School of
ENGINEERING
DUKE UNIVERSITY

A THEORY OF CONTROL
FOR A CLASS OF ELECTRONIC POWER PROCESSING SYSTEMS:
ENERGY-STORAGE DC-TO-DC CONVERTERS

by

William W. Burns, III

Prepared under Research Grant No. NGL 34-001-001, Supplement 16

April 25, 1977

A THEORY OF CONTROL FOR A CLASS OF ELECTRONIC POWER PROCESSING SYSTEM: ENERGY-STORAGE DC-TO-DC CONVERTERS

by

William W. Burns, III

April 25, 1977

Prepared under Research Grant No. NGL 34-001-001, Supplement 16

Department of Electrical Engineering

School of Engineering

Duke University

Durham, North Carolina

for

NATIONAL AERONAUTICS AND SPACE ADMINISTRATION

A THEORY OF CONTROL FOR A CLASS OF ELECTRONIC POWER PROCESSING SYSTEMS: ENERGY-STORAGE DC-TO-DC CONVERTERS

by

William W. Burns, III

Department of Electrical Engineering
Duke University

Date: April 25, 1977

Approved:

Thomas G. Wilson, Supervisor

Dissertation submitted in partial fulfillment of the requirements for the degree of Doctor of Philosophy in the Department of Electrical Engineering in the Graduate School of Arts and Sciences of Duke University
1977

ABSTRACT
(Electrical Engineering)

A THEORY OF CONTROL FOR A CLASS OF ELECTRONIC POWER PROCESSING SYSTEMS: ENERGY-STORAGE DC-TO-DC CONVERTERS

by

William W. Burns, III

Department of Electrical Engineering
Duke University

Date: April 25, 1977

Approved:

Thomas G. Wilson
Thomas G. Wilson, Supervisor

Harry A. Owen, Jr.

W. T. Jones

Devendra P. Garg

Dissertation submitted in partial fulfillment of the requirements for the degree of Doctor of Philosophy in the Department of Electrical Engineering in the Graduate School of Arts and Sciences of Duke University
1977

ABSTRACT

The principal function of energy-storage dc-to-dc converters is to extract electrical energy from a given source at some unregulated voltage level, but at a controlled rate, in order to provide a precisely regulated dc supply of power to an electrical load at some other specified voltage level. The only means available for controlling this rate of energy extraction is the turning on and off of the converter power switch in a systematically determined sequence. It is the principal task of the converter control subsystem to determine this switching sequence. Thus the behavior of the system and its subsequent level of performance are very much dependent on the particular control function employed to generate the switching decisions. Because of the highly nonlinear nature of dc-to-dc converter systems, classical analysis techniques have been unable to provide adequate guidance for the design and development of these control subsystems, and consequently most converter control techniques have been derived heuristically, with an inadequate understanding of the cause and effect relationships which exist between the action of the controller and the converter power stage performance which results from it. Thus, it is usually very difficult to predict the performance characteristics of dc-to-dc converter systems over a range of specified operating

conditions, and it is even more difficult to determine what elements are required in a control subsystem to alleviate the tendency of these highly nonlinear systems toward instability.

This dissertation presents an analytically derived approach to the control of energy-storage dc-to-dc converters which enables improved system performance and an extensive understanding of the manner in which this improved performance is accomplished. The control approach is derived from a state-plane analysis of dc-to-dc converter power stages which enables a graphical visualization of the movement of the system state during both steady-state and transient operation. This graphical representation of the behavior of dc-to-dc converter systems yields considerable qualitative insight into the cause and effect relationships which exist between various commonly used converter control functions and the system performance which results from them. Furthermore, this theoretical insight has led to the conceptual development of a state-trajectory control law which utilizes all of the information available from the converter power stage to determine the unique system equilibrium condition which yields the desired steady-state output characteristics of the converter and the exact switching sequence which is needed to move the state of the system from any initial condition to that steady-state trajectory in one cycle of control.

Systems operating in conjunction with this control law exhibit short response times to external disturbances, precise static regulation, and inherently stable operation over an entire range of specified operating conditions. This performance is achieved by making the control decision based on the location of the state of the system relative to a state-plane switching boundary which is a function of the converter power stage component values, the desired steady-state operating characteristics, and the extern-

ally imposed operating conditions. The influence of parasitic losses in the converter power stage on the shape and location of this switching boundary, and consequently on the behavior of a converter controlled by it, is investigated, and modifications to the mathematical representation of this boundary are presented which accommodate these losses. Additionally, simplifications to the mathematical representation of the switching boundary are presented which require less complex circuitry to implement but at the same time yield less precise operational characteristics, and discussions of the tradeoff between converter performance and the complexity of the control implementation required to achieve that performance are presented. Digital computer simulation data and oscillograms from an experimental converter system are presented to illustrate and verify the theoretical discussions and subsequent control law presented.

ACKNOWLEDGEMENTS

This research was supported in part by the National Aeronautics and Space Administration under Research Grant NGL-34-001-001 to Duke University.

I would like to express my sincere appreciation to Professors Thomas G. Wilson, my faculty advisor, and Harry A. Owen, Jr., member of my faculty advisory committee, for their immeasurable contributions to the work described in this dissertation in particular and to my graduate education in general. Their skill and generosity as teachers and friends is heartily acknowledged.

I would also like to thank Mr. Stephen D. Huffman for his programming and instrumentation of the control law implementation described in Chapter VI; Mr. Jimmy Hartley for his drafting of many of the figures in this dissertation; and Mrs. Margrid Casseday for her skillful and cheerful typing of this manuscript.

I would especially like to thank my wife Sandy, not only for her typing of drafts of this dissertation, but more importantly for her loving patience and much needed support throughout this endeavor.

W. W. Burns, III

CONTENTS

LIST OF FIGURES

LIST OF TABLES

A THEORY OF CONTROL FOR A CLASS OF ELECTRONIC POWER PROCESSING SYSTEMS: ENERGY-STORAGE DC-TO-DC CONVERTERS

Chapter I

INTRODUCTION

One of the most useful and far reaching accomplishments of modern technology has been the generation and harnessing of electric power for purposes of performing work and processing information for man's benefit. Numerous techniques have been devised for generating electric power in both direct current and alternating current forms, and a veritable multitude of devices have been invented which use the power so generated to perform a wide variety of useful tasks from lighting homes and offices to performing complex scientific experiments onboard orbiting spacecraft. It is of course necessary that the electrical characteristics of the source of power in each of these applications be compatible with those of the electrical loads so that safe and efficient operation can ensue. The great majority of electrical devices in use today are designed to operate from the well-regulated alternating current supplied by the electric utilities industry and meet this compatibility requirement very well. However, increasingly more devices are being developed for a wide variety of applications which either require power in some other form or, in some cases, must operate from an unconventional source of power which has widely varying terminal characteristics and fluctuating supply capabilities. Such applications often present compatibility problems which must be resolved before the source can be effectively and safely applied to the load.

Examples of such interface problems can be found in most unmanned spacecraft systems. The electrical loads on board these spacecraft are often complex scientific experiments and telemetry systems which must be supplied with precisely regulated dc power at several different voltage levels. Because of the size and weight limitations imposed on the spacecraft, however, the only source of electric power available is often a solar array whose terminal characteristics vary with intensity of sunlight, temperature, and the load current being withdrawn. Thus, before this source of power can meet the requirements of the spacecraft loads, some additional manipulation and management of the raw source power must be performed.

Classical ac-to-ac transformation and ac-to-dc rectification are two such power handling processes which are widely-used and well-established applications of electro-technology. These processes cannot meet all electric power interface requirements, however, and two additional power management processes which are becoming increasingly more important in the development of electric power are the processes of dc-to-ac inversion and dc-to-dc conversion. The study and development of these two electric power transformation processes is the principal objective of the relatively new and still evolving discipline known as "electronic power processing" or "electronic power conditioning." There are two particularly important and distinguishing features of the power conversion processes treated in this field. First, the inversion from direct to alternating current is accomplished entirely with static electronic components, without the aid of rotating machines or other mechanical devices. Secondly, the regulation of dc voltages or currents is accomplished non-dissipatively whereby the only power wasted is that which is unintentionally lost in nonideal circuit components, thus distinguishing these processes from the more familiar and less complex

dissipative regulation techniques which intentionally discard unneeded energy in a controlled manner so as to maintain a regulated output voltage or current.

An early exploration into the fundamental nature of these power processing techniques revealed that one or more switching elements must be present in the power paths of these networks in order to be able to achieve the dc-to-ac or dc-to-dc power conversion processes [1]. This requirement hindered the early exploration and development of the field of power processing because of a lack of suitably fast and efficient switching devices. Static power conversion, in principle, had been recognized for many years [2], but the relatively poor operational characteristics of available switching devices such as mercury-vapor discharge tubes rendered further exploration and development practically unfeasible. With the invention and rapid development of the power transistor and the silicon controlled rectifier (SCR), however, substantial research efforts began to emerge in the still somewhat undefined area of electronic power processing [3], and the significance and applicability of this branch of technology has since continued to evolve and grow.

One widely used subclass of electronic power processing systems is that which is commonly known as "energy-storage dc-to-dc converters." Other names often assigned to this class of circuits include "switching regulators," "pulse-modulated controlled dc/dc regulators," and "switched dc-dc converters." The lack of conformity to an established terminology is yet another indication of the still rapidly evolving stature of this field. As can be inferred from all of these names, however, the principal purpose of this class of electronic networks is to process power from an unregulated dc source with a possibly varying terminal voltage in such a way as to provide

a well-regulated dc supply of power to a load at some other specified voltage level. The conversion process is accomplished statically and requires the use of one or more switching devices as described above. It is non-dissipative and efficiencies approaching 100% are theoretically possible and greater than 90% have been achieved practically. Converters in this class can accomplish step-up as well as step-down transformations of the source voltage, which again distinguishes these systems from dissipative regulators which can only step-down the source voltage.

Dc-to-dc converters have become quite popular during the past two decades and are currently found in a wide variety of power-conditioning applications. Because the dc-to-dc conversion process is dependent on the presence and action of high speed switching devices in the converter power paths, these systems are highly nonlinear and consequently difficult to analyze. The well established theories of linear systems analysis are, of course, invalid when studying nonlinear systems such as these, but even many of the more appropriate, although less complete, theories of nonlinear systems analysis are not directly applicable to this class of closed-loop switching systems. Because of this analytical complexity, the most frequently used tools over the years for the design and development of dc-to-dc converters have been engineering intuition and technical experience. As the effectiveness and widening applicability of these converters and other static power processing systems became apparent, however, increasingly more effort has been expended in developing analysis and design tools to aid in the understanding and advancement of this new branch of power technology.

Numerous approaches to the study of energy-storage dc-to-dc converters have been pursued during the past decade, and many analysis and design techniques with varying degrees of usefulness and applicability have been pro-

posed. Some of the more significant contributions are described in references 4 through 21. Each of these efforts is an attempt to explain and/or develop design guidelines for various aspects of particular dc-to-dc conversion circuits which had been previously developed through engineering ingenuity and experience as described above. This, of course, is one of the principal purposes of investing time and talent in pursuing mathematical analyses of physical systems, but another equally important and potentially profitable goal of circuit and system analysis is to evoke, through the insight and understanding gained, new ideas and inventions which reveal previously unexplored but potentially fruitful approaches to the systems and to enable the development of improvements in them. This dissertation presents such an analytically derived contribution to the field of power processing which takes the form of a new theory of control for energy-storage dc-to-dc converters. The application of this conceptually developed control theory enables the accomplishment of converter performance that approaches theoretical limits which are revealed through a state-plane analysis of this class of systems. Furthermore, because of its sound mathematical basis, the nature of the operation of the resultant control technique is easily understood and additional developments and extensions of it can be readily accomplished to meet particular application requirements or system performance constraints as desired.

The analysis approach which has led to the development of this theory of control is based on a state-space visualization of the overall performance of converter systems, including large as well as small signal behavior. A major shortcoming of many of the analysis approaches referenced above is that they yield information concerning only the small signal behavior of systems operating about predetermined equilibrium conditions. This limita-

tion is due largely to the fact that most of these techniques are based on linearization or averaging approximations which sometimes tend to obscure the fundamental nonlinear nature of the systems. The apprcach pursued in this dissertation, on the other hand, chooses to embrace the system nonlinearities rather than to avoid them, and it is found that in so doing considerably greater insight into the fundamental nature of these systems and a more complete understanding of their behavioral characteristics can be achieved. This desire to preserve the nonlinear nature of these systems throughout the analysis is based on the conviction that although it is the system nonlinearities which usually are the principal cause of difficulty in analyzing and understanding the behavior of such systems, it is also these same nonlinearities which usually are the keystone for successful circuit operation and which consequently hold the most promise for yielding further understanding and improved developments of them.

One of the most powerful features of this approach is its ability to clearly portray the manner in which various control techniques accomplish the task of turning the system switching elements on and off in order to achieve the conversion and regulation processes desired. Both the steady-state and the transient characteristics of converter systems are very much dependent on the particular type of control technique employed, and different control subsystems applied to a common converter power stage can result in systems with drastically different behavioral characteristics and performance capabilities. This modular character of dc-to-dc converter systems is illustrated conceptually in Fig. 1.1.

Since the development and successful application of the basic power-handling configurations of this class of networks, increasingly more attention has been focused on developing new control techniques which can enable those

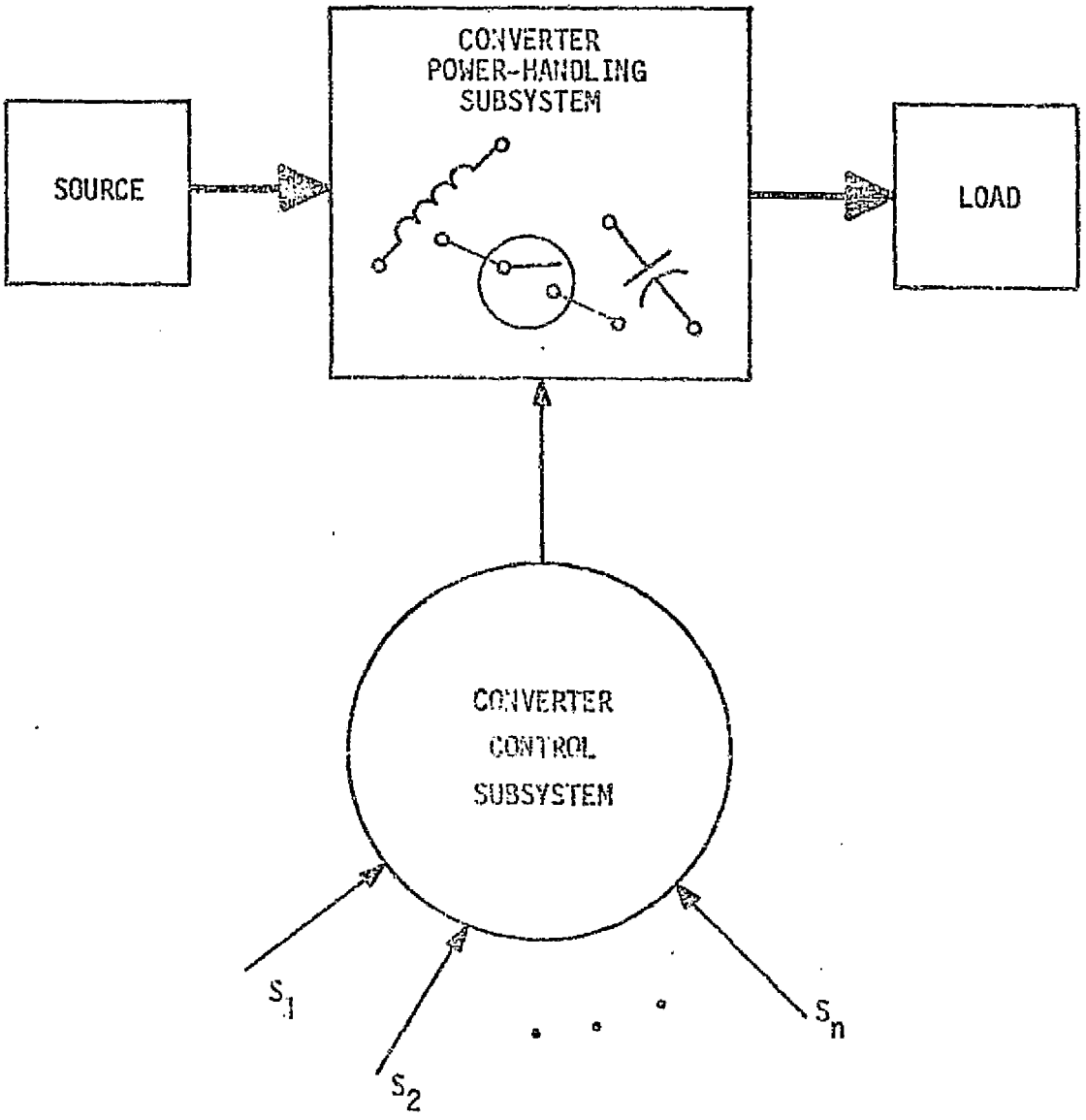

Fig. 1.1 Modular nature of energy-storage dc-to-dc converter systems. The converter power stage is comprised of some combination of linear inductors, capacitors, and switches. $S_1, S_2, \ldots S_n$ represent signals from the power stage which are used by the controller to determine a switching sequence for the power stage switches.

basic power stages to meet more stringent static and dynamic converter system performance specifications. The converter analysis techniques referenced above so far appear to have been of little apparent use in this endeavor because the approximations inflicted on the systems in order to be able to apply the well established and time proven analysis and design tools found in linear system theory usually have rendered these newer analysis approaches inadequate for the purposes of studying the nonlinear nature of dc-to-dc converter control. Consequently, most of the converter control techniques, like the power stages themselves, have been developed through engineering intuition and design experience rather than through analytical derivations. The resultant converter systems usually display improvements in some aspect or aspects of the system performance, but the majority of the performance indicators remain unchanged or, in some cases, even degrade. Converters operating under the influence of these heuristically determined control configurations can successfully achieve good steady-state voltage regulation over a specified range of operating conditions, but they do so by a more or less iterative process, and as a result, the transient convergence of the systems to steady-state operation is usually rather slow, and sometimes unstable operation results. In any event, the system performance which results when employing many of these controllers cannot be precisely predicted or explained, and any additional improvements or modifications in the system must again be accomplished through trial-and-error design based on engineering experience.

The control technique proposed in this dissertation, on the other hand, is completely founded in a state-plane analysis of a widely used class of energy-storage dc-to-dc converters. The analysis has provided considerable insight into the fundamental elements of control which are required

for the successful operation of these converters, and it has enabled a critical comparison of various conventional control techniques which reveals strengths and weaknesses of each. This insight has led to the postulation of the control theory presented in this dissertation and to the subsequent development of a state-trajectory control law which employs information available from the converter power stage to determine the precise switching sequence needed to move the system to a desired equilibrium condition in one "on/off" cycle of control regardless of the system's initial state or externally imposed operating conditions. The performance of converters operating under the influence of this control technique can be accurately predicted for an entire range of specified operating conditions, and all aspects of the system performance are incorporated in the control process. It is the purpose of this dissertation to present the analytical background, conceptual development, and practical investigation and evaluation of this control technique as applied to a widely used class of electronic power processing systems.

A detailed description of the state-plane analysis technique employed in this endeavor and its application to a class of energy-storage dc-to-dc converters is presented in Chapter II. After briefly describing the principal function and distinguishing characteristics of the family of converters, normalized models of each of three representative converter power stages are developed for use in subsequent analytic derivations and illustrative examples. Within this normalized framework, the behavior of the converters is characterized in the system state plane with particular attention being given to observing how the behavior varies when subjected to changes in internal parameters or externally imposed operating conditions. Both the static and the dynamic performance of converters can be observed

in this way, and examples of system trajectories are presented to illustrate all aspects of this approach.

As stated previously, this analysis approach is particularly well suited for studying the manner in which various control techniques determine a switching sequence for the converter power stage. Chapter III exploits this feature and presents a discussion of some fundamental elements which are required for the control of these systems and an evaluation of the strengths and weaknesses of several particular control approaches as revealed through the system state plane. Conditions for the stability of systems employing one of the control approaches are discussed and explained in terms of the system state trajectories, and measures which can be taken to alleviate stability problems are proposed. Digital computer simulations of converter systems operating under the influence of each of the control techniques discussed are presented, and comparisons of the system responses to step changes in the source voltage and the load current are made.

From the analytical background presented in Chapters II and III, a state-trajectory control law for dc-to-dc converters is derived in Chapter IV. After presenting a qualitative description of the fundamental concept of this approach, detailed derivations of equations which are needed to implement the control law are presented. The performance capabilities of systems operating with this control technique are discussed with respect to both steady-state and transient operation, and simulations of converter systems are presented. The same converter power stages are used in these tests as are used in Chapter III so that meaningful comparisons between this control technique and the techniques presented in Chapter III can be made.

For the sake of clarity in developing and explaining this state-trajectory control technique, all of the data presented in Chapters II, III,

and IV are based on the models of the physical converters presented early in Chapter II. Chapter V extends the development and understanding of this new technique by considering some practical aspects of its application to actual converter systems. The effects of lossy elements such as inductor winding resistance, capacitor equivalent series resistance (ESR), and semiconductor voltage drops and bulk resistances on the converter behavior and their subsequent relationship to the control technique proposed are discussed. Modifications to the equations derived in Chapter IV are presented which accommodate the changes in system behavior caused by these lossy elements, and, in a similar vein, additonal modifications to these equations which yield simpler controller implementations but less precise converter performance are explored, and tradeoffs between various aspects of converter system performance and the complexity of the control law implementation required to achieve that performance are discussed. Digital computer simulations of converter systems are again presented to illustrate each of these considerations.

The physical realizability of this mathematically derived control theory and its applicability to actual converter systems is demonstrated in Chapter VI. The particular approach described in this chapter employs digital processing of the system variables to generate the derived control function, but other approaches which employ analog signal processing or hybrid combinations of digital and analog techniques are equally feasible. After briefly outlining the steps involved in this digital implementation, the behavior of an experimental dc-to-dc converter circuit operating under its control is presented and discussed with respect to the performance measures described in Chapter IV, and the experimentally measured response of this system is compared to the simulated and theoretically predicted

responses described in previous chapters.

The merits and usefulness of the analysis approach and resultant control technique presented in this dissertation are discussed in Chapter VII. Possible further developments of the control law for dc-to-dc converters are proposed and the applicability of this control approach to other types of dc-to-dc converters in particular and power processing systems in general is discussed. Because this approach is both general and straightforward to apply, its usefulness is by no means limited to the particular applications presented herein, and it is hoped that the reader will emerge from this dissertation with an interest in applying this approach to other systems as well as with a better understanding of an important class of electronic power processing systems.

Chapter II

STATE TRAJECTORIES USED TO OBSERVE ENERGY-STORAGE DC-TO-DC CONVERTERS

2.1 Introduction

The theory of control presented in this dissertation is derived from a qualitative state-plane analysis of a widely used class of energy-storage dc-to-dc converters. This analysis approach and its application to three representative dc-to-dc converters is described in this chapter. After discussing the principal function and behavioral characteristics of the converters in general, normalized models of three particular converter power stages which are used throughout this dissertation to illustrate the concepts and theories developed are presented. Based on these models, a general discussion of converter behavior as it can be portrayed in the system state plane is presented, with particular attention being given to observing how the system behavior changes when subjected to changes in internal parameters or externally imposed operating conditions. To aid in the visualization of the various concepts and aspects of converter system performance described, numerous graphical illustrations and examples of actual converter characteristics are presented and discussed.

2.2 Class of Converters

The class of energy-storage dc-to-dc converters treated in this

dissertation can be represented by the three basic networks depicted in Figs. 2.1, 2.2, and 2.3. There exist numerous other converter configurations which are also members of this family, but the fundamental operational characteristics of each of them can be found in one or the other of the three basic configurations shown, and consequently an understanding of the operation of these three configurations leads directly to an understanding of all of the others. Each of these dc-to-dc converter systems is comprised of two principal subsystems -- a power-handling stage and a control subsystem. Only the converter power stages are shown in Figs. 2.1-2.3 because there are a myriad of different control techniques which have been developed for these systems. The surprisingly simple circuit topologies depicted in these figures can efficiently and reliably achieve the relatively complex dc-to-dc conversion process described in Chapter I. For each of the basic power-handling configurations, the overall system performance with respect to such features as output voltage overshoot or system response times to transient disturbances is, to a large extent, dependent on the manner in which the control function is accomplished. The state-space analysis approach pursued in this dissertation enables a clear visualization of this cause and effect relationship between the system control function and the resultant converter behavior, and these relationships are examined in considerable detail in this and the following chapter.

The primary function of energy-storage dc-to-dc converters is to extract electrical energy from a given dc source at some unregulated voltage level, but at a controlled rate, in order to deliver precisely regulated dc power to an electrical load at some other specified voltage level. The relative magnitudes of the input supply voltage available and the regulated output voltage desired is the criterion that determines which type of con-

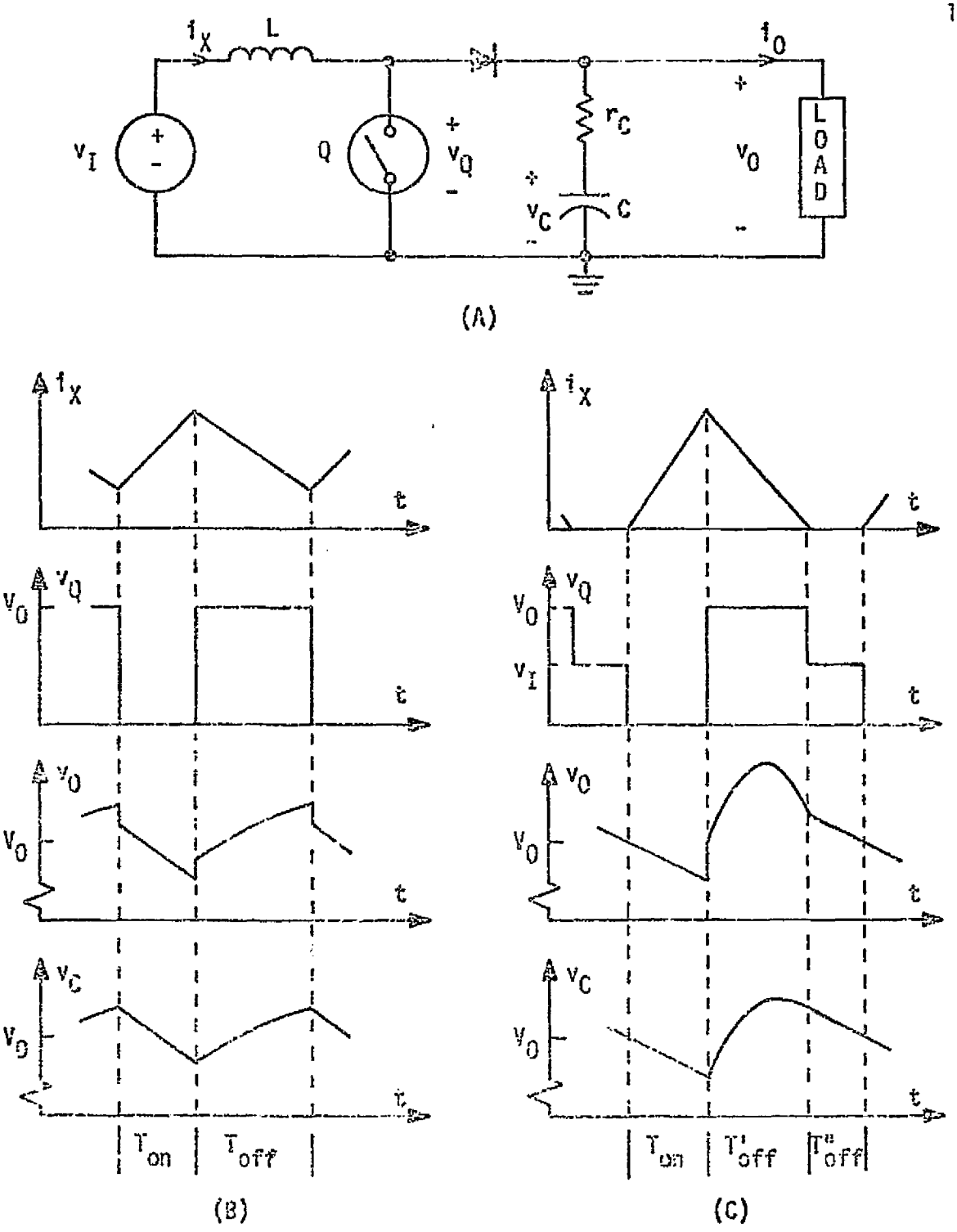

Fig. 2.1 (A) Schematic diagram of voltage step-up dc-to-dc converter. Characteristic waveforms for (B) operation in the continuous conduction mode, and (C) operation in the discontinuous conduction mode. Example circuit values are: L=0.253mH, C=400μF, r_C = 0.05Ω, $V_{O,rated}$ = 28.0V, $v_{I,nominal}$ = 21.0V, and $i_{O,rated}$ = 4.0A.

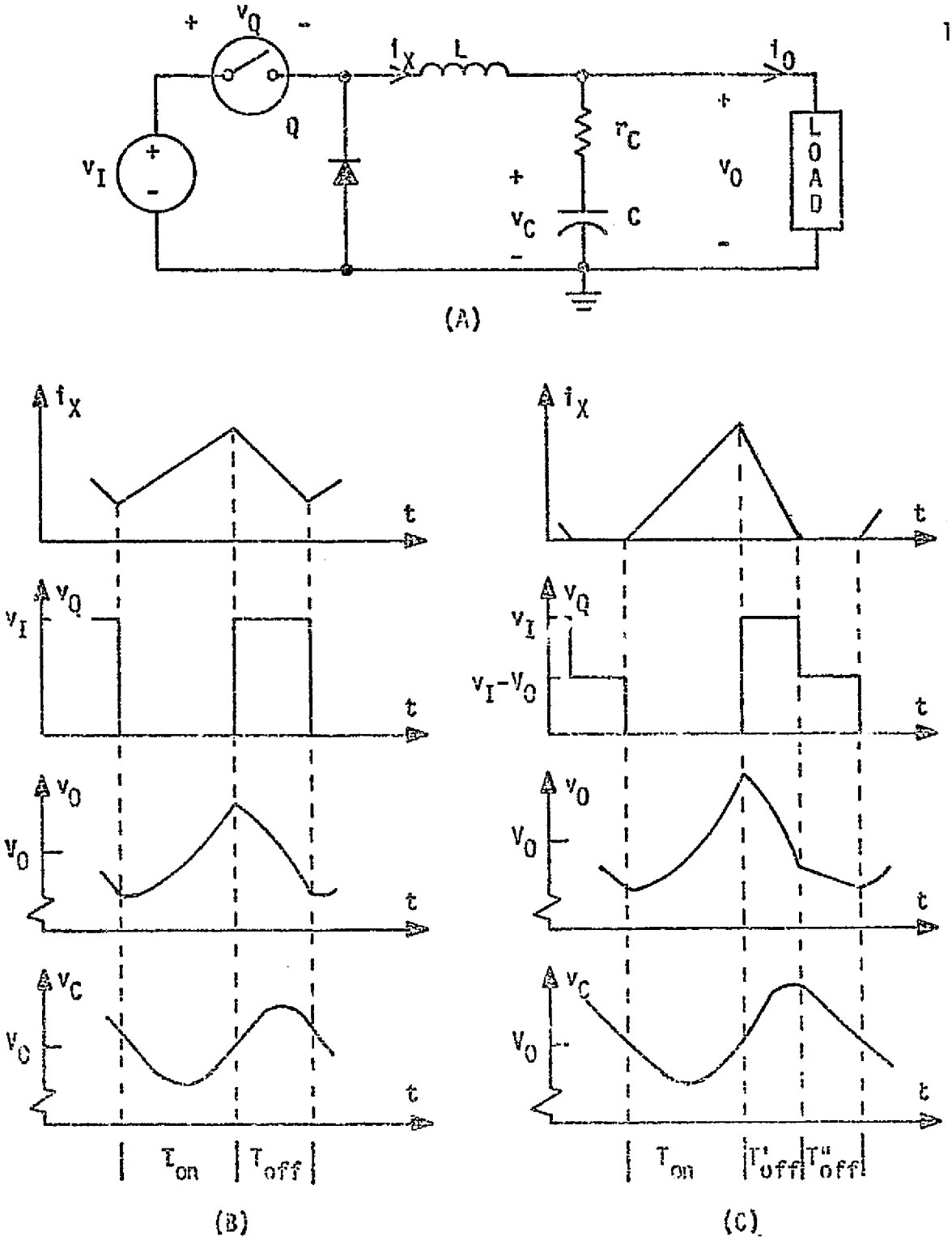

Fig. 2.2 (A) Schematic diagram of current step-up dc-to-dc converter. Characteristic waveforms for (B) operation in the continuous conduction mode, and (C) operation in the discontinuous conduction mode. Example circuit values are: L=0.23mH, C=300μF, r_C = 0.05Ω, $v_{O,rated}$ = 20.0V, $v_{I,nominal}$ = 30.0V, and $i_{O,rated}$ = 2.0A.

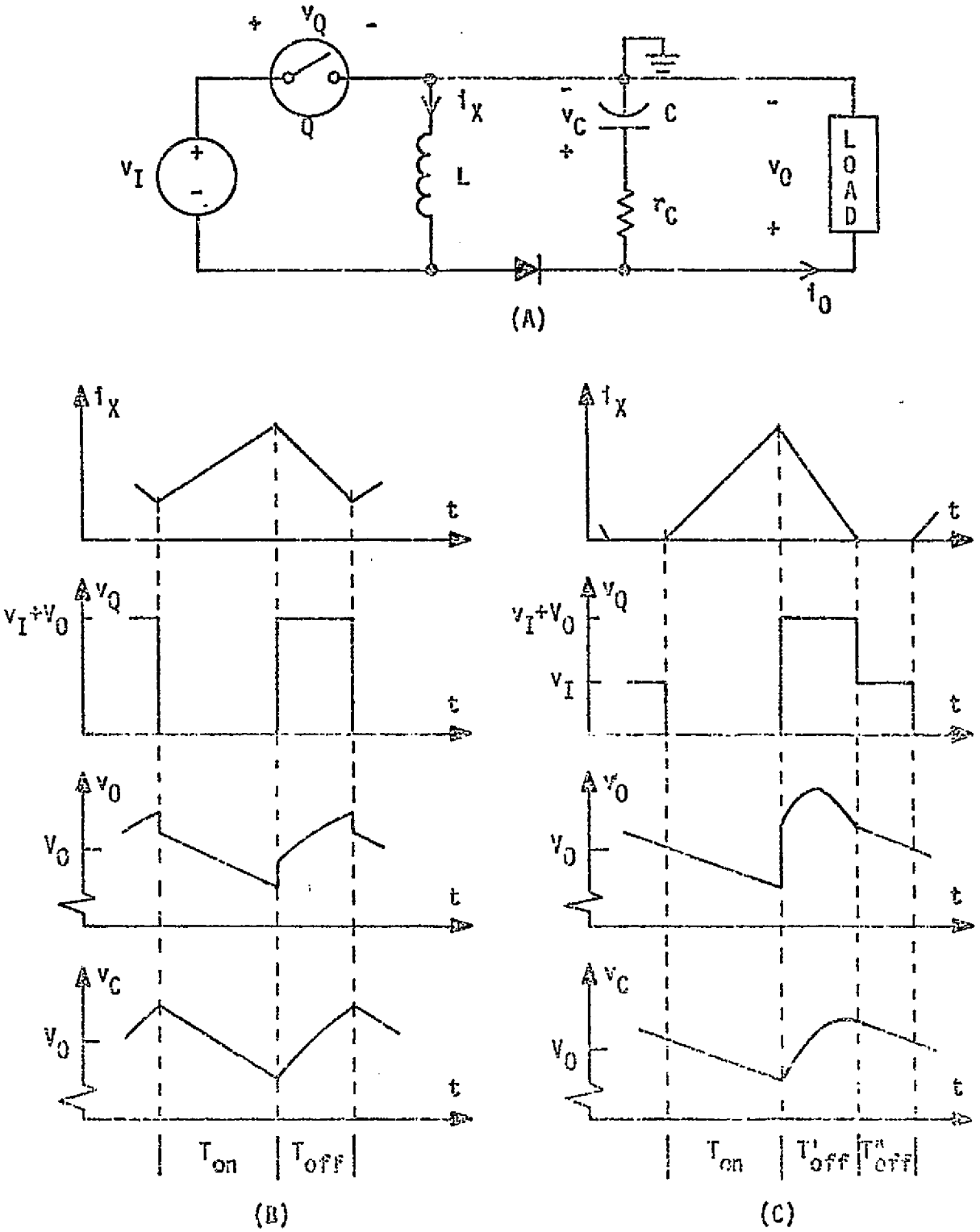

Fig. 2.3 (A) Schematic diagram of current-or-voltage step-up dc-to-dc converter. Characteristic waveforms for (B) operation in the continuous conduction mode, and (C) operation in the discontinuous conduction mode. Example circuit values are: L=0.211mH, C=400μF, r_C = 0.05Ω, $v_{O,rated}$ = 28.0V, $v_{I,nominal}$= 21.0V, and $i_{O,rated}$ = 4.0A.

verter configuration should be used for a given application. The converter depicted in Fig. 2.1, for example, is capable of delivering power to a load at a regulated voltage level which is greater than that of its source. This configuration is commonly known as the "voltage step-up" or "boost" converter. The converter shown in Fig. 2.2, on the other hand, is capable of supplying power to a load at a higher current level than is drawn from the source, and consequently it is known as the "current step-up" or "buck" converter. The third configuration, shown in Fig. 2.3, is known as the "current-or-voltage step-up" or "buck/boost" converter because it is capable of accomplishing either of the functions described above depending on the duty cycle of the power switch Q and the relative magnitudes of the input supply voltage and the desired average output voltage.

For the sake of clarity and conciseness in the presentation of this dissertation, detailed discussions of the concepts and theories derived are presented as they are developed for the voltage step-up configuration only. Equivalent characteristic data and examples for the other two representative configurations are also presented, but because the procedures for deriving and utilizing these data are essentially the same for all three configurations, the discussions of the current step-up and the current-or-voltage step-up converters are limited to highlighting any differences or unusual features which may be peculiar to one but not the others. The voltage step-up configuration has been chosen for the more complete presentation because it has been found to exhibit more severe stability problems and greater analytical difficulties than the other two configurations, and thus can more fully illustrate the power of this approach.

The rate at which dc-to-dc converters extract electrical energy from a source is controlled by successively opening and closing a power switch

so as to periodically interrupt the flow of energy from the source to the load. These switches, denoted as Q in Figs. 2.1-2.3, are often silicon power transistors in actual applications, but the type of switch employed is of no consequence in the analysis and theory presented in this dissertation, and so the more general symbol for a switch is used in these circuit diagrams rather than the particular symbol for a transistor. During the time that the power switch is closed, energy is extracted from the source and stored in a magnetic field in the linear inductor L. During this same time period, energy which had previously been stored in an electric field between the plates of the output capacitor C is released to the load. During the time that the switch is open, the energy stored in the inductor during the previous halfcycle is released to the load and to the capacitor to replenish the energy which was lost during the switch closure time. The lengths of time that the switch is open, T_{off}, and closed, T_{on}, in both steady-state and transient operation determine how much and how quickly energy is transferred to the load and consequently are very important parameters in the study of dc-to-dc converters. A more complete discussion and qualitative explanation of this aspect of performance and the behavior of these three converter configurations in general is presented in Reference 6. The brief discussion presented here is intended only to introduce the basic function of this class of electronic networks and to give a basis for interpreting some of the data presented in this and succeeding chapters.

Pertinent characteristic waveforms for each of the three representative configurations are presented in the (B) and (C) portions of Figs. 2.1-2.3. As indicated in the figures, two distinct modes of operation -- the "continuous conduction" and the "discontinuous conduction" modes -- are possible for each configuration. This distinction is based

on the behavior of the current, i_x, in the energy-storage reactor. If this current falls to zero during the time that the power switch is open, the converter is said to be operating in the discontinuous conduction mode. Otherwise it is said to be in the continuous conduction mode. In recent years considerable attention has been given to this distinction, and some researchers in the field of power processing have attributed superior performance capabilities to systems which are designed to operate solely in one or the other of these modes. A study of the relative merits of each of these modes of operation is not presented in this dissertation *per se*, but discussions and examples of systems operating in each mode are presented in the course of the development of this thesis, and some advantages and disadvantages of each do become apparent.

Another useful distinction which is illustrated in these series of waveforms is the difference between the voltage, v_C, across ideal output capacitors and the actual output voltage, v_0, which is present across non-ideal capacitors. This difference is due to the presence of the parasitic equivalent series resistance (ESR), shown as r_C in the diagrams, which is always present to some degree in actual physical capacitors. This parasitic effect has been included, even in these simplified diagrams, because it has been found to play an important and sometimes dominant role in establishing converter system behavior [5]. Some examples of the effect of capacitor ESR on the behavior of various converter/controller systems are presented in Chapter III.

2.3 Normalized Converters and Models

For purposes of generality and to facilitate relative comparisons of converter performance characteristic, the three basic converter power

stages described above have been normalized as shown in Fig. 2.4. Normalization factors have been chosen so that the normalized rated average output voltage is unity, the normalized rated output current is unity, and a normalized time of 2π corresponds to the undamped natural period of the inductor-capacitor combination in the unnormalized converter power stage. In a system normalized in this manner, the magnitudes of all voltages represent some portion of the desired average output voltage. Thus, an input voltage of 0.75 corresponds to a voltage of 75% of the desired average output voltage, and an instantaneous peak output voltage of 1.05 corresponds to an output voltage overshoot of 5%. Likewise, the values of all normalized system currents represent some multiple of the rated output current, and a reactor current of 2.0 corresponds to twice the rated current, whereas a current of 0.5 corresponds to one half of the rated output current. The third normalization factor, $T_{ref} = \sqrt{LC}$, enables a quick evaluation of the converter switching frequency relative to the natural frequency of the system. This is a very important consideration when designing switching converters such as these, and normally the successful operation of them is dependent on having a switching frequency considerably higher than the natural frequency of the LC combination in the power stage. Thus, the switching period of the normalized system should be considerably less than 2π to meet this criterion. Most of the data presented in this dissertation are in normalized form, and the symbols introduced in Fig. 2.4 with the subscripts N are used to distinguish normalized variables and parameters from their unnormalized counterparts.

To be amenable to a mathematical analysis, any physical system must be modeled in such a way as to capture those aspects of the system behavior which are essential to its operation and which, additionally, focus

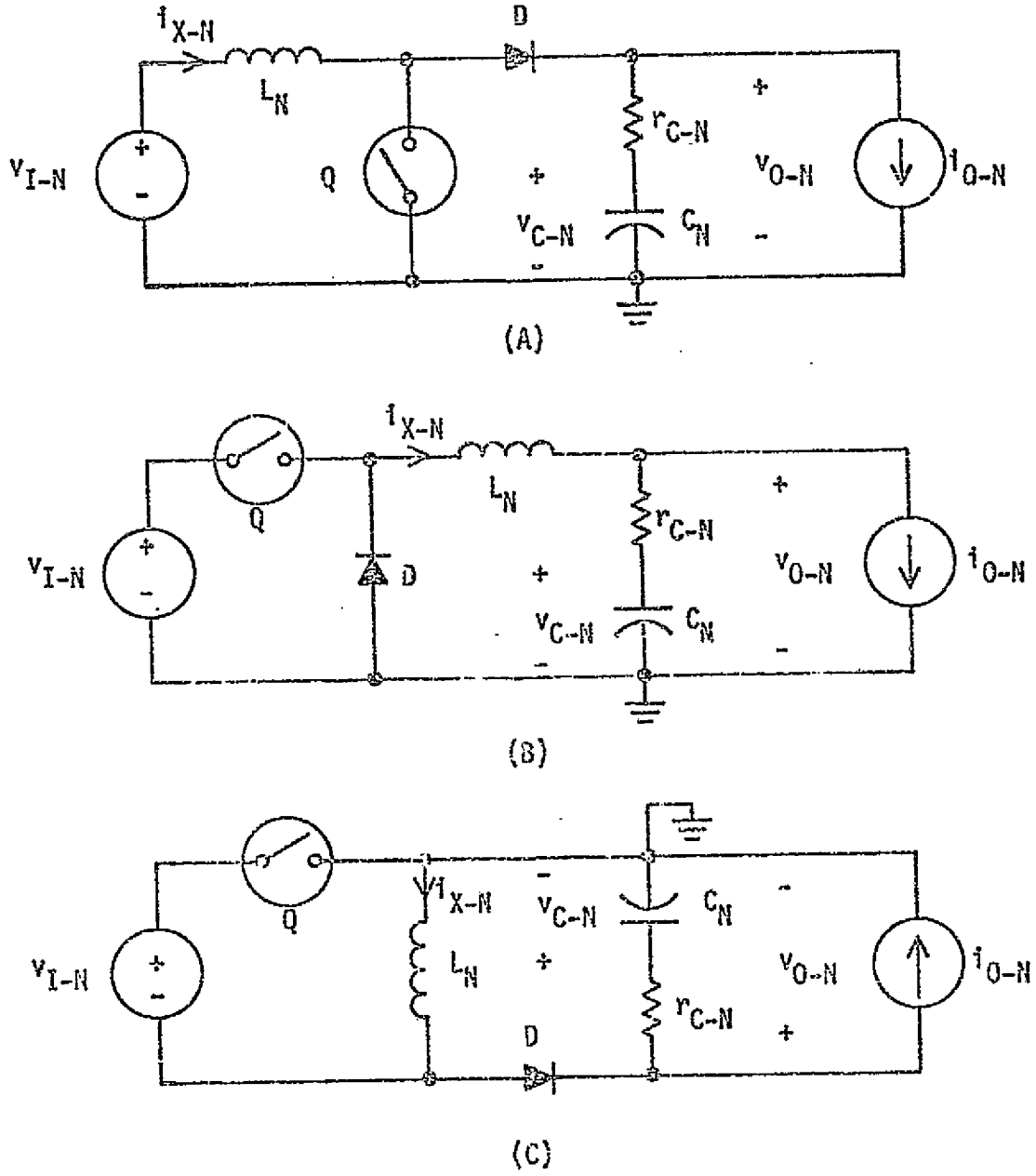

Fig. 2.4 Normalized representations of power stages for (A) voltage step-up, (B) current step-up, and (C) current-or-voltage step-up converters with normalization factors $V_{ref} = V_{O,rated}$, $I_{ref} = I_{O,rated}$, and $T_{ref} = \sqrt{LC}$. Normalized circuit parameters and variables in terms of original network values are:

$$L_N = \frac{I_{ref}}{V_{ref} T_{ref}} L \qquad v_{I-N} = \frac{v_I}{V_{ref}} \qquad v_{O-N} = \frac{v_O}{V_{ref}}$$

$$C_N = \frac{V_{ref}}{I_{ref} T_{ref}} C \qquad i_{X-N} = \frac{i_X}{I_{ref}} \qquad i_{O-N} = \frac{i_O}{I_{ref}}$$

$$r_{C-N} = \frac{I_{ref}}{V_{ref}} r_C \qquad v_{C-N} = \frac{v_C}{V_{ref}} \qquad t_N = \frac{t}{T_{ref}}$$

attention on items of particular interest. The simplified schematic diagrams presented in Figs. 2.1 - 2.3 and the normalized networks of Fig. 2.4 are examples of such abstractions of physical dc-to-dc converter systems. Another model of each of these converters is presented in Figs. 2.5, 2.6, and 2.7. The (A) portion of each of these figures represents the respective converter power stage during the time that the power switch Q is closed or "on," while part (B) represents the converter during the time that the switch is open or "off." The models portrayed in these figures have relatively simple mathematical representations but, at the same time, retain the essential behavioral characteristics of the actual physical systems. Thus, for the sake of convenience in generating desired data and to avoid obscuring fundamental concepts in unessential details, these simplified models are used in the development of this and the next two chapters. It should be noted, however, that the validity of the theoretical treatment presented in this chapter is not dependent on the particular simplified converter models depicted in these figures. The same arguments and equivalent data can be generated for converter models of arbitrary complexity. A complete discussion and evaluation of various levels of modeling as it affects the control theory developed in this dissertation is presented in Chapter V.

As can be surmised from Figs. 2.5-2.7, the power switches in these converters are assumed to be ideal; i.e., they switch between ideal open circuits and ideal closed circuits instantly on command. Likewise the diodes are assumed to be ideal with no losses and no switching delays. These two approximations enable a piecewise-linear treatment of these circuits which can readily be justified given the quality of currently available semiconductor switching devices. In addition, the converter output

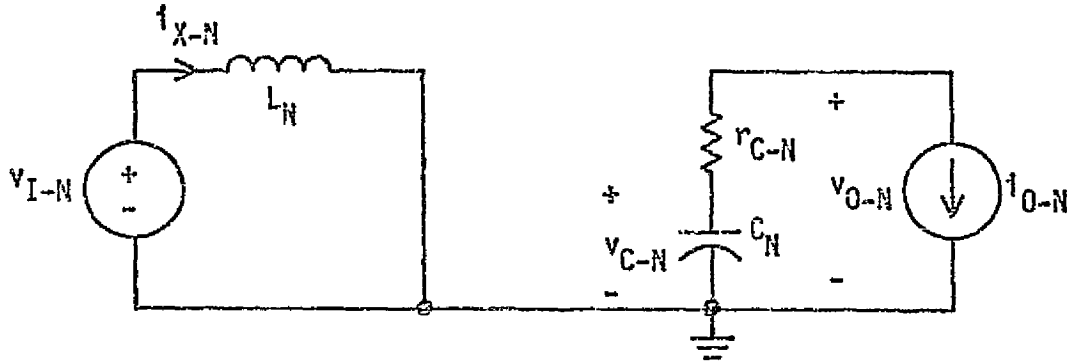

$$\frac{di_{X-N}}{dt_N} = \frac{v_{I-N}}{L_N} \qquad \frac{dv_{C-N}}{dt_N} = -\frac{i_{O-N}}{C_N}$$

(A)

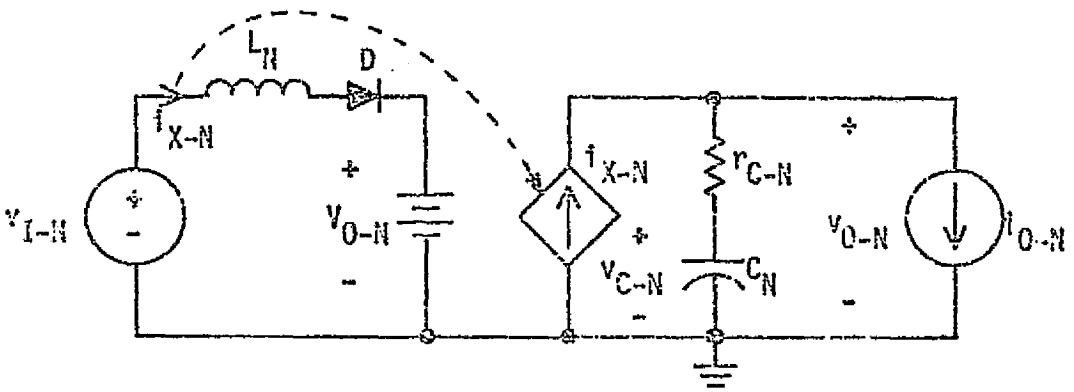

$$\frac{di_{X-N}}{dt_N} = \frac{v_{I-N} - v_{O-N}}{L_N} \qquad \frac{dv_{C-N}}{dt_N} = \frac{1}{C_N}\left(i_{X-N} - i_{O-N}\right)$$

(B)

Fig. 2.5 Voltage step-up converter model and mathematical representation during (A) power switch on-time, and (B) power switch off-time. Diamond shaped symbol represents a dependent current source.

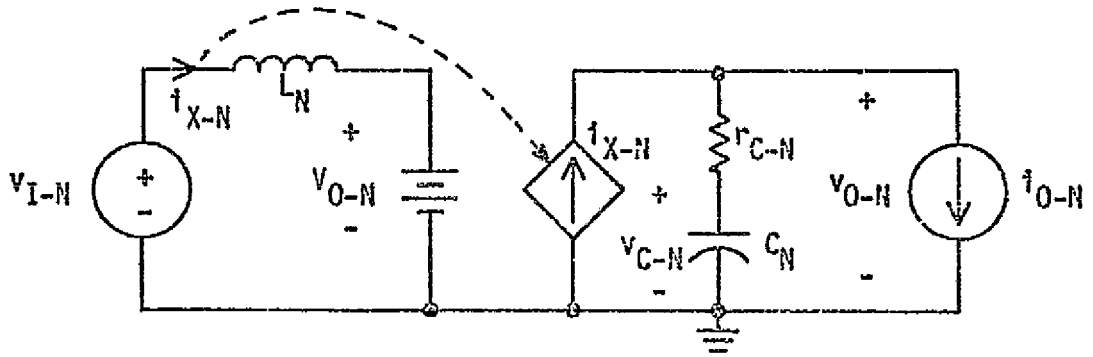

$$\frac{di_{X-N}}{dt_N} = \frac{V_{I-N} - V_{O-N}}{L_N} \qquad \frac{dv_{C-N}}{dt_N} = \frac{1}{C_N}\left(i_{X-N} - i_{O-N}\right)$$

(A)

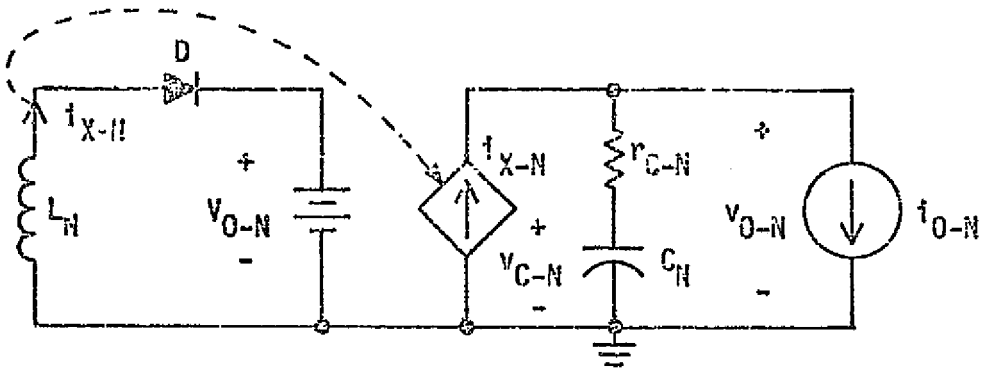

$$\frac{di_{X-N}}{dt_N} = -\frac{V_{O-N}}{L_N} \qquad \frac{dv_{C-N}}{dt_N} = \frac{1}{C_N}\left(i_{X-N} - i_{O-N}\right)$$

(B)

Fig. 2.6 Current step-up converter model and mathematical representation during (A) power switch on-time, and (B) power switch off-time. Diamond shaped symbols represent dependent current sources.

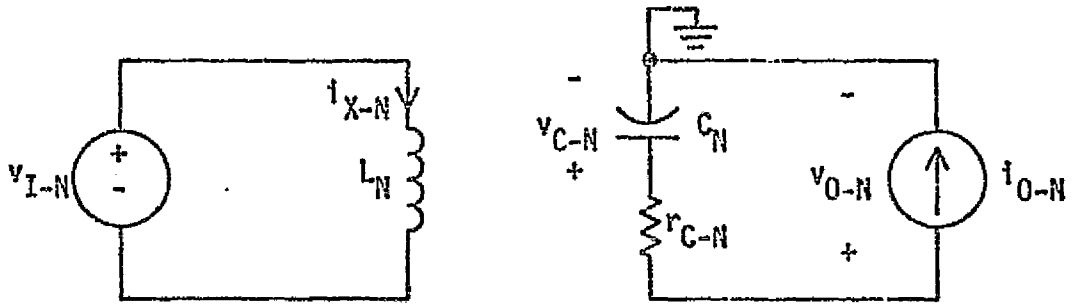

$$\frac{di_{X-N}}{dt_N} = \frac{v_{I-N}}{L_N} \qquad \frac{dv_{C-N}}{dt_N} = -\frac{i_{O-N}}{C_N}$$

(A)

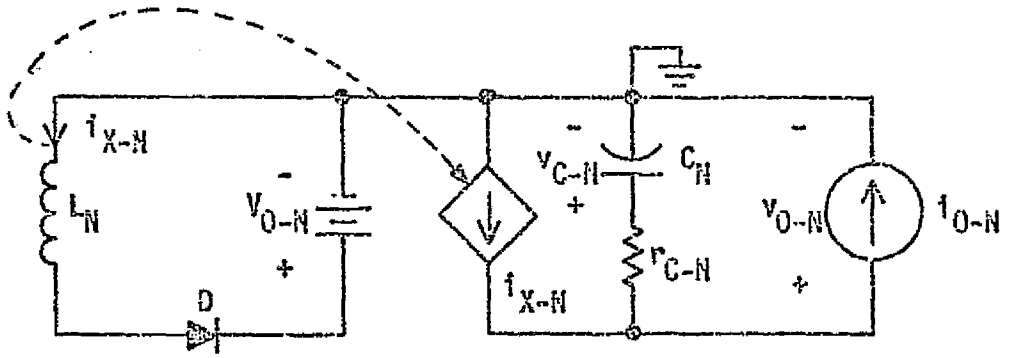

$$\frac{di_{X-N}}{dt_N} = -\frac{V_{O-N}}{L_N} \qquad \frac{dv_{C-N}}{dt_N} = \frac{1}{C_N}(i_{X-N} - i_{O-N})$$

(B)

Fig. 2.7 Current-or-voltage step-up converter model and mathematical representation during (A) power switch on-time, and (B) power switch off-time. Diamond shaped symbol represents a dependent current source.

voltage is assumed to be sufficiently well-regulated in the case of a constant load resistance that the load can be represented as a constant current sink, and when v_{I-N} is constant, the inductor current can be assumed to rise with a constant slope during the switch on-time and fall with a constant slope during the switch off-time. This triangular inductor current i_{L-N} is used, in conjunction with the independent output current, i_{O-N}, to compute the current into capacitor C_N and subsequently the capacitor voltage v_{C-N}.

The mathematical representations of these models are given below their respective diagrams in the form of pairs of first order differential equations. The solutions to these state equations are algebraic functions of time and thus are easy to visualize. The primary justification for the assumptions on the shape of the inductor current and the magnitude of the peak to peak output voltage ripple relative to its average value can be found in the design restriction stated above that the converter switching frequency should be at least one order of magnitude greater than the natural frequency of the inductor-capacitor combination in the converter power stage. A more detailed evaluation of these assumptions and their affect on the accuracy of analyses can be found in the literature [20] and is not presented here; for as stated previously, this model has been chosen merely for convenience and for the sake of clarity of presentation and is not cruical to the development of this control theory. More exact models of these systems yield solutions to the state equations which, although transcendental in nature, are equally amenable to this state-plane treatment but are less readily visualized without the aid of detailed computation.

2.4 Converter Behavior in the State Plane

The converter system state variables employed in this study are

the normalized reactor current i_{X-N} and the normalized capacitor voltage v_{C-N}. The behavior of the converters can be represented mathematically by means of a sequence of pairs of differential equations which can be solved explicitly to yield time-domain solutions for the state of the system. The mathematical representations for the models described in the preceding section are given in Figs. 2.5-2.7. If the independent variable, normalized time, is eliminated in the solutions $i_{X-N}(t_N)$ and $v_{C-N}(t_N)$, a sequence of equations of the form $v_{C-N} = g(i_{X-N})$ results in which time is an implicit parameter. These implicit equations, when plotted in the state plane of i_{X-N} versus v_{C-N}, define what is called the solution curve, or the system state trajectory. Those portions of a solution curve which result when the power switch is on are referred to as on-time trajectories, and those portions corresponding to the power switch being off are referred to as off-time trajectories. The complete transient response of a converter thus can be portrayed in the state plane as a sequence of connected on-time and off-time trajectories. Normal steady-state operation of a converter is indicated by a closed curve in the state plane consisting of a single on-time trajectory and a single off-time trajectory.

A typical family of on-time and family of off-time trajectories for a particular voltage step-up dc-to-dc converter, whose equations are derived below, are presented in Fig. 2.8. Each trajectory corresponds to a different pair of initial conditions or initial state of the system. The family of off-time trajectories, whose initial states have been arbitrarily selected as uniformly spaced points along the translated ordinate axis, are shown as solid lines and also include segments of the v_{C-N} axis. Paths, such as these are the ones which the system state must follow whenever the power switch is turned off. Similarly, the on-time trajectories, shown

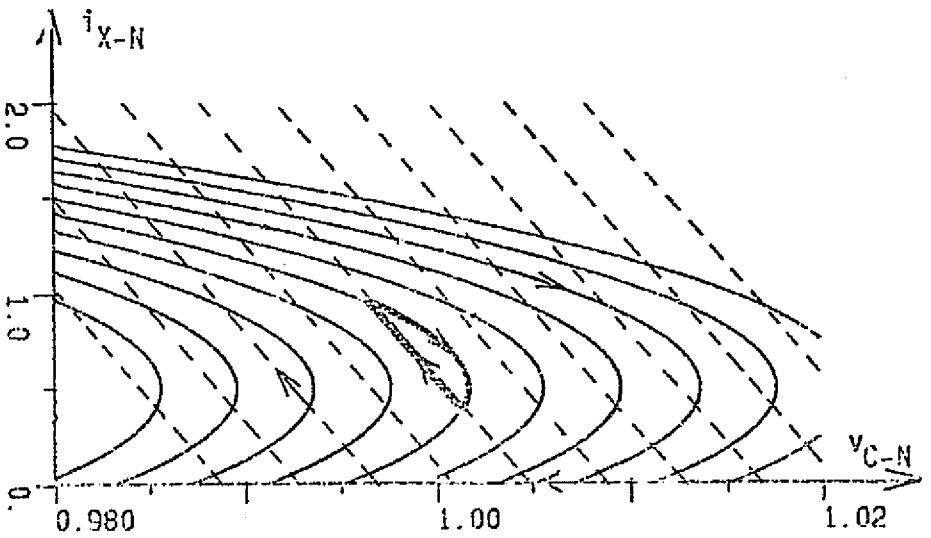

Fig. 2.8 Families of on-time trajectories (dashed lines) and off-time trajectories (solid lines) in the state plane of i_{X-N} vs v_{C-N} for the voltage step-up converter shown in Fig. 2.1 with v_{I-N} = 0.75, and i_{O-N} = 0.5. Highlighted closed curve is the steady-state solution trajectory corresponding to nominal conditions used as a reference in subsequent figures.

as dashed lines, are the paths which the state must follow during the time that the power switch is closed. As indicated previously, time is an implicit parameter in these state trajectories and, as time increases, the system state moves in the direction indicated by the arrow heads; i.e., decreasing reactor current and peaking capacitor voltage, or simply decreasing capacitor voltage if the reactor current is zero, for the off-time trajectories,[1] and increasing reactor current and decreasing capacitor voltage for the on-time trajectories. Any converter solution curve, or solution trajectory, is made up of a sequence of such off-time segments and on-time segments.

2.4.1 Equations of Trajectories

When modeling the voltage step-up converter as portrayed in Fig. 2.5, these solution curves are found to be parabolas for the off-time trajectories with reactor current greater than zero and straight lines for the on-time trajectories as derived below. Using Kirchoff's voltage and current laws, the sequence of state equations corresponding to the model of Fig. 2.5 and given in that figure can be readily derived. Calling t_N^0 the arbitrary initial time and $i_{X-N}(t_N^0)$ and $v_{C-N}(t_N^0)$ the arbitrary initial state variables of the converter, the time-domain solution of the network of Fig. 2.5(A) for the time interval T_{on-N} that the power switch is closed is

$$\begin{aligned} i_{X-N} &= \frac{v_{I-N}}{L_N} t_N + i_{X-N}(t_N^0) \\ v_{C-N} &= -\frac{i_{O-N}}{C_N} t_N + v_{C-N}(t_N^0) \end{aligned} \tag{2.1}$$

[1] Notice that the off-time trajectories peak at $i_{X-N} = i_{O-N}$.

for $t_N^0 \leq t_N < t_N^0 + T_{on-N}$. Let the time instant $(t_N^0 + T_{on-N})$ that the power switch opens be called t_N^1 as illustrated in Fig. 2.9(A) for the continuous conduction case and 2.9(B) for the discontinous conduction case. Then, for that portion of the power switch off-time period T'_{off-N} that the inductor current i_{X-N} is greater than zero in Fig. 2.5(B), the solutions for the two system state variables are

$$\begin{aligned} i_{X-N} &= -\frac{V_{O-N} - v_{I-N}}{L_N} t_N + i_{X-N}(t_N^1) \\ v_{C-N} &= -\frac{V_{O-N} - v_{I-N}}{2L_N C_N} t_N^2 + \frac{i_{X-N}(t_N^1) - i_{O-N}}{C_N} t_N + v_{C-N}(t_N^1) \end{aligned} \tag{2.2}$$

for $t_N^1 \leq t_N < t_N^1 + T'_{off-N}$. Similarly, let the time instant $(t_N^1 + T'_{off-N})$ that the inductor current i_{X-N} falls to zero and the diode D becomes reverse biased or "open" be called t_N^2. Then, for that portion of the power switch off-time period T''_{off-N} that the inductor current i_{X-N} is equal to zero in Fig. 2.5(B), the solutions for the two system state variables are

$$\begin{aligned} i_{X-N} &= 0 \\ v_{C-N} &= -\frac{i_{O-N}}{C_N} t_N + v_{C-N}(t_N^2) \end{aligned} \tag{2.3}$$

for $t_N^2 \leq t_N < t_N^2 + T'_{off-N}$. To simplify this notation for subsequent derivations, the initial values of inductor current and capacitor voltage when the converter is operating in steady state are defined as illustrated in Fig. 2.9 and as listed below.

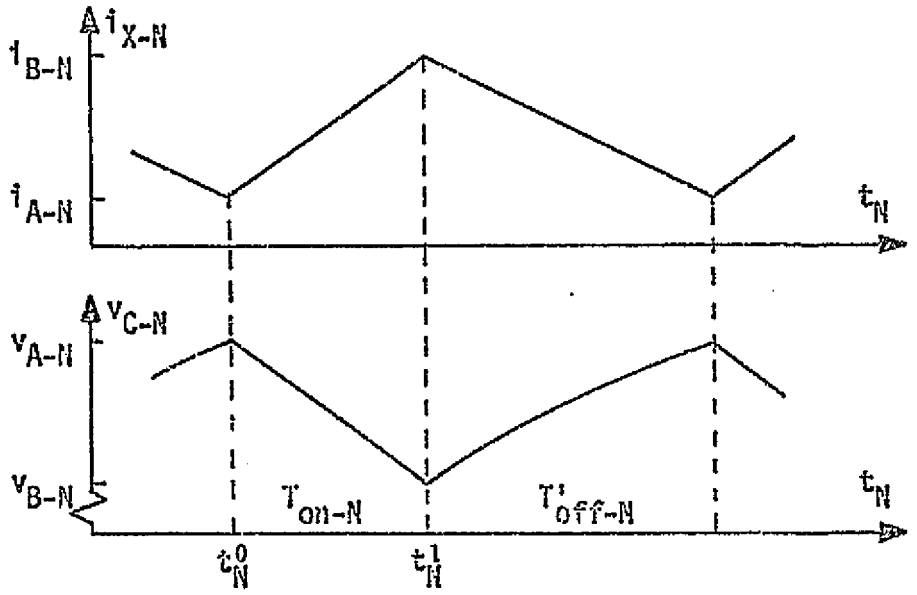

(A)

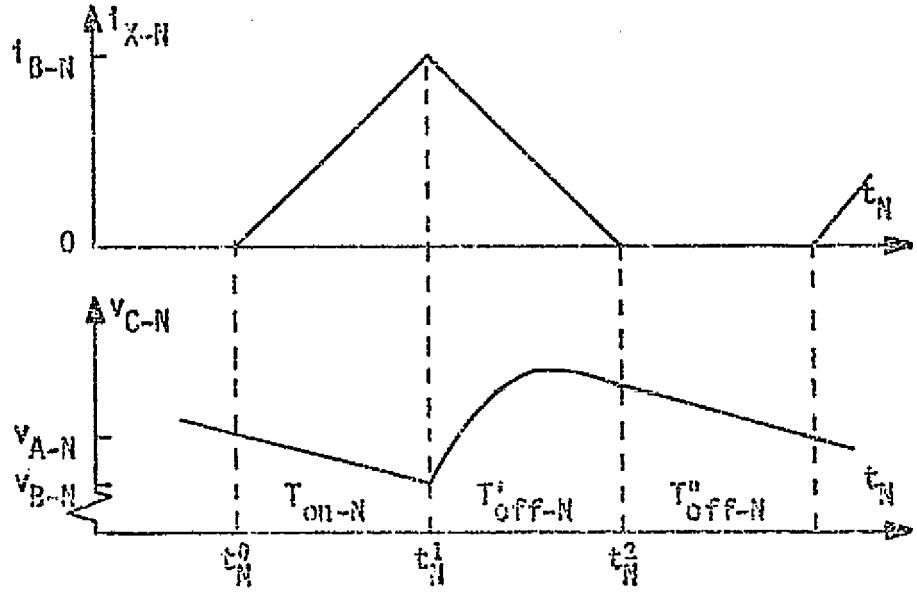

(B)

Fig. 2.9 Time waveforms illustrating symbols assigned to initial states for on-time and off-time trajectories for (A) steady-state continuous conduction operation, and (B) steady-state discontinuous conduction operation.

$$i_{X-N}(t_N^0) = i_{A-N}$$

$$v_{C-N}(t_N^0) = v_{A-N} \tag{2.4}$$

$$i_{X-N}(t_N^1) = i_{B-N}$$

$$v_{C-N}(t_N^1) = v_{B-N} \tag{2.5}$$

It should be noted that if the converter is operating in the continuous conduction mode, the inductor current never falls to zero and only two sets of equations, (2.1) and (2.2), are needed to completely describe the system.

The independent variable, t_N, in each of the pairs of solutions presented above can be eliminated to yield the following sequence of equations which defines the system state trajectory during each of the three possible time intervals, where again only the first two equations are appropriate if the system is operating in the continuous conduction mode.

$$v_{C-N} = - \frac{L_N \, i_{O-N}}{C_N \, v_{I-N}} i_{X-N} + K_1 \tag{2.6}$$

$$v_{C-N} = - \frac{L_N}{2C_N(V_{O-N} - v_{I-N})} i_{X-N}^2 + \frac{L_N i_{O-N}}{C_N(V_{O-N} - v_{I-N})} i_{X-N} + K_2 \tag{2.7}$$

$$i_{X-N} = 0 \tag{2.8}$$

K_1 and K_2 are constants which are functions of the circuit component

values, the converter operating conditions, and the particular initial states for the respective switching intervals, and for steady-state operation are given by[2]

$$K_1 = \frac{L_N\, i_{O-N}}{C_N\, v_{I-N}}\, i_{A-N} + v_{A-N} \tag{2.9}$$

$$K_2 = \frac{L_N}{2C_N(V_{O-N} - v_{I-N})}\, i_{B-N}^2 - \frac{L_N\, i_{O-N}}{C_N(V_{O-N} - v_{I-N})}\, i_{B-N} + v_{B-N} \tag{2.10}$$

Thus, for the converter model chosen, the system on-time trajectories are defined by (2.6) which gives the family of straight lines of Fig. 2.8. Likewise, the portions of the off-time trajectories which occur during T'_{off-N} are defined by (2.7) which gives the family of parabolas of Fig. 2.8. The portions of off-time trajectories corresponding to T''_{off-N} are defined by (2.8) and are simply segments of the v_{C-N} axis with the direction of movement of the state when on this axis being toward the origin of the plane. The trajectories defined by (2.8) occur during the zero-current dwell time of the system when operating in the discontinuous conduction mode.

The trajectories plotted in Fig. 2.8 are shown only in a localized region of the state plane with a voltage range of $\pm$2% of the rated output voltage and a current range of 0 to 2 times the rated output current. This particular region of the plane is displayed because it includes the steady-state trajectory of the example converter operating with the input voltage and output current specified. This steady-state trajectory is highlighted with bold lines near the center of Fig. 2.8 and is seen to be comprised of segments of one off-time trajectory and one on-time trajectory. The particular closed trajectory illustrated there corresponds to steady-state operation in the continuous conduction mode at half the rated output current

[2] See page 125 for further discussion of i_{A-N}, v_{A-N}, i_{B-N}, and v_{B-N}.

and with an input voltage equal to 75% of the rated output voltage, and it is used as a reference condition in subsequent illustrative data. It should be noted that the average reactor current for the voltage step-up converter is equal to V_{O-N}/v_{I-N} times the average output current, which for this example is $\frac{4}{3}\, i_{O-N}$. Examples of discontinuous conduction trajectories, consisting of three distinct segments as described in the preceding paragraph, are presented later in this chapter.

Given any initial state within this plane, the transient trajectory which the system state follows in attempting to reach a steady-state condition is determined by the sequence of power switch closings and openings as established by the converter controller. As long as the power switch is off, the system state must follow the particular off-time trajectory which passes through the state at the instant the switch is opened. At the instant the switch is turned on, the state must begin to follow the particular on-time trajectory which passes through the final state of the preceding off-time trajectory. In this manner, the state of the system alternately follows off-time and on-time trajectories around the state plane and eventually, if the converter system is functioning properly, converges to a closed steady-state trajectory. Such a sequence of trajectories is illustrated in Fig.2.10.

From the initial state marked with an X in the i_{X-N} vs. v_{C-N} plane, the system state follows the on-time trajectory which passes through this initial state until the power switch is turned off at some time by the action of the converter's controller. The off-time trajectory which passes through the final on-time is then followed until the switch is again turned on by the controller. In this example, the converter, operating under the influence of a fictitious controller, converges to the closed two-segment steady-state trajectory near the center of the figure in two "on/off" cycles of control. The families of curves shown in this figure

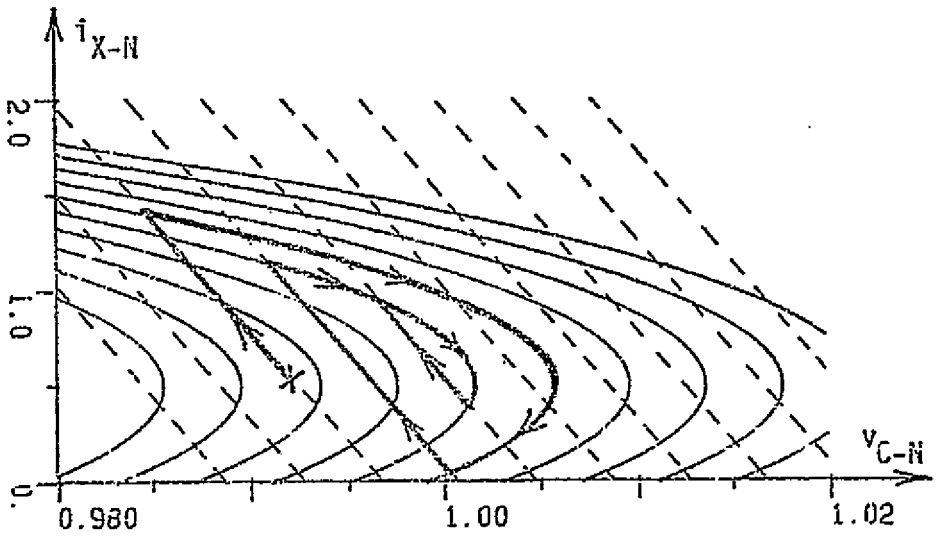

Fig. 2.10 Example of a transient trajectory which converges to a steady-state trajectory for the voltage step-up converter of Fig. 2.1 with $v_{I-N} = 0.75$ and $i_{O-N} = 0.5$.

are the same as those in Fig. 2.8, and the steady-state trajectory highlighted in both figures is the same. The fictitious controller employed in this example enables the system state to converge very quickly and efficiently to the desired steady-state trajectory. Most conventional controllers usually are not capable of achieving such quick and accurate transient solutions, however, and in some cases unstable converter operation results whereby the system state diverges from the desired steady-state trajectory or converges to some other steady-state trajectory which does not meet the system specifications adequately. Examples of transient trajectories for systems operating with some commonly employed control techniques and illustrations of various types of unstable operation in converters are presented in Chapter III.

As discussed previously, time is an implicit parameter in these state trajectories, and it can be extracted if desired to reveal the more familiar current and voltage vs. time waveforms. The relationship between a system state trajectory and its corresponding time waveforms is illustrated in Fig. 2.11. Selected instants of the implicit parameter t_N are indicated in the state plane as small circles on the state trajectory. The same values of current and voltage are similarly marked on the i_{X-N} vs. t_N and v_{C-N} vs. t_N plots. It should be noted that the distance traversed by the system state in the state plane is not necessarily a good indication of the length of time required to accomplish that movement. The state of the system can move quickly or slowly around the state plane as determined by the system time constants which are revealed in the state equations.

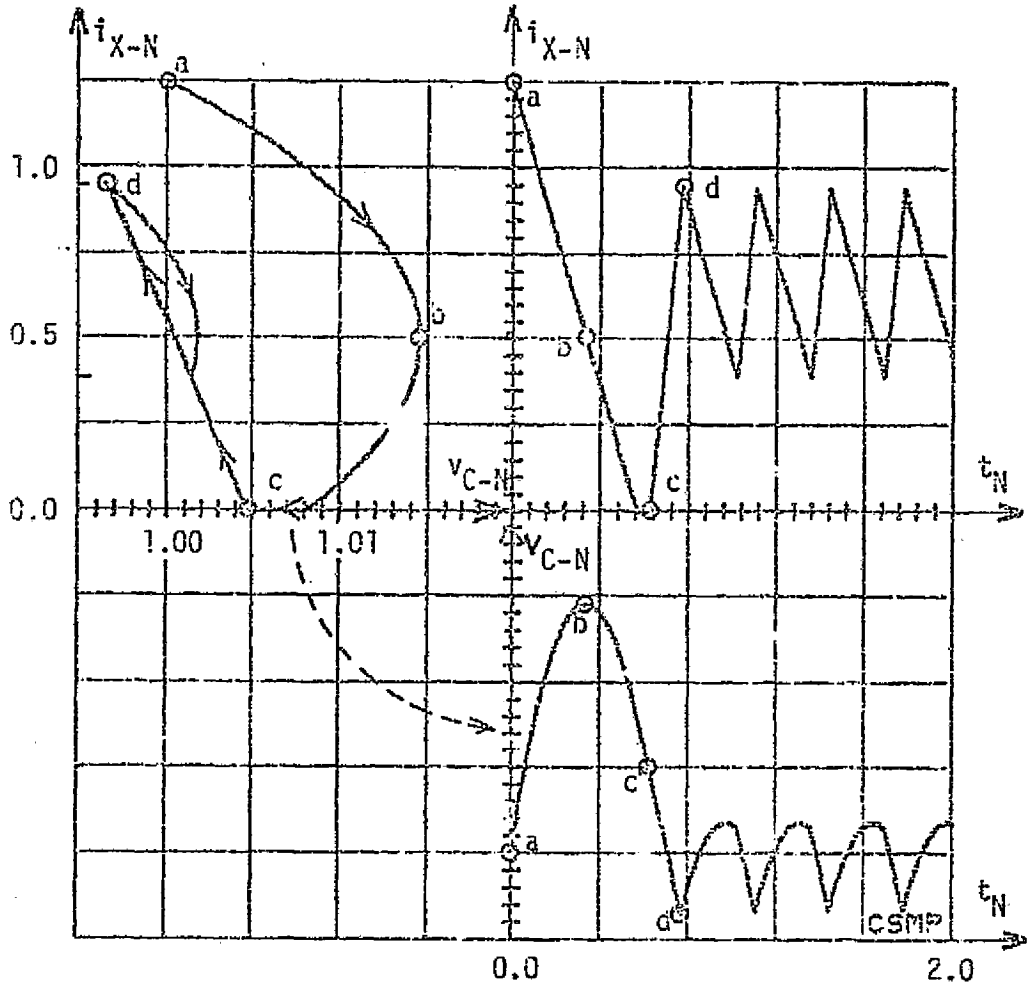

Fig. 2.11 Illustration of relationship between state-plane solution trajectory (upper left) and state-variable time waveshapes (right) for the voltage step-up converter. The solution trajectory is comprised of segments from the two families of trajectories displayed in Fig. 2.8.

2.4.2 Equations of Trajectories for the Current Step-Up and the Current-or-Voltage Step-Up Converters

The general discussion presented at the beginning of section 2.4 applies equally well to the other members of this class of dc-to-dc converters. Families of on-time trajectories and off-time trajectories for the current step-up and current-or-voltage step-up converters shown in Figs. 2.2 and 2.3 are presented in Figs. 2.12 and 2.13 respectively. The derivation of the equations for these trajectories follows precisely the derivation presented for the voltage step-up configuration given in section 2.4.1 and is not repeated here. The equations for the current step-up converter trajectories are found to be parabolas during both the power switch on-time interval and the portion of the switch off-time interval when the reactor current is greater than zero as seen in equations (2.11) and (2.12) respectively. During T_{on-N}

$$v_{C-N} = - \frac{L_N}{2C_N(V_{O-N} - v_{I-N})} i_{X-N}^2 + \frac{i_{O-N} L_N}{C_N(V_{O-N} - v_{I-N})} i_{X-N} + K_1 \qquad (2.11)$$

During T'_{off-N}

$$v_{C-N} = - \frac{L_N}{2C_N v_{O-N}} i_{X-N}^2 + \frac{i_{O-N} L_N}{C_N v_{O-N}} i_{X-N} + K_2 \qquad (2.12)$$

During T''_{off-N}

$$i_{X-N} = 0 \qquad (2.13)$$

with

$$K_1 = \frac{L_N}{2C_N(V_{O-N} - v_{I-N})} i_{A-N}^2 - \frac{i_{O-N} L_N}{C_N(V_{O-N} - v_{I-N})} i_{A-N} + v_{A-N} \qquad (2.14)$$

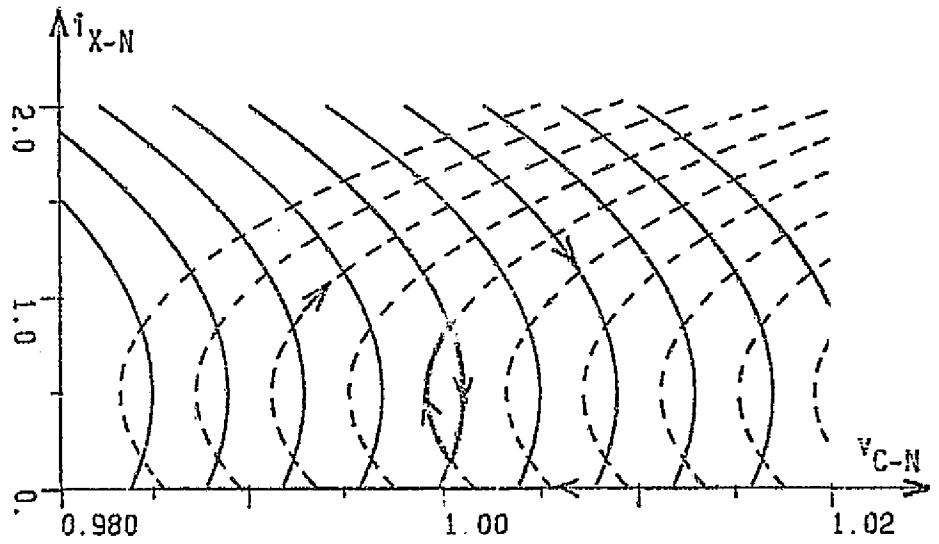

Fig. 2.12 Families of on-time trajectories (dashed lines) and off-time trajectories (solid lines) in the state plane of i_{X-N} vs. v_{C-N} for the current step-up converter shown in Fig. 2.2 with $v_{I-N} = 1.5$ and $i_{O-N} = 0.5$. Highlighted closed curve is the steady-state solution trajectory corresponding to nominal conditions used as a reference in subsequent figures.

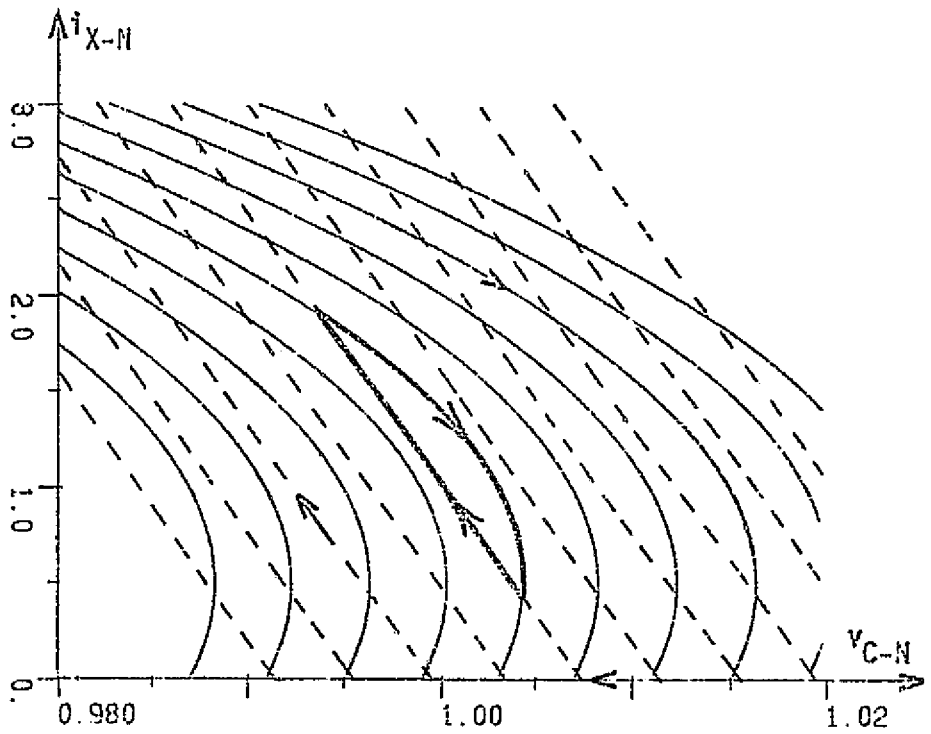

Fig. 2.13 Families of on-time trajectories (dashed lines) and off-time trajectories (solid lines) in the state plane of i_{X-N} vs. v_{C-N} for the current-or-voltage step-up converter shown in Fig. 2.3 with $v_{I-N} = 0.75$ and $i_{O-N} = 0.5$. Highlighted closed curve is the steady-state solution trajectory corresponding to nominal conditions used as a reference in subsequent figures.

and

$$K_2 = \frac{L_N}{2C_N V_{O-N}} i_{B-N}^2 - \frac{i_{O-N} L_N}{C_N V_{O-N}} i_{B-N} + v_{B-N} \qquad (2.15)$$

The equations which determine the state trajectories for the current-or-voltage step-up configuration are given as equations (2.16) and (2.17).

During T_{on-N}

$$v_{C-N} = - \frac{i_{O-N} L_N}{V_{I-N} C_N} i_{X-N} + K_1 \qquad (2.16)$$

During T'_{off-N}

$$v_{C-N} = - \frac{L_N}{2C_N V_{O-N}} i_{X-N}^2 + \frac{L_N i_{O-N}}{C_N V_{O-N}} i_{X-N} + K_2 \qquad (2.17)$$

During T''_{off-N}

$$i_{X-N} = 0 \qquad (2.18)$$

with

$$K_1 = \frac{i_{O-N} L_N}{V_{I-N} C_N} i_{A-N} + v_{A-N} \qquad (2.19)$$

and

$$K_2 = \frac{L_N}{2C_N V_{O-N}} i_{B-N}^2 - \frac{L_N i_{O-N}}{C_N V_{O-N}} i_{B-N} + v_{B-N} \qquad (2.20)$$

As in the case for the voltage step-up converter, the on-time trajectories for the current-or-voltage step-up converter are straight lines, while the off-time trajectories for reactor current greater than zero are parabolas. The range of i_{X-N} illustrated in Fig. 2.13 is greater than that in Figs.

2.12 and 2.8 because the two-segment steady-state trajectory for the current-or-voltage step-up converter operating under nominal conditions occurs at a higher average normalized current than the steady-state trajectories for the other two cases. This difference in current levels is particularly interesting in view of the fact that both the voltage step-up and the current-or-voltage step-up converter systems are operating under the same conditions and with approximately the same circuit component values. Further comparisons between these configurations are possible, but it is not a purpose of this dissertation to make a comparative study of converter power stages, and consequently detailed evaluations of them are not proposed. Examples of transient trajectories from arbitrary initial states to the desired steady-state trajectories for the current step-up and the current-or-voltage step-up converters and corresponding time waveforms are presented in Figs. 2.14 and 2.15 respectively.

2.4.3 Changes in System Operating Conditions and Parameters

As discussed and derived in preceding sections of this chapter, the shapes of converter system state trajectories are well defined and known functions of network parameters, such as the system inductance and capacitance, and of the externally imposed operating conditions such as the source voltage and the load current. Thus, a change in a system parameter or, more likely, a change in operating conditions, causes the shapes of these trajectories to change accordingly. For example, Fig. 2.16(A) illustrates how, starting from common initial states, the shapes of the off-time and on-time trajectories for the voltage step-up converter presented previously change when the converter output current increases from no load to full load. The initial state for the off-time trajectories,

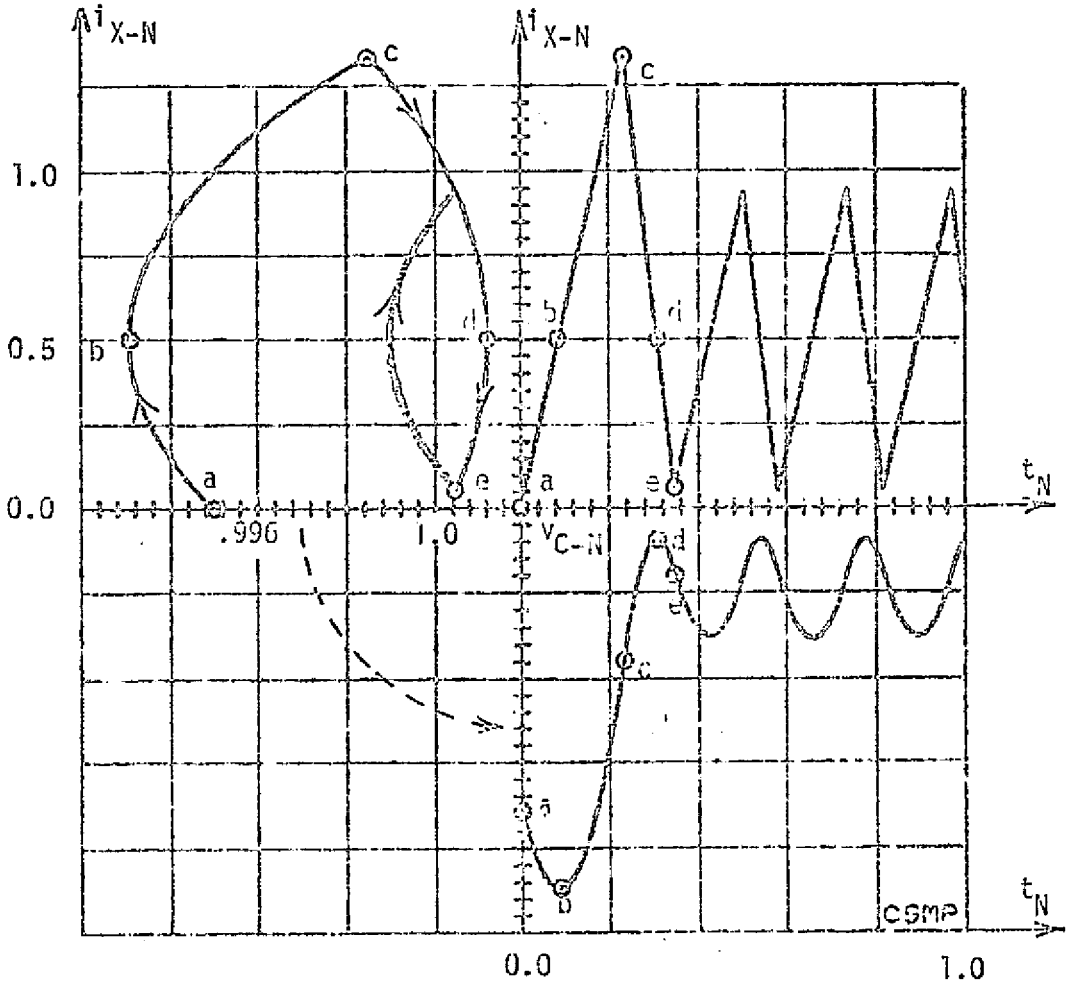

Fig. 2.14 Illustration of relationship between state-plane solution trajectory (upper left) and state-variable time waveshapes (right) for the current step-up converter. The solution trajectory is composed of segments from the two families of trajectories displayed in Fig. 2.12.

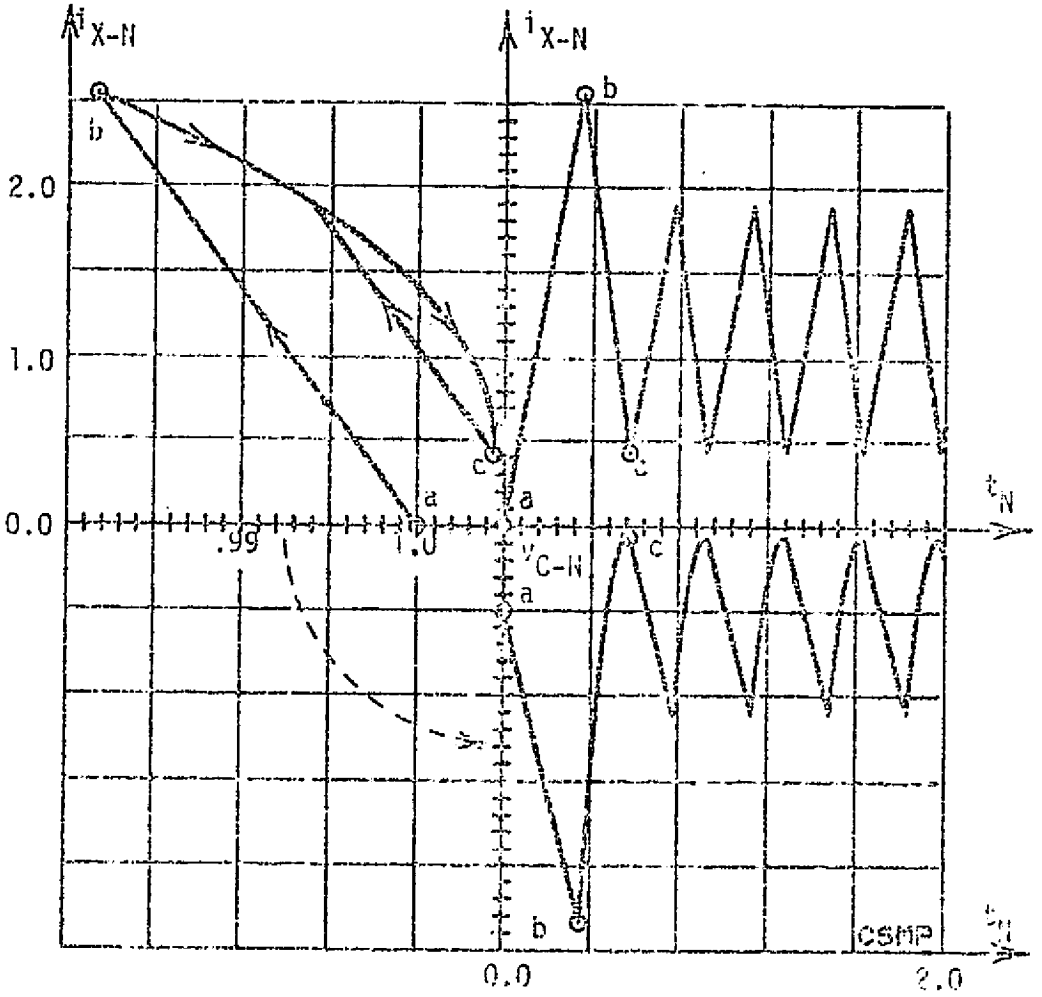

Fig. 2.15 Illustration of relationship between state-plane solution trajectory (upper left) and state-variable time wave-shapes (right) for the current-or-voltage step-up converter. The solution trajectory is composed of segments from the two families of trajectories displayed in Fig. 2.13.

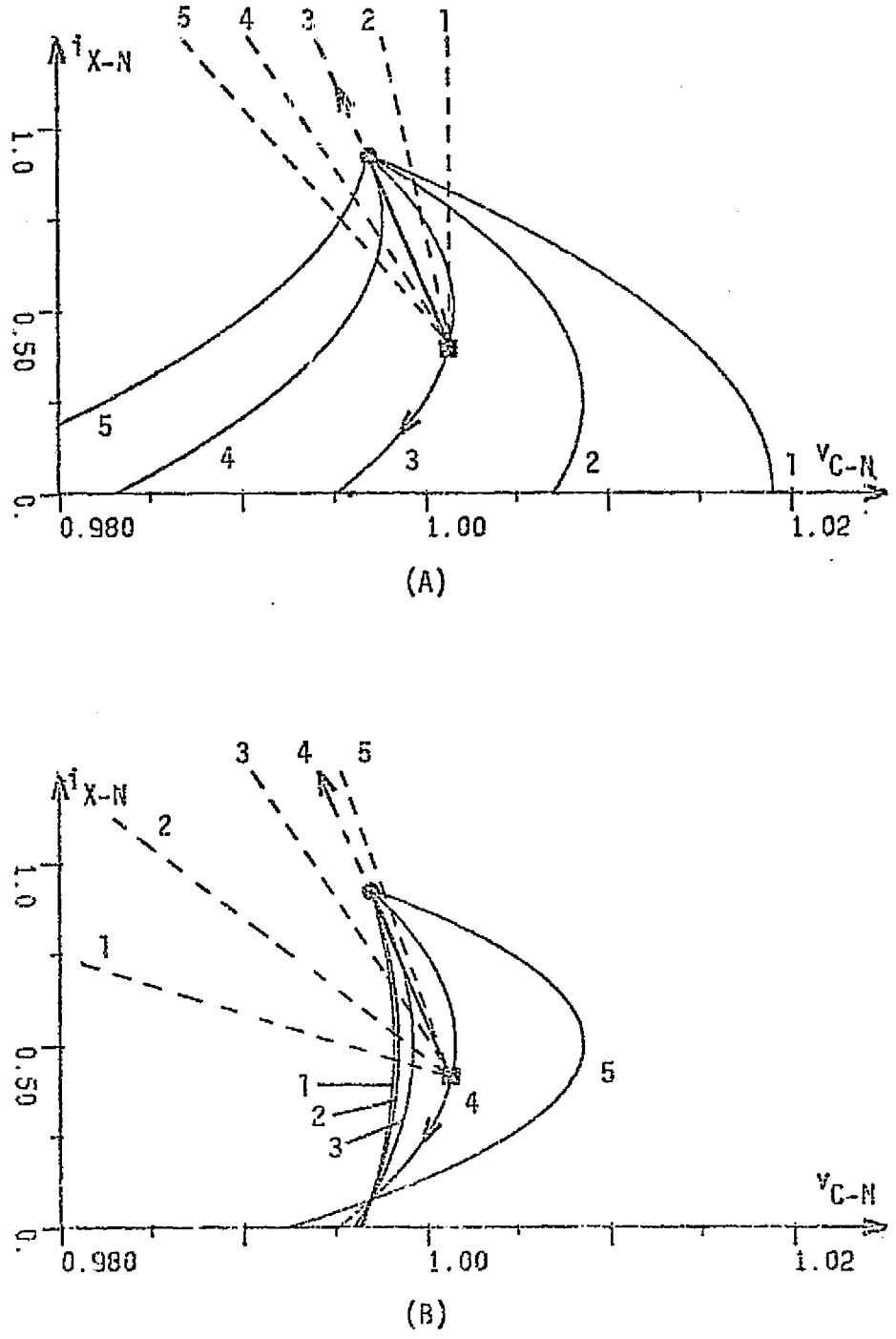

Fig. 2.16 Changes in shape of on-time trajectories (dashed lines) and off-time trajectories (solid lines) for the voltage step-up converter with
(A) v_{I-N} constant at 0.75 and i_{O-N} = 1) 0.0, 2) 0.25, 3) 0.5, 4) 0.75, and 5) 1.0.
(B) i_{O-N} constant at 0.5 and v_{I-N} = 1) 0.1, 2) 0.25, 3) 0.5, 4) 0.75, and 5) 0.9.

indicated by the dot in the figure, corresponds to the instant in the steady-state cycle of Fig. 2.8 when the power switch turns off. Likewise, the initial state for the five on-time trajectories, indicated by the square in the figure, is chosen as the switch-on instant in the same steady-state cycle. This reference steady-state solution trajectory can also be seen in Fig. 2.16(A) as the solid closed curve made up of segments corresponding to one half of the rated output current and indicated on the figure as load condition number three. Note that the range of the reactor current in this figure is 0 to 1 unit rather than 0 to 2 units as in Fig. 2.8 so that the steady-state trajectory appears enlongated in the vertical direction. A similar example of how the shapes of the trajectory segments change for various values of input voltage is presented in Fig. 2.16(B) where the same initial states are used, and the reference steady-state trajectory of Fig. 2.8 is again displayed as the closed curve consisting of segments corresponding to input-voltage condition number four.

In each of the examples of system state trajectories presented in this chapter, a closed two-segment steady-state trajectory for the given converter system and externally imposed operating conditions has been noted. These closed paths have been referred to as the *desired* steady-state trajectories implying that these, and only these trajectories satisfy all of the converter specifications. On examining the positions of these steady-state trajectories in the system state-plane, one can see that they are more or less centered about the voltage $v_{C-N} = 1.0$ and about some value of reactor current i_{X-N} which is commensurate with the output current required. A method for determining the exact location of the steady-state trajectory that satisfies a given converter specification is presented in Chapter IV. It is sufficient for the purposes of this chapter

to point out that the position and shape of the steady-state trajectory of a converter operating under a given set of externally imposed operating conditions change, as do the shapes of the on-time and off-time trajectories in general, when there is a change in the externally imposed operating conditions.

To illustrate this concept, consider the system of Fig. 2.1 operating in steady-state under the input voltage and output current conditions shown in Fig. 2.8. If the load current required suddenly changes from 50% to 10% of the rated value (due, perhaps, to the switching off of some experiment on an orbiting spacecraft system), the system state must suddenly follow the families of on-time and off-time trajectories corresponding to the new load condition, depicted in Fig. 2.17, rather than those shown in Fig. 2.8 as it had been doing. The steady-state trajectory corresponding to the original operating conditions has been superimposed on the new families of trajectories in Fig. 2.17. If the load switch occurs, for example, when the system state is at the point marked X, a possible transient trajectory which converges to the new equilibrium condition in three off/on cycles of control is shown as the bold sequence of connected off-time and on-time trajectory segments. Again the switching from off-time trajectories to on-time trajectories is determined by the system controller which is, in this case, purely fictitious. The new steady-state trajectory, consisting of a three-segment closed path, illustrates the discontinuous conduction mode of operation and centers about the desired average output voltage and a level of reactor current which enables the supply of the required output current at that voltage. As stated previously, the accomplishment of this desired steady-state trajectory is in reality a difficult task, and usually the precise steady-

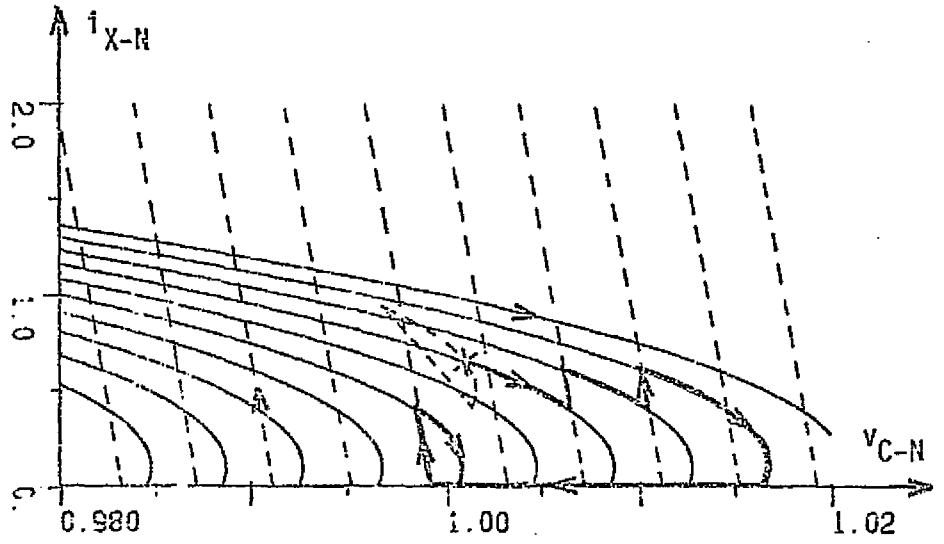

Fig. 2.17 Example of a transient trajectory (bold broken line) for the voltage step-up converter responding to a step-change in output current from i_{O-N} = 0.5 to 0.1.

state trajectory which yields exactly the desired average output voltage cannot be achieved for more than one set of externally imposed operating conditions. A more likely response of this system to a decrease in output current would result in an average output voltage which is higher than the desired value. Examples of such behavior are presented in Chapter III.

Similar changes in the shapes of the state trajectories for changes in output current and input voltage for the current step-up and the current-or-voltage step-up converters can be observed as illustrated in Figs. 2.18 and 2.19 respectively. Notice, however, that in these figures, the shapes of the off-time trajectories are independent of variations in the input voltage. This independence is apparent by the absence of v_{I-N} in equations (2.12) and (2.17) for the off-time trajectories of these converters, but it can also be explained by observing in Figs. 2.2 and 2.3 that the input voltage source is completely decoupled from the converter power stages during the time that the power switch is open, and consequently cannot influence the behavior of them during that time. Notice also that the range of i_{X-N} displayed in Fig. 2.19 is twice that displayed in Figs. 2.18 and 2.16. This is due, again, to the fact that higher current levels are observed in the current-or-voltage step-up configuration than in the voltage step-up or the current step-up converters for comparable power conversion tasks. Examples of transient trajectories for the current step-up and the current-or-voltage step-up configurations moving from one equilibrium condition to another due to a step change in load current and a step change in input voltage respectively are illustrated in Figs. 2.20 and 2.21. The controllers are again fictitious, and the final steady-state trajectories achieved are those which precisely meet the new system operating conditions.

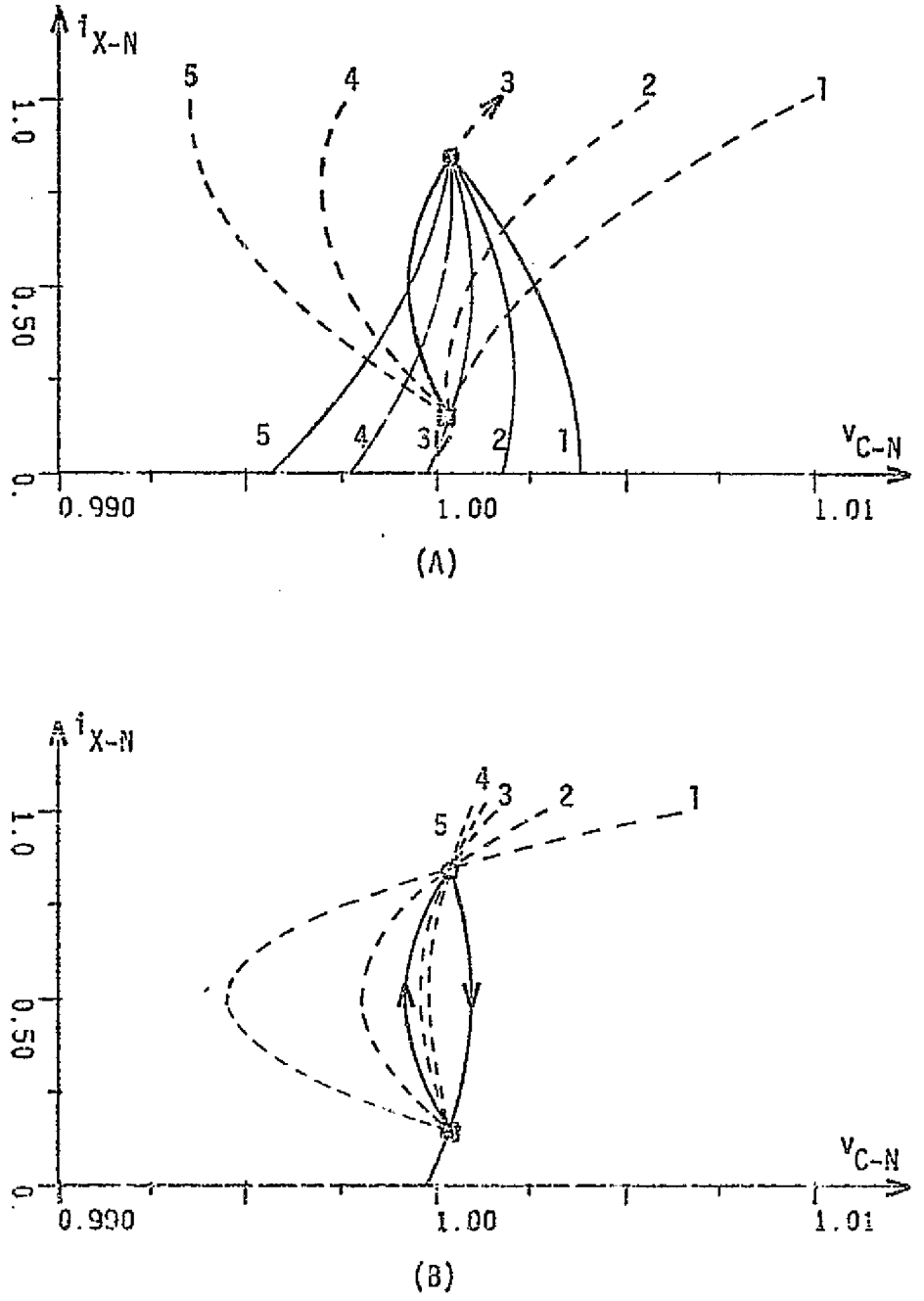

Fig. 2.18 Changes in shape of on-time trajectories (dashed lines) and off-time trajectories (solid lines) for the current step-up converter with
(A) v_{I-N} constant at 1.5 and i_{O-N} = 1) 0.0, 2) 0.25, 3) 0.5, 4) 0.75, and 5) 1.0.
(B) i_{O-N} constant at 0.5 and v_{I-N} = 1) 1.1, 2) 1.25, 3) 1.5, 4) 1.75, and 5) 2.0.

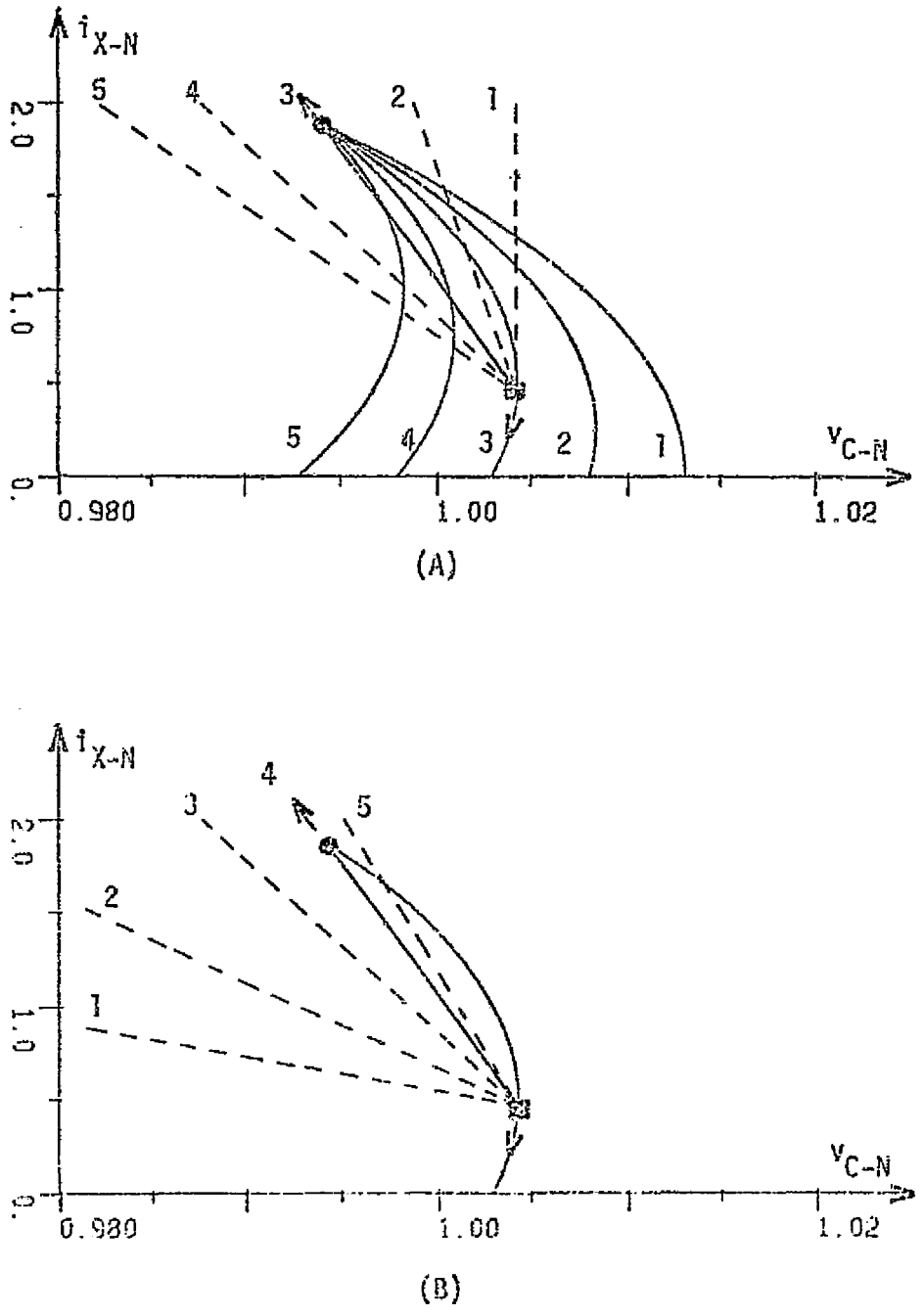

Fig. 2.19 Changes in shape of on-time trajectories (dashed lines) and off-time trajectories (solid lines) for the current-or-voltage step-up converter with
(A) v_{I-N} constant at 0.75 and i_{O-N} = 1) 0.0, 2) 0.25, 3) 0.5, 4) 0.75, and 5) 1.0.
(B) i_{O-N} constant at 0.5 and v_{I-N} = 1) 0.1, 2) 0.25, 3) 0.5, 4) 0.75, and 5) 0.9.

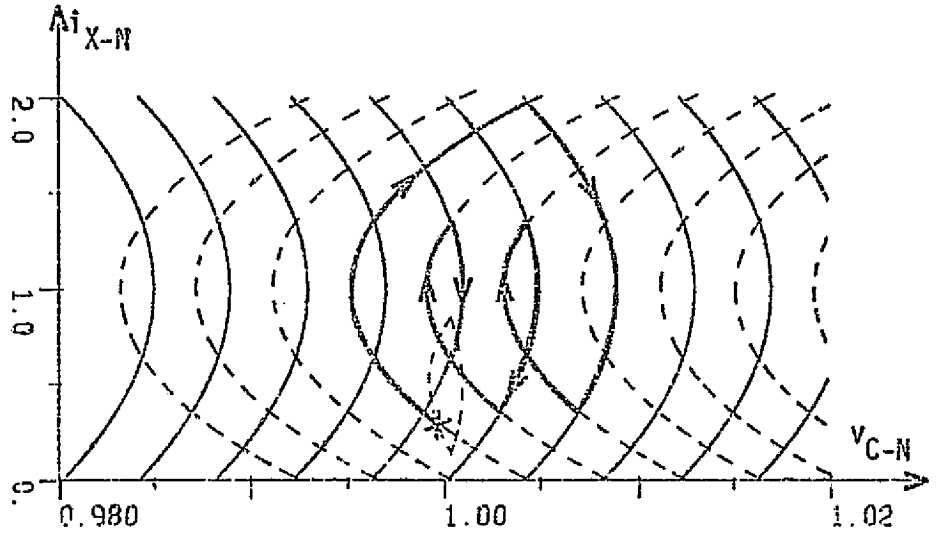

Fig. 2.20 Example of a transient trajectory (bold broken line) for the current step-up converter responding to a step change in output current from i_{O-N} = 0.5 to 1.0.

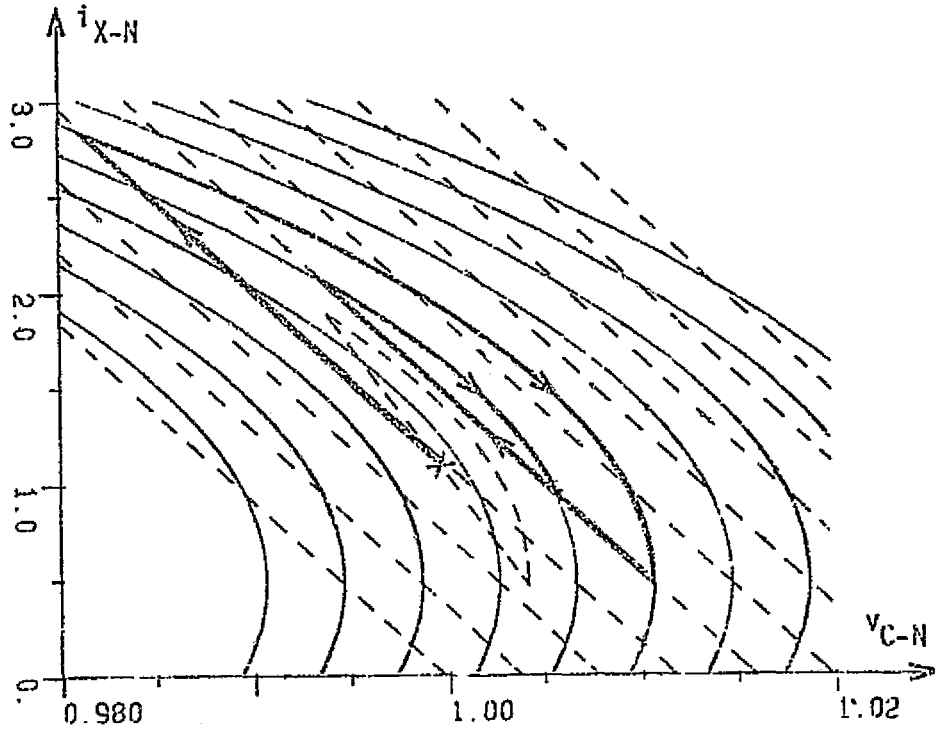

Fig. 2.21 Example of a transient trajectory (bold broken curve) for the current-or-voltage step-up converter responding to a step change in input voltage from v_{I-N} = 0.75 to 0.5.

As mentioned previously, the shapes of the system state trajectories, in addition to depending on the circuit operating conditions, are also dependent on the values of the system parameters. Of particular interest to converter designers in recent years has been the effect of changing the value of the energy-storage inductance. The value of inductance often is chosen to insure converter operation in either the continuous or the discontinuous conduction mode over a specified range of operating conditions. Fig. 2.22 presents the off-time trajectories and the on-time trajectories for three different values of inductance in voltage step-up converters which are otherwise identical and which are running under the same set of operating conditions. The trajectories labeled 2 correspond to the value of inductance which has been used as the reference value in previous illustrations. One can see the now familiar reference steady-state trajectory near the center of the figure. As one might expect, the steady-state trajectories which exist for the other two illustrative values of inductance are quite different. All three of these trajectories are shown in Fig. 2.23 for the same values of input supply voltage, average output voltage, and average load current. For large values of inductance, steady-state operation is in the continuous conduction mode, Figs. 2.23(A) and (B). With sufficiently small values of inductance the steady-state operation of the converter is in the discontinuous conduction mode as can be seen in Fig. 2.23(C) where the solution trajectory incorporates a portion of the axis of abscissas corresponding to zero reactor current during a portion of the power switch off-time. Thus, one can see that these three converters, which are identical except for the values of inductance, accomplish the same power processing task but in markedly different manners which are consistent with the requirements of

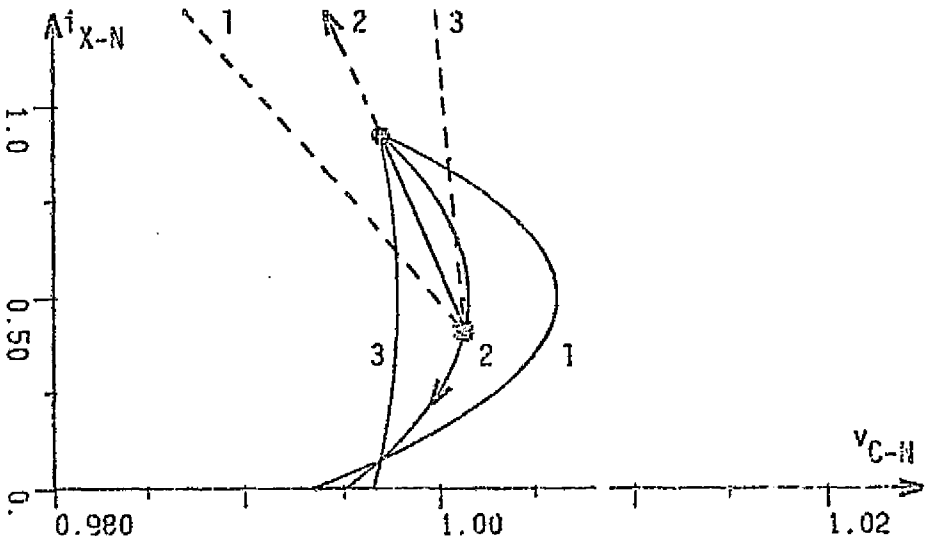

Fig. 2.22 Changes in shape of on-time trajectories (dashed lines) and off-time trajectories (solid lines) for the voltage step-up converter with $v_{I-N} = 0.75$, $i_{O-N} = 0.5$, and decreasing values of inductance L_N = 1) 0.1597, 2) 0.1136, and 3) 0.0505.

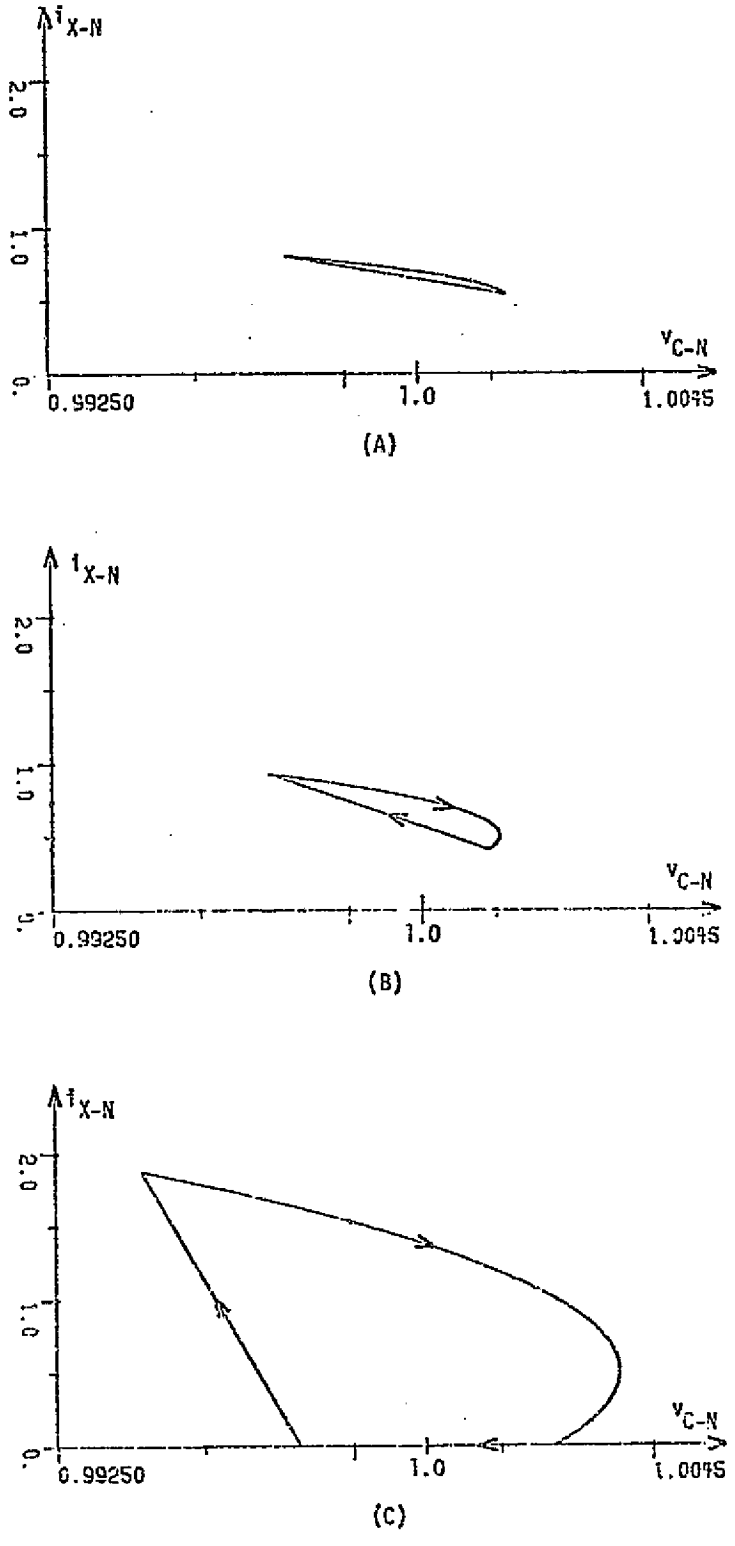

Fig. 2.23 Steady-state trajectories for the voltage step-up converter operating at v_{I-N} = 0.75, i_{O-N} = 0.5, and successively smaller values of inductance: (A) L_N = 0.1597, (B) L_N = 0.1136, and (C) L_N = 0.0505.

the individual shapes of their respective on-time and off-time trajectories.

Similar behavior is observed for the current step-up configuration as illustrated in Figs. 2.24 and 2.25 and for the current-or-voltage step-up configuration as illustrated in Figs. 2.26 and 2.27. Again there are observable aspects which are peculiar to each of the converter configurations presented, but the fundamental nature of each of them is quite similar, and information learned about one is usually helpful when studying the others.

2.5 Conclusions

The primary purpose of this chapter has been to demonstrate how the behavior of energy-storage dc-to-dc converters can be portrayed in the system state plane by means of families of trajectories which the converter state must follow during both transient and steady-state operation. The shapes of these trajectories are established by the physical laws which govern the operation of the systems, and mathematical representations of them can be derived in terms of the system component values and externally imposed operating conditions. The particular sequence of off-time and on-time trajectories which a system state follows in both steady-state and transient operation is determined by the action of the system controller and establishes the static and dynamic performance characteristics of the converter. A particular converter power stage operating in conjunction with a fixed set of operating conditions can exhibit the same steady-state trajectory when functioning under different control laws provided that the power switch duty cycle is the same for each and the controller can be adjusted to yield the same average output voltage. When the operating conditions change, however, the transient response of each system is

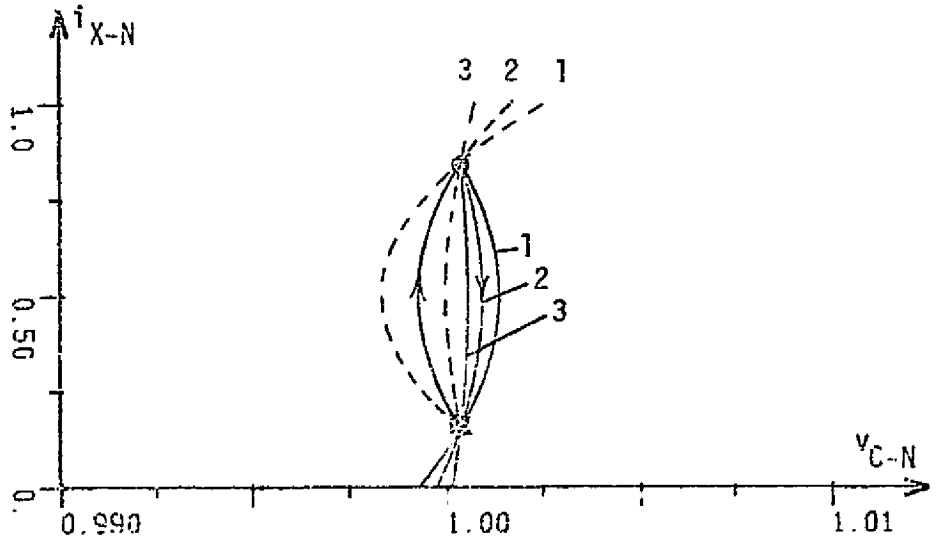

Fig. 2.24 Changes in shape of on-time trajectories (dashed lines) and off-time trajectories (solid lines) for the current step-up converter with v_{I-N} = 1.5, i_{Q-N} = 0.5, and decreasing values of inductance L_1 = 1) 0.1291, 2) 0.0978, and 3) 0.0577.

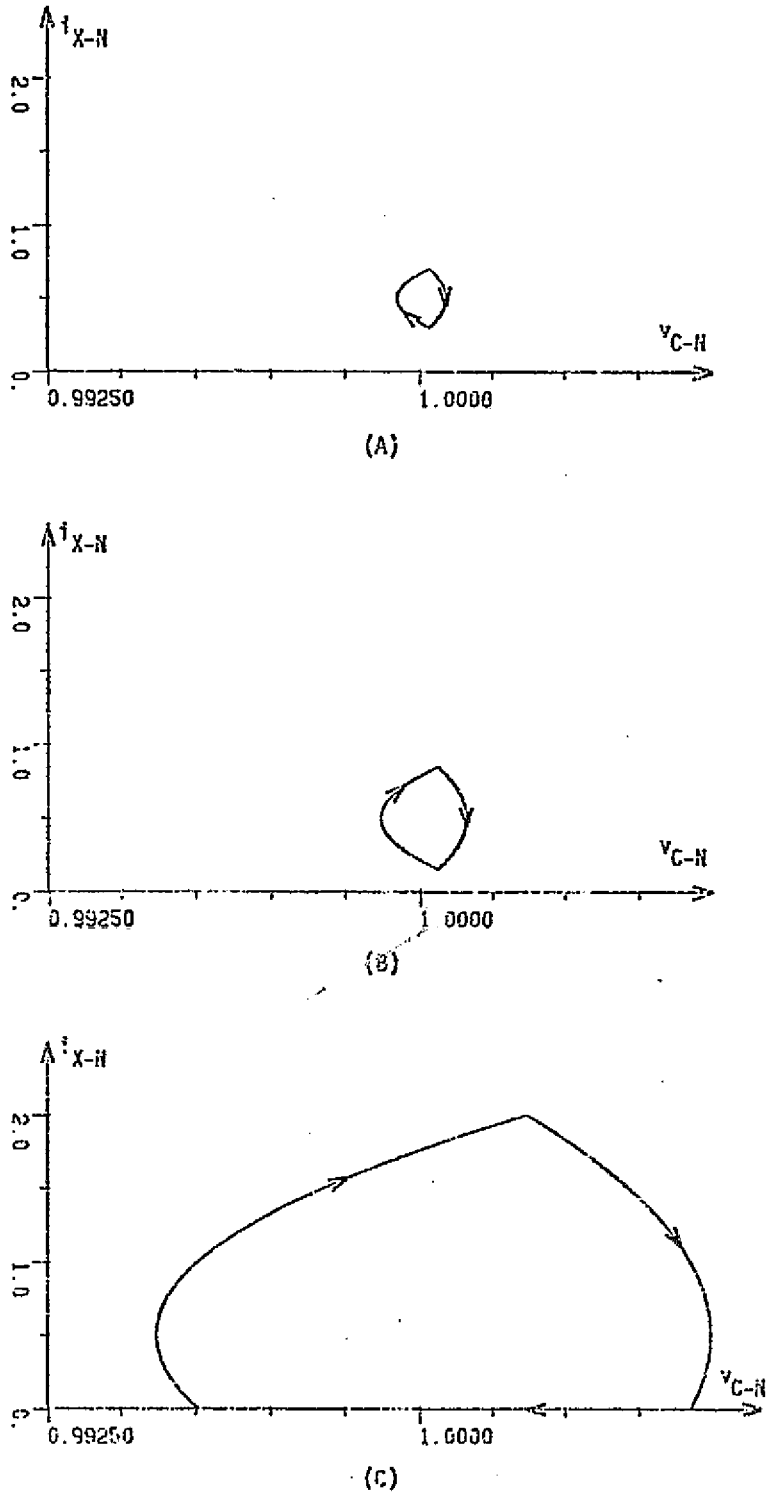

Fig. 2.25 Steady-state trajectories for the current step-up converter operating at $v_{I-J} = 1.5$, $i_{O-J} = 0.5$, and successively smaller values of inductance: (A) $L_J = 0.1291$, (B) $L_J = 0.0978$, and (C) $L_J = 0.0577$.

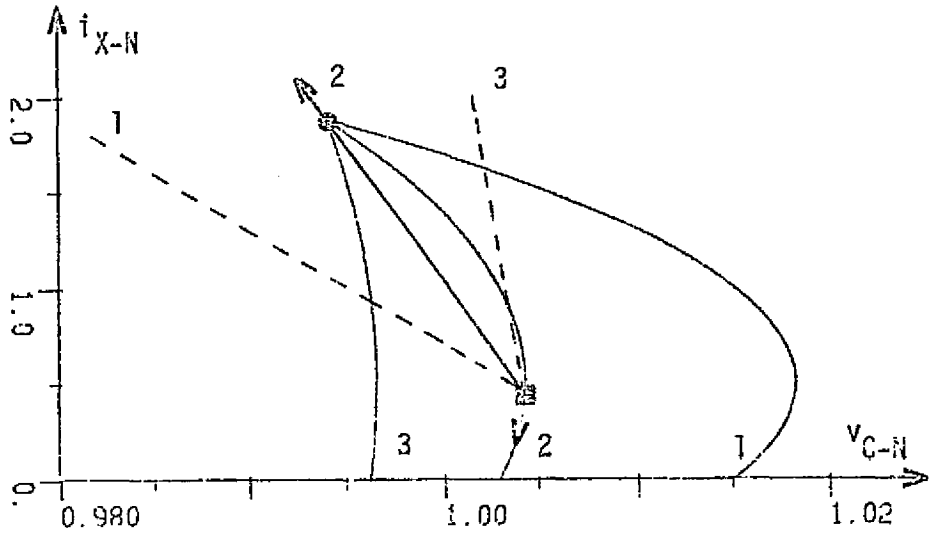

Fig. 2.26 Changes in shape of on-time trajectories (dashed lines) and off-time trajectories (solid lines) for the current-or-voltage step-up converter with $v_{I-N} = 0.75$, $i_{O-N} = 0.5$, and decreasing values of inductance L_N = 1) 0.1597, 2) 0.1038, and 3) 0.0595.

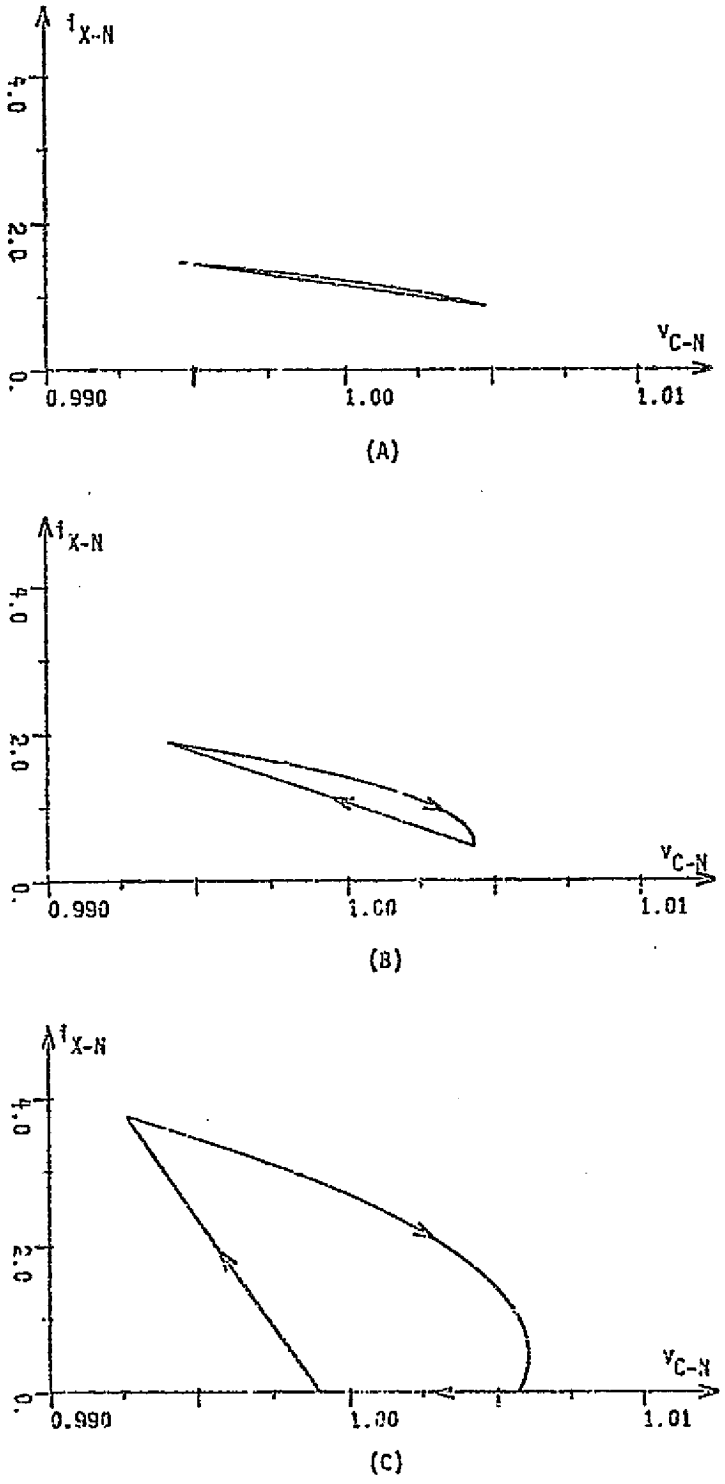

Fig. 2.27 Steady-state trajectories for the current-or- voltage step-up converter operating at v_{I-N} = 0.75, i_{O-N}= 0.5, and successively smaller values of inductance: (A) L_N = 0.1597, (B) L_N = 0.1038, and (C) L_N = 0.0505.

quite different as determined by the particular controller employed. The same families of off-time and on-time trajectories, as established by the converter power stage, must be followed in each case, but the particular switching instants and intervals, and consequently the complete transient trajectory, are determined by the controller employed and usually are quite different for each system.

An understanding of the system state trajectories and knowing how they change for changes in system parameters and externally imposed operating conditions reveal certain fundamental limitations in the performance of the converter power stage which cannot be exceeded no matter what control technique is employed. This ability to observe the movement of the system state enables one to examine and compare various control techniques which can be used to determine when to turn the converter power switch on and off, and to determine strengths and weaknesses in these techniques. The primary purpose of the remainder of this dissertation is to investigate this task of controlling energy-storage dc-to-dc converters and to present the derivation of a highly responsive control technique which is based on the findings of this chapter.

CHAPTER III

CONVERTER CONTROL FUNCTIONS PORTRAYED IN THE STATE PLANE

3.1 Introduction

As discussed in the preceding chapter, the specific trajectories which a converter state follows in both transient and steady-state operation are selected by the action of the converter control subsystem. The state-plane analysis approach developed in Chapter II enables a useful visualization of the manner in which various converter control functions accomplish this task of determining a switching sequence for the converter power stage. This visualization, in turn, enables a meaningful comparison and understanding of the strengths and weaknesses of these various control approaches. The purpose of this chapter is to illustrate, by example, how converter control functions can be portrayed in the system state plane, and to demonstrate how this portrayal can be used to reveal the cause and effect relationships which exist between the action of the control function and the converter power stage behavior which results from it.

After discussing the basic characteristics of converter controllers in general, several control techniques which are commonly used in converter applications are described and evaluated. Examples of converters operating under the influence of these control functions are presented in the form of digital computer simulations, and comparisons and discussions of the strengths and weaknesses of each of them are made. Although the

state-plane analysis approach described in Chapter II can be used to extensively analyze and predict the performance of these converter/controller systems, the presentation in this chapter is intended only to give the necessary background for an understanding of the development of the new control technique which is presented in Chapter IV.

3.2 Categories of Converter Controllers

One of the most important points discussed in Chapter II is the fact that the movement of the state of any dc-to-dc converter system is restricted to specific families of trajectories as established by the governing physical laws of the system. For second order systems, these trajectories can be represented by curves in a two-dimensional state plane as illustrated in Chapter II. For higher order systems, these trajectories become curves in an n-dimensional state space which are less easily visualized, but nonetheless represent completely the behavior of the system. In either case, however, the only means available for controlling the behavior of these systems is to switch the movement of the state from one type of trajectory to another. The criterion used by the system controller to determine when to make such a switch is the principal feature which distinguishes one control technique from another and which enables a particular controller to accomplish improvements in certain aspects of converter system performance while other techniques enable superior performance for some other aspects.

In recent years it has become apparent that each of the control techniques developed for dc-to-dc converters can be conveniently grouped into one of four classes based on a characteristic timing feature of the control function. These four classes of converter controllers are commonly

referred to as the "constant frequency," "constant on-time," "constant off-time," and "free running" types of controllers. These class distinctions are based on the manner in which one of the two controller switching decisions, turn-off or turn-on, is made. For example, a constant on-time controller turns the converter power switch off after it has been on for a pre-determined constant time interval, designated T_{on}, regardless of all other circuit conditions. Many different criteria can be used to determine the switch-on instant, but the switch is always opened after a specified on-time interval. Similarly, constant off-time controllers close the converter power switch after a specified off-time interval, T_{off}, without regard to the circuit conditions at that instant. With the on-time or the off-time switching interval fixed in this manner, the overall converter switching frequency often must vary as the system operating conditions vary; for as discussed previously and as described in Ref. [6], the converter power switch duty-cycle ratio, $T_{on}/(T_{on}+ T_{off})$, is a very important parameter in determining the general behavior of most converter systems, and particularly in determining the input to output voltage transformation ratio.

The third class of converter controllers listed above are characterized by a fixed switching interval, with a variable ratio of on-time to off-time within that interval to maintain the volatage regulation desired. Inherent in this type of controller are limitations on the maximum on-time and off-time periods which are possible per cycle of operation, because their sum, $T_{on} + T_{off}$, for each cycle must equal the total switching period T. Constant frequency controllers can be designed so that either the switch-off instant or the switch-on instant occurs at the beginning of the fixed interval, T, with the other switching instant occuring sometime

during the interval as determined by some other controller criterion. The final category of controllers listed above is the free-running class which involves no system timing constraints whatsoever and makes both the switch-on and the switch-off decision based on some untimed control function. These four converter control categories, summarized pictorially in Fig. 3.1, are discussed in considerable detail in Ref. [22]. Examples of particular constant on-time and constant frequency controllers, and digital computer simulations of the performance of converters operating in conjunction with them, are presented and discussed in the next two sections of this chapter.

3.3 Constant On-Time Controllers

Two examples of constant on-time, or pulse frequency modulation, controllers are presented in this section. The first example is a classical single-loop controller which senses the converter output voltage and makes its switch-on decision based on the magnitude of this voltage relative to a fixed reference value. The second example is a more recently developed two-loop control configuration which combines the converter output voltage with the voltage across the energy storage reactor, integrates this composite voltage, and compares the resultant signal to a fixed threshold level to determine the converter switch-on instant. A detailed description of the development of this latter control technique is presented in Ref. [23].

3.3.1 Conventional Single-Loop Controller

A conventional single-loop constant on-time controller is depicted conceptually in Fig. 3.2. The controller monitors the output voltage, v_{0-1},

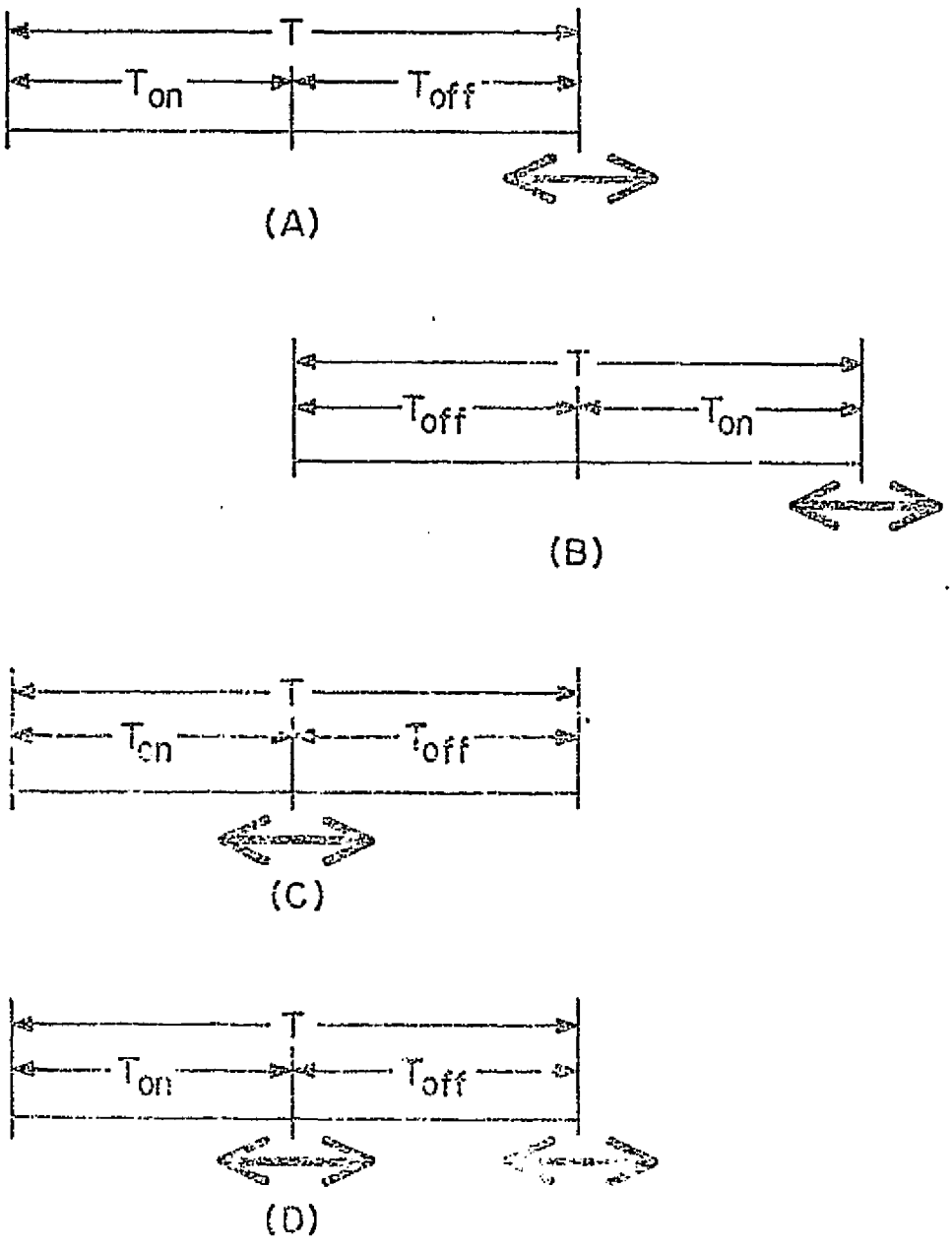

Fig. 3.1 Pictorial representation of (A) constant on-time, (B) constant off-time, (C) constant frequency, and (D) free-running types of converter controllers.

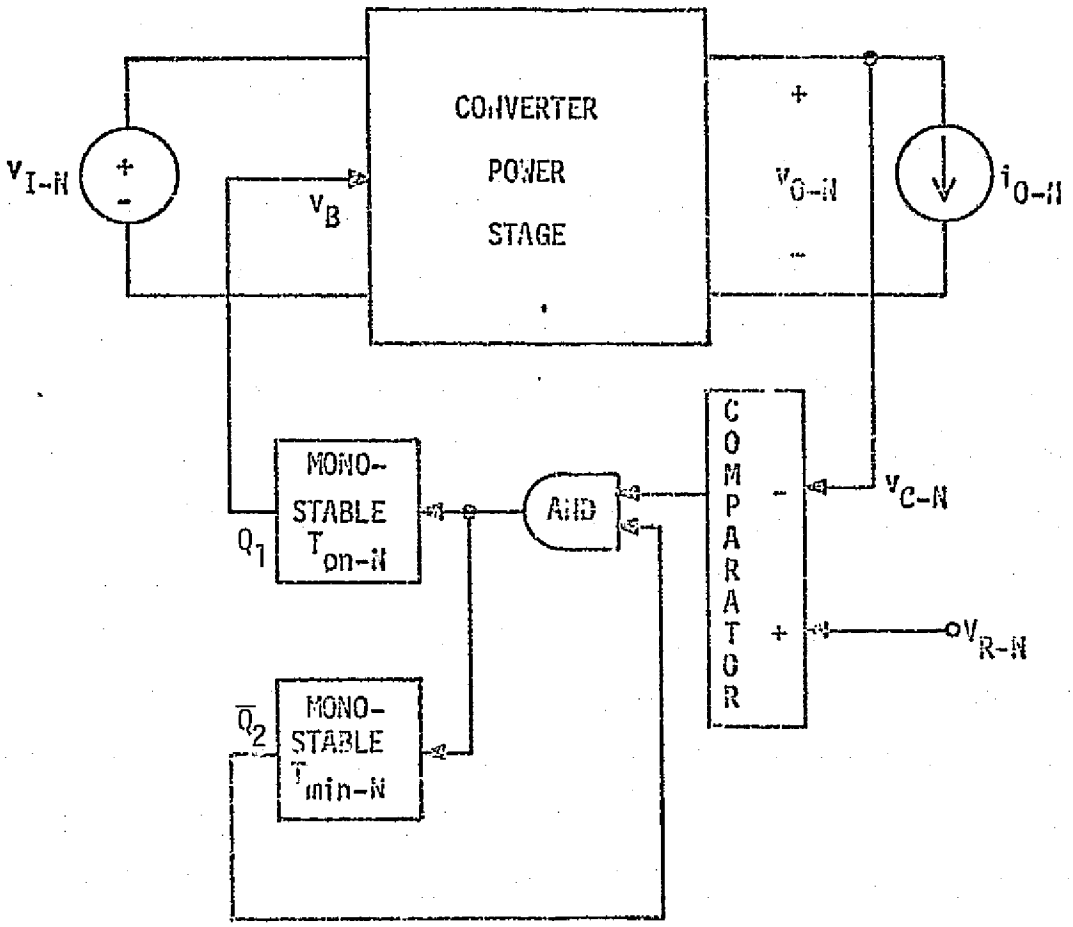

Fig. 3.2 Conceptual diagram of a single-loop constant on-time converter system.

of the converter power stage and compares it to a constant reference voltage, V_{R-N}. When the output voltage is less than the reference voltage, two monostable multivibrators are activated; one produces a pulse of width T_{on-N}, equal to the constant on-time specified, and the other produces a pulse of width equal to the on-time plus a specified minimum off-time which yields, in effect, a minimum switching period equal to T_{min-N}. The output of the upper monostable multivibrator turns the converter power switch on for the specified time interval, T_{on-N}, whereas the complementary output from the lower multivibrator gives a negative input to the AND gate. This insures that the upper multivibrator cannot be activated again until after waiting a minimum time, T_{min-N}, even if the output voltage never exceeds the reference. If after this minimum period the output voltage still does not exceed the reference level, the output of the AND gate goes positive and a turn-on signal is again issued. If the output voltage does rise above the reference level within the minimum off-time interval, however, the upper input to the AND gate is negative and the turn-on signal cannot be activated.

A minimum off-time interval is incorporated into this control process to allow the energy which is stored in the inductor during the power switch on-time intervals to be released to the load and the output capacitor, and thus enable the output voltage to rise. This feature is absolutely essential to the successful operation of the voltage step-up and the voltage-or-current step-up configurations which, as illustrated in Figs. 2.8 and 2.13 respectively, sustain decreasing output capacitor voltages during the switch on-time intervals so that the output voltage is always less than the reference level at the switch-off instant. This feature is also needed when any of the three converter power stages discussed in

Chapter II undergo start-up or are subjected to sudden increases in load current which cause the output voltage to fall considerably below the reference level. Under these conditions, the minimum switching period enables the output voltage to gradually build up to the reference level and accomplish the desired threshold turn-on mode of operation. In each cycle of normal steady-state operation, however, the converter output voltage does increase to a value which is greater than the reference level within the minimum specified off-time interval, and the power switch remains open until the output voltage falls back to cross the reference level. At that instant, the desired threshold turn-on signal is issued and a fixed on-time interval ensues. The minimum-period turn-on feature is incorporated in this control function only as a backup measure to help accommodate severe transient disturbances. If the operating conditions of the converter are such that it must depend on this feature for the power switch turn-on signal, unstable operation results as described and illustrated below.

This constant on-time control function can be portrayed in the system state plane as illustrated in Fig. 3.3(A) and (B), where in Fig. 3.3(B) the state variables are the reactor current, i_{X-N}, and the capacitor voltage, v_{C-N}, as they are in the plots in Chapter II, but in Fig. 3.3(A) the state variables have been chosen to be the reactor current and the output voltage, v_{O-N}. The output voltage has replaced v_{C-N} in Fig. 3.3(A) because it is the signal normally monitored in actual circuit implementations rather than the ideal capacitor voltage, and as can be seen by comparing Fig. 3.3(A), to Fig. 3.3(B), a somewhat different portrayal of the system behavior results. These figures present a family of off-time trajectories and a particular transient trajectory for the voltage step-up converter of Fig. 2.1 operating under the nominal conditons specified in Fig. 2.8.

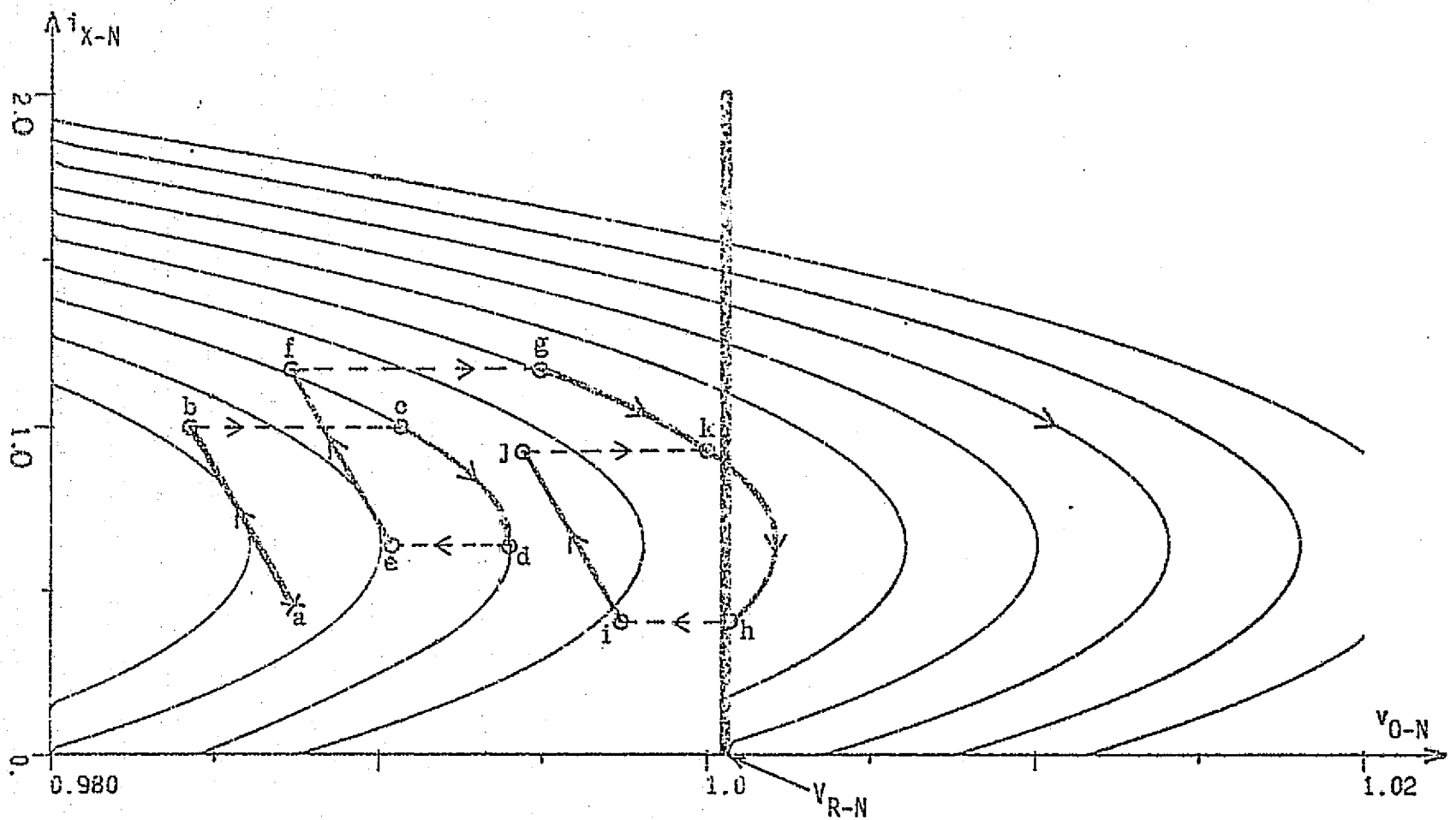

Fig. 3.3 (A) Illustrative transient trajectory plotted in the i_{X-N} vs. v_{O-N} plane for a voltage step-up converter operating in conjunction with the constant on-time controller of Fig. 3.2. The bold vertical line represents the reference level switching line.

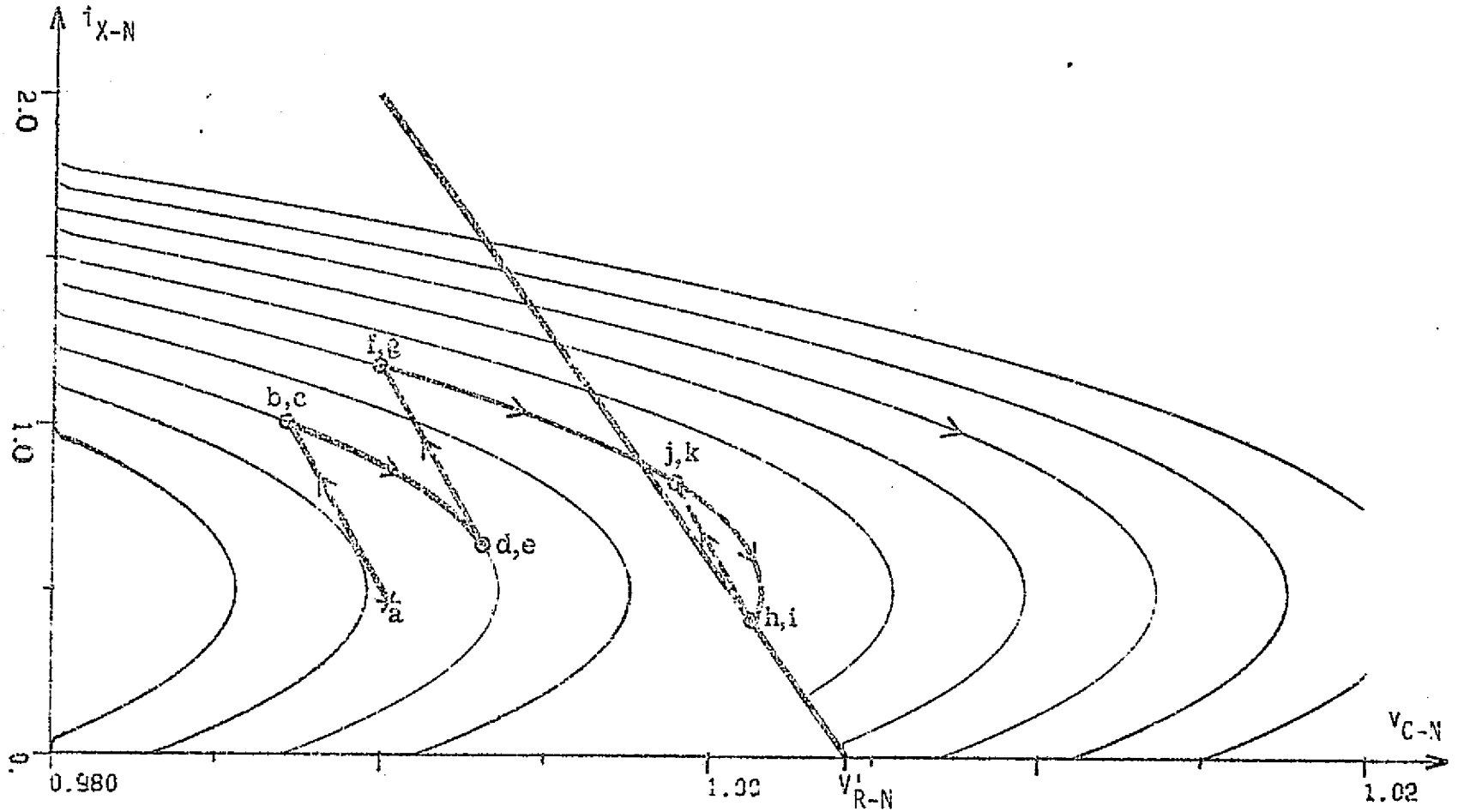

Fig. 3.3(B, Trajectories of Fig. 3.3(A) mapped into the i_{X-N} vs. v_{C-N} plane. The vertical switching line of Fig. 3.3(A) maps into the slanted switching line of Fig. 3.3(B).

The on-time and off-time trajectories in the i_{X-N} vs. v_{O-N} plane can be determined from the more familiar trajectories in the i_{X-N} vs. v_{C-N} plane from equations (3.1) and (3.2) respectively.

During T_{on-N},

$$v_{O-N} = v_{C-N} - i_{O-N} r_{C-N} \tag{3.1}$$

During T_{off-N},

$$v_{O-N} = v_{C-N} + (i_{X-N} - i_{O-N}) r_{C-N} \tag{3.2}$$

The transient trajectory displayed in these figures is purely fictitious and is intended only to illustrate the various features of the constant on-time control technique described above.

The broad vertical line displayed in Fig. 3.3(A) represents the reference voltage, V_{R-N}, which is used as a threshold value for the comparator of Fig. 3.2. For purposes of illustration, consider the state of the system to be initially at the point marked by an X and indicated by the letter *a*. This state is to the left of the vertical switching line and thus the system controller initially issues a turn-on signal and the state follows an on-time trajectory to point *b*. The length of this on-time trajectory is fixed by the specified time interval, T_{on-N}, as are all on-time trajectories for systems controlled in this manner. At the instant the power switch is turned off, the state of the system jumps horizontally from point *b* to point *c*. This jump, indicated by the dashed line in Fig. 3.3(A), is due to the sudden change in current which flows through the output capacitor ESR at the switching instant. The magnitude of this jump in output voltage is $i_{X-N} r_{C-N}$ as can be seen by subtracting equation (3.1) from (3.2). From point *c*, the system state follows an off-time trajectory to point *d*, which it reaches after the specified minimum off-time interval. This point is still in the switch-on region of the state plane, and thus the backup

minimum off-time criterion issues a switch-on signal. The particular off-time trajectory which the state follows from point c to point d illustrates the need for this minimum off-time switching criterion, for as can be seen, the system state can never cross the switching line while following this off-time trajectory because it peaks to the left of the line and thus never intersects it. Off-time trajectories such as these are the ones which the system state follows during converter startup or after severe changes in operating conditions.

At the instant the power switch turns on, the state of the system jumps horizontally from point d to point e, again because of the change of current through r_{C-N}. In this case, however, the output voltage instantaneously decreases by the magnitude $i_{X-N}r_{C-N}$. A constant on-time trajectory follows this jump with the final on-time state occuring at point f. At that instant the power switch again opens and the state of the system jumps horizontally to point g. From g the appropriate off-time trajectory is followed, and during this off-time interval, the state of the system crosses the vertical switching line before the minimum period switch-on signal is issued. Thus the next switch-on signal is not issued until the state falls back to cross the switching line at point h, at which time the desired reference level turn-on signal is issued. The power switch is closed at that instant and the system state jumps to point i and follows an on-time trajectory to point j. At that instant, the switch is opened and the state jumps to point k and again follows an off-time trajectory into the right-hand portion of the state plane within the minimum specified off-time interval. Thus, the system is seen to be in steady-state operation about the trajectory h-i-j-k.

The off-time trajectories which peak to the right of the vertical

switching line are the ones which the system state follows when the converter is operating in the desired reference level turn-on mode. All of these trajectories terminate at their lower intersection with the switching line, because at those points the power switch is closed and the state must begin to follow an on-time trajectory. The off-time trajectories which peak to the left of the switching line, on the other hand, never intersect the line and consequently the desired reference level turn-on signal cannot be achieved when the system state is following one of those trajectories. Thus, if a steady-state trajectory which meets the requirements of a given converter and specified operating conditions falls within a region of the state plane where the off-time trajectories do not peak, see for example Fig. 2.23(A), the converter cannot operate in the desired reference level turn-on mode and unstable operation results. An example of this unstable condition is presented later in this section.

The same off-time trajectories and transient trajectory which are illustrated in Fig. 3.3(A) have been mapped into the more familiar i_{X-N} vs. v_{C-N} plane in Fig. 3.3(B). Since the voltage across an ideal capacitor cannot change instantaneously, no horizontal jumps are observed in this plane, and the end points of the horizontal dashed lines in Fig. 3.3(A) map into one point in Fig. 3.3(B). The vertical switching line in Fig. 3.3(A) maps into a slanted line in Fig. 3.3(B) with slope $-1/r_{C-N}$ and with a v_{C-N} axis intercept defined by equation 3.3

$$V'_{R-N} = V_{R-N} + i_{O-N}r_{C-N} \tag{3.3}$$

where r_{C-N} is the value of the output capacitor ESR. If the capacitor ESR is neglected, the switch-on line becomes vertical, whereas larger values of

ESR cause the switching line to slant even more. Thus, one effect of the capacitor ESR on converter performance with this type of controller is made evident; i.e., more off-time trajectories can cross the system switching line when the output capacitor has a larger ESR, thus enabling this particular control technique to accommodate a wider range of operating conditions than it can with a smaller value of ESR.

From this brief discussion of the constant on-time control function portrayed in Figs. 3.2 and 3.3, several observations concerning the stability of such converter systems can be made. First, the minimum switching period, T_{min-N}, must be long enough to allow the converter state to move to the right of the reference switching line during steady-state operation over the entire range of specified operating conditions. Secondly, for those combinations of operating conditions which require that the system steady-state trajectory occur in a region of the state plane where the output voltage does not peak, unstable operation results. To avoid this unstable condition, the value of inductance, L_N, can be decreased until the desired steady-state trajectory does incorporate a peaking off-time trajectory for those conditions. This feature is illustrated in Fig. 2.23, where it is demonstrated that the same power processing task can be achieved with markedly different performance characteristics for different values of inductance. As can be seen in that figure, decreasing the value of inductance increases the output voltage ripple magnitude and increases the peak inductor current, but these conditions must be accepted in exchange for the stable operation desired.

A third observation on the stability of these systems concerns operation in the discontinuous conduction mode. As described previously, steady-state trajectories of systems in the discontinuous conduction mode

of operation always incorporate a peaking off-time trajectory segment and a portion of the v_{C-N} axis which is traversed during the time that the energy-storage reactor current is zero. Thus, whenever these systems are operating in the discontinuous conduction mode, the desired reference level turn-on signal is always issued at the same output voltage level, $v_{O-N} = V_{R-N}$, regardless of the system operating conditions. Consequently, the system on-time trajectories are always initiated at the state $v_{O-N} = V_{R-N}$, $i_{X-N} = 0$, and proceed for a fixed length as determined by the specified on-time interval, T_{on-N}. Thus, if the minimum off-time interval is specified properly so that the state of the system can move to the right of the switching line within that time interval, the desired reference level turn-on condition can always be achieved.

Some of the features described above are illustrated in the following two examples of this type of controller applied to a voltage step-up and a current-or-voltage step-up converter power stage.[3] Although the discussions presented above and the trajectories displayed in Fig. 3.3 are developed explicitly for the voltage step-up configuration only, the observations made can also be applied to the current-or-voltage step-up converter because the on-time and the off-time trajectories for each of these systems are of the same nature. The first example illustrates a stable transition from one operating condition to another, while the second example illustrates one of the unstable conditions described above.

Example 1. Consider the current-or-voltage step-up converter of Fig. 2.3 in steady-state operation at the nominal conditions of $v_{I-N} = 0.75$ and $i_{O-N} = 0.5$ as given in Fig. 2.13. If the output current is suddenly reduced from 50% to 10% of its rated value, the state of the system must

[3]The energy-storage inductors used in these examples and the other examples in this dissertation were designed using the procedure described in Ref. [9].

follow different families of on-time and off-time trajectories in attempting to reach a new steady-state trajectory which satisfies the new load condition. The response of this converter to such a disturbance when operating under the influence of the constant on-time controller described above is illustrated in Fig. 3.4. These data and the data for the other examples presented in this chapter were generated by means of a modified Continuous System Modeling Program (CSMP) with extended graphic display capabilities.[4]

The state trajectory of this system moving from the original equilibrium condition to steady-state operation for the new load condition is presented in Fig. 3.4(A). This figure again displays i_{X-N} vs. v_{C-N} rather than i_{X-N} vs. v_{O-N} because the horizontal jumps which occur in the i_{X-N} vs. v_{O-N} plane tend to clutter the figure and thus obscure the points of interest. The original steady-state trajectory is represented by the two-segment closed curve which occurs between the steady-state switch-off and switch-on points marked *a* and *b* respectively in the figure. This steady-state trajectory is the same as that displayed at the center of Fig. 2.13. The controller reference level, V_{R-N}, has been specified so as to yield a normalized steady-state average output voltage of 1.0 at these nominal operating conditions, and consequently the steady-state trajectory is centered about 1.0 on the v_{C-N} axis.

The load change arbitrarily occurs when the system state is at point *e* in Fig. 3.4(A). At that instant the state of the system must follow the new on-time trajectory which passes through that point for the remainder of the fixed on-time interval. At the end of this on-time interval, point *d* in Fig. 3.4(A), the power switch is opened and the off-time trajectory corresponding to the new load condition and passing through

[4]See note concerning this simulation program on page 80-A.

NOTE

The structure of this CSMP simulation program is such that the particular converter system being investigated is entered into the computer in terms of the system state equations. These state equations are integrated by means of a second order Runge-Kutta integration scheme to yield the time domain solution of the system. If the converters are modeled as piecewise linear systems, see for example Figs. 2.5-2.7, two sets of state equations must be programmed, one set for the power switch on-time interval and one set for the off-time interval. The converter control function, programmed in the same manner, determines whether the power switch should be on or off at each integration step and thus which set of equations should be integrated during each interval. Thus, a given converter power stage which is programmed in this manner can yield significantly different solution curves for different control functions as can be seen by comparing the examples presented in this chapter to the examples presented in Chapter IV.

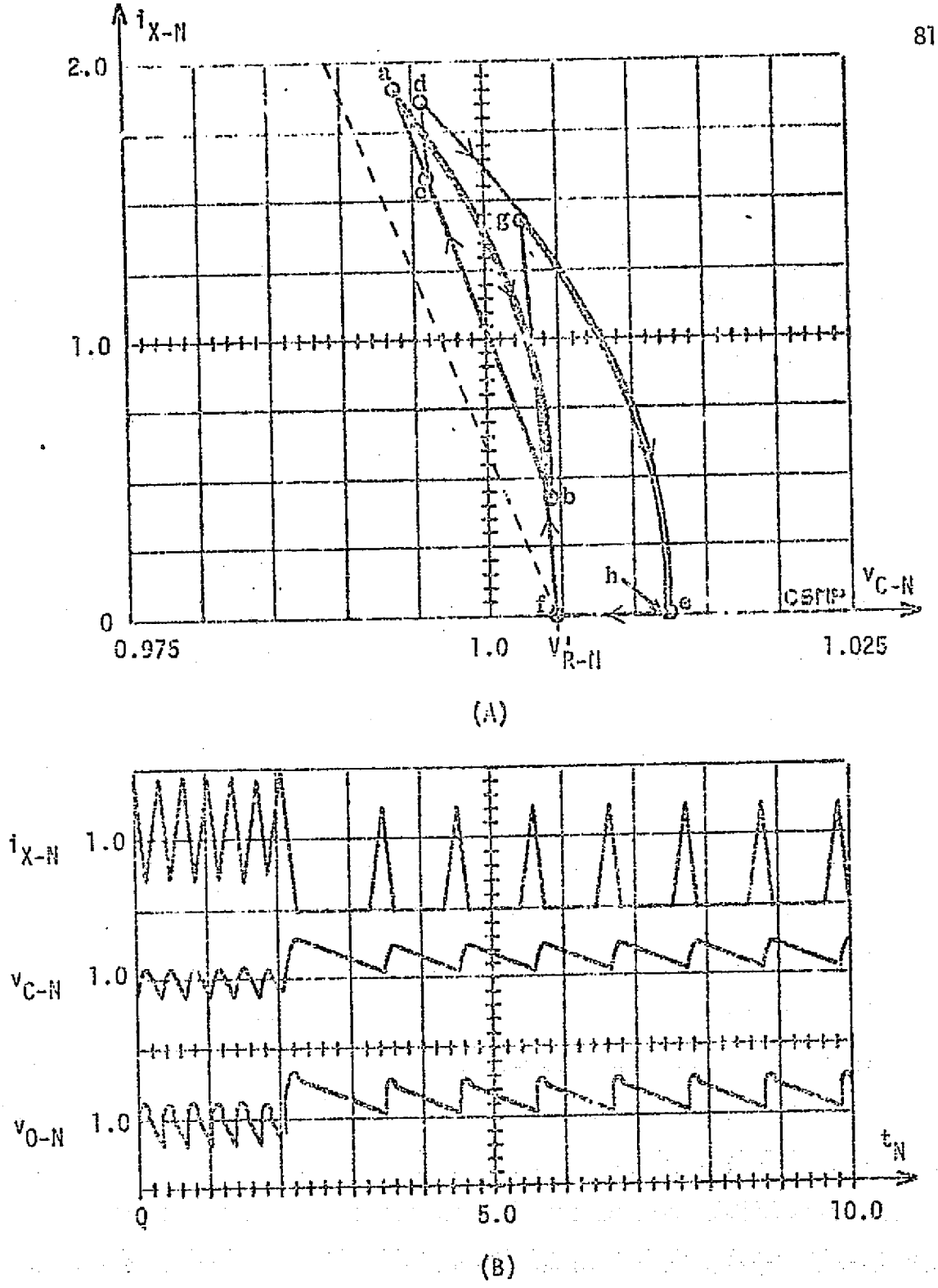

Fig. 3.4 CSMP generated response of current-or-voltage step-up converter of Fig. 2.3 operating with the constant on-time controller of Fig. 3.2 for a step decrease in V_{C-N} from 0.5 to 0.1. Controller parameters are V_{R-N} = 1.004, T_{on-N} = 0.2 and T_{min-N} = 0.3. Scale factors for the time waveforms are, in normalized units per major division: i_{X-N}, 1.0/div, v_{C-N}, 0.025/div; and v_{O-N}, 0.025/div.

point *d* is followed. Point *d* is to the right of the switching line, which is indicated by the slanted dashed line in this figure, and thus this off-time trajectory is followed until the reactor current falls to zero at point *e*. At that time, the state moves to the left along the v_{C-N} axis until the switching line is crossed at point *f*. On crossing this threshold, the converter power switch is closed for the fixed time interval, T_{on-N}, and the system is seen to be in steady-state operation in the discontinuous conduction mode as represented by the three segment closed curve *f-g-h*.

It should be noted that the switching line displayed in Fig.3.4(A) corresponds to the second load condition of $i_{O-N} = 0.1$ but not to the original condition of $i_{O-N} = 0.5$. The slope of this switching line is constant at, $-1/r_{C-N}$, for all operating conditions, but the v_{C-N} axis intercept, as given by equation (3.3), is a function of the output current and thus is not the same for both of the load conditions displayed in Fig. 3.4. The switching line corresponding to the original operating conditions is a straight line parallel to the dashed switching line shown in Fig. 3.4(A), but it passes through point *b* rather than point *f*. Thus, the decrease in load current is seen to shift the switching line to the left. It should also be noted that the magnitude of the slope of the on-time trajectories for this system operating under the lighter load condition is greater than the magnitude of the slope of the switching line. Thus, the state of the system is always to the right of the switching line when operating under this light load condition and consequently the minimum off-time switching criterion is not employed.

Plots of i_{X-N}, v_{C-N} and v_{O-N} vs.time for this same test case are displayed in Fig.3.4(B). The vertical jumps observed in the v_{O-N} vs.t_N waveform

are again the result of the instantaneous change of current which flows through the output capacitor ESR as a result of the converter power switch turning on or off. The magnitude of these jumps can be computed from a consideration of equations (3.1) and (3.2). Before the load change occurs at $t_N = 2.0$, v_{O-N} is seen to undergo a vertical jump at both the switch-off and the switch-on instants. After the load change occurs, however, the system operates in the discontinuous conduction mode, and the instantaneous jumps in v_{O-N} occur only at the switch-off instants because at the switch-on instants $i_{X-N} = 0$. As illustrated in this figure, the converter switching frequency at the lighter load condition is less than it is for the nominal conditions, but the power switch on-time interval remains constant for each cycle of operation.

This particular example illustrates two characteristic features of dc-to-dc converters which operate with this type of controller. First, constant on-time converters are able to respond very quickly to disturbances which require the release of energy from the converter power stage; i.e., to decreases in load current or changes in input voltage which bring v_{I-N} closer to the regulated output voltage, V_{O-N}. For either of these two types of disturbances, the system must release some of its stored energy in order to accomodate the lighter operating conditions, and this release of energy can only be accomplished by opening the converter power switch. This type of controller puts no limitation on the length of time that the switch can remain open and thus permits the release of as much energy as is needed to satisfy a change in operating conditions. Conversely, an increase in load current, or a change in input voltage such that the difference $|v_{I-N} - V_{O-N}|$ increases, requires additional energy storage within the converter power stage, but the converter switch

on-time is restricted to T_{on-N} and thus cannot respond as quickly to this type of disturbance.

A second feature of this type of system concerns the fixed threshold reference level V_{R-N}. As stated previously, the particular value of V_{R-N} used in this example has been chosen so that the normalized average output voltage of the converter when operating in steady state under nominal conditions is 1.0. For any other set of operating conditions, this fixed reference level is not the value which will yield an average output voltage of 1.0. This feature is illustrated in Fig. 3.4 where the average output voltage of the converter operating at the lighter load condition is seen to be greater than 1.0. For heavier load conditions, an average output voltage of less than 1.0 results. In order to be able to achieve the desired average output voltage for all possible operating conditions, the converter controller must employ a reference signal which adapts to changes in those conditions. Such an adaptable reference level is incorporated in the new control technique which is developed in Chapter IV.

Example 2. An example of the application of the single loop constant on-time controller to the voltage step-up converter of Fig. 2.1 operating under the nominal conditions of $v_{I-N} = 0.75$ and $i_{O-N} = 0.5$ is presented in Fig. 3.5. The steady-state trajectory which corresponds to these operating conditions can be seen in the i_{X-N} vs. v_{C-N} plane in Fig. 3.5(A) with the steady-state switch-off and switch-on points indicated by the letters *a* and *b* respectively. At $t_N = 2.0$, the output current is changed from 50% to 100% of its rated value, and the resultant system response, as can be seen in both the state plane and the time domain, leads to an unstable mode of operation.

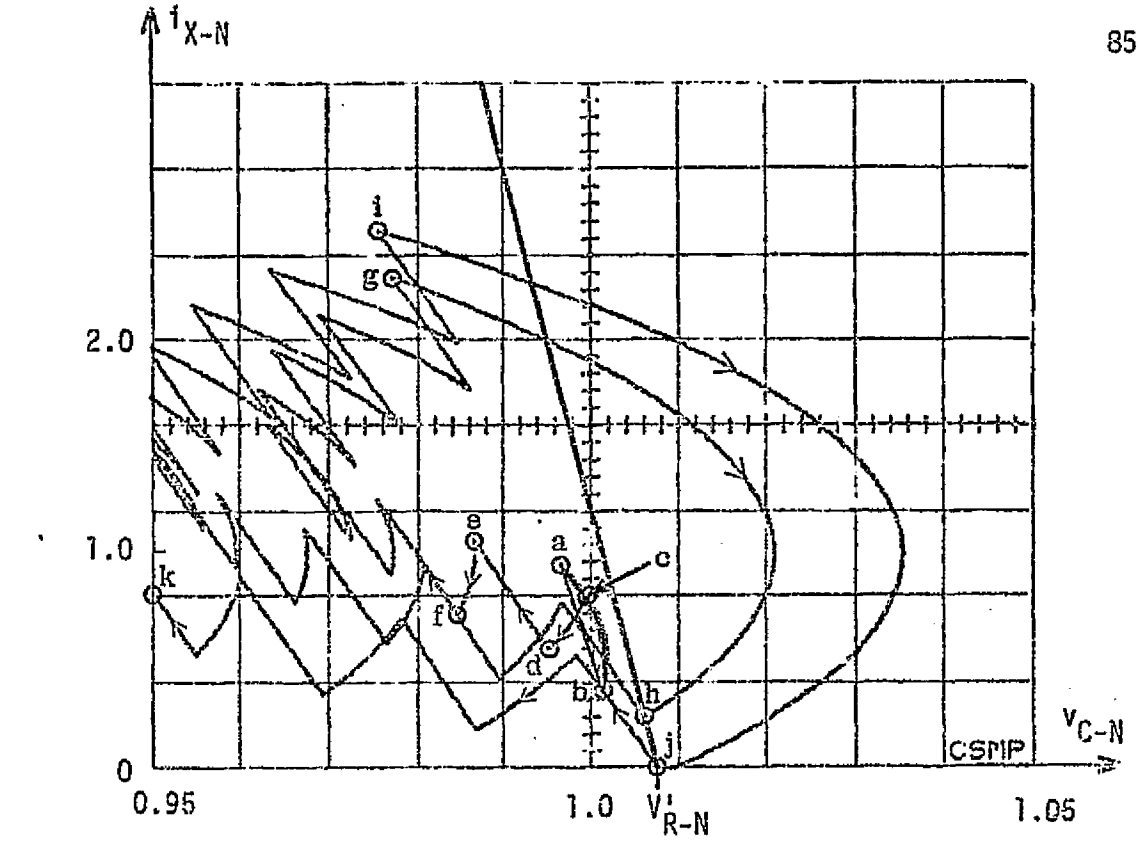

(A)

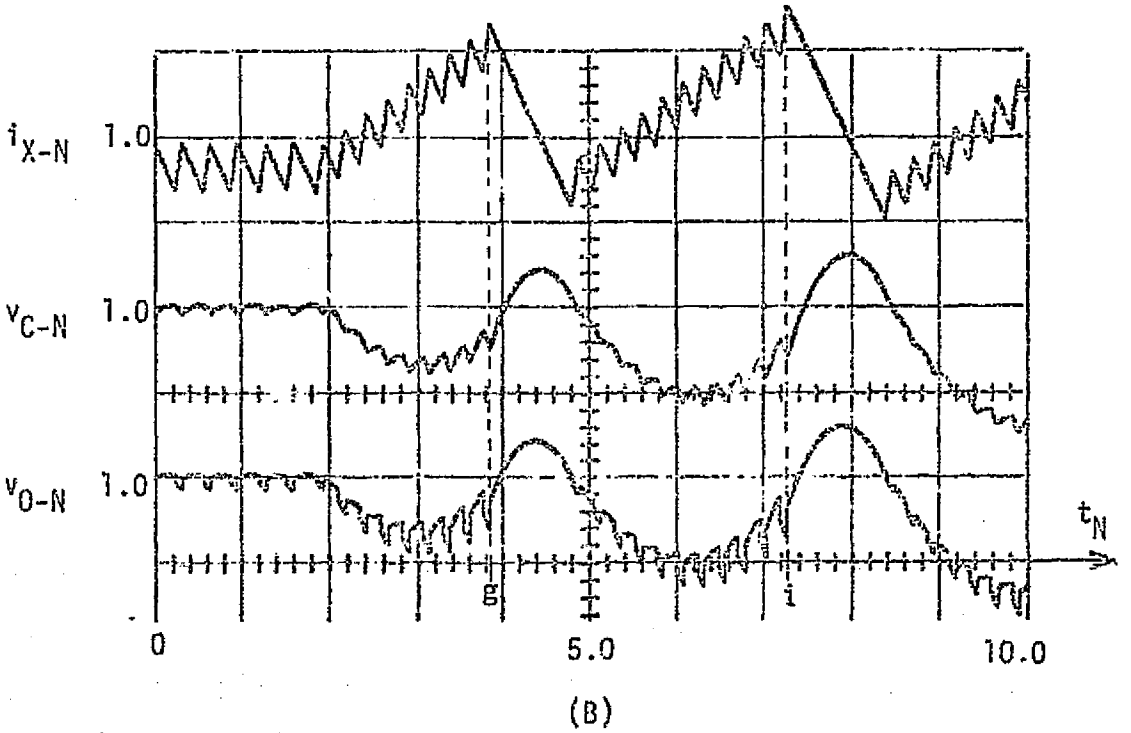

(B)

Fig. 3.5 CSMP generated response of voltage step-up converter of Fig. 2.1 operating with the constant on-time controller of Fig. 3.2 for a step increase in i_{O-N} from 0.5 to 1.0. Controller parameters are V_{R-N} = 1.0007, T_{on-N} = 0.08 and T_{min-N} = 0.24. Scale factors for the time waveforms are, in normalized units per major division: i_{X-N}, 1.0/div; v_{C-N}, 0.05/div; and v_{O-N}, 0.05/div.

At the instant of the load switch, the state of the system is at point c as indicated in Fig. 3.5(A). At that same instant, the system switching line shifts to the right to accomodate the higher load current, as indicated in equation (3.3), and the system state is suddenly to the left of the switching line. The state of the system, located on the original steady-state off-time trajectory at the load-change instant, begins to follow an off-time trajectory which corresponds to the new load condition, and it continues to follow this particular trajectory until the end of the specified minimum off-time interval, which began even before the load change occurred. After this minimum off-time interval, the state of the system is at point *d* and the backup minimum period switch-on signal is issued. After a fixed on-time interval, the state is at point *e* and begins to follow the off-time trajectory which passes through that point. After another minimum off-time interval, the converter state is at point *f* and the power switch is again closed for the fixed on-time interval, T_{on-N}. As can be seen in Fig. 3.5, this backup switch-on criterion issues the converter turn-on signal for the first eight cycles of the system's transient response, because during each of these cycles, the state of the system cannot move to the right of the system switching line within the specified minimum off-time period. After the eighth on-time interval, however, the reactor current has increased to a value large enough to enable the state of the system to move to the right of the switching line before the backup turn-on signal is issued. The state of the system at this switch-off instant is indicated by point *g* in Fig. 3.5(A). At this state, however, the reactor current is much larger than that which is needed to meet the output conditions, and thus a relatively long power switch off-time interval ensues while the system state follows

an off-time trajectory from point g around to the reference level switch-on line at point h. At that point, the reactor current is again too low to accomodate the 100% load condition, and the fixed on-time/minimum off-time switching syndrome again is observed until the state of the system is able to move to the right of the switch-on line within the specified minimum off-time period. A second crossing of the switching line occurs when the converter power switch opens at point j in Fig. 3.5(A). This behavioral pattern continues indefinitely, and the unstable subswitching-frequency mode of operation illustrated in Fig. 3.5 results. This response is an example of the unstable operation which results when the region of the state plane around the desired average output voltage and the required average reactor current does not contain peaking off-time trajectories.

3.3.2 Two-Loop Controller

A second example of a constant on-time control technique as it is applied to a current step-up converter power stage is illustrated in Fig. 3.6. This system, commonly referred to as a two-loop controlled converter, is described and analyzed in considerable detail in Ref. [15] and is presented here only as an illustrative example of an advanced dc-to-dc converter control technique. The system has been normalized as described in Chapter II so that the data presented in the following two examples are consistent with the other data presented in this dissertation. The unnormalized component values, as presented in Ref. [15], and their normalized counterparts are presented in Table 3.1.

The principal difference between this two-loop control technique and the single loop approach presented in the preceding section is found

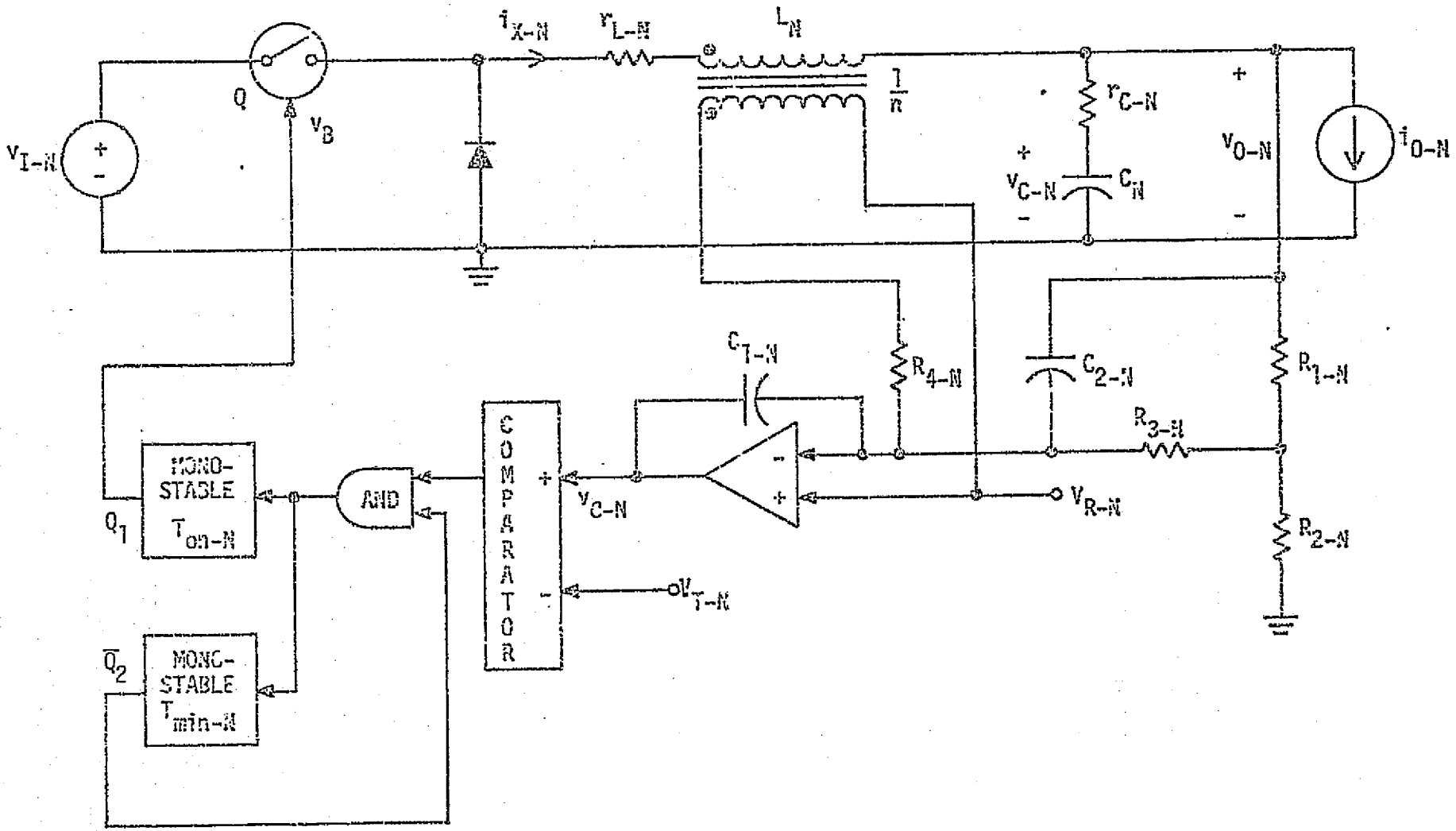

Fig. 3.6 A two-loop constant on-time current step-up converter system. System component values and parameters are given in Table 3.1.

Table 3.1

System Component Values and Parameters for the Two-Loop Constant on-Time Current Step-Up Converter System of Fig. 3.6

Component or Parameter	Actual Value	Normalized Value
$V_{I,nominal}$	30.0 V	1.5
$i_{O,nominal}$	2.0 A	1.0
V_R	6.4 V	0.32
V_T	8.0 V	0.4
L	0.25 mH	0.09
C	300 μF	10.9
r_L	0.015 Ω	0.0015
r_C	0.077 Ω	0.0077
R_1	28.7 KΩ	2870.
R_2	13.5 KΩ	1350.
R_3	10 KΩ	1000.
R_4	100 KΩ	10000.
C_1	.0022 μF	.00008
C_2	.022 μF	.0008
n	0.65	0.65
T_{on}	20 μsec	0.07
T_{min}	25 μsec	0.09

in the manner in which the analog control signal, v_{C-N}, is formed.[5] For the controller depicted in Fig. 3.2, v_{C-N} is simply equal to the converter output voltage. For the controller depicted in Fig. 3.6, this signal is formed by integrating a combination of the converter output voltage and the voltage across the energy-storage inductor, L_N. Whenever this analog control signal exceeds the specified threshold level, V_{T-N}, a fixed power switch on-time interval is initiated. If after this fixed on-time interval, v_{C-N} is less than V_{T-N}, the power switch opens and remains open until v_{C-N} again exceeds V_{T-N}. If, however, v_{C-N} has not fallen below V_{T-N} after the fixed on-time interval, the power switch remains open for a specified minimum off-time interval, after which another fixed on-time interval is initiated. Thus, this controller employs the same type of fixed on-time/minimum off-time switching criterion as is used in the previous example. It should be noted, however, that the positive input to the comparator in this example is the analog control signal, v_{C-N}, rather than the fixed threshold level as it is in the previous example. This difference is due to the nature of the analog control signal for each system.

As mentioned previously, a detailed analysis of this system is presented in Ref. [15] and is not repeated here. The system model and mathematical representation presented in Ref. [15] have been used in this work to generate the computer simulated responses presented as Examples 3 and 4 below. Because of the presence of energy storage elements in the control subsystem, this converter is not a second order system, and thus its behavior cannot be completely represented in a two dimensional plane as has been the case for Examples 1 and 2 above. However, the movement of the state of the converter power stage is still restricted to specific

[5]Note the distinction between v_{C-N}, *control* voltage, and v_{C-N}, *capacitor* voltage.

families of off-time and on-time trajectories in the i_{X-N} vs. v_{C-N} plane regardless of the order of the control subsystem. Thus, the response of the converter power stage still can be observed by means of trajectories in the i_{X-N} vs. v_{C-N} plane although the complete state of the system, and consequently the system switching criterion, is not represented in these trajectories. Examples of trajectories in the i_{X-N} vs. v_{C-N} plane and corresponding time waveforms for the system of Fig. 3.6 are presented below.

Example 3. The response of the constant on-time current step-up converter system of Fig. 3.6 to a step change in load current from 100% to 50% of its rated value is illustrated in Fig. 3.7. The load switch occurs at $t_N = 0.8$ during a power switch on-time interval, and thus the system state initially follows an on-time trajectory which corresponds to the new load condition, point *a* to point *b* in Fig. 3.7(A). Within three switching cycles, the state of the system has reached the general vicinity of the new steady-state trajectory, but convergence to a final closed trajectory is very slow and the new equilibrium condition has still not been achieved after 30 cycles of operation as can be seen in Fig. 3.7(B). As observed previously in Example 1, the average output voltage for this system operating at the lighter load condition is greater than it is for the heavier load. This steady-state error in the average output voltage is again due to the fact that although the analog control signal, v_{C-N}, is a carefully formed combination of pertinent system variables, the power switch turn-on signal is still issued when this analog signal intersects a predetermined fixed threshold level which does not change as the operating conditions change.

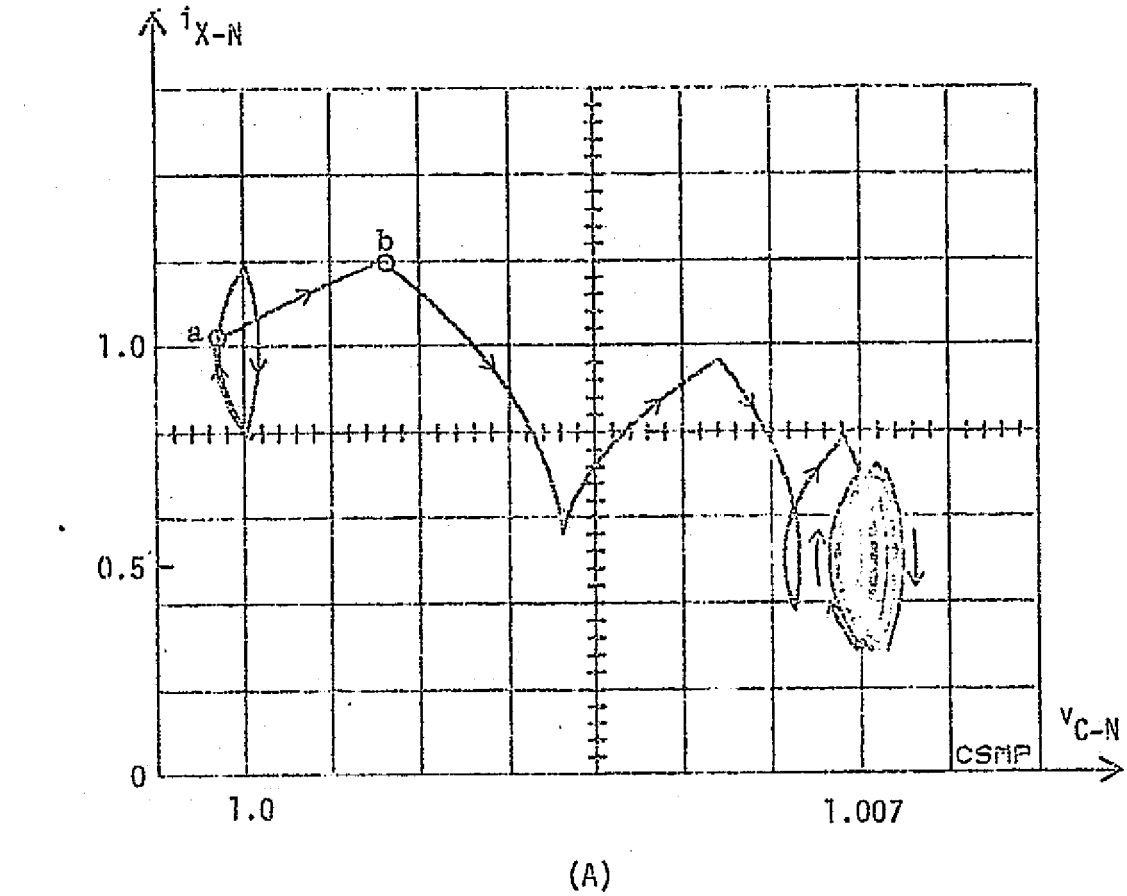

(A)

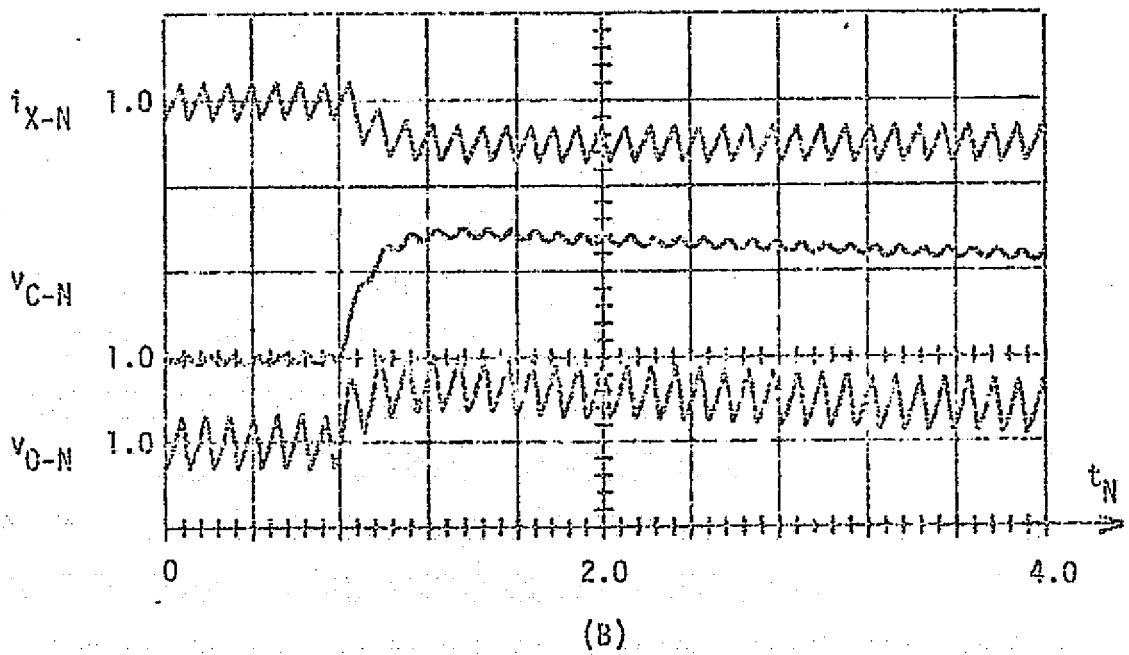

(B)

Fig. 3.7 CSMP generated response of converter system of Fig. 3.6 for a step decrease in i_{O-N} from 1.0 to 0.5. Scale factors for the time waveforms are, in normalized units per major division: i_{X-N}, 1.0/div; v_{C-N}, 0.005/div; and v_{O-N}, 0.005/div.

Example 4. A second example of the behavior of this converter/controller system is presented in Fig. 3.8. During the first seven cycles displayed in this figure, the system is in steady-state operation with an input voltage equal to 1.5 times the rated average output voltage, and an output current equal to 100% of its rated value. The steady-state trajectory under these conditions is seen in Fig. 3.8(A) between points *a* and *b*. At $t_N = 0.8$, point *c* in Fig. 3.8(A), the input voltage changes to twice the rated average output voltage, and the shapes of the system on-time trajectories change accordingly. In this example, after only two cycles of transient operation, the system state has reached the vicinity of the new steady-state trajectory, but again convergence to the final equilibrium condition is slow. Only six cycles of the transient response are displayed in Fig. 3.8(A) because the trajectories begin to overlap for displays of longer duration, which tends to obscure the visualization of the system behavior.

3.4 Constant Frequency Controller

One of the most popular approaches to the control of energy-storage dc-to-dc converters is the constant frequency, or pulse width modulation, approach. Many different techniques have been devised for implementing this type of control function, and it has been used extensively with all types of converter power stages and for all types of applications. One very commonly used embodiment of this approach is the constant frequency coincidence detector controller illustrated conceptually in Fig. 3.9. In this configuration, the converter output voltage is subtracted from a fixed reference voltage, V_{R-N}, and the difference, v_{E-N}, is amplified by a factor -A. The resultant analog control signal, v_{C-N}, is compared to

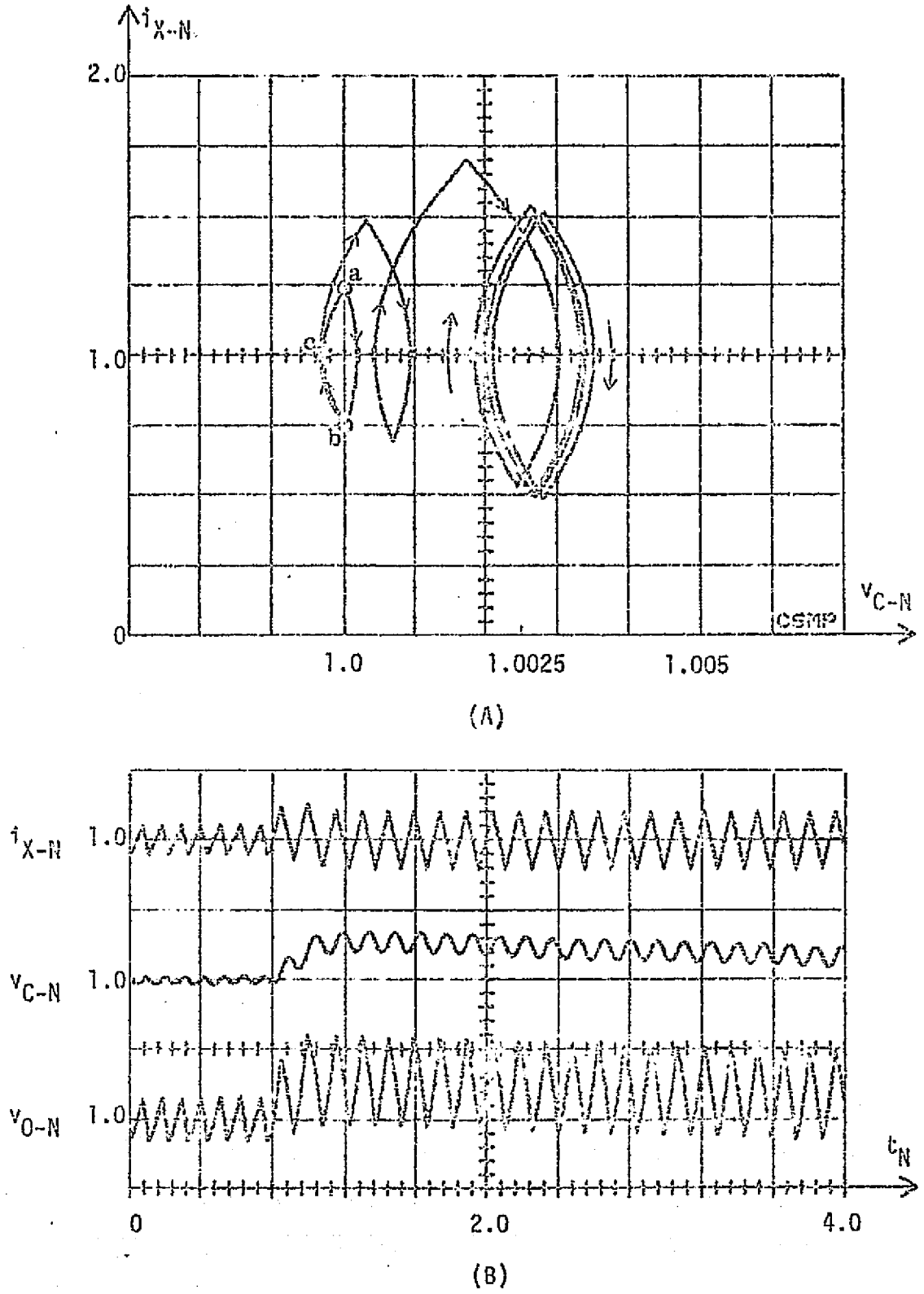

Fig. 3.8 CSMP generated response of system of Fig. 3.6 for a step increase in v_{I-N} from 1.5 to 2.0. Scale factors for the time waveforms are, in normalized units per major division: i_{X-N}, 1.0/div; v_{C-N}, 0.005/div; and v_{O-N}, 0.005/div.

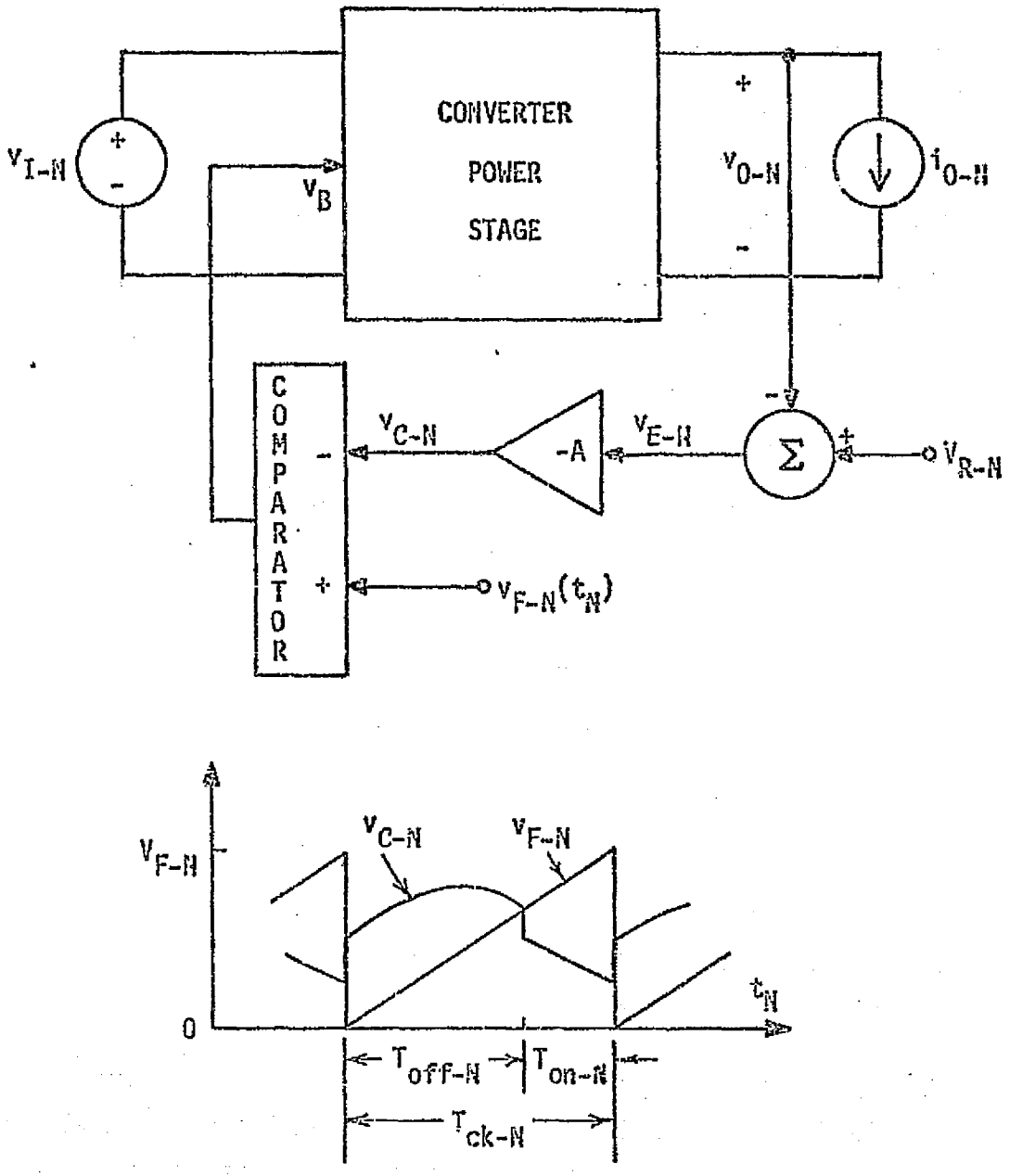

Fig. 3.9 Conceptual diagram of a constant frequency coincidence detector converter system.

a constant frequency sawtooth function, $v_{F-N}(t_N)$, and the converter power switch turn-on signal is issued when these two signals are coincident. The switch remains closed until the end of the fixed period, T_{ck-N}, at which time the sawtooth function falls to zero, the output of the comparator goes negative, and the power switch turns off. Examples of the application of this control technique to each of the three converter power stages being treated in this dissertation are presented below.

Example 5. The response of the voltage step-up converter of Fig. 2.1 to a step change in load current from 50% to 10% of its rated value when operating under the influence of the constant frequency coincidence detector controller described above is illustrated in Fig. 3.10. The steady-state trajectory corresponding to the nominal operating conditions of $v_{I-N} = 0.75$ and $i_{O-N} = 0.5$ is displayed near the center of Fig. 3.10(A) between points a and b. After the load switch occurs at $t_N = 2.0$, point c in Fig. 3.10(A), the system state begins to follow the families of off-time and on-time trajectories which correspond to the new load condition, and steady-state operation in the discontinuous conduction mode is approximately achieved within seven cycles of control. This new equilibrium condition yields an average output voltage which is higher than the rated value, however, and thus this example illustrates once again the steady-state error which results when employing a fixed reference level in the controller subsystem.

The initial transient off-time trajectory, point c to point d in Fig. 3.10(A), is interrupted at point d by the action of the coincidence detector controller. If this system were being controlled by the constant on-time controller described in section 3.3.1, this off-time trajectory

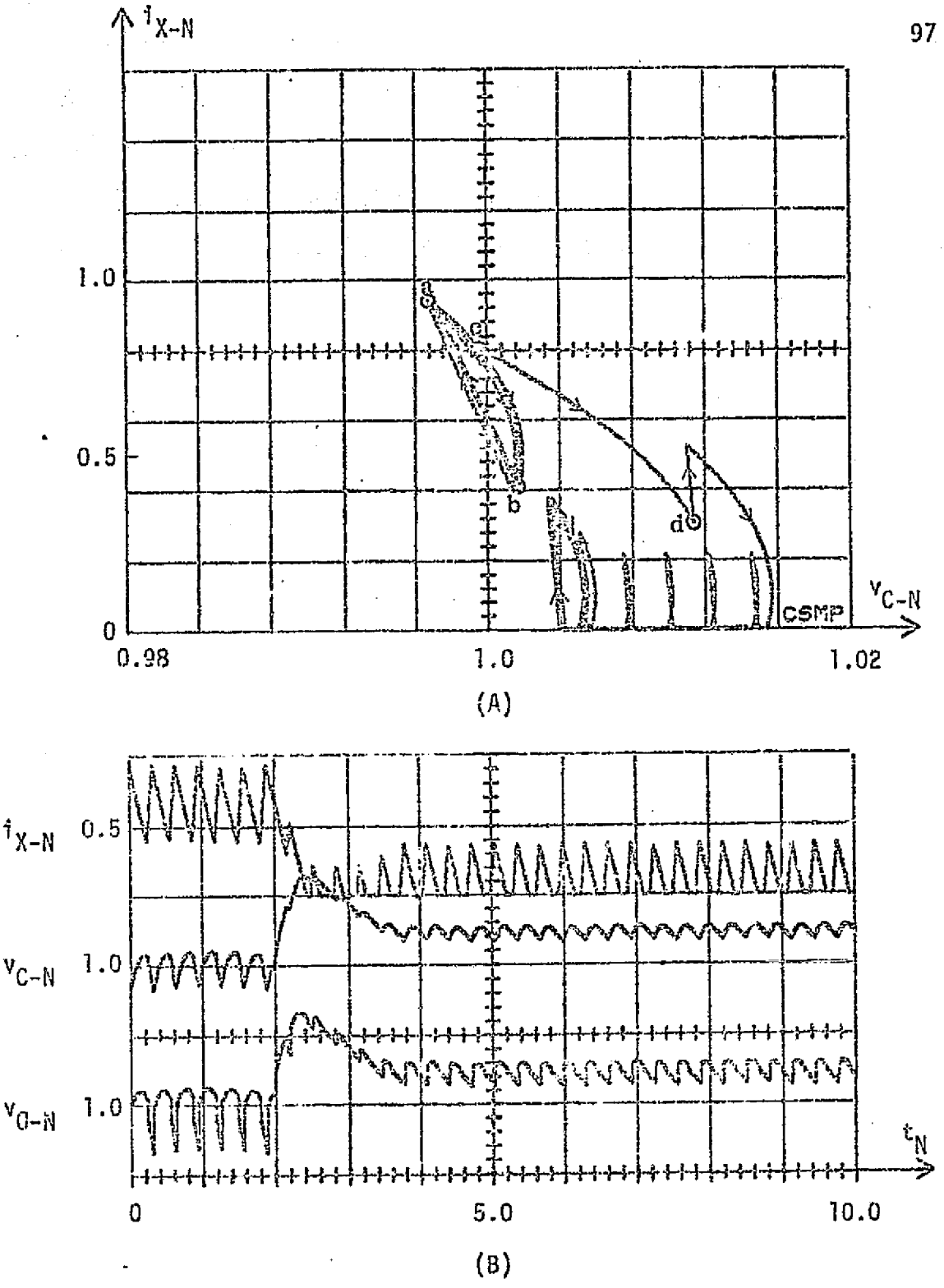

Fig. 3.10 CSMP generated response of voltage step-up converter of Fig. 2.1 operating with the constant frequency controller of Fig. 3.9 for a step decrease in i_{O-N} from 0.5 to 0.1. Controller parameters are V_{R-N} = 0.97, V_{F-N} = 0.04, T_{ck-N} = 0.3, and A = 1.0. Scale factors for the time waveforms are, in normalized units per major division: i_{X-N}, 0.5/div; v_{C-N}, 0.01/div; and v_{O-N}, 0.01/div.

would not be terminated until the state of the system reached a peak and fell back to cross the reference level switching line. Thus, the peak output voltage overshoot is greater for this disturbance than it would have been if the system were controlled by the constant on-time technique of Fig. 3.2.

Example 6. The response of this same converter/controller system to a step change in input voltage from 75% to 50% of the rated average output voltage is presented in Fig. 3.11. After two units of normalized time, the system state begins to follow trajectories which correspond to the lower input voltage, and as illustrated in the figure, unstable operation results. The final time of the state trajectory plot in Fig. 3.11(A) is again less than the final time of Fig. 3.11(B) because after 6 units of time the state trajectories begin to overlap and obscure the visualization of the system behavior. The states of the system at the switching instants between $t_N = 2.0$ and $t_N = 4.0$ are marked with black dots in Fig. 3.11(A) to help distinguish the transient trajectory which occurs during that time from the trajectory which occurs from $t_N = 4.0$ to $t_N = 6.0$. The states marked with the letters *a* and *b* in Fig. 3.11(A) correspond to the peak reactor currents which are similarly marked in Fig. 3.11(B). The final state plotted in Fig. 3.11(A) is labeled point *c*.

Example 7. The constant frequency coincidence detector controller applied to the current-or-voltage step-up converter power stage of Fig. 2.3 is illustrated in Fig. 3.12. The response shown in this figure corresponds to a step increase in load current from 10% to 50% of the rated value. Steady-state operation before the load change occurs is in the discontin-

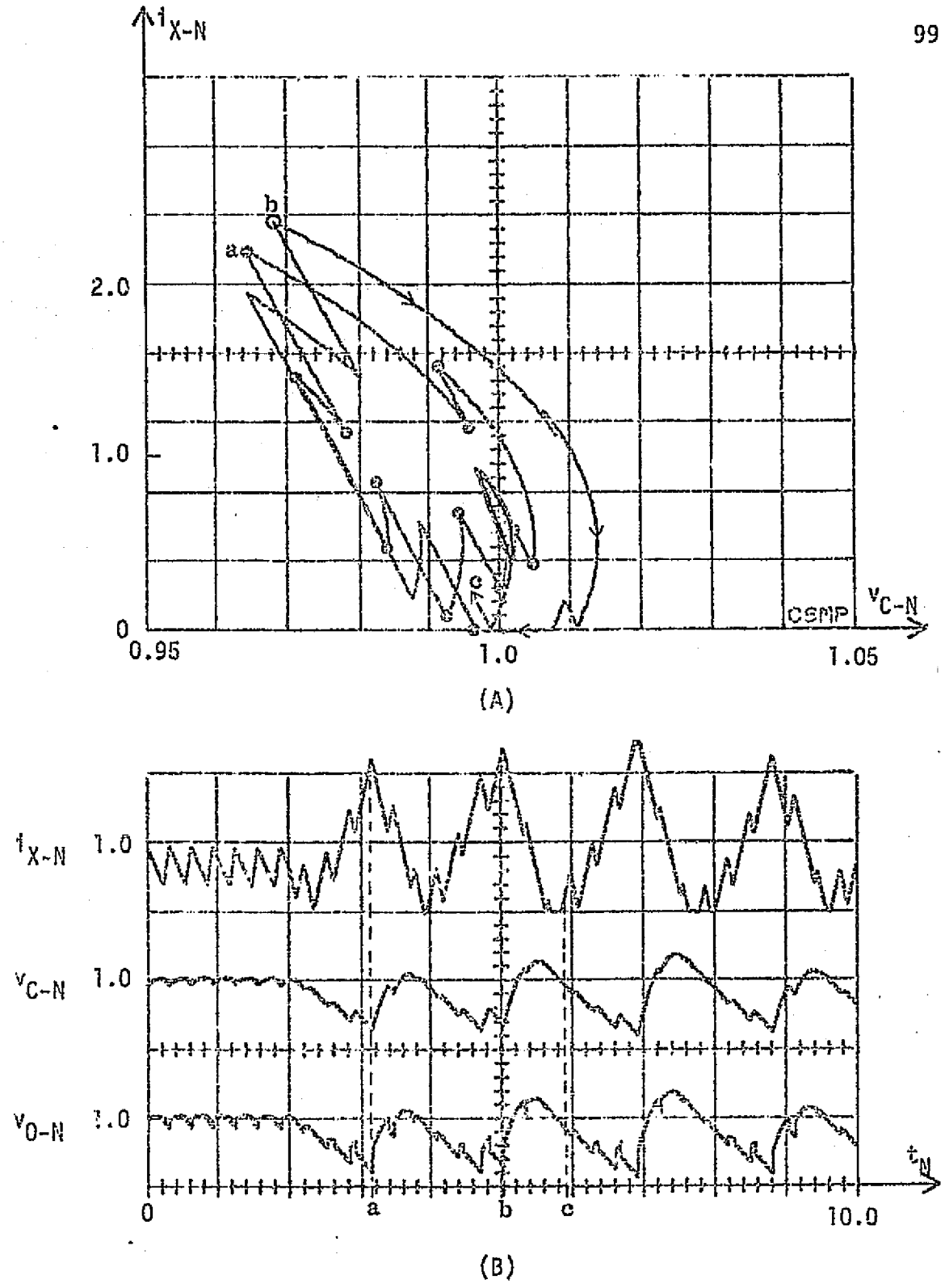

Fig. 3.11 CSMP generated response of voltage step-up converter of Fig. 2.1 operating with the constant frequency controller of Fig. 3.9 for a step decrease in V_{I-N} from 0.75 to 0.5. Controller parameters are V_{R-N} = 0.97, V_{F-N} = 0.04, T_{ck-N} = 0.3, and A=1.0. Scale factors for the time waveforms are, in normalized units per major divisions: i_{X-N}, 1.0/div; v_{C-N}, 0.05/div, and v_{O-N}, 0.05/div.

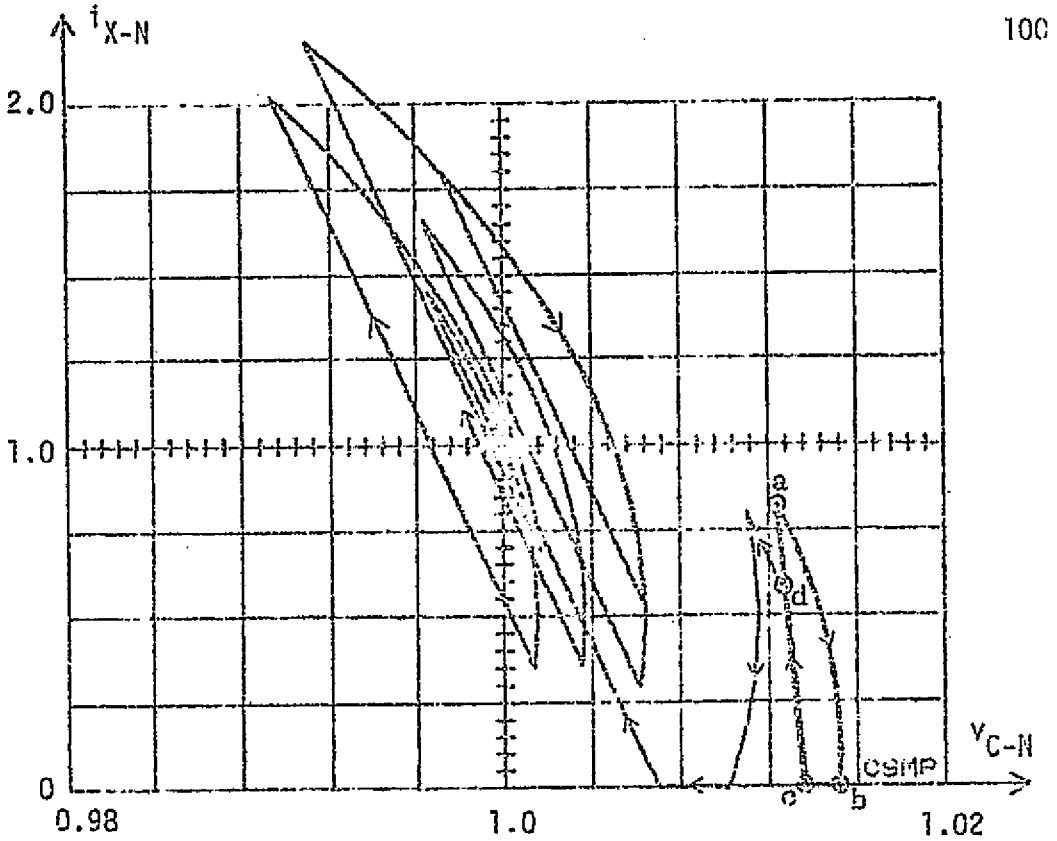

(A)

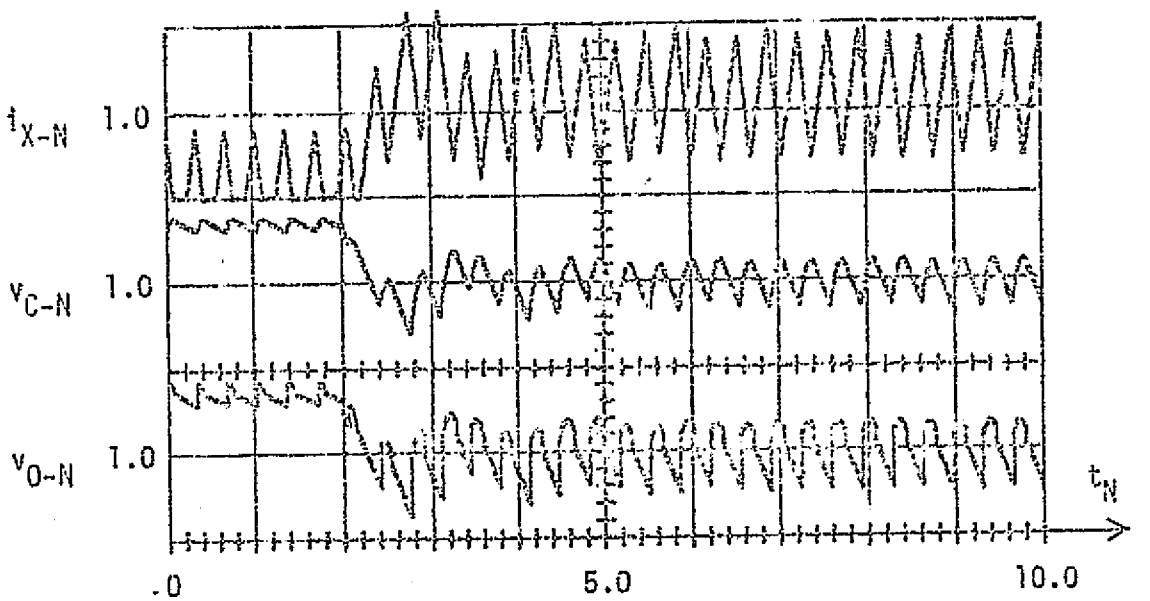

(B)

Fig. 3.12 CSMP generated response of current-or-voltage step-up converter of Fig. 2.3 operating with the constant frequency controller of Fig. 3.9 for a step increase in i_{O-N} from 0.1 to 0.5. Controller parameters are V_{R-N} = 0.99, V_{F-N} = 0.04, T_{ck-N} = 0.3, and A=1.0. Scale factors for the time waveforms are, in normalized units per major division: i_{X-N}, 1.0/div; v_{C-N}, 0.02/div; and v_{O-N}, 0.02/div.

uous conduction mode with an average output voltage approximately 1.5% greater than desired. This steady-state operation is represented in Fig. 3.12(A) by the three segment closed trajectory labeled *a-b-c*. After the load is switched at t_N = 2.0 units, point *d* in Fig. 3.12(A), the families of trajectories for the new load condition are followed to the unique steady-state trajectory that yields the desired average output voltage for this converter operating under nominal conditions. The average output voltage of this system running under these operating conditions is equal to the rated value because the fixed reference level, V_{R-N}, has been specified to accommodate them. As in previous examples, the plot of the system state trajectory in Fig. 3.12(A) was terminated before the final steady-state trajectory was reached in order to prevent obscuring the nature of the transient response. The shape of the final steady-state trajectory for these operating conditions can be seen in Fig. 2.13.

Example 8. The final example of this chapter illustrates the application of the constant frequency coincidence detector controller to the current step-up converter power stage of Fig. 2.2. The response of this system to a step change in input voltage from 1.5 to 1.25 times the rated average output voltage is presented in Fig. 3.13. The original steady-state trajectory shown at the center of Fig. 3.13(A) between points *a* and *b* is the same as that displayed in Fig. 2.12. Six cycles of the transient trajectory are shown in Fig. 3.13(A). The time waveforms in Fig. 3.13(B) show that after 17 cycles of transient operation, the system is still not in an equilibrium condition, but that the system is stable for v_{I-N} = 1.25 and i_{O-N} = 0.5, and an average output voltage approximately 1% below the rated value results.

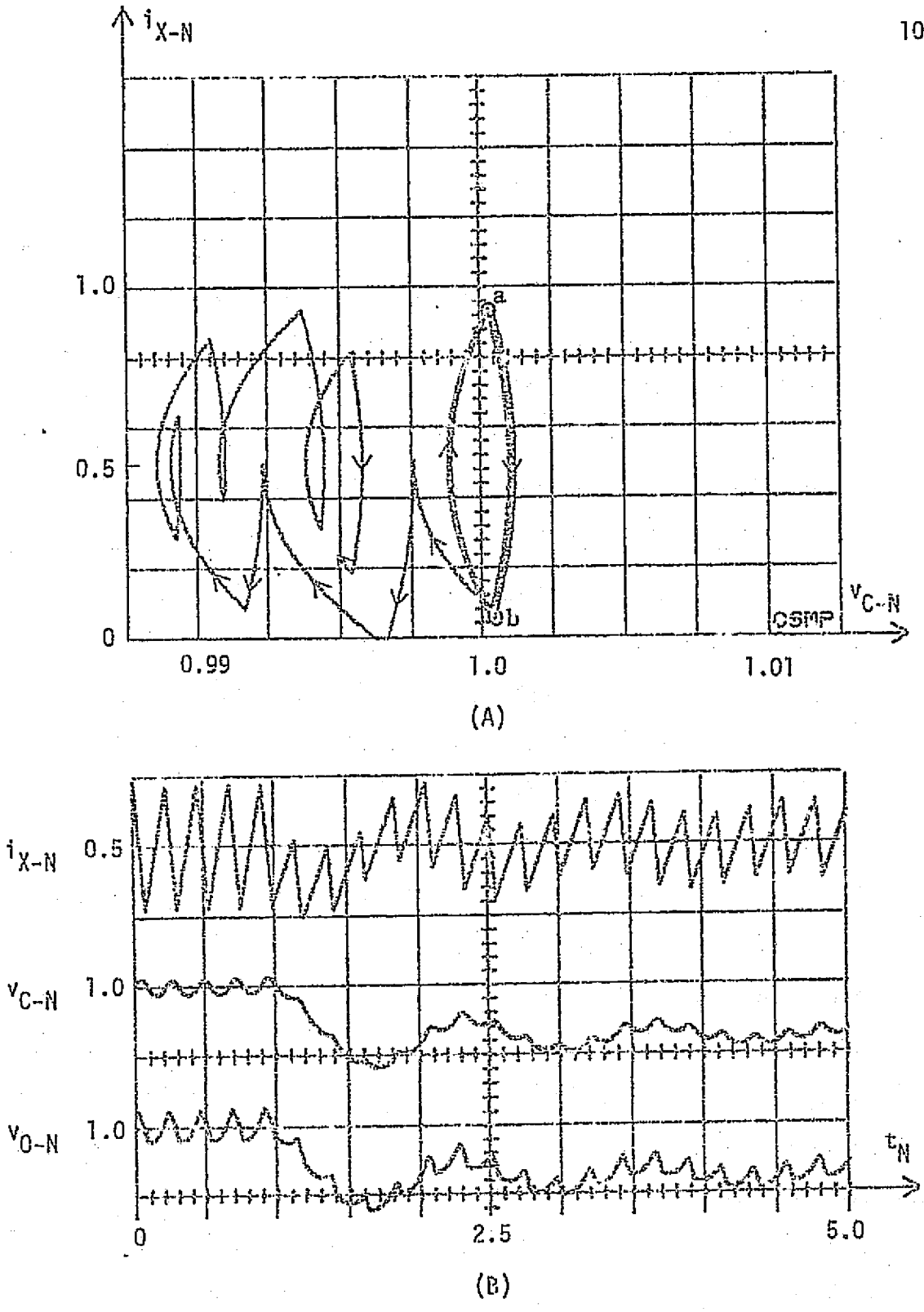

Fig. 3.13 CSMP generated response of current step-up converter of Fig. 2.2 operating with the constant frequency controller of Fig. 3.9 for a step decrease in v_{I-N} from 1.5 to 1.25. Controller parameters are V_{R-N} = 0.98, V_{F-N} = 0.05, T_{ck-N} =0.2, and A=1.0. Scale factors for the time waveforms are, in normalized units per major division: i_{X-N}, 0.5/div; v_{C-N}, 0.01/div; and v_{O-N}, 0.0./div.

3.5 Conclusions

As illustrated by the examples in this chapter, the behavior of dc-to-dc converters is very much dependent on the manner in which the system control function accomplishes its task of determining a switching sequence for the converter power stage. Different control techniques applied to the same converter power stage can be adjusted to yield precisely the same steady-state trajectory for one specified operating point. The response of each of these systems to any disturbance in the nominally specified operating conditions is quite different, however, and the resultant steady-state trajectories achieved by each system for the new operating conditions are also quite different and usually do not yield the desired average output voltage. This feature is illustrated in Examples 1 and 7 above in which the current-or-voltage step-up converter exhibits the same steady-state solution trajectory under nominal operating conditions when functioning under both a single-loop constant on-time controller and a constant frequency coincidence detector controller. Likewise, examples 2 and 5 illustrate this feature for the voltage step-up converter configuration.

Individual converter control subsystems usually are able to respond very well to certain types of system disturbances, but other types, or disturbances of sufficient magnitude, often result in poor converter performance and even, in some cases, unstable operation as illustrated in Examples 2 and 6 above. It sometimes is possible to readjust controller parameters, such as V_{R-N} or T_{min-N}, in order to accommodate such disturbances, but this can be done only at the expense of the system performance over some other range of the specified operating conditions. One of the major

causes of this inability of converter controllers to respond to wide variations in operating conditions is the fact that the controller parameters are fixed and cannot adapt to changes in the system operating conditions. As revealed in Chapter II, the shapes of the system trajectories change as the externally imposed operating conditons change, and consequently parameters computed for one particular operating point do not necessarily adequately satisfy all possible conditions.

Another limitation in converter system performance is caused by timing restrictions which are usually inflicted on conventional control techniques. Each system disturbance requires a redistribution of energy within the converter power stage in order to accommodate new operating conditions. This redistribution of energy can usually be adequately accomplished for moderate disturbances in the system operating conditions, regardless of the controller timing restrictions; but for relatively large disturbances, the timing limitations, such as minimum off-times or minimum on-times, often play a dominant role in determining the converter switching sequence, and the converter power stage is not able to process the necessary amount of energy sufficiently quickly to maintain the desired average output voltage. To meet the converter performance specifications for all possible disturbances in externally imposed operating conditions, the system controller must be given sufficient flexibility in terms of establishing threshold levels and switch timing sequences. The next chapter presents the development of an analytically derived control function which does incorporate these considerations.

CHAPTER IV

DERIVATION OF A STATE-TRAJECTORY CONTROL LAW FOR DC-TO-DC CONVERTERS

4.1 Introduction

The use of the system state plane as a vehicle for studying and understanding the behavior of dc-to-dc converters is extensively described in Chapters II and III. Both the fundamental physical constraints in the performance of the basic converter power stages and the manner in which various control techniques accomplish the task of regulating the flow of energy through them are discussed. The purpose of this chapter is to demonstrate how the insight gained through this theoretical investigation can be used to develop a new state-trajectory control law for a class of dc-to-dc converters which enables the accomplishment of system performance that approaches the theoretical limits revealed in Chapter II. The control approach derived in this chapter is conceptually quite simple and can be easily visualized in the system state plane.

After presenting a qualitative description of the control technique, switching lines in the system state plane are derived for each of the converter configurations discussed in Chapter II. The performance capabilities of these dc-to-dc converter systems operating under the influence of this control law are discussed and evaluated, and digital computer simulations of such systems in both steady-state and transient operation are presented to illustrate and verify the theoretical dis-

cussions presented. The particular converter power stages and operating conditions used as examples in this chapter are identical to those used in Chapter III so that comparisons of the behavior of these systems when functioning with the various control techniques can be made.

4.2 Conceptual Development of the Control Law

In Chapter II, several figures are presented which display, in the state plane, families of off-time and on-time trajectories for various converter power stages. In most of these figures, a particular combination of an off-time and an on-time trajectory segment which together yield a closed path in the system state plane is highlighted and referred to as the *desired* steady-state trajectory for the given converter operating at a specified switching frequency, input voltage, and output current. This steady-state trajectory centers about 1.0 on the v_{C-N} axis, and about a value of reactor current which is commensurate with the converter input and output conditions on the i_{X-N} axis. No other closed path in the system state plane can precisely meet these conditions at the specified operating frequency, and consequently it is used as the cornerstone for the development of the state-trajectory control law as described below.

The switching criterion employed by this state-trajectory control law is illustrated in Fig. 4.1. This figure displays the same on-time and off-time trajectories for the voltage step-up converter as are shown in Fig. 2.8, but in this case, the state plane has been divided into two regions, with the off-time trajectories being confined to the upper right-hand region and the on-time trajectories to the lower left. The boundary between the regions consists of segments of a particular off-time trajectory and a

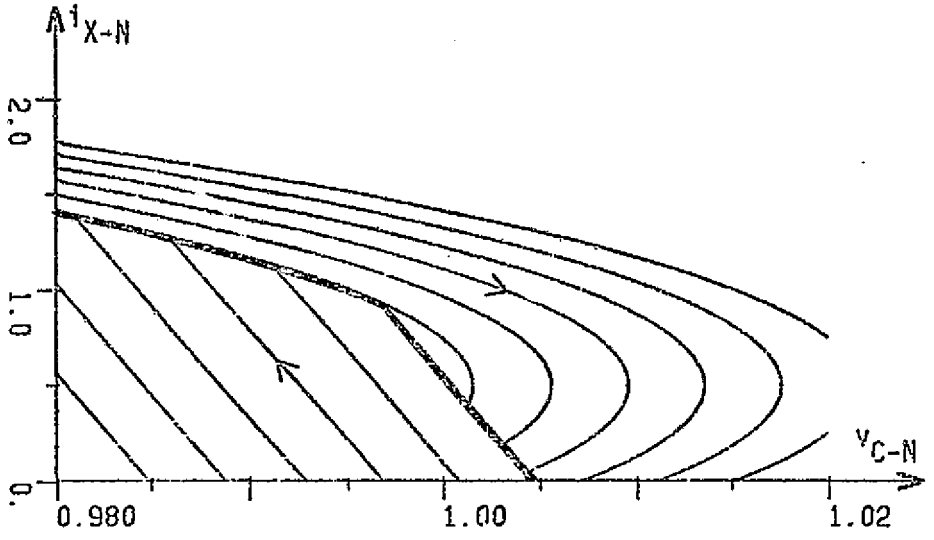

Fig. 4.1 Off-time and on-time trajectories for the voltage step-up converter of Fig. 2.1 with $v_{I-N} = 0.75$ and $i_{O-N} = 0.5$. Bold line separates state plane into an on-region and an off-region.

particular on-time trajectory which are shown as bold lines in the figure. The particular trajectories chosen to construct this boundary line are the ones that also include the steady-state off-time and on-time trajectory segments which yield the desired converter output characteristics for the given operating conditions. The actual desired steady-state trajectory for this converter operating with $v_{I-N} = 0.75$ and $i_{O-N} = 0.5$ is represented by the closed curve at the intersection of the two segments that make up the boundary line. The steady-state trajectory shown in this figure is the same trajectory that has been used throughout this dissertation as a reference case for the voltage step-up converter.

The information contained in this figure can be used to determine a converter power stage switching sequence which enables the converter to achieve the desired steady-state operation in one on/off cycle of control, regardless of the system's initial state and for any imposed operating conditions. For example, if the initial state of the system is in the region of the plane below the boundary line, and if the control law is such that the power switch is closed when the state is in this region, the system state must follow the corresponding on-time trajectory upward and to the left toward the bold boundary line. If, in addition, the controller is such that it uses this boundary as a switch-off line, the converter power switch opens the instant the state reaches this boundary and the off-time trajectory which coincides with the boundary line is subsequently followed. If the controller likewise uses the on-time segment of the boundary line as a switch-on line, the system state immediately converges to the steady-state trajectory shown adjacent to the boundary lines. Similarly, if the control law is such that the power switch is off whenever the system state is above the boundary line, a state in this upper

region must initially follow an off-time trajectory until the switch-on boundary is reached. At that instant the power switch closes and the on-time trajectory which coincides with the boundary line is followed to the desired steady-state trajectory. Thus, it is evident that if this boundary is used as a switching line, the desired system steady-state trajectory can be reached within one precisely determined cycle of control; i.e., with one on-time and one off-time, or vice versa, depending on which region of the plane contains the initial state. Two examples of transient trajectories for a converter operating under the control of this law are illustrated in Fig. 4.2. The portions of the transient trajectories in this figure which do not coincide with the switching boundaries are represented by bold *dashed* lines rather than by solid lines so that the switching boundaries themselves are not obscured.

The same switching criterion is valid for the current step-up and the current-or-voltage step-up converter configurations as illustrated in Figs. 4.3 and 4.4 respectively. These figures display the same on-time and off-time trajectories as are shown in Figs. 2.12 and 2.13, but again the state planes have been divided into an on-region and an off-region by a particular combination of an off-time and an on-time trajectory. If the control law is such that the power switch is turned on when the state of the system is in the region to the left of the boundary, and off when the state of the system is to the right of the boundary, the desired steady-state trajectory for each configuration can be achieved within one cycle of control as illustrated in Figs. 4.3 and 4.4. The transient trajectories which begin in the off-region of the state plane in these two figures incorporate a portion of the

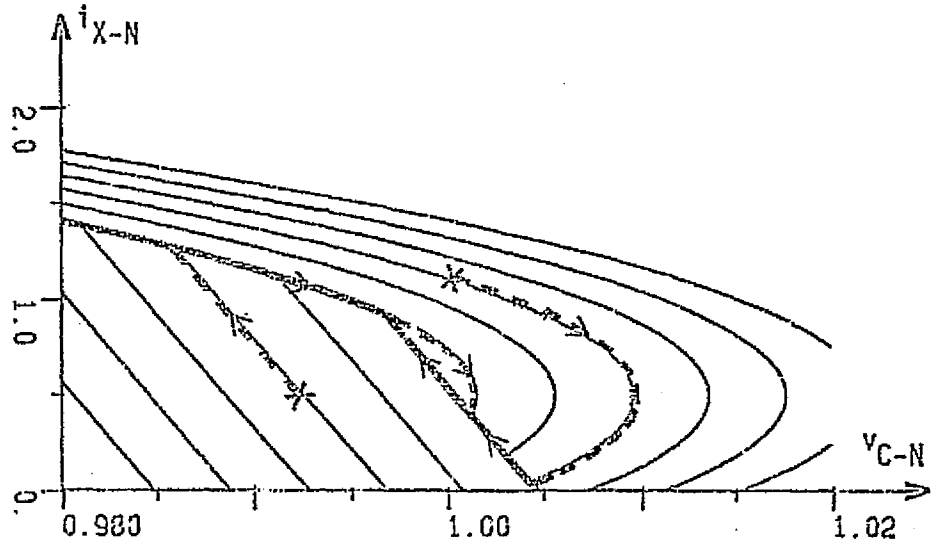

Fig. 4.2 Two examples of transient trajectories which reach steady-state operation in one control cycle. Initial states are indicated by X.

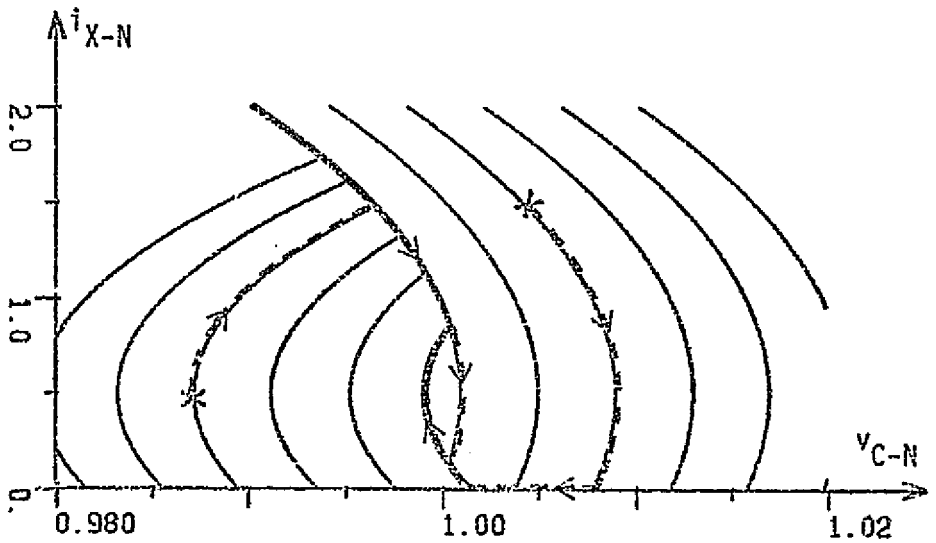

Fig. 4.3 Switching boundary (solid bold line) and two examples of transient trajectories for the current step-up converter of Fig. 2.2 with $v_{I-N} = 1.5$ and $i_{O-N} = 0.5$. Initial states are indicated by X.

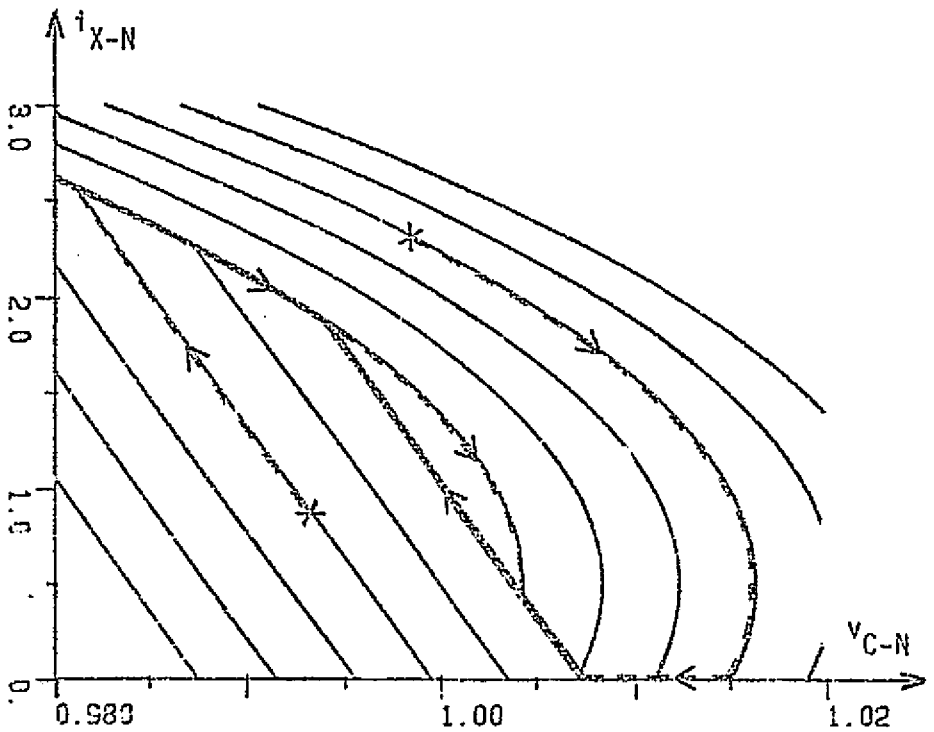

Fig. 4.4 Switching boundary (solid bold line) and two examples of transient trajectories for the current-or-voltage step-up converter of Fig. 2.3 with $v_{I-N} = 0.75$ and $i_{O-N} = 0.5$. Initial states are indicated by X.

v_{C-N} axis as part of their off-time trajectories. The abrupt change in direction which the system state undergoes at the instant the reactor current falls to zero is caused by the diode in the converter power stage becoming reverse biased, rather than by a switching signal from the system controller.

No timing restrictions are imposed on the converter power switch during these transient trajectories so that the switch can remain open or closed for as long a period as is needed for the system state to reach the switching boundary. Any switching prior to the intersection of the state with this boundary, whether it be caused by a controller timing constraint or a fixed reference level which was chosen to accommodate some other operating point, can only cause delays in the accomplishment of the desired steady-state condition or, in some cases, cause the state of the system to converge to some other undesired equilibrium condition. As a final observation on these figures, one can see that no matter how far the initial state is from the desired equilibrium condition, the direction of movement of the state is always toward the switching line rather than away from it, and thus these converters operating in conjunction with such a control law are inherently stable in the large.

4.3 Derivation of the Switching Line

To implement the control concept described above, one must be able to precisely determine for a given converter and operating conditions, the location, in the system state plane, of the steady-state trajectory which yields the desired converter output characteristics. As demonstrated in Chapters II and III, the location of this equilibrium trajectory is very much dependent on the values of the converter input voltage, output

current, and the values of the components in the converter power stage. The location of this steady-state trajectory is also a function of the specified converter steady-state operating frequency or of a specified power switch on-time or power switch off-time if preferred. These relationships and the equations which are needed to determine the location of the desired converter steady-state trajectory for any externally imposed operating conditions or timing specifications are derived in the following subsections.

4.3.1 Steady-State Switch-Off Point

Given the piecewise linear nature of this class of dc-to-dc converters, a sufficient criterion for locating the desired steady-state trajectory is to specify the system state at the instant that the power switch should be turned off. This steady-state switch-off point is the initial state for the system off-time trajectory and the final state for the on-time trajectory for each cycle of steady-state operation. Thus, since only one off-time trajectory and one on-time trajectory can pass through a given point in the system state plane, specifying this point completely specifies the system steady-state trajectory. The steady-state switch-on point corresponding to this trajectory is simply the lower intersection of the appropriate on-time and off-time trajectories for continuous conduction operation, or the intersection of the on-time trajectory with the v_{C-N} axis for discontinuous conduction operation.

The precise location of this equilibrium switch-off state can be determined from a static analysis of the particular converter power stage. The specification of this point takes the form of a pair of algebraic equations which give the converter reactor current, i_{X-1}, and

capacitor voltage, v_{C-N}, at the steady-state switch-off instant in terms of the converter power stage component values, the externally imposed operating conditions, and a designer specified timing parameter. For convenience, these variables have been assigned the symbols i_{B-N} and v_{B-N} as illustrated in Fig. 2.9. The equations derived for these variables are, of course, dependent on the particular model used to describe the actual converter power stage. The equations and data presented in this chapter are derived from the models presented in Chapter II. An evaluation of the accuracy of these models and the resultant state-plane switching lines, and the development of other switching lines based on different converter models are presented in Chapter V.

The equation for the value of peak reactor current, i_{B-N}, can be derived from a consideration of the average reactor current and the power switch duty-cycle ratio required to yield the desired converter output characteristics. The value of capacitor voltage at the steady-state switch-off instant, v_{B-N}, can be derived by averaging, over one cycle, the expressions derived in Chapter II for v_{C-N} as a function of time. This averaging procedure yields an expression for the average output voltage, V_{O-N}, as a function of v_{B-N}, and consequently v_{B-N} in terms of V_{O-N}. Expressions for i_{B-N} and v_{B-N} must be derived for both the continuous and the discontinuous conduction modes of operation if the converter is required to function in both modes over the specified range of operating conditions. If converter operation is restricted to one mode or the other, only the expressions corresponding to that mode are needed to specify the switching boundary for all possible operating conditions. Detailed derivations of these expressions for both the continuous and the discontinuous conduction modes of operation are presented in Appendix A. The

resultant expressions for each of the three converter configurations being treated in this dissertation are given in Table 4.1.

4.3.2 Steady-State Timing Parameter

The expressions listed in Table 4.1 are all functions of the power stage components, L_N and C_N, the externally imposed operating conditions, v_{I-N} and i_{O-N}, the desired average output voltage, V_{O-N}, and a timing parameter which, in these equations, is the normalized switching period T_N. The shape and location of the steady-state trajectory which satisfies a particular set of operating conditions for a converter is very much dependent on the frequency at which the state of the system switches from the steady-state on-trajectory segment to the off trajectory. As the converter switching frequency increases, the steady-state trajectory contracts about a point which corresponds to the desired average output voltage and the required average reactor current. In the limit, as $T_N \rightarrow 0$, the steady-state trajectory actually approaches that single state as can be demonstrated mathematically by letting $T_N = 0$ in the equations of Table 4.1. This condition is, of course, not physically realizable, and in practice converters rarely are designed to operate above 100 KHz because with currently available switching components, system efficiencies begin to decrease severely at that frequency and higher. Conversely, converters operating at low frequencies tend to display large excursions of reactor current about the required average value and large peak-to-peak ripples on the converter output voltage. This dependence of the system steady-state trajectory on the converter operating frequency is illustrated in Fig. 4.5 where steady-state trajectories for the same voltage step-up converter operating under the same externally imposed operating conditions but at different switching frequencies are displayed.

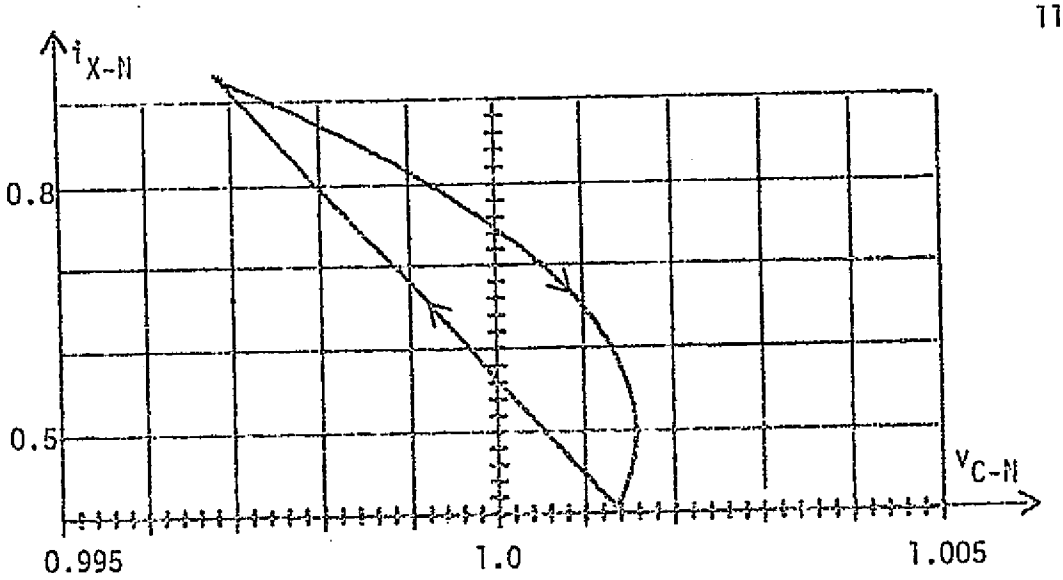

(A)

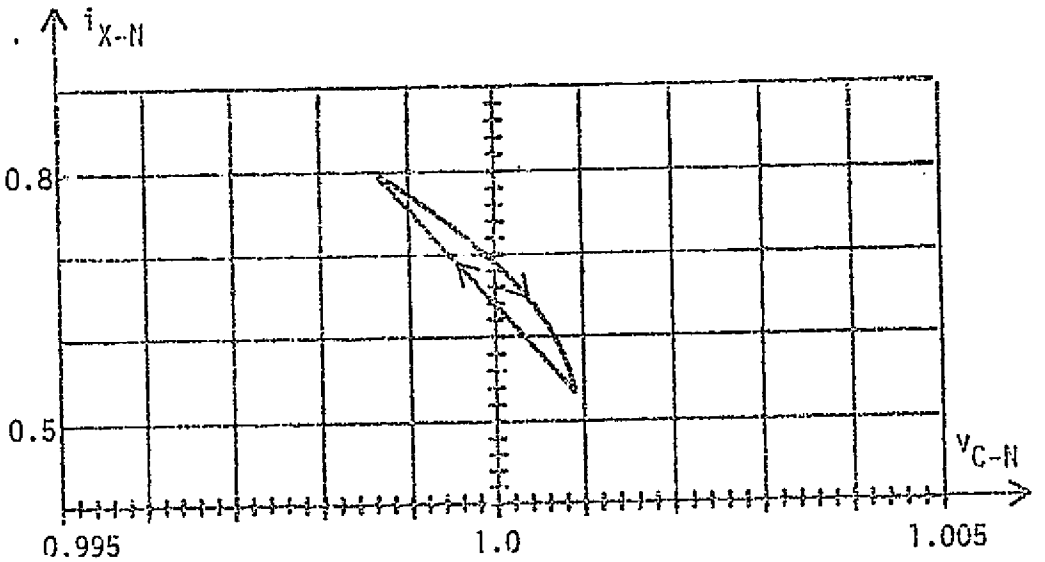

(B)

Fig. 4.5 Steady-state trajectories for the voltage step-up converter of Fig. 2.1 operating with $v_{I-N} = 0.75$, $i_{O-N} = 0.5$, and a switching frequency of (A) 10 KHz, and (B) 20 KHz.

Table 4.1(A)

Location of Steady-State Switch-Off Point for Constant Frequency Operation in the Voltage Step-Up Converter

CONTINUOUS CONDUCTION OPERATION

$$i_{B-N} = \frac{i_{O-N}\, V_{O-N}}{v_{I-N}} + \frac{T_N v_{I-N}(V_{O-N} - v_{I-N})}{2L_N V_{O-N}} \qquad (4.1)$$

$$v_{B-N} = V_{O-N} - \frac{(V_{O-N} - v_{I-N}) i_{O-N}\, T_N}{2C_N\, V_{O-N}} - \frac{(V_{O-N} - v_{I-N}) v_{I-N}^{3}\, T_N^{2}}{12L_N C_N\, V_{O-N}^{3}} \qquad (4.2)$$

DISCONTINUOUS CONDUCTION OPERATION

$$i_{B-N} = \sqrt{\frac{2\, T_N\, i_{O-N}\, (V_{O-N} - v_{I-N})}{L_N}} \qquad (4.3)$$

$$v_{B-N} = V_{O-N} - \frac{i_{O-N}\, T_N}{2C_N} + \frac{i_{O-N}}{3C_N}\sqrt{\frac{2\, i_{O-N}\, L_N\, T_N}{(V_{O-N} - v_{I-N})}} \qquad (4.4)$$

Table 4.1(B)

Location of Steady-State Switch-Off Point for Constant Frequency Operation in the Current Step-Up Converter

CONTINUOUS CONDUCTION OPERATION	
$i_{B-N} = i_{O-N} + \frac{V_{O-N}\,(v_{I-N} - V_{O-N})\,T_N}{2L_N\,v_{I-N}}$	(4.5)
$v_{B-N} = V_{O-N} + \frac{(v_{I-N} - 2V_{O-N})\,(v_{I-N} - V_{O-N})\,V_{O-N}T_N^2}{12\,L_N\,C_N\,v_{I-N}^2}$	(4.6)
DISCONTINUOUS CONDUCTION OPERATION	
$i_{B-N} = \sqrt{\frac{2\,T_N\,i_{O-N}(v_{I-N} - V_{O-N})\,V_{O-N}}{L_N\,v_{I-N}}}$	(4.7)
$v_{B-N} = V_{O-N} + \frac{(v_{I-N} - 2V_{O-N})\,i_{O-N}}{3C_N}\sqrt{\frac{2\,i_{O-N}\,L_N\,T_N}{v_{I-N}V_{O-N}(v_{I-N}-V_{O-N})}} - \frac{T_N\,i_{O-N}(v_{I-N} - 2V_{O-N})}{2C_N\,v_{I-N}}$	(4.8)

Table 4.1(C)

Location of Steady-State Switch-Off Point for Constant Frequency Operation in the Current-or-Voltage Step-Up Converter

CONTINUOUS CONDUCTION OPERATION

$$i_{B-N} = \frac{i_{O-N}\,(v_{I-N} + V_{O-N})}{v_{I-N}} + \frac{T_N\,V_{O-N}\,v_{I-N}}{2L_N\,(V_{O-N} + v_{I-N})} \qquad (4.9)$$

$$v_{B-N} = V_{O-N} - \frac{i_{O-N}\,V_{O-N}\,T_N}{2\,C_N\,(V_{O-N} + v_{I-N})} - \frac{V_{O-N}\,v_{I-N}^3\,T_N^2}{12L_N\,C_N\,(V_{O-N} + v_{I-N})^3} \qquad (4.10)$$

DISCONTINUOUS CONDUCTION OPERATION

$$i_{B-N} = \sqrt{\frac{2\,T_N\,i_{O-N}\,V_{O-N}}{L_N}} \qquad (4.11)$$

$$v_{B-N} = V_{O-N} - \frac{i_{O-N}\,T_N}{2\,C_N} + \frac{i_{O-N}}{3\,C_N}\sqrt{\frac{2\,i_{O-N}\,L_N\,T_N}{V_{O-N}}} \qquad (4.12)$$

The timing parameter used to determine the point (v_{B-N}, i_{B-N}) is by no means restricted to the switching period, T_N. As discussed in Chapter III, there are three basic timing specifications which can be incorporated into a converter control function and which are widely used in practical systems. A converter can be designed to operate at a constant frequency with a fixed period, T_N, or with a constant switch on-time, T_{on-N}, or a constant switch off-time, T_{off-N}. Any one of these three timing parameters can be used in specifying the steady-state switch-off point with the resulting converter steady-state behavior displaying the appropriate timing characteristics. Table 4.2 presents the relationships between the various timing parameters which can be substituted into the equations of Table 4.1 to yield the proper expressions for each of these conditions. The time relationships given in Table 4.2 are derived in Appendix B.

Operational timing characteristics in conventionally controlled converters are normally achieved by using explicit elements such as frequency clocks or monostable multivibrators. The state-trajectory control law presented in this chapter requires no such timing elements, however, and yet achieves the desired steady-state timing characteristics implicitly by incorporating the appropriate timing parameter in the equations which determine the converter steady-state switch-off point. Thus, systems operating in conjunction with this control law are free-running in the sense that no external timing elements are involved in the switching decisions, but at the same time they can be designed to operate in any of the three timing modes described above during steady-state operation over the entire range of externally imposed operating conditions. The free-running nature of these systems allows them to close or open the system power switch at any

Table 4.2(A)

Timing Parameter Relationships for the Voltage Step-Up Converter

CONTINUOUS CONDUCTION OPERATION	
$T_N = \frac{V_{O-N}}{V_{O-N} - v_{I-N}} \; T_{on-N}$	(4.13)
$T_N = \frac{V_{O-N}}{v_{I-N}} \; T_{off-N}$	(4.14)
DISCONTINUOUS CONDUCTION OPERATION	
$T_N = \frac{v_{I-N}^2}{2L_N \, i_{O-N}(V_{O-N} - v_{I-N})} \; T_{on-N}^2$	(4.15)
$T_N = T_R$ where T_R is the larger root of the quadratic $T_R^2 - 2(T_{off-N} + \frac{i_{O-N} \, L_N \, (V_{O-N} - v_{I-N})}{v_{I-N}^2}) \; T_R + T_{off-N}^2 = 0$	(4.16)

Table 4.2(B)

Timing Parameter Relationships for the Current Step-Up Converter

CONTINUOUS CONDUCTION OPERATION
$T_N = \frac{V_{I-N}}{V_{O-N}} T_{on-N}$ (4.17)
$T_N = \frac{V_{I-N}}{V_{I-N} - V_{O-N}} T_{off-N}$ (4.18)
DISCONTINUOUS CONDUCTION OPERATION
$T_N = \frac{V_{I-N}(V_{I-N} - V_{O-N})}{2 L_N i_{O-N} V_{O-N}} T_{on-N}^2$ (4.19)
$T_N = T_R$ where T_R is the larger root of the quadratic $T_R^2 - 2\left(T_{off-N} + \frac{i_{O-N} L_N V_{O-N}}{V_{I-N}(V_{I-N} - V_{O-N})}\right) T_R + T_{off-N}^2 = 0$ (4.20)

Table 4.2(C)

Timing Parameter Relationships for the Current-or-Voltage Step-Up Converter

CONTINUOUS CONDUCTION OPERATION	
$T_N = \frac{V_{O-N} + v_{I-N}}{V_{O-N}} \; T_{on-N}$	(4.21)
$T_N = \frac{V_{O-N} + v_{I-N}}{v_{I-N}} \; T_{off-N}$	(4.22)
DISCONTINUOUS CONDUCTION OPERATION	
$T_N = \frac{v_{I-N}^2}{2 L_N i_{O-N} V_{O-N}} \; T_{on-N}^2$	(4.23)
$T_N = T_R$ where T_R is the larger root of the quadratic $T_R^2 - 2 \left(T_{off-N} + \frac{i_{O-N} L_N V_{O-N}}{v_{I-N}^2}\right) T_R + T_{off-N}^2 = 0$	(4.24)

time and for as long as needed during a transient cycle to move the system from one steady-state condition to another in one on/off cycle. As described in Chapter III, it is very often the timing restrictions imposed on conventional controllers which prevent them from responding adequately to severe transient disturbances. By eliminating these restrictions, the converter is better able to achieve its maximum performance capability as established by the physical laws of the power stage. Examples of free-running converter systems operating in conjunction with this state-trajectory control law in the constant frequency and constant on-time modes are presented in succeeding sections of this chapter.

4.3.3 Constructing the Switching Line

Having determined the steady-state switch-off point as presented in Table 4.1, the state-plane switching boundary is established by selecting the system off-time and on-time trajectories which pass through that point. This selection is accomplished mathematically by substituting the derived values of i_{B-N} and v_{B-N} into the expressions for K_1 and K_2 which are derived in Chapter II and are given as equations (2.9) and (2.10) for the voltage step-up converter, equations (2.14) and (2.15) for the current step-up converter, and equations (2.19) and (2.20) for the current-or-voltage step-up configuration. It should be noted that the expressions for K_1 involve i_{A-N} and v_{A-N} rather than i_{B-N} and v_{B-N}, but since both the steady-state switch-on point and the steady-state switch-off point must be on that on-time trajectory, the two points can be used interchangeably. Thus, the converter power stage switching signals, for both steady-state and transient operation, are issued when the system state trajectory intersects this well-defined switching line which corresponds to the particular converter power stage components, desired output characteristics, and extern-

ally imposed operating conditions.

A conceptual picture of this free-running control process for the voltage step-up converter is presented in Fig. 4.5. As illustrated in this figure, four signals from the converter power stage are required by the controller to accomplish the decision making process described above. These signals correspond to the two externally imposed operating conditions of the system, v_{I-N} and i_{O-N}, and the system state variables, v_{C-N} and i_{X-N}. The instantaneous values of input voltage and output current are used, in conjunction with the power stage component values, the designer-specified timing parameter, and the desired average output voltage, to construct the two-segment switching line derived above and illustrated graphically in Fig. 4.6(B) with the functional representation $f(V_{O-N}, L_N, C_N, \tau_N, v_{I-N}, i_{O-N}) = 0$, where τ_N represents the designer specified timing parameter. The controller compares the measured value of the system state to this computed switching boundary and turns the converter power switch on if the state is in region R and off otherwise. Since the values of the externally imposed operating conditions are continuously monitored, any change in them is immediately reflected as a change in the switching boundary, and consequently the converter switching sequence, thus eliminating all delays in the response of the system to that disturbance. Such delays in response often occur in conventionally controlled systems which must wait for the disturbance to manifest itself in some internal system signals. This fast response is illustrated by example in the next section of this chapter.

To determine whether or not the state of the system is contained within region R, the state variables, i_{X-N} and v_{C-N}, must also be continuously monitored. As described in Chapter II, the ideal capacitor volt-

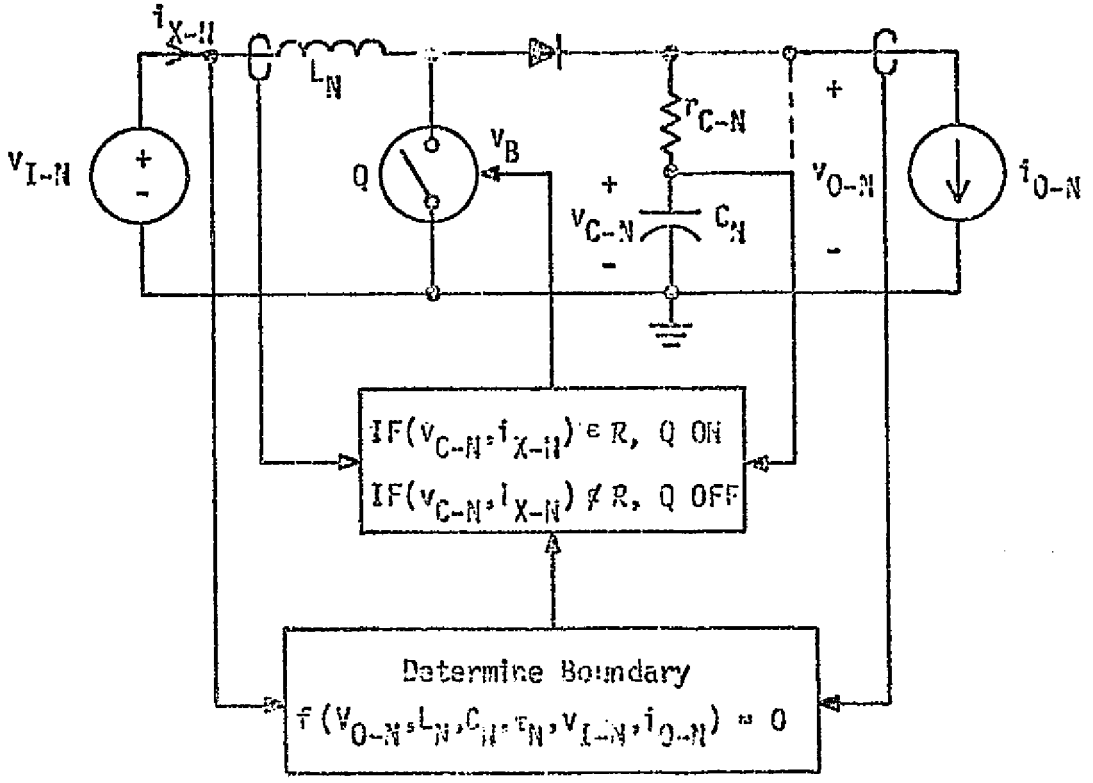

(A)

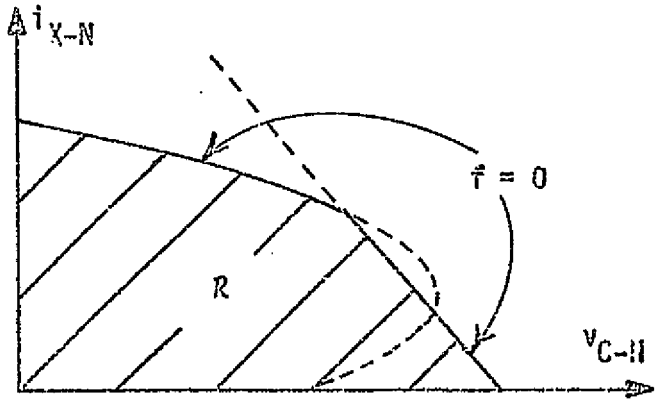

(B)

Fig. 4.6(A) Conceptual diagram of state-trajectory control law for a voltage step-up converter. (B) Definition of function f and region R.

age usually is not physically obtainable, and thus the actual output voltage, v_{O-N}, is shown in Fig. 4.6(A) as an alternative input to the control process. In this case, the function f must be modified accordingly to yield an f', which is also a function of the capacitor ESR. This modified function, as well as the original function f, is given in Appendix C. The computer simulations presented later in this chapter use the output voltage as a controller input rather than the ideal capacitor voltage.

Similar visualizations of the application of this control theory to the current step-up and the current-or-voltage step-up converter configurations are illustrated in Figs. 4.7 and 4.8 respectively. The same four system signals are required in each case although the resultant switching boundary and region R for each configuration are different. Examples of each of these converters operating under the influence of the state-trajectory control law are presented in the next section.

4.4 System Performance

In Chapter II, a fairly complete study of the dependence of the shapes of converter on-time and off-time trajectories on system parameters and externally imposed operating conditions is presented, and as described in the preceding section, this information is used by the system controller to determine how it should respond to changes in these conditions. System state trajectories and switching boundaries for the voltage step-up converter of Fig. 2.1 for three different load conditions are presented in Fig. 4.9. If the system is operating in steady state at 50% of the rated output current, the system state follows the closed trajectory at the center of Fig. 4.9(B). If the load current is reduced to 10% of the rated value, the trajectories plotted in Fig. 4.9(C) subsequently must be

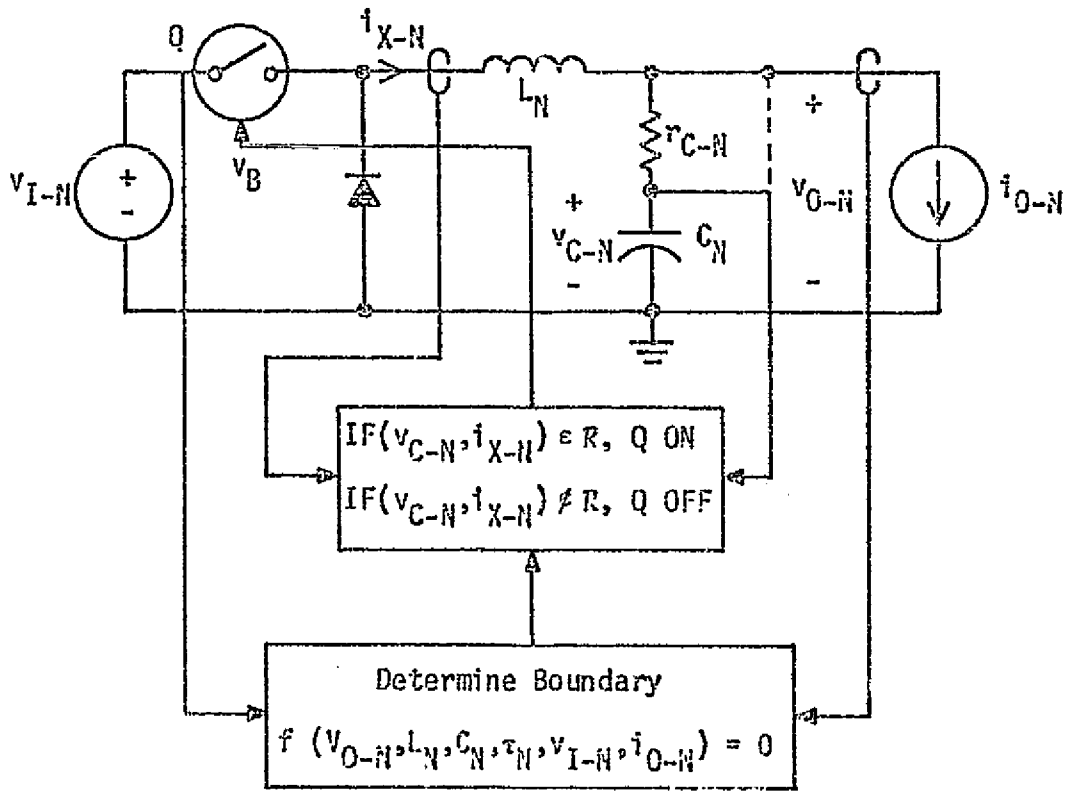

(A)

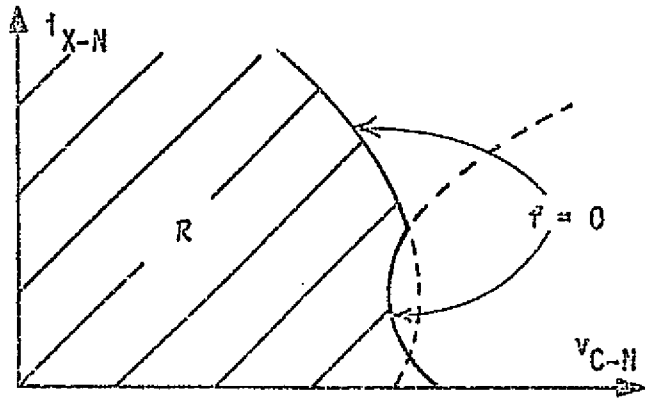

(B)

Fig. 4.7 (A) Conceptual diagram of state-trajectory control law for a current step-up converter. (B) Definition of function f and region R.

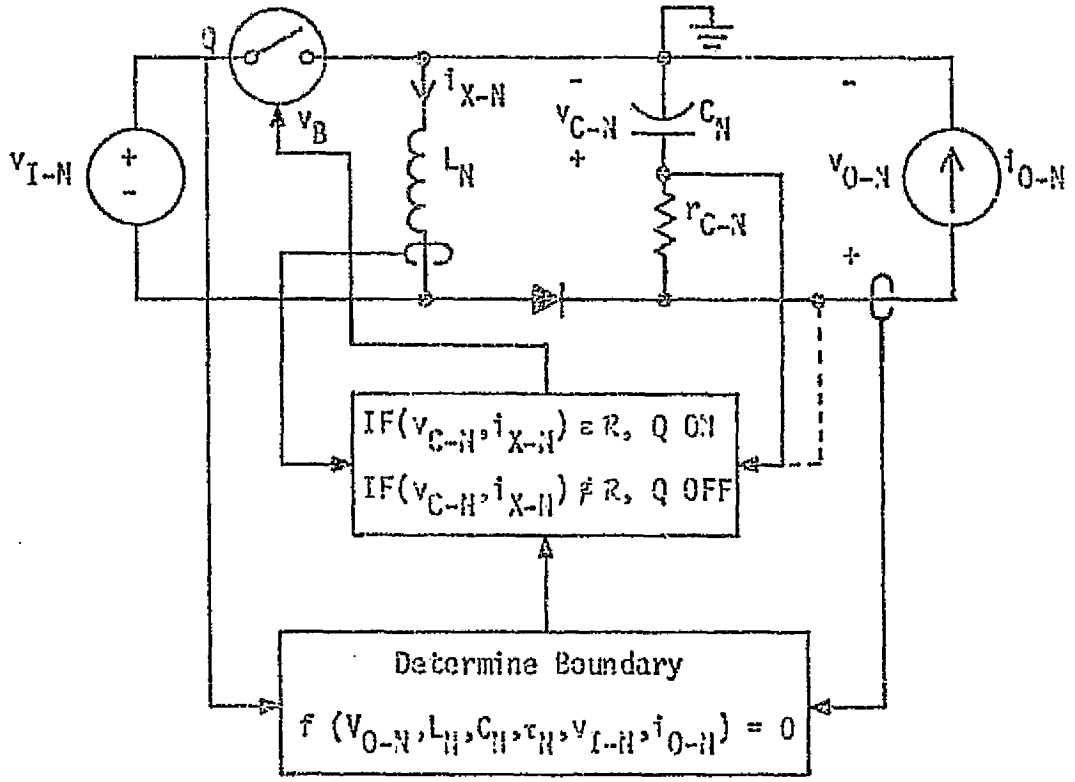

(A)

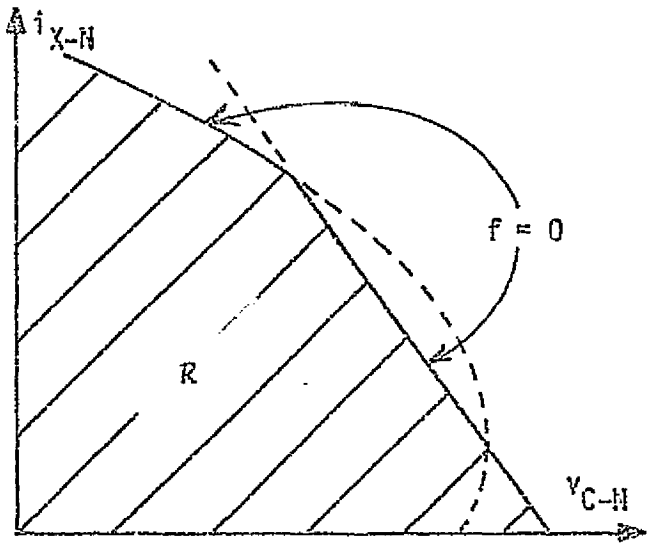

(B)

Fig. 4.8 (A) Conceptual diagram of state trajectory control law for a current-or-voltage step-up converter. (B) Definition of function f and region R.

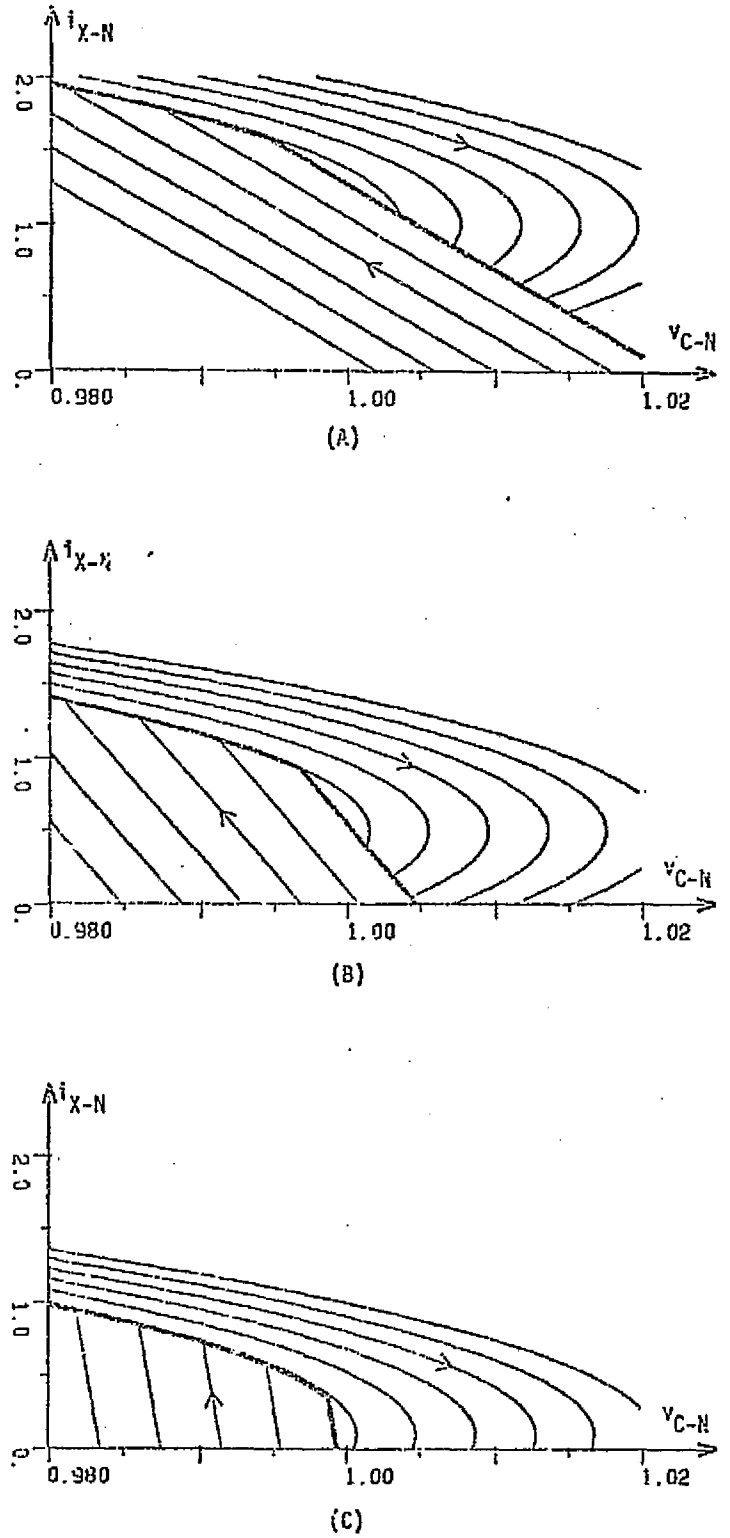

Fig. 4.9 State trajectories and switching boundaries (bold lines) for the voltage step-up converter of Fig. 2.1 with $v_{I-N} = 0.75$ and $i_{O-N} =$ (A) 1.0, (B) 0.5, and (C) 0.1.

followed, and the bold switching line shown there should be used in the switching decision making process. Similarly, if the load current is increased to 100% of its rated value, the trajectories shown in Fig. 4.9(A) must be followed, and if the switching line shown there is used to determine the converter power stage switching sequence, the steady-state trajectory in the upper central portion of that figure results. For each of these load conditions, the steady-state trajectory displayed adjacent to the intersection of the switch-off and switch-on lines yields the desired average output voltage. The behavior of this system when switching between these various load conditions is described below.

4.4.1 Transient Trajectories

Consider first this system in steady-state operation under the conditions depicted in Fig. 4.9(B). If the load current is suddenly reduced to 10% of its rated value, the transient state trajectory which results when the system is operating under the influence of the state-trajectory control law is illustrated in Fig. 4.10(A). The trajectories and the switching boundary shown in this figure are the same as those displayed in Fig. 4.9(C), with the original steady-state trajectory of Fig. 4.9(B) superimposed on the plane as the dashed closed curve. Let the change in load current arbitrarily occur when the system state is at the point marked with an X in Fig. 4.10(A). At that instant, the switching boundary and the system trajectories change to accommodate the change in load current, and the system state begins to follow the new off-time trajectory which passes through the state at that instant. The reactor current eventually falls to zero at which time the converter power stage diode becomes reverse biased and the output capacitor voltage continues to decay along the v_{C-N} axis

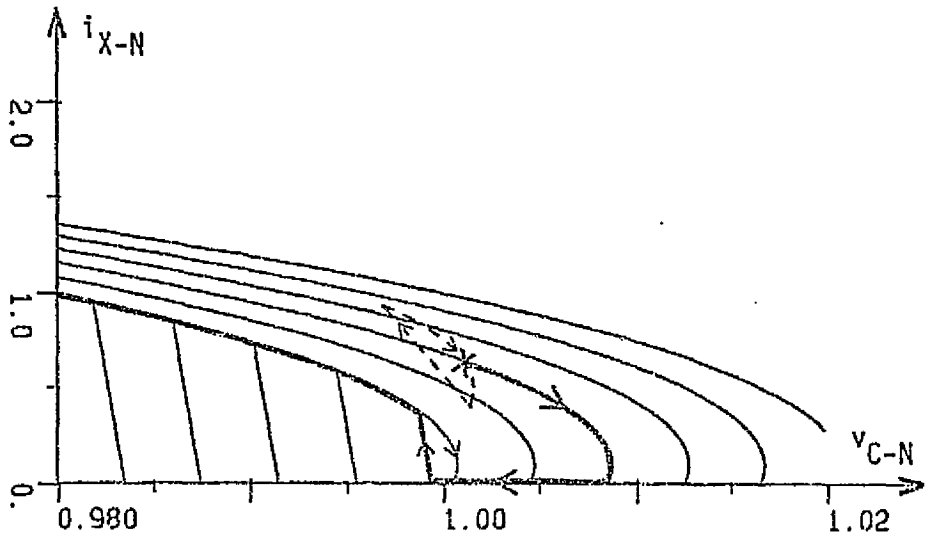

(A)

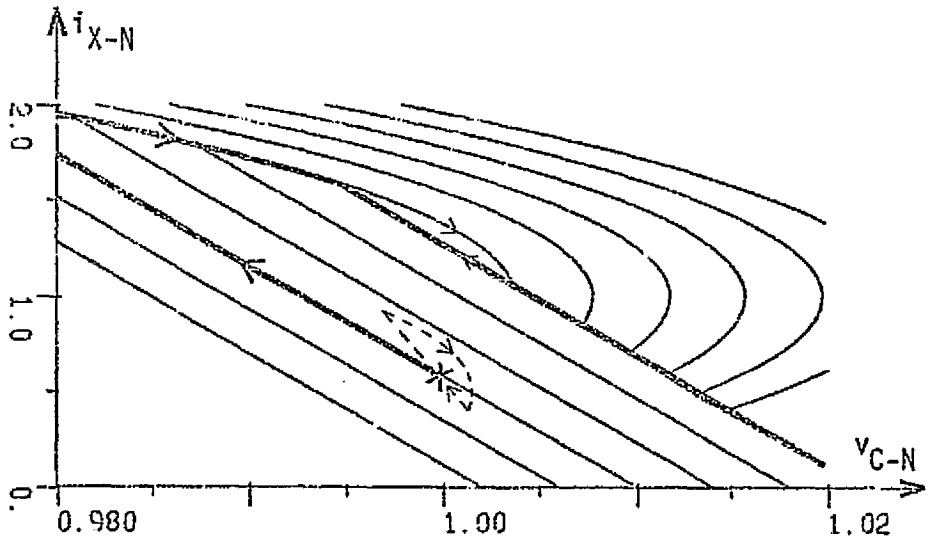

(B)

Fig. 4.10 Transient response of free-running voltage step-up converter system to step changes in i_{O-N} from 0.5 to (A) 0.1, and (B) 1.0. Dashed closed curves represent the original steady-state trajectory corresponding to $v_{I-N} = 0.75$ and $i_{O-N} = 0.5$.

until the switch-on boundary line is reached. A switch-on signal is issued at that instant, and the new steady-state condition, which is in the discontinuous conduction mode, has been attained within one cycle of control. It should be noted that no matter when the load switch occurs within the original steady-state trajectory, whether it be during a power switch on-time or a switch off-time, the power switch, if it is not already off, is immediately opened at that instant because the original steady-state trajectory is suddenly located entirely within the off region. This response is again in contrast to that which is observed with conventional control techniques which often must wait to complete a fixed on-time or off-time interval before a new control command can be issued. The transient trajectory which results for a step change in load current from 50% to 100% of the rated value is illustrated in Fig. 4.10(B). In this case, the system state is in the on-region of the state plane immediately following the load change, but it again reaches the new steady-state condition within one cycle of control.

The same principles of operation apply when the system is subjected to changes in input voltage as illustrated in Fig. 4.11. The state trajectories and switching boundary displayed in Fig. 4.11(A) correspond to this voltage step-up converter system operating with an input voltage equal to 50% of the desired average output voltage rather than the nominal 75% as in Fig. 4.9(B), and the conditions depicted in Fig. 4.11(B) correspond to an input voltage of 90% of the rated output voltage. The transient trajectories which result when the system is subjected to step changes in input voltage from 75% to 50% and 90% of the desired average output voltage are illustrated in Figs. 4.11(A) and (B) respectively in the same way that they are displayed in Fig. 4.10.

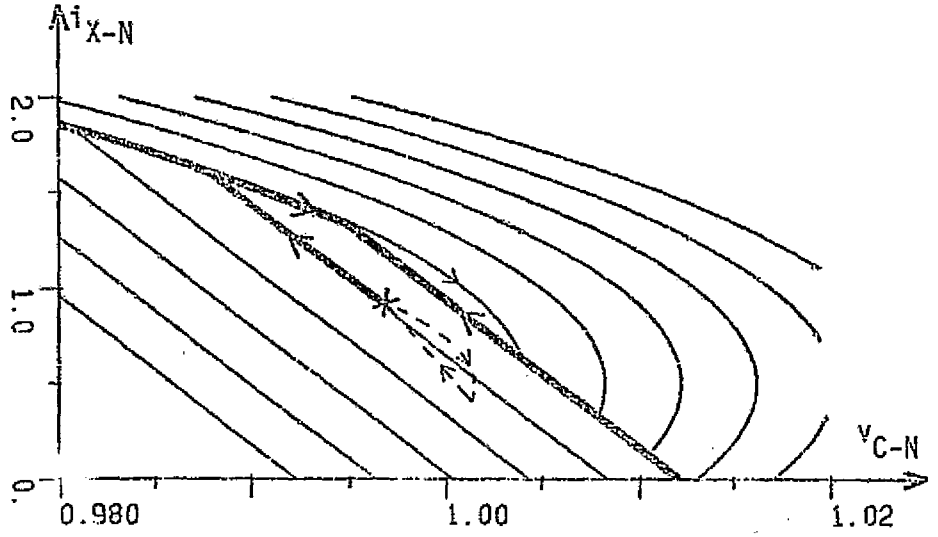

(A)

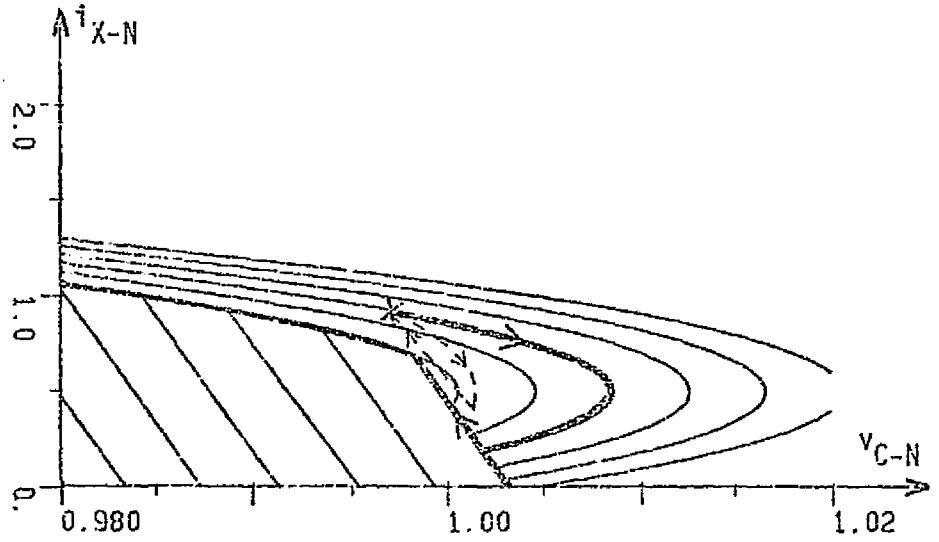

(B)

Fig. 4.11 Transient response of free-running voltage step-up converter system to step changes in v_{I-N} from 0.75 to (A) 0.5, and (B) 0.9. Dashed closed curves represent the original steady-state trajectory corresponding to $v_{I-N} = 0.75$ and $i_{O-N} = 0.5$.

Additionally, examples of transient trajectories for the current step-up and the current-or-voltage step-up converters are illustrated in Figs. 4.12 through 4.16. As discussed previously, the off-time trajectories for these two converter configurations do not change shape for changes in input voltage. This characteristic is clearly illustrated in Figs. 4.14 and 4.16 where for the cases in which the change in input voltage occurs during a power switch off-interval, no apparent change in the converter trajectory occurs until either the original or the new switching boundary is crossed. Note also that some of the examples presented in these figures illustrate changes in operating conditions whereby the new steady-state trajectory completely encompasses the original trajectory or *vice versa*. In these cases, the system transient trajectory results in no voltage or current overshoot or undershoot. The principles of operation for these converters are precisely the same as those described above so that no additional discussion of these cases is necessary.

4.4.2 Computer Simulated Responses

To illustrate and verify the theoretical discussions presented above, digital computer simulations of dc-to-dc converters operating under the influence of this state-trajectory control law are presented in this section. The simulation tool used to generate the data presented in this chapter is the same CSMP program that was used to obtain the data presented in Chapter III.[6] Also, the same converter power stages and the same external disturbances in the system operating conditions are used in these examples as are used in Chapter III so that useful comparisons between the various control techniques might be made.

[6]See page 80-A for a discussion of the simulation tool.

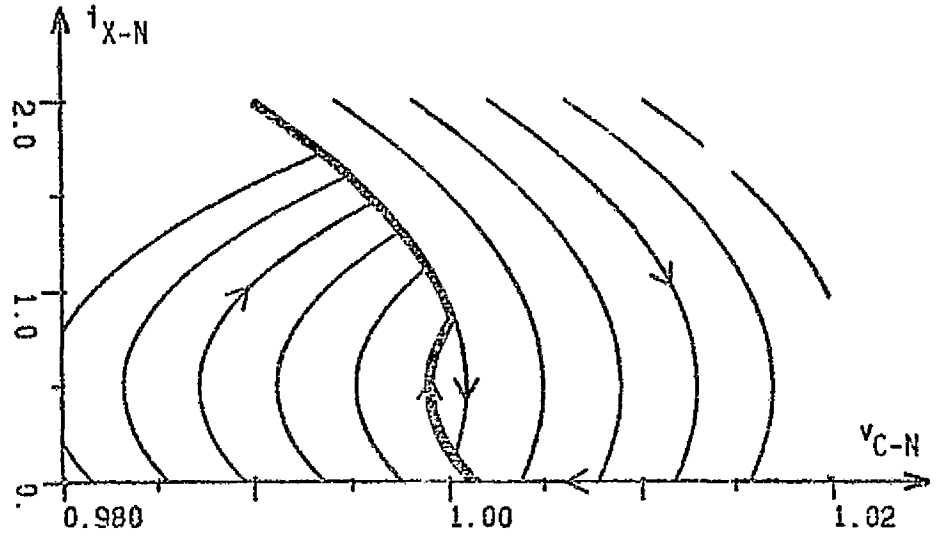

(A)

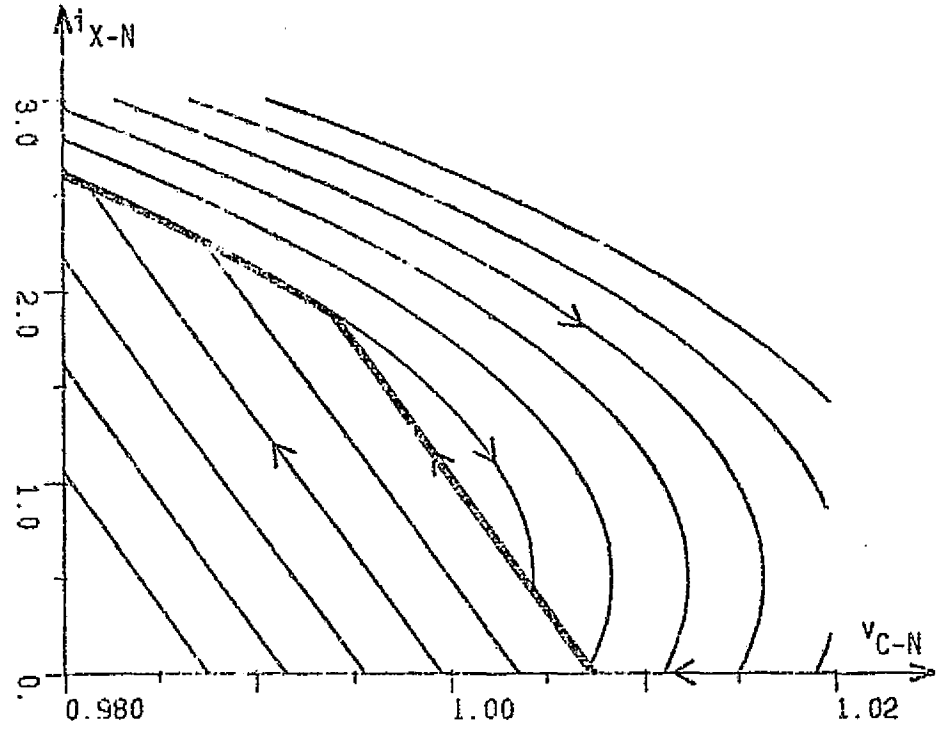

(B)

Fig. 4.12 State trajectories and switching boundaries (bold lines) for (A) the current step-up converter of Fig. 2.2 with $v_{I-N} = 1.5$ and $i_{O-N} = 0.5$, and (B) the current-or-voltage step-up converter of Fig. 2.3 with $v_{I-N} = 0.75$ and $i_{O-N} = 0.5$.

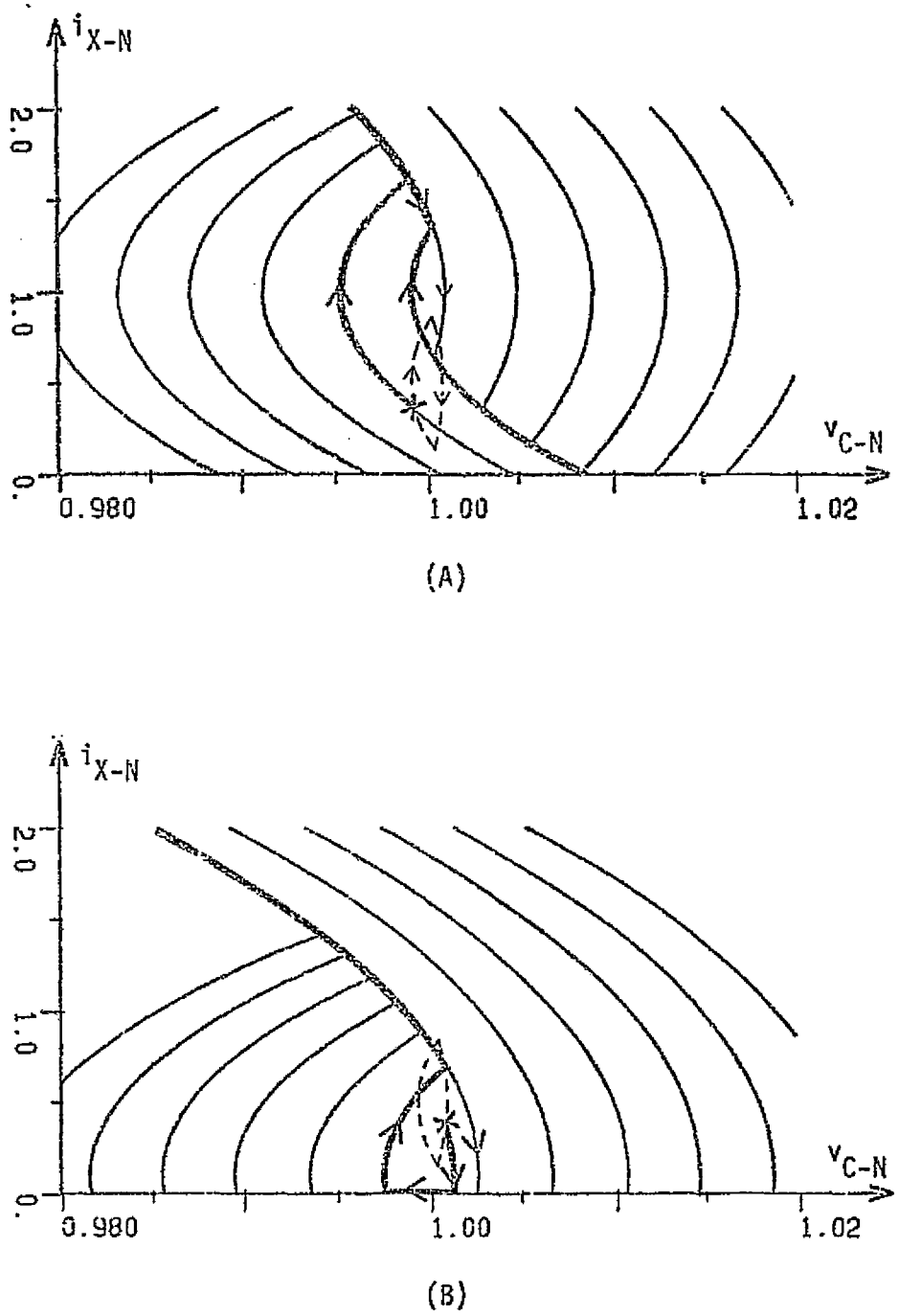

Fig. 4.13 Transient response of free-running current step-up converter system to step changes in i_{O-N} from 0.5 to (A) 1.0, and (B) 0.1. Dashed closed curves represent the original steady-state trajectory corresponding to $v_{I-N} = 1.5$ and $i_{O-N} = 0.5$.

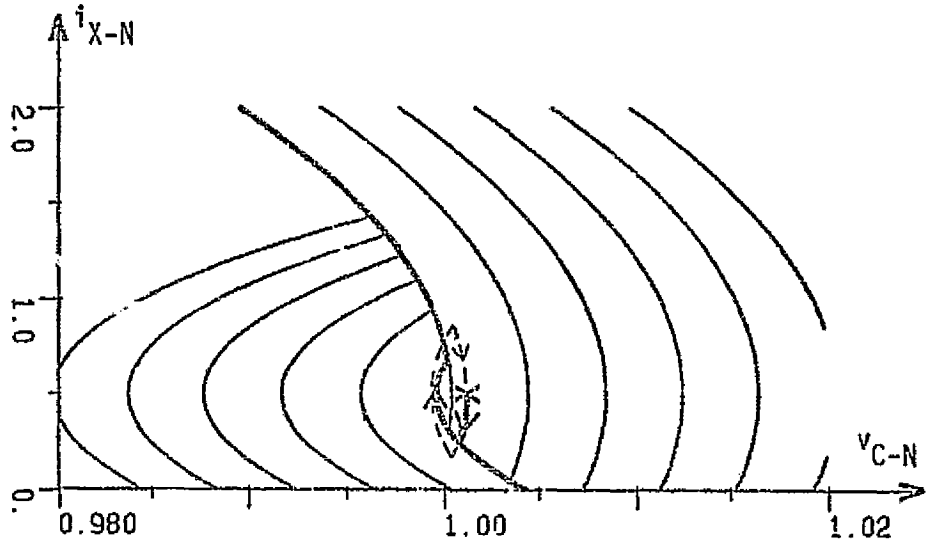

(A)

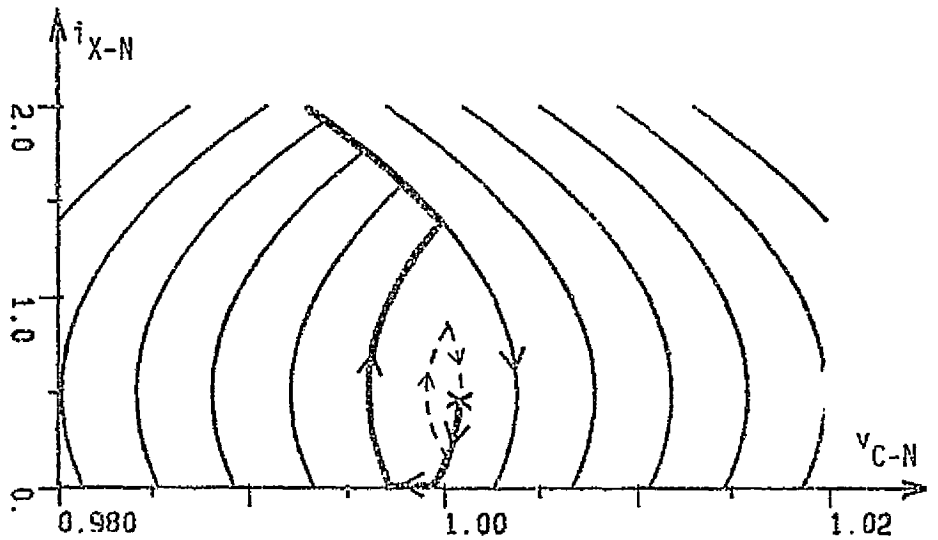

(B)

Fig. 4.14 Transient response of free-running current step-up converter system to step changes in v_{I-N} from 1.5 to (A) 1.25, and (B) 2.0. Dashed closed curves represent the original steady-state trajectory corresponding to $v_{I-N} = 1.5$ and $i_{O-N} = 0.5$.

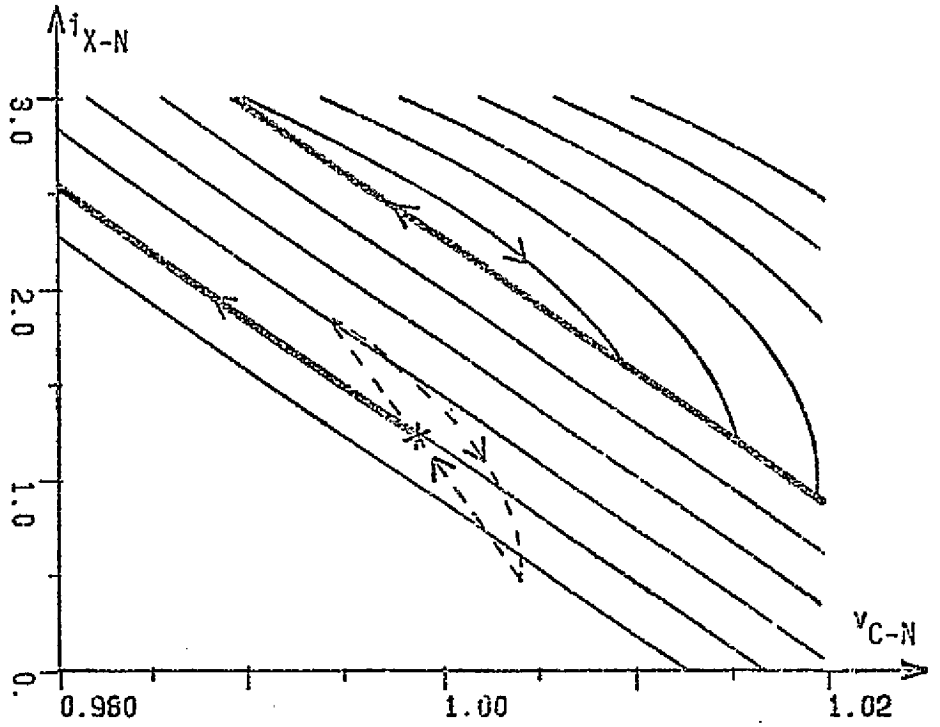

(A)

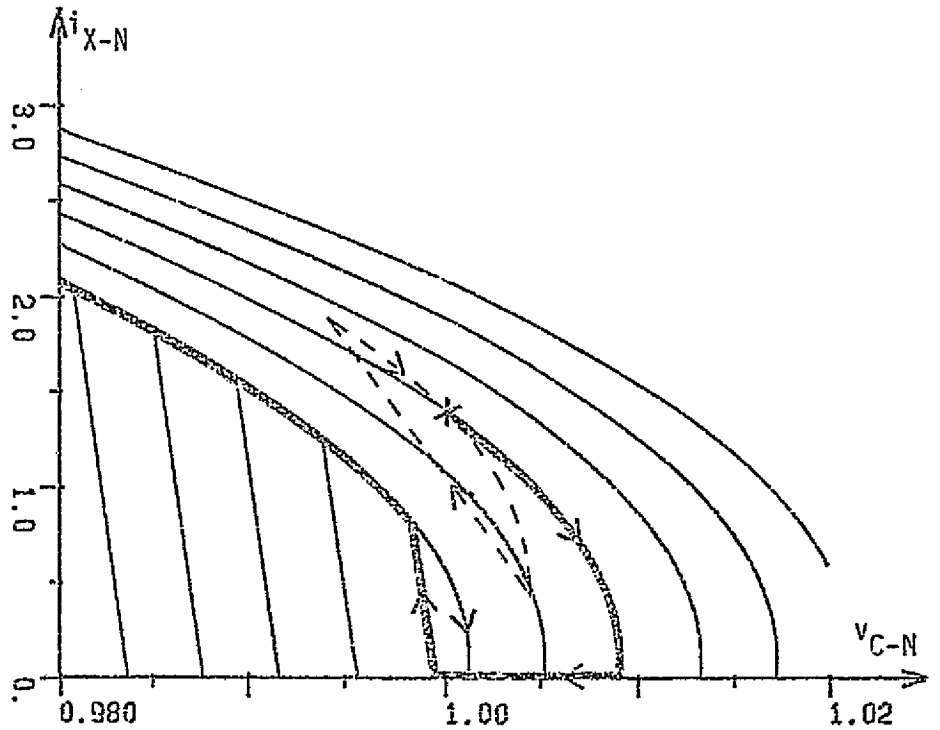

(B)

Fig. 4.15 Transient response of free-running current-or-voltage step-up converter system to step changes in i_{O-N} from 0.5 to (A) 1.0 and (B) 0.1. Dashed closed curves represent the original steady-state trajectory corresponding to $v_{I-N} = 0.75$ and $i_{O-N} = 0.5$.

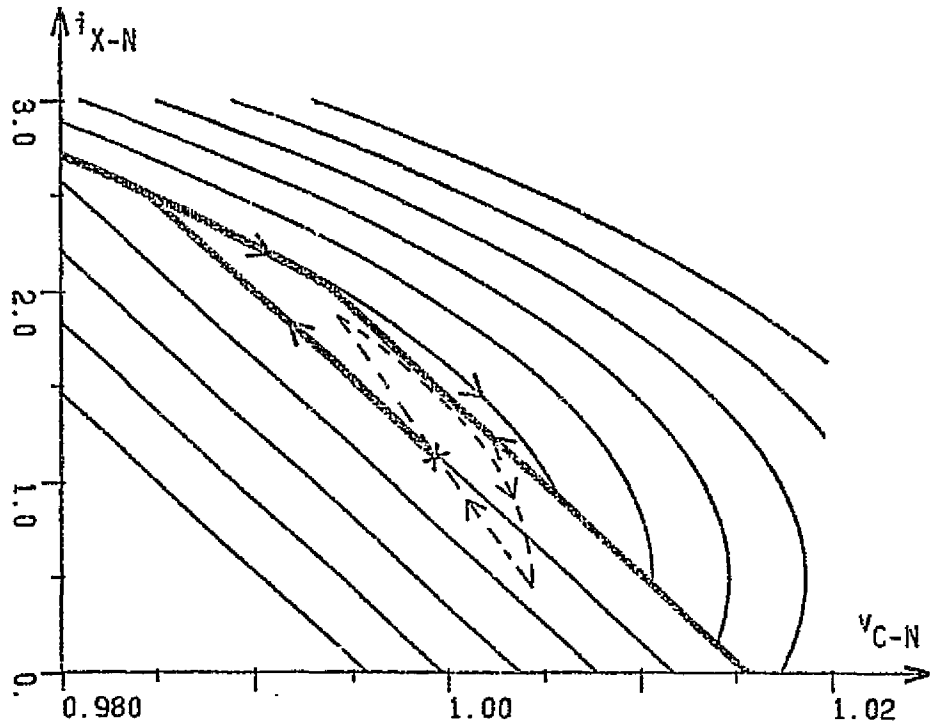

(A)

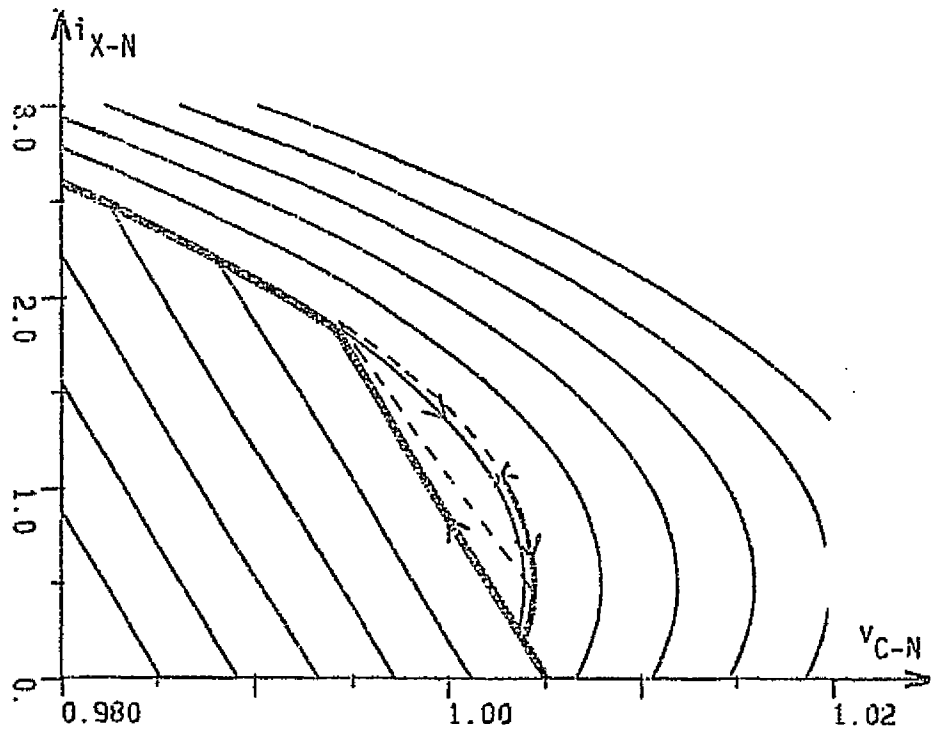

(B)

Fig. 4.16 Transient response of free-running current-or-voltage step-up converter system to step changes in v_{I-N} from 0.75 to (A) 0.5 and (B) 0.9. Dashed closed curves represent the original steady-state trajectory corresponding to $v_{I-N} = 0.75$ and $i_{O-N} = 0.5$.

Example 1. The response of the voltage step-up converter of Fig. 2.1 to a step change in output current from 50% to 100% of its rated value when operating under the influence of the state-trajectory control law is presented in Fig. 4.17. The timing parameter specified for this example is T_{on-N}=0.08 so that the conditions of this example correspond precisely to those of Example 2 in Chapter III with results shown in Fig. 3.5. The system state initially follows the steady-state trajectory which corresponds to the nominal operating conditions of this system as can be seen in both Figs. 4.17(A) and 3.5(A). The steady-state switch-off and switch-on points of this trajectory are indicated by the letters *b* and *a* respectively in Fig. 4.17(A). The load changes in these two examples occur at the same instant in time, but they are not synchronized to the same point on the initial steady-state trajectory so that the transient state trajectories in Figs. 4.17(A) and 3.5(A) do not begin at precisely the same point in the system state plane. The nature of the transient response of each of these systems is not dependent on the particular state at the instant of the load change, however, and thus qualitative comparisons of these data are justified. The same scale factors have been used for each of these figures to facilitate comparison of the data.

The change in load current in this example occurs after two units of normalized time. At t_N=2.0, the state-plane switching boundary immediately changes to accommodate the new load condition, and the system state, located at point *b* in Fig. 4.17(A), is suddenly well within the switch-on region of the plane and begins to follow an on-time trajectory toward the new switch-off line. After reaching this boundary at point *c* in the state plane, the converter power switch is turned off and the system state follows that off-time trajectory to the new steady-state condition. The

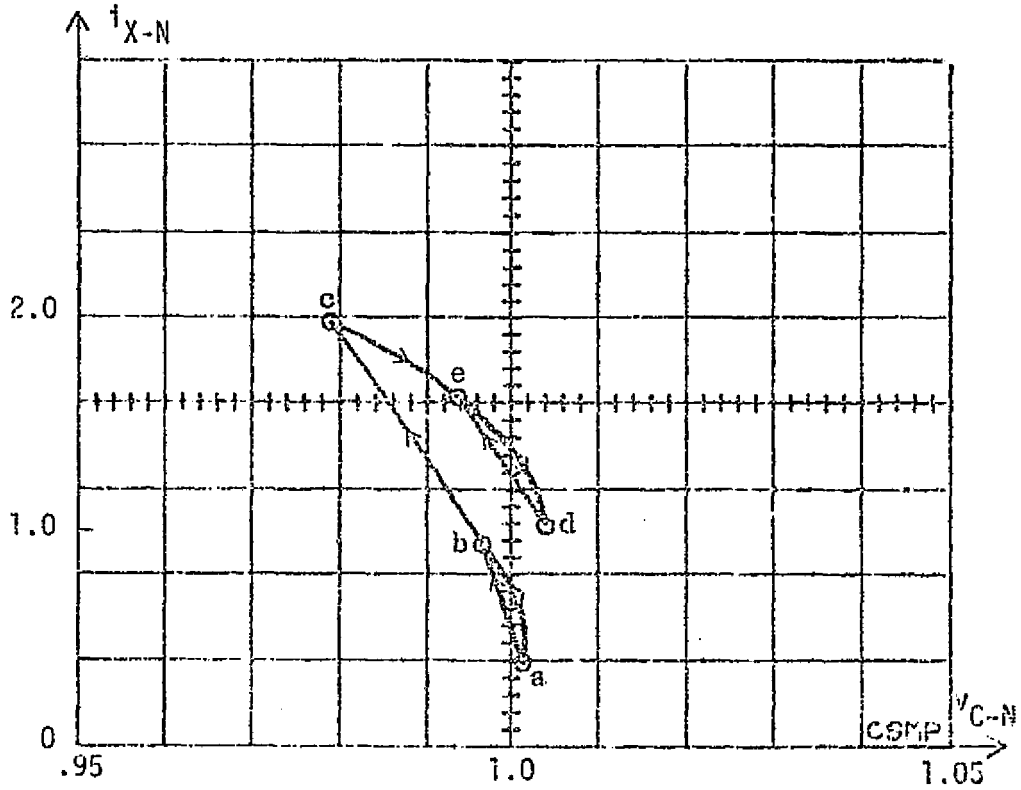

(A)

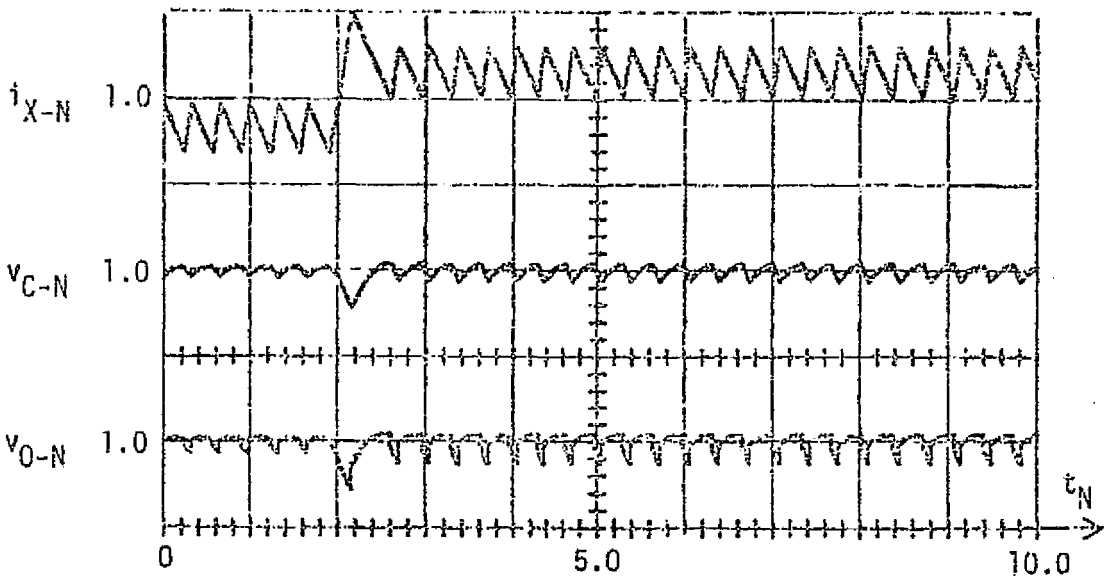

(B)

Fig. 4.17 CSMP generated response of free-running voltage step-up converter system for a step increase in i_{O-N} from 0.5 to 1.0. Scale factors for the time waveforms are, in normalized units per major division: i_{X-N}, 1.0/div; v_{C-N}, 0.05/div; and v_{O-N}, 0.05/div. The control law is in the constant on-time mode.

new steady-state switch-off and switch-on points are indicated by the letters *e* and *d* respectively in Fig. 4.17(A). The time waveforms presented in Fig. 4.17(B) illustrate the free-running nature of this converter during the single on/off transient cycle in which the on-time interval and the off-time interval are different from all of the other cycles. Before and after this transient cycle, the system operates with the specified fixed on-time, T_{on-N}, and because this system is operating in the continuous conduction mode for both load conditions, the switch duty cycle, and consequently the overall system switching frequency, is the same in both steady-state conditions.

The steady-state trajectory achieved for the new load condition is the only closed trajectory for this system which yields precisely the desired average output voltage for the given operating conditions and specified timing parameter, T_{on-N}. The peak-to-peak output voltage ripple for this heavier load condition is greater than it is for operation at 50% of the rated load, but it is the minimum which is physically obtainable with the given converter power stage components and externally imposed operating conditions. The ability of this system to achieve the desired steady-state trajectory at more than one operating point is possible because no fixed reference levels are imposed on the converter control subsystem. Also, the very fast and precise response of this system as observed in Fig. 4.17 is possible because no timing restrictions, such as minimum or maximum switching intervals, are imposed on this control function as they are, of necessity, in the conventional controllers described in Chapter III.

Example 2. The converter response illustrated in Fig. 4.18 corresponds to the same power stage configuration and the same load-switch conditions as are presented in Example 3 of Chapter III and illustrated in Fig. 3.7. This example illustrates the behavior of a constant on-time current step-up converter responding to a step-decrease in load current from 100% to 50% of its rated value. The new steady-state condition is achieved in this case in one off/on cycle of control, and again it is seen to yield the desired average output voltage for the new load condition.

Example 3. The response of a current-or-voltage step-up converter to a step-increase in load current from 10% to 50% of its rated value is presented in Fig. 4.19. This load-change condition and the converter power stage are the same as those presented in Example 7 of Chapter II and illustrated in Fig. 3.12. The system switching line for this example has been specified to yield a constant steady-state switching frequency when in both the continuous and the discontinuous conduction modes of operation. A single on/off transient cycle again leads to the desired steady-state trajectory for the new load condition, and except for the single transient cycle, the desired constant switching frequency is maintained.

Example 4. The current step-up converter of Fig. 2.2 operating in conjunction with the state trajectory control law in a constant switching frequency mode is illustrated in Fig. 4.20. The transient response displayed in this figure is to a step-decrease in input voltage from 1.5 to 1.25 times the rated average output voltage. The converter power stage and operating conditions for this example are the same as those presented in Example 8 of Chapter III and illustrated in Fig. 3.13. Since the

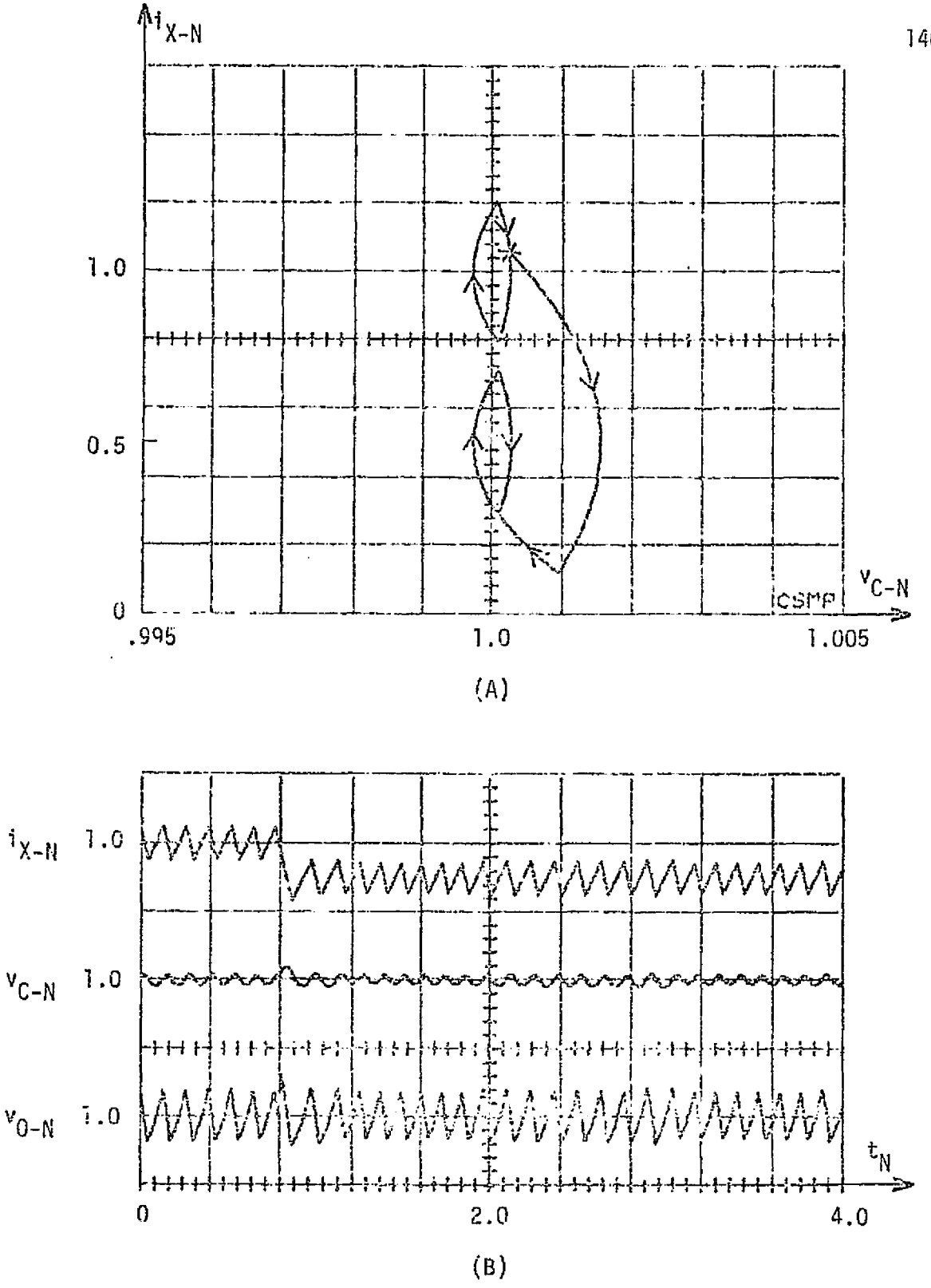

Fig. 4.18 CSMP generated response of free-running current step-up converter system for a step decrease in i_{O-N} from 1.0 to 0.5. Scale factors for the time waveforms are, in normalized units per major division: i_{X-N}, 1.0/div; v_{C-N}, 0.005/div; and v_{O-N}, 0.005/div. The control law is in the constant on-time mode.

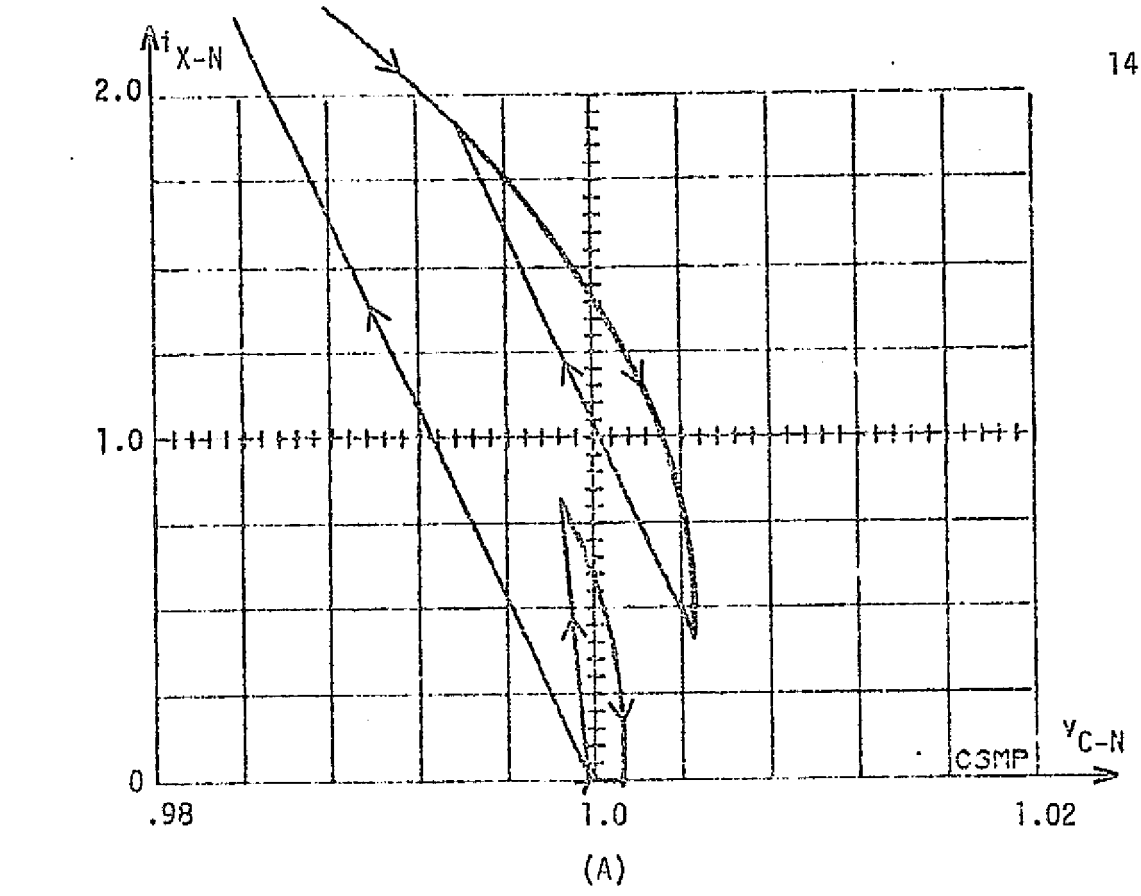

(A)

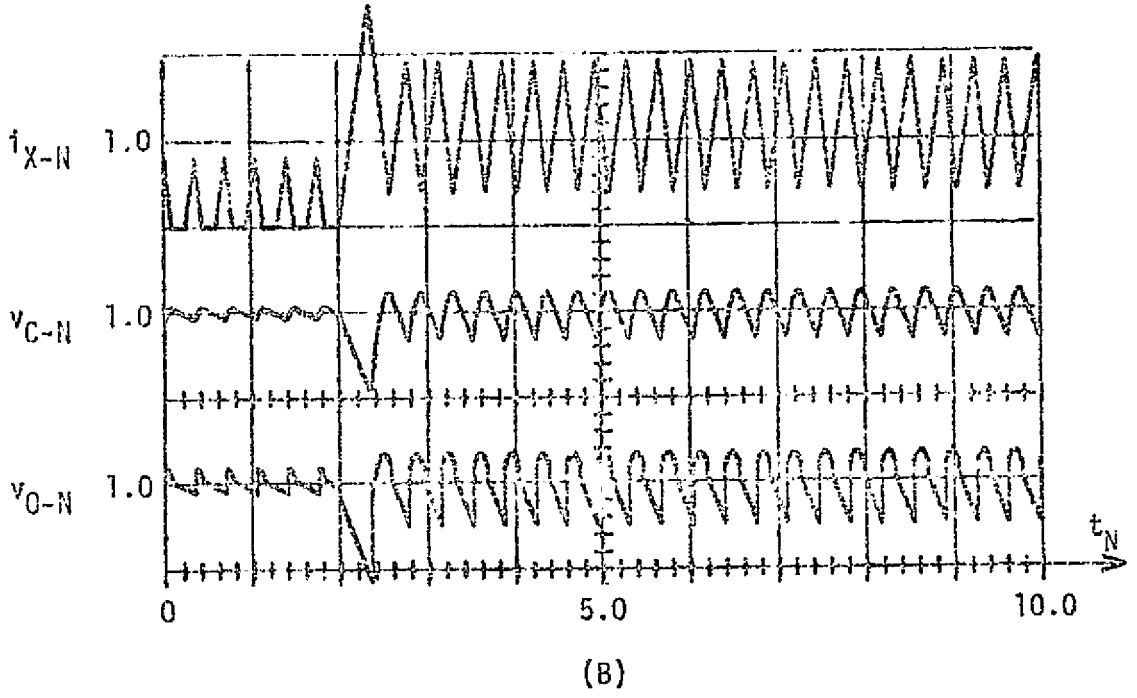

(B)

Fig. 4.19 CSMP generated response of free-running current-or-voltage step-up converter system for a step-increase in i_{O-N} from 0.1 to 0.5. Scale factors for the time waveforms are, in normalized units per major division: i_{X-N}, 1.0/div; v_{C-N}, 0.02/div; and v_{O-N}, 0.02/div. The control law is in the constant frequency mode.

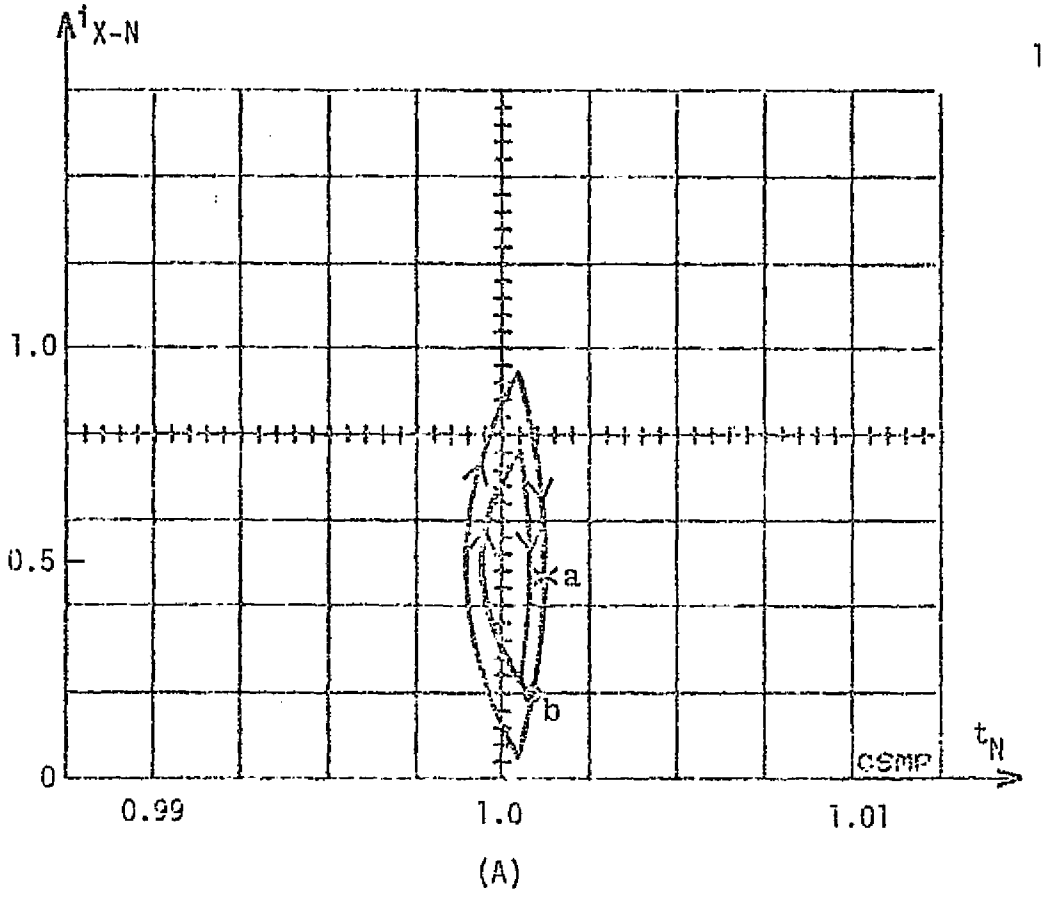

(A)

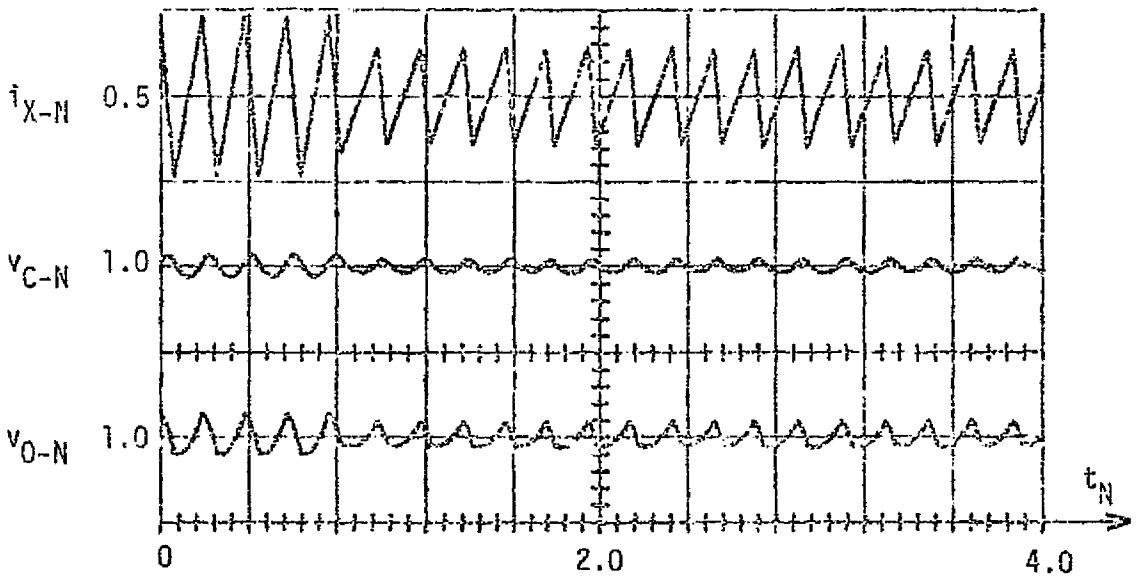

(B)

Fig. 4.20 CSMP generated response of free-running current step-up converter system for a step decrease in v_{I-N} from 1.5 to 1.25. Scale factors for the time waveforms are, in normalized units per major division: i_{X-N}, 0.5/div; v_{C-N}, 0.01/div; and v_{O-N}, 0.01/div. The control law is in the constant frequency mode.

shapes of the system off-time trajectories for the current step-up converter configuration are independent of the input voltage, v_{I-N}, the system state trajectory in this example does not appear to change at the instant of the input voltage change, point *a* in Fig. 4.20(A), because this change occurs during a power switch off-time. The system switching line does change at the instant of the input voltage change, however, and when the new switch-on boundary is crossed at point *b*, the power switch is closed and the new steady-state trajectory is very quickly attained with no output voltage or inductor current overshoot or undershoot. The off-time segment of the new steady-state trajectory is the same shape as the original off-time trajectory, but it is displaced to the left yielding a smaller peak-to-peak output voltage ripple.

4.5 Conclusions

The qualitative insight gained through observing the behavior of energy-storage dc-to-dc converters in the system state plane has led to the development of a state-trajectory control law for dc-to-dc converters. The control law is conceptually quite simple and is easily visualized in the system state plane. It can be represented mathematically by means of relatively simple algebraic equations which can be used to implement the graphical conception. The realizability of this control law and the excellent static and dynamic performance which result for converters operating in conjunction with it have been demonstrated through digital computer simulations of actual converter systems.

The mathematical foundation of this control technique enables one to predict, *a priori*, the performance characteristics of any converter system which is controlled by it. Such measures as overshoot or undershoot

of voltages and currents, and transient settling times of the system variables can be computed from simple algebraic expressions which can be derived from the converter power stage models presented in Chapter II. The control function is completely free of the usual limiting constraints, such as fixed operating frequencies, fixed power switch on-time intervals, or fixed reference threshold levels which cannot adapt to changes in the system operating conditions and thus tend to hinder the successful performance of converter systems. Moreover, this control technique is based on a knowledge of the behavioral characteristics of the converter power stages as revealed through the system state plane, and it uses this knowledge to guide the system state to a desired location in that plane. Thus, converter systems which employ this control technique offer a unique combination of excellent performance--inherent stability, precise static regulation, and fast dynamic response--and a straightforward understanding of the manner in which this performance is accomplished and the design procedures which enable its implementation.

Chapter V

PRACTICAL CONSIDERATIONS OF THE STATE-TRAJECTORY CONTROL LAW

5.1 Introduction

The state-trajectory control law presented in Chapter IV is based on a general conceptual visualization of the behavior of dc-to-dc converters and can, in theory, be formulated from converter models of arbitrary complexity. The particular equations used in Chapter IV to illustrate the mathematical implementation of this control concept are derived from the converter models presented in Chapter II in which most of the elements are assumed to be ideal components. Because of the nonideal nature of actual circuit components, however,the state trajectories of actual dc-to-dc converters do not precisely coincide with those of such approximate mathematical models. Consequently, if switching boundaries which are derived from idealized converter models are applied to actual physical systems which are comprised of nonideal components, the resultant system performance does not meet the theoretical limits described in Chapter IV, and the deviation of the actual performance from the theoretical limits can be predicted from a consideration of the nature and severity of the approximations which are incorporated into the converter power stage model.

A principal purpose of this chapter is to demonstrate how the state-plane analysis technique described in Chapter II can be used to ex-

plore the influence of various converter modeling assumptions on the shape and location of the state-trajectory switching boundaries which are derived from those models, and to describe the deviations in system behavior which result from using those switching boundaries in the converter control process. Throughout this chapter, the voltage step-up converter is used to illustrate and verify theoretical discussions and to provide computer simulation data for further clarification of the concepts presented. A relatively complex mathematical model of this converter is presented, and the shapes of the state trajectories which correspond to it are compared to those which are presented in previous chapters and which correspond to the less complex model presented in Chapter II. The behavior of this complex model when operating in conjunction with the state-plane switching boundary derived in Chapter IV is illustrated by means of a digital computer simulation and compared to the theoretical behavior which is described in Chapter IV. From the insight gained in this investigation, a third model of the voltage step-up dc-to-dc converter is proposed which incorporates those elements of the complex model which are the primary contributors to the discrepancies observed in the behavior of the two previously described models. The state-plane switching boundary derived from this third converter model is applied to the complex model and the resultant system performance is again compared to the theoretical limits described previously.

A fundamental tenet held throughout the development of this dissertation is the belief that the theoretical limits in converter performance which are revealed through a state-plane analysis can be achieved only if all of the information which is available in the converter power stage is properly used in the control decision making process. As demonstrated in

Chapter III, however, the control of dc-to-dc converters can be successfully accomplished with a less complete processing of the system information, but the resulting system performance degrades accordingly. Likewise, it is possible, if desired, to make additional approximations to the state-plane switching boundaries presented in Chapter IV in order to simplify their implementation and still achieve good system performance, although not the theoretical limits predicted through analysis. Thus, a second purpose of this chapter is to introduce the nature of such simplifications to the implementation of the switching boundaries and to indicate a basic approach to exploring them. Because of the mathematical nature of this control law, numerous possibilities exist for such modifications, and the discussions presented in this chapter are intended only to indicate the types of results which are possible and to give an example of such a control law modification. Additional features which can be incorporated into the control function to accommodate particular converter application requirements are also indicated in this chapter, but the details of these investigations are left to the reader.

5.2 Effects of Modeling Assumptions on the Switching Boundary

Most of the state trajectories which are presented as examples throughout this dissertation are comprised of segments of parabolas and straight lines as established by the mathematical models presented in Chapter II and given by equations (2.6) through (2.8) for the voltage step-up converter, (2.11) through (2.13) for the current step-up converter, and (2.16) through (2.18) for the current-or-voltage step-up configuration. More detailed models of these converter systems yield solution trajectories which are combinations of logarithmic spirals and generalized parabolas[7] One

[7] Parabolas of the form $v_{C-N} = \alpha i_{X-N}^{\beta} + \gamma$, where α, β and γ are constants with $\beta > 0$.

such model of the voltage step-up converter is presented in Fig. 5.1. This model includes resistive parasitic elements such as source resistance, r_{S-N}, inductor winding resistance, r_{X-N}, and semiconductor bulk resistances, r_{D-N} for the diode, and r_{Q-N} for the power switch, which cause a loss of efficiency in the converter operation. Also included in this model are a switch saturation voltage drop, V_{Q-N}, and a diode forward voltage drop, V_{D-N}. No assumptions are made concerning the relative magnitudes of the peak to peak output voltage ripple and the average value of the output voltage, and the validity of this model is not dependent on the converter switching frequency beirg much greater than the natural frequency of the inductor-capacitor combination in the converter power stage. The piecewise linear approximation to this switching system is preserved in this model, however, as the switches are assumed to be ideal open circuits during their off-time intervals, and the transition from an open to a closed condition and *vice versa* is assumed to occur instantly on command.

The solutions to the state equations which represent the behavior of this model are logarithmic spirals during the power switch off-time intervals and parabolas during the switch on-time intervals. The shapes of these trajectories relative to the shapes of the state trajectories which correspond to the model of the voltage step-up converter presented in Fig. 2.5 are illustrated in Fig. 5.2. From point *A*, the off-time trajectory for the converter model of Fig. 2.5 is plotted as the parabola labeled *a*, whereas the logarithmic spiral corresponding to the model of Fig. 5.1 is shown as plot *b*. In the region of the state plane which corresponds to normal steady-state operation, the shapes of these two trajectories are quite similar, with the observable differences between them being caused by the parasitic losses which are included in the model of Fig. 5.1 but assumed

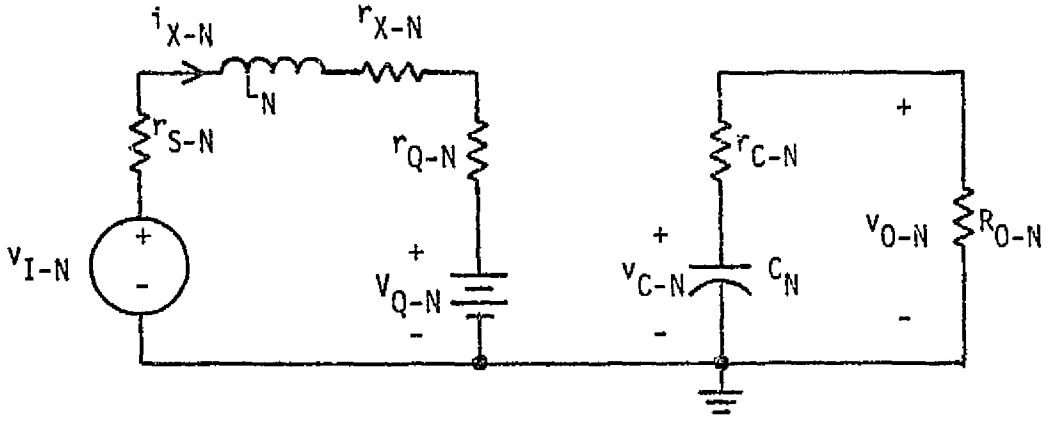

$$\frac{di_{X-N}}{dt_N} = -\frac{(r_{S-N} + r_{X-N} + r_{Q-N})}{L_N} i_{X-N} + \frac{v_{I-N} - V_{Q-N}}{L_N}$$

$$\frac{dv_{C-N}}{dt_N} = -\frac{1}{C_N(r_{C-N} + R_{O-N})} v_{C-N}$$

(A)

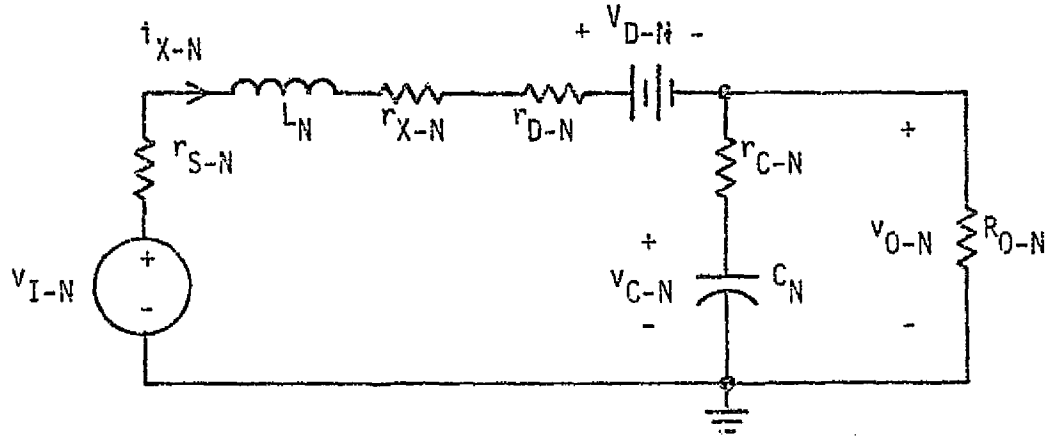

$$\frac{di_{X-N}}{dt_N} = -\frac{(r_{S-N} + r_{X-N} + r_{D-N} + r_{C-N}R_{O-N}/(r_{C-N} + R_{O-N}))}{L_N} i_{X-N}$$

$$- \frac{R_{O-N}}{L_N(r_{C-N} + R_{O-N})} v_{C-N} + \frac{v_{I-N} - V_{D-N}}{L_N}$$

$$\frac{dv_{C-N}}{dt_N} = \frac{R_{O-N}}{C_N(r_{C-N} + R_{O-N})} i_{X-N} - \frac{1}{C_N(r_{C-N} + R_{O-N})} v_{C-N}$$

(B)

Fig. 5.1 Detailed model and mathematical representation of the voltage step-up converter during (A) power switch on-time, and (B) power switch off-time.

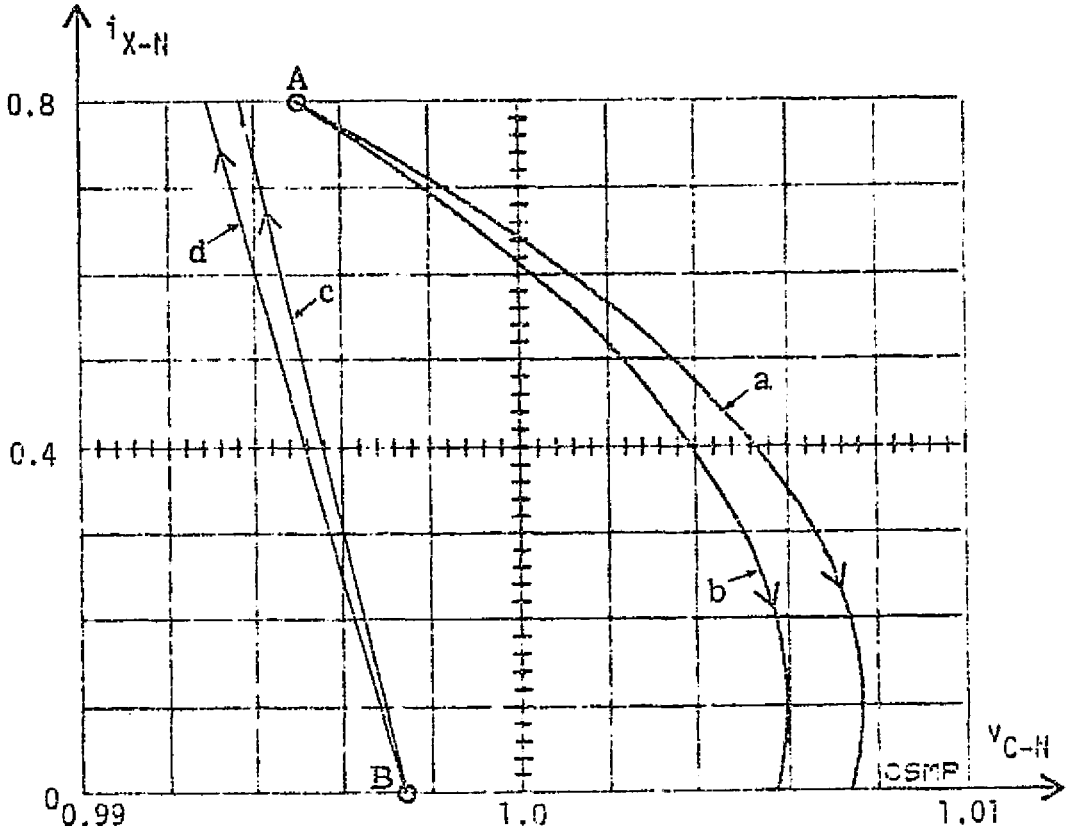

Fig. 5.2 Comparison of shapes of state trajectories for two different models of the voltage step-up converter. Off-time trajectory *a* and on-time trajectory *c* correspond to the model of Fig. 2.5. Trajectories *b* and *d* correspond to the model of Fig. 5.1.

negligible in the model of Fig. 2.5. Because of these losses, the same initial value of reactor current in the system of Fig. 5.1 is unable to charge the output capacitor during the power switch off-time intervals as fully as the system of Fig. 2.5 which is lossless. Similarly, the on-time trajectories for these two models emanating from the common initial state marked *B*, spread apart as time increases because the effective voltage across the inductor for trajectory *d* is less than it is for trajectory *c* and consequently the reactor current cannot rise as quickly.

If the switching boundary derived in Chapter IV, which is based on the model of Fig. 2.5, is used to control a converter whose behavior more nearly corresponds to the model of Fig. 5.1, the system performance which is predicted and illustrated in Chapter IV does not result. An example of the type of behavior which does result under these conditions is illustrated in Fig. 5.3. In this figure, the steady-state off-time and on-time trajectories, and consequently the state-plane switching boundary, derived from the model of Fig. 2.5 for $v_{I-N} = 0.75$ and $i_{O-N} = 0.5$ are shown as bold lines. As illustrated in Fig. 5.2, however, the actual off-time trajectory for the converter model of Fig. 5.1 curves inside of the trajectory which corresponds to the idealized model, and consequently the state of the system crosses the switch-on line at point *a* with a higher value of current and a lower voltage level than it would have if the simulated power stage were lossless--point *b*. The on-time trajectory which ensues has a lower slope than the switch-on line and subsequently intersects the switch-offboundary at point *c* rather than point *d*, and the steady-state trajectory which results is *a-c-a* rather than *b-d-b* which is predicted in theory. Thus, one can see that the basic principles of operation of the state-trajectory control law as developed in Chapter IV still apply for this case, but that the steady-state trajectory which results in this system does not

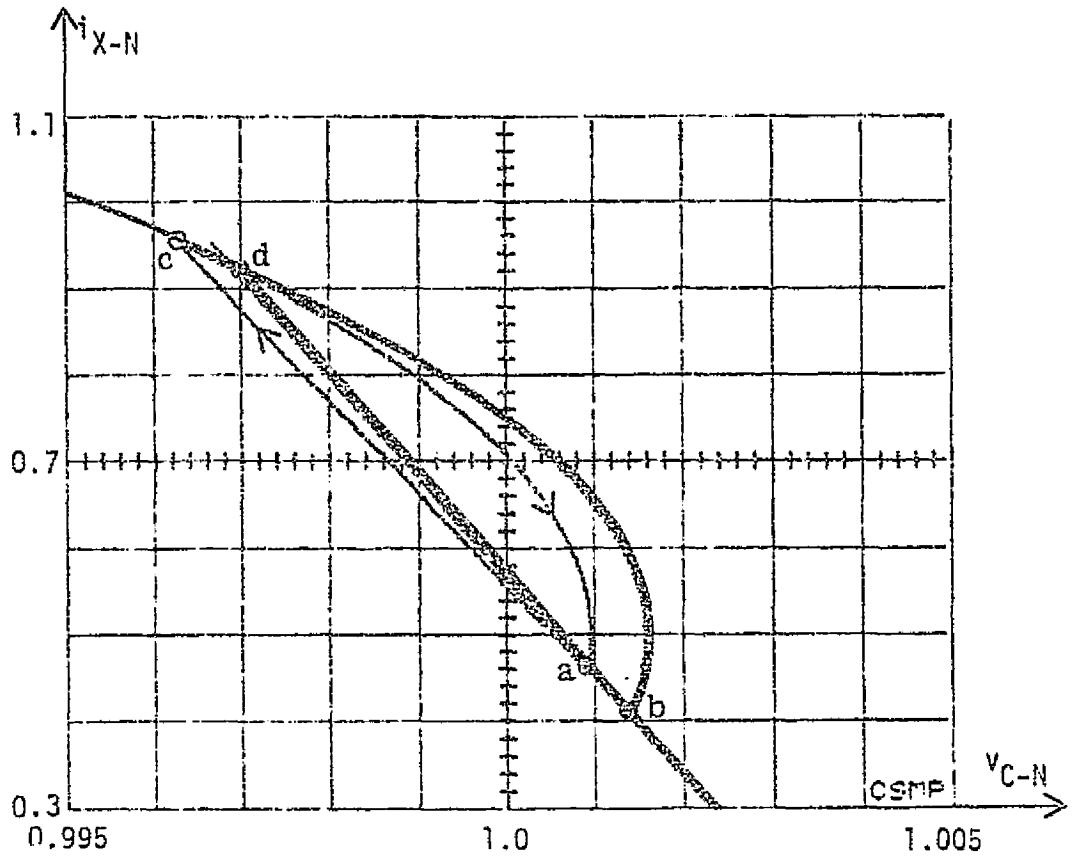

Fig. 5.3 Steady-state trajectory, a-c-a, of the voltage step-up converter of Fig. 2.1 with $v_{I-N} = 0.75$ and $i_{O-N} = 0.5$[8] modeled as shown in Fig. 5.1 but controlled with a switching boundary, bold line, derived from the simplified converter model of Fig. 2.5.

[8] In the model of Fig. 5.1, the load condition is determined by the value of resistance, R_{O-N}. The value of R_{O-N} used in simulating this model is computed from $R_{O-N} = V_{O-N}/i_{O-N}$, where i_{O-N} is considered to be the desired average output current. Thus, $i_{O-N} = 0.5$ for the model of Fig. 2.5 corresponds to $R_{O-N} = 2.0$ for the model of Fig. 5.1.

coincide with the unique desired solution, and as would be expected intuitively, the average output voltage in this case is less than the desired average output voltage because of the loss of power in the converter power stage. To compensate for this loss of power, the location of the desired steady-state trajectory must be shifted to accommodate higher reactor current levels as illustrated later in this section.

A more complete illustration of this dependence of the converter behavior on the particular switching boundary generated in the control process is presented in Figs. 5.4 and 5.5. The response of the voltage step-up converter of Fig. 2.1 modeled as shown in Fig. 2.5 is presented in Fig. 5.4. The state-plane switching boundary used in the control of this system is derived from the same converter model, and thus the shapes of the system trajectories coincide with the shape of the switching boundary and the theoretically predicted response of this system to a step change in load current from 100% to 50% of its rated value is observed in the simulation. The format of this and succeeding examples is the same as the format used in previous chapters so that comparisons of the data can be made if desired. As can be seen in Fig. 5.4, the desired average output voltage for this system is achieved for both load conditions, and the transition from one steady-state condition to another is accomplished in one off/on cycle of control.

Using the same switching boundary to control the voltage step-up converter model depicted in Fig. 5.1 results in the system behavior illustrated in Fig. 5.5. As discussed previously, the losses within this converter power stage model cause the average output voltage to fall below the desired value. At higher power levels, rated load for example, these losses increase and the average output voltage falls even more as the steady-

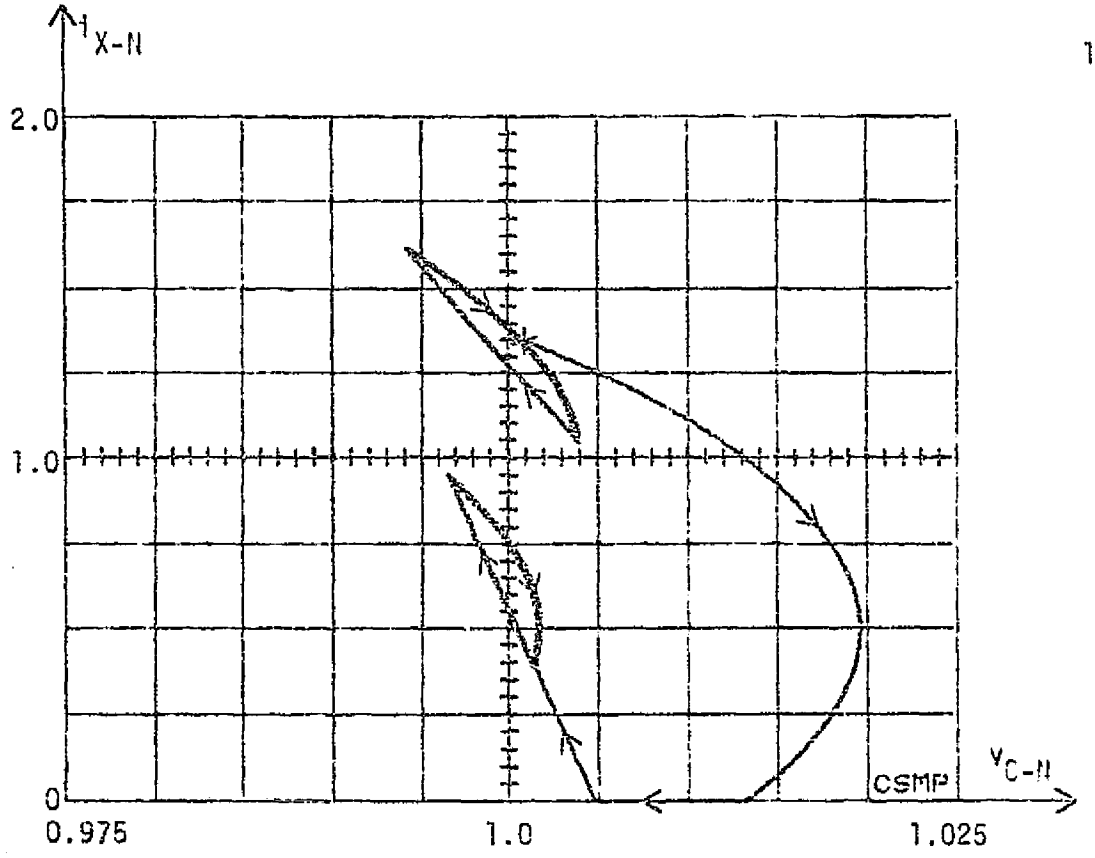

(A)

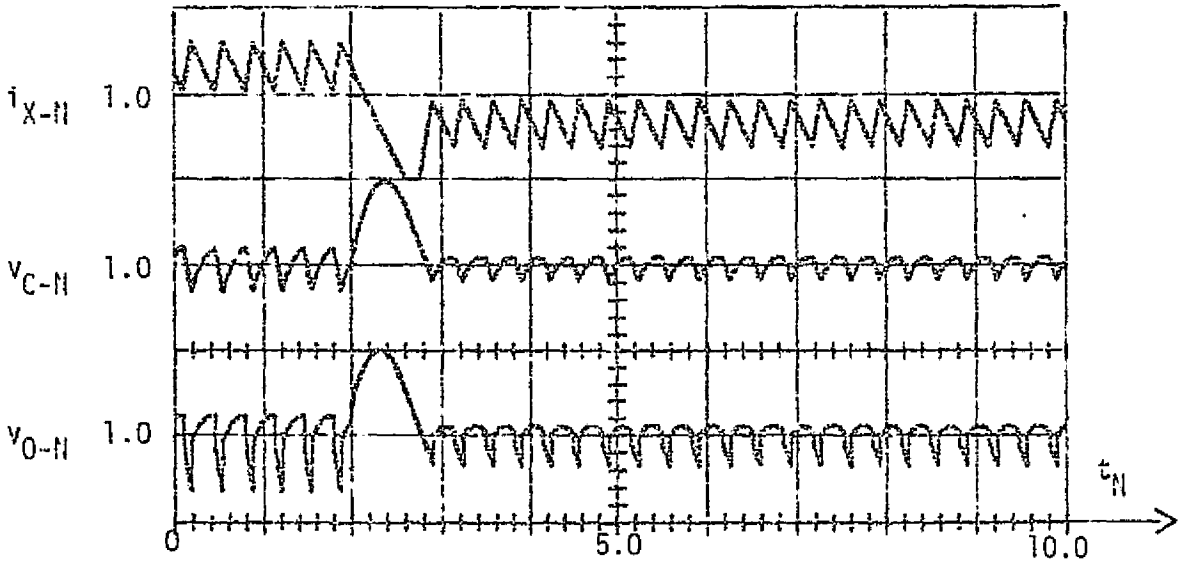

(B)

Fig. 5.4 CSMP generated response of the voltage step-up converter of Fig. 2.1 modeled as shown in Fig. 2.5 and controlled with a switching boundary derived from the same model. The operating conditions are $v_{I-N} = 0.75$ and i_{O-N} switches from 1.0 to 0.5 at $t_N = 2.0$. Scale factors for the time waveforms are, in normalized units per major division: i_{X-N}, 1.0/div; v_{C-N}, 0.02/div; and v_{O-N}, 0.02/div.

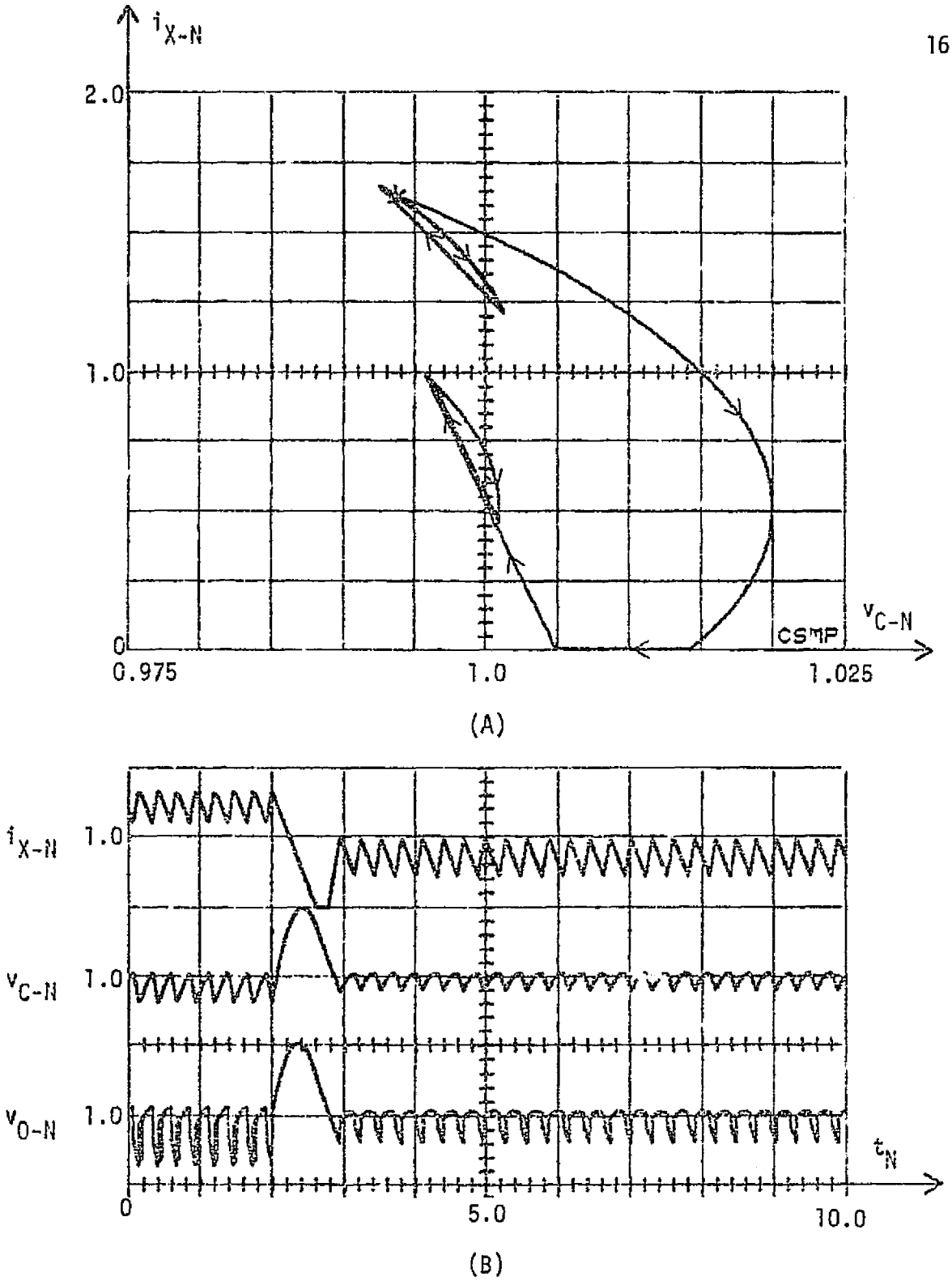

Fig. 5.5 CSMP generated response of the voltage step-up converter of Fig. 2.1 modeled as shown in Fig. 5.1 but controlled with a switching boundary derived from the model of Fig. 2.5. The operating conditions are v_{I-N} = 0.75 and i_{O-N} switches from 1.0 to 0.5[9] at t_N = 2.0. Scale factors for the time waveforms are, in normalized units per major division: i_{X-N}, 1.0/div; v_{C-N}, 0.02/div; and v_{O-N}, 0.02/div.

[9] R_{O-N} switches from 1.0 to 2.0.

state trajectory shifts to the left. Also, since the unique desired steady-state trajectory cannot be achieved under these conditions, the frequency of operation deviates from the specified value, for as discussed in section 4.3.2, the frequency of operation of these converter configurations is very much dependent on the particular steady-state trajectory being traversed, and any change in the location of this equilibrium trajectory causes a change in the system's operating frequency. In spite of these inaccuracies in the static performance characteristics of the converter, however, the basic switching decision process is the same as specified in theory and the transition from one steady-state condition to another is again accomplished in one off/on cycle of control.

5.3 Modified Switching Boundary

With an understanding of the effects of parasitic losses in the converter power stage on the shapes of the system state trajectories, it is possible to derive a state-trajectory switching boundary which can accommodate those internal losses and consequently enable actual systems to more nearly accomplish the theoretical performance described previously. Such a switching boundary can be derived from the converter model depicted in Fig. 5.6. This model is the same as that shown in Fig. 2.5 except that the effects of the parasitic losses in the power stage components are included. The switch saturation voltage drops are modeled as constant voltage sources of amplitude V_{Q-N} for the converter power switch during an on-time interval and V_{D-N} for the diode during the converter off-time intervals. The effects of the resistive losses are modeled as voltage sources whose amplitudes are dependent on the value of the output current, i_{O-N}. This approximation eliminates the exponential terms in the system solutions and

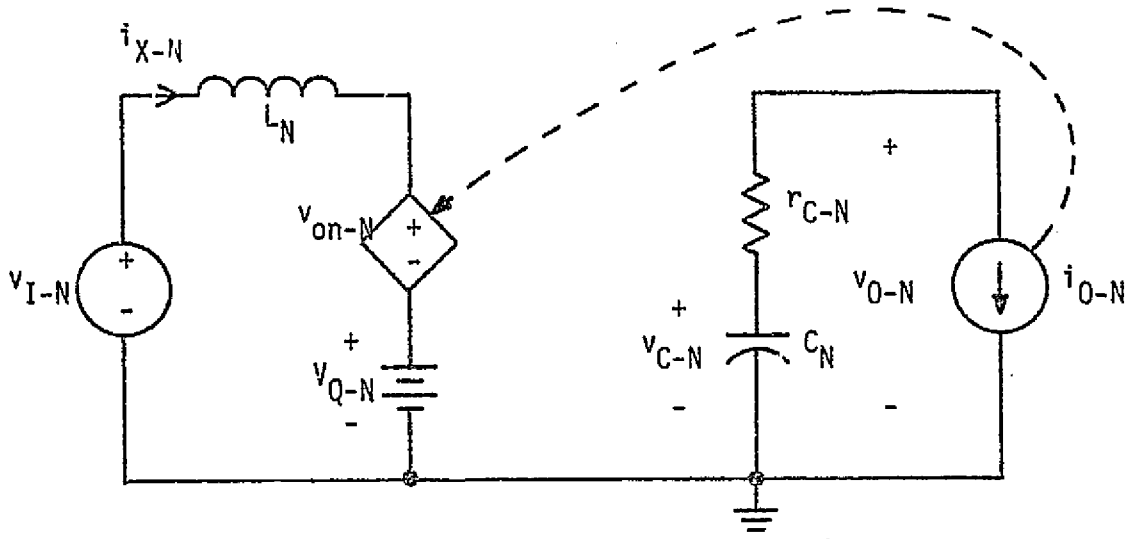

$$\frac{di_{X-N}}{dt_N} = \frac{v_{I-N} - v_{on-N} - V_{Q-N}}{L_N} \qquad \frac{dv_{C-N}}{dt_N} = -\frac{i_{O-N}}{C_N}$$

where $v_{on-N} = (r_{S-N} + r_{X-N} + r_{Q-N})\, i_{O-N}$

(A)

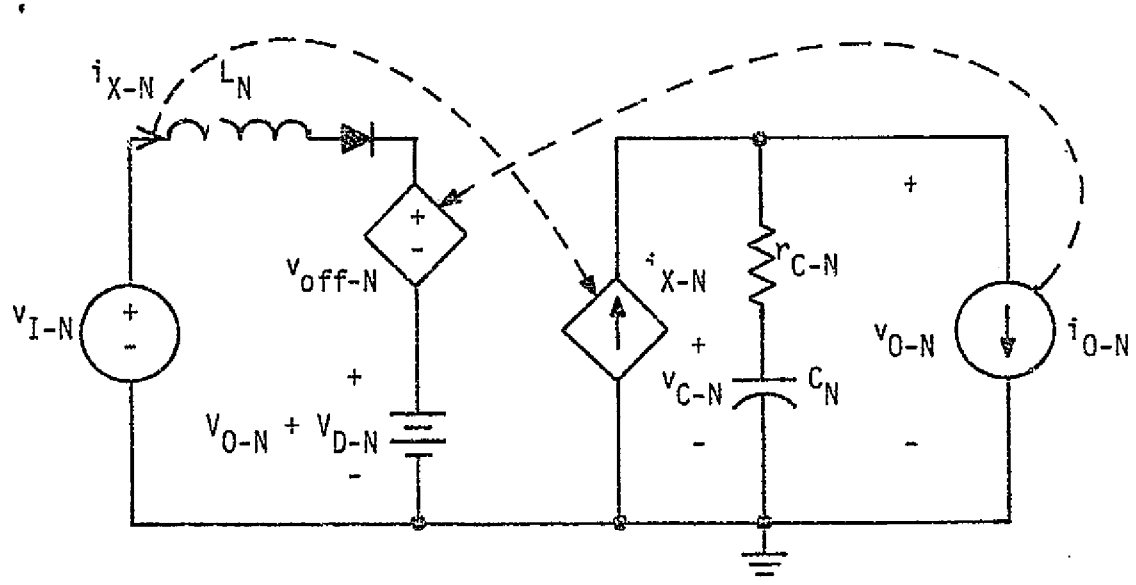

$$\frac{di_{X-N}}{dt_N} = \frac{v_{I-N} - v_{off-N} - V_{O-N} - V_{D-N}}{L_N} \qquad \frac{dv_{C-N}}{dt_N} = \frac{1}{C_N}(i_{X-N} - i_{O-N})$$

where $v_{off-N} = (r_{S-N} + r_{X-N} + r_{D-N} + r_{C-N})\, i_{O-N}$

(B)

Fig. 5.6 Model and mathematical representation which includes the effects of parasitic losses but preserves the parabolic shape of the off-time trajectories for the voltage step-up converter.

thus preserves the parabolic nature of the converter off-time trajectories and the linear nature of the on-time trajectories. The dependency of these voltage sources on the value of the output current enables this model to accommodate the effect of higher output currents causing greater resistive losses within the converter power stage as described previously. Other values of current, such as the average reactor current, could also be used to determine the magnitudes of these dependent sources, but the output current has been chosen in this case because it is the simplest to implement.

The solution trajectories corresponding to this model are parabolas during the power switch off-time intervals and straight lines during the switch on-time intervals as given by equations (5.1) through (5.3).

$$v_{C-N} = - \frac{L_N \, i_{O-N}}{C_N \, (v_{I-N} - v'_N)} \; i_{X-N} + K_1 \tag{5.1}$$

$$v_{C-N} = - \frac{L_N}{2 \, C_N \, (v''_N - v_{I-N})} \; i^2_{X-N} + \frac{L_N \, i_{O-N}}{C_N \, (v''_N - v_{I-N})} \; i_{X-N} + K_2 \tag{5.2}$$

$$i_{X-N} = 0 \tag{5.3}$$

where

$$v'_N = V_{Q-N} + (r_{S-N} + r_{X-N} + r_{Q-N}) \; i_{O-N} \tag{5.4}$$

and

$$v''_N = V_{O-N} + V_{D-N} + (r_{S-N} + r_{X-N} + r_{D-N} + r_{C-N}) \; i_{O-N} \tag{5.5}$$

K_1 and K_2 are constants which are functions of the circuit component values,

the converter operating conditions, and the particular initial states for the respective switching intervals and are given by

$$K_1 = \frac{L_N\, i_{O-N}}{C_N\,(v_{I-N} - v_N')}\, i_{X-N}\,(t_N^\circ) + v_{C-N}\,(t_N^\circ) \tag{5.6}$$

and

$$K_2 = \frac{L_N}{2\,C_N\,(v_N'' - v_{I-N})}\, i_{X-N}^2\,(t_N') - \frac{L_N\, i_{O-N}}{C_N\,(v_N'' - v_{I-N})}\, i_{X-N}\,(t_N') + v_{C-N}\,(t_N') \tag{5.7}$$

Thus, following the procedure established in Chapter IV, a switching boundary can be established by selecting the off-time and on-time trajectories which correspond to steady-state operation for the given system. The steady-state switch-off point for this model can be derived as demonstrated in Appendix A, and the resultant expressions for the voltage step-up converter in the constant frequency mode of operation are presented in Table 5.1.

A comparison of the shapes of the off-time and on-time trajectories which correspond to the models of Fig. 5.6 and 5.1 is presented in Fig. 5.7, and as can be seen in this figure, the shapes of these trajectories are nearly identical in the displayed region of the state plane. The off-time trajectory corresponding to the model of Fig. 5.1 and labeled *a* curves slightly under that of the model of Fig. 5.6, trajectory *b*, but the on-time trajectories coincide exactly. Thus, the inclusion of the power stage losses in the converter model has improved the effectiveness of the switching boundary considerably, even though the approximations which

Table 5.1

Location of Steady-State Switch-Off Point for the Modified Model of the Voltage Step-Up Converter

CONTINUOUS CONDUCTION OPERATION
$$i_{B-N} = \frac{v''_N - v'_N}{v_{I-N} - v'_N} i_{O-N} + \frac{T_N (v_{I-N} - v'_N)(v''_N - v_{I-N})}{2 L_N (v''_N - v'_N)} \quad (5.6)$$
$$v_{B-N} = V_{O-N} - \frac{(v''_N - v_{I-N}) i_{O-N} T_N}{2 C_N (v''_N - v'_N)} - \frac{(v''_N - v_{I-N})(v_{I-N} - v'_N)^3 T_N^2}{12 L_N C_N (v''_N - v'_N)^3} \quad (5.7)$$
DISCONTINUOUS CONDUCTION OPERATION
$$i_{B-N} = \sqrt{\frac{2 T_N i_{O-N} (v''_N - v_{I-N})}{L_N}} \quad (5.8)$$
$$v_{B-N} = V_{O-N} - \frac{i_{O-N} T_N}{2 C_N} + \frac{i_{O-N}}{3 C_N} \sqrt{\frac{2 T_N L_N i_{O-N}}{(v''_N - v_{I-N})}} \quad (5.9)$$

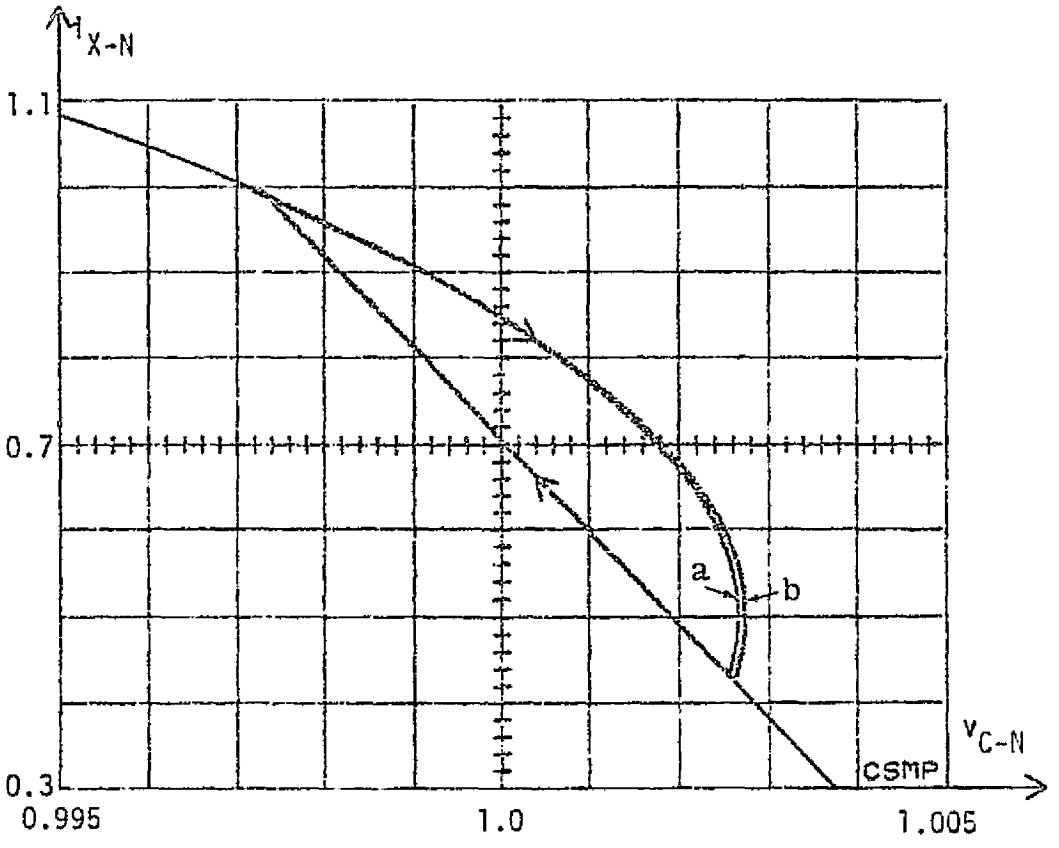

Fig. 5.7 Comparison of shapes of state trajectories for voltage step-up converter models of Fig. 5.1, trajectory *a*, and Fig. 5.6, trajectory *b*.

lead to parabolic and linear trajectories are retained.[10]

To demonstrate the improved performance which results when using this modified switching boundary, the same test conditions as are illustated in Figs. 5.4 and 5.5 are repeated in Fig. 5.8 for the same converter power stage but operating with the modified switching boundary. The converter power stage model simulated in this example is the detailed model displayed in Fig. 5.1. As can be seen in Fig. 5.8, the performance of this system operating with the modified switching boundary again approaches the theoretical limits revealed through analysis. The desired average output voltage is accomplished for both load conditions and the steady-state switching frequency is again stable at the specified value. On comparing the data of Fig. 5.8 to the response of the lossless converter model as illustrated in Fig. 5.4, one can see that the average reactor current for this system is higher than it is for the lossless converter model displayed in Fig. 5.4 as it must be to accommodate the losses in the converter power paths. Thus, by adjusting the shape and location of the switching boundary, the performance characteristics described and demonstrated in Chapter IV can be achieved.

5.4 Simplification of the Switching Boundary

As demonstrated in the preceding section, the performance of a converter system operating in conjunction with the state-trajectory control law is very much dependent on the location and shape of the switching boundary which is generated by the control function. If the theoretical converter performance described in Chapter IV is desired, the shape of the system switching boundary must closely match the shapes of the actual converter trajectories, and the steady-state switch-off point which is used

[10] The degree of improvement can be seen by comparing Fig. 5.7 to Fig. 5.3.

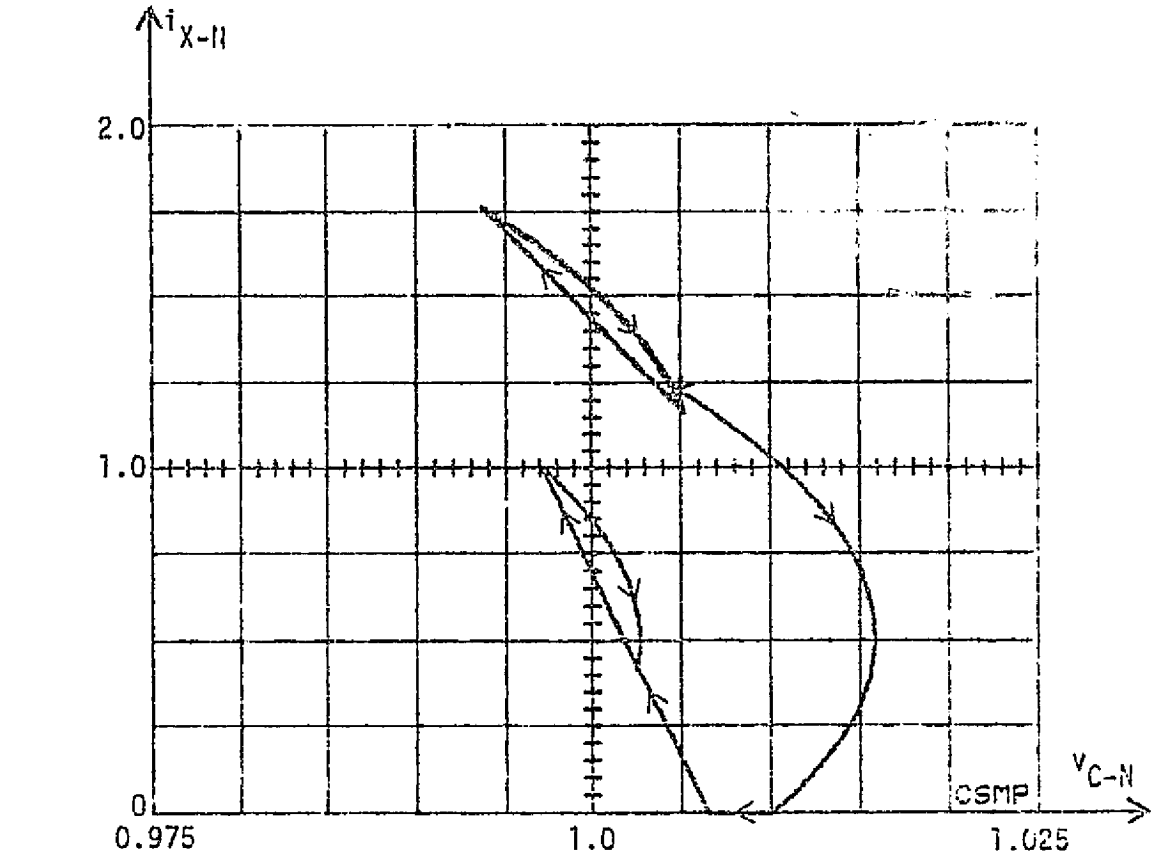

(A)

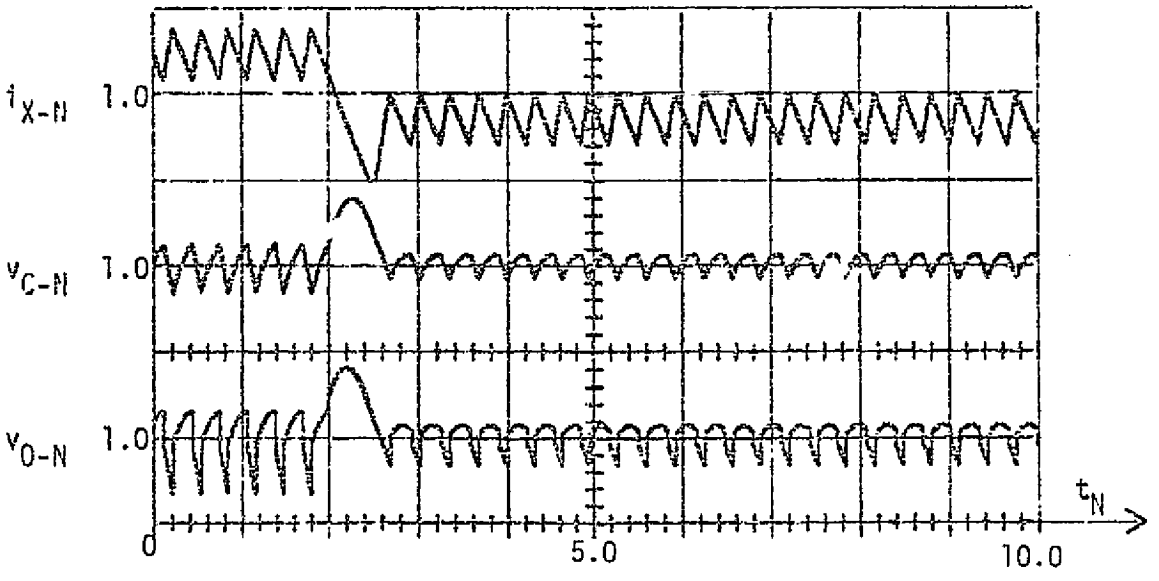

(B)

Fig. 5.8 CSMP generated response of the voltage step-up converter of Fig. 2.1 modeled as shown in Fig. 5.1 but controlled with a switching boundary derived from the model of Fig. 5.6. The operating conditions are $v_{I-N} = 0.75$ and i_{O-N} switches from 1.0 to 0.5 at $t_N = 2.0$. Scale factors for the time waveforms are, in normalized units per major division: i_{X-N}, 1.0/div; v_{C-N}, 0.02/div; and v_{O-N}, 0.02/div.

to locate the switching boundary must be derived with a consideration of the losses within the converter power stage so that additional power from the source can be processed to compensate for the parasitic losses within the system. However, if a particular application does not require such stringent performance characteristics, simplifications can be introduced into the construction of the switching boundary so that adequate system performance can be achieved with a more easily implemented control function

The possibilities for such control function simplifications are too numerous to treat in detail in this dissertation, but an example of one switching line approximation is presented in this section to illustrate the nature and approach to this process. As discussed previously, the state-trajectory control law derived in this dissertation is based on two fundamental observations. First, the state of a converter power stage follows specifically shaped trajectories during the power switch on-time and off-time intervals as determined by the governing physical laws of the system. The shapes of these trajectories can be approximated to arbitrary degrees of accuracy with mathematical expressions which can be derived from conceptual models of the physical system. Secondly, the particular combination of off-time and on-time trajectory segments which a converter state follows during steady-state operation establishes the static performance characteristics of that system. Thus, by either adjusting the shape of the switching boundary or by changing its location in the system state plane, the overall performance of a converter system can be changed. As more approximations are introduced into the specification of the switching boundary, the deviation of the resultant converter performance from the theoretical limits discussed in Chapter IV increases, but the complexity of implementing the corresponding control function decreases.

As an example of how the generation of a state-trajectory switching boundary can be simplified, consider the equations which give the location of the steady-state switch-off point for the voltage step-up converter as presented in Table 4.1(A). This table presents mathematical expressions which give the exact coordinates of the steady-state switch-off point for both continuous and discontinuous conduction operation of a voltage step-up converter modeled as shown in Fig. 2.5. Given the values of the system power stage components, L_N and C_N, the desired system steady-state operating characteristics, V_{O-N} and T_N, and a nominally specified operating point, v_{I-N} and i_{O-N}, the value of capacitor voltage, v_{B-N}, which should occur at the steady-state switch-off instant for these conditions can be computed. If this value of capacitor voltage is used in determining the location of the switching boundary for all operating conditions, rather than computing a new value for each condition from equations (4.2) and (4.4), considerable computation can be saved in the control process with relatively little loss in the accuracy of the steady-state performance characteristics. This type of simplification is illustrated graphically in Figs. 5.9 and 5.10.

The families of off-time and on-time trajectories displayed in Fig. 5.9(A) correspond to the voltage step-up converter of Fig. 2.1 operating with $v_{I-N} = 0.75$ and $i_{O-N} = 0.5$. These trajectories are derived from the model of Fig. 2.5 and consequently are the same as those displayed in Fig. 4.9(B), and the steady-state switch-off point for these condiditions, marked with an X in Fig. 5.9(A), is given by equations (4.1) and (4.2) in Table 4.1(A). If the output current being withdrawn from this system is 100% of the rated value rather than 50%, the families of trajectories displayed in Fig. 5.9(B) are followed and a different steady-state switch-off point can

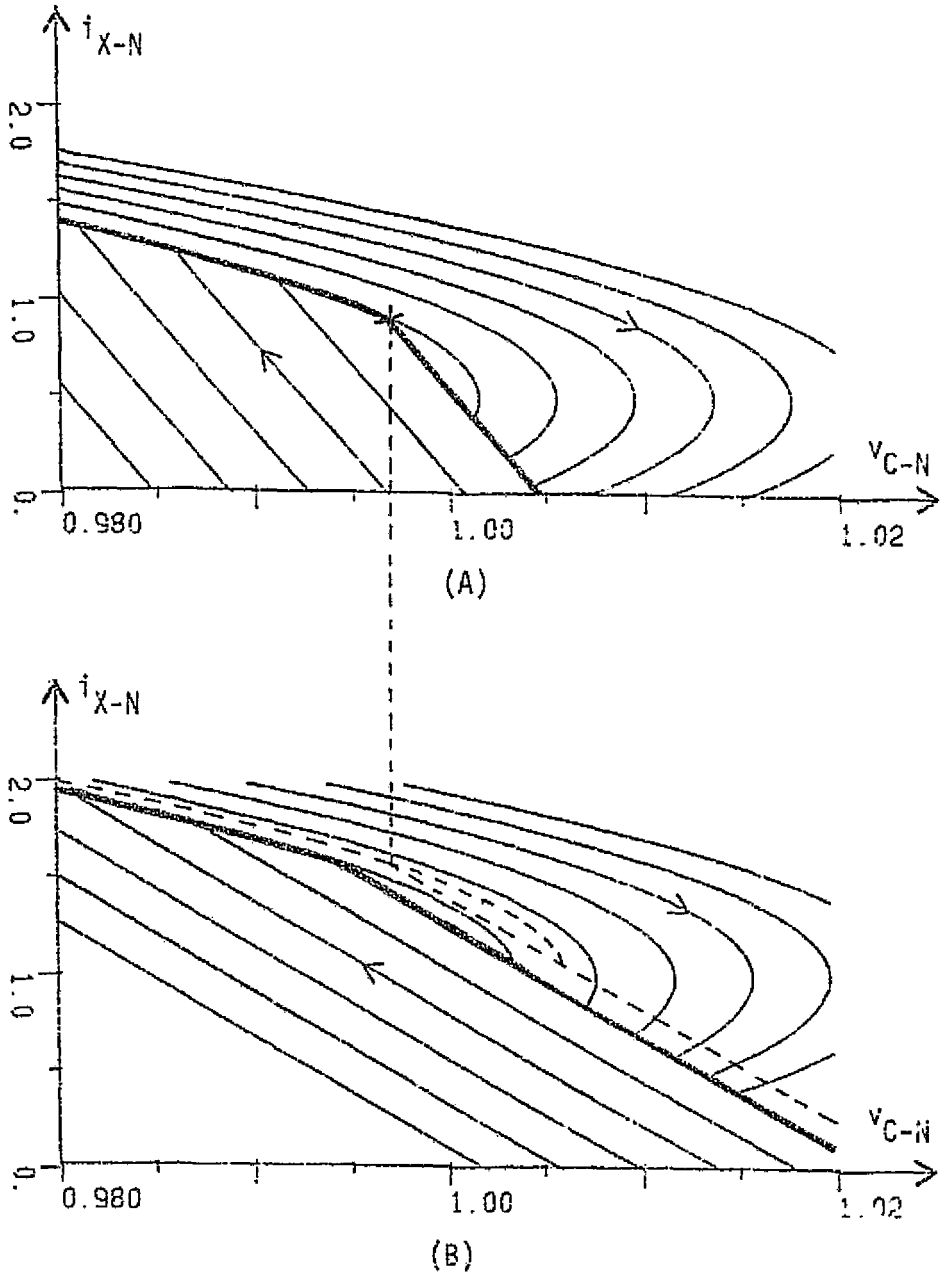

Fig. 5.9 State trajectories and switching boundaries (bold lines) for the voltage step-up converter of Fig. 2.1 modeled as shown in Fig. 2.5 with $v_{I-N} = 0.75$ and i_{O-N} = (A) 0.5 and (B) 1.0. Dashed switching boundary in (B) results if the value of v_{B-N} computed for $i_{O-N} = 0.5$ is used to locate the steady-state switch-off point.

be determined from equations (4.1) and (4.2). If instead of recomputing a value of v_{B-N} for $i_{O-N} = 1.0$, however, the value computed for $i_{O-N} = 0.5$ is used to determine the location of the switching boundary for this heavier load condition, the dashed boundary shown in Fig. 5.9(B) results. By using this value of v_{B-N}, which is greater than the value that corresponds to operation at $i_{O-N} = 1.0$, the state-trajectory switching boundary is shifted slightly upward and to the right, and the steady-state trajectory which results from using this switching boundary also shifts to the right yielding an average output voltage which is approximately 0.25% greater than the desired value.

If the value of v_{B-N} which corresponds to $i_{O-N} = 0.5$ is used to locate a switching boundary for this converter operating with $i_{O-N} = 0.1$, the dashed boundary of Fig. 5.10(B) results. Since v_{B-N} for $i_{O-N} = 0.1$ is greater than v_{B-N} for $i_{O-N} = 0.5$, using the smaller value of v_{B-N} tends to pull the switching boundary and the resultant system steady-state trajectory to the left. Thus, the average output voltage of the converter operating with this switching boundary is slightly less than the desired value, but neither this steady-state error nor the error displayed in Fig. 5.9(B) is as great as the errors encountered with conventional control techniques as presented in Chapter III. Thus, qualitatively at least, approximating v_{B-N} with a constant value which corresponds to a nominally specified operating point still enables good system performance with a less complex mathematical implementation of the state-trajectory control law.

Digital computer simulations which illustrate the response of a voltage step-up converter operating in conjunction with the simplified state-trajectory control law are presented in Figs. 5.11 and 5.12. The converter power stage model simulated in these examples is the more complex model

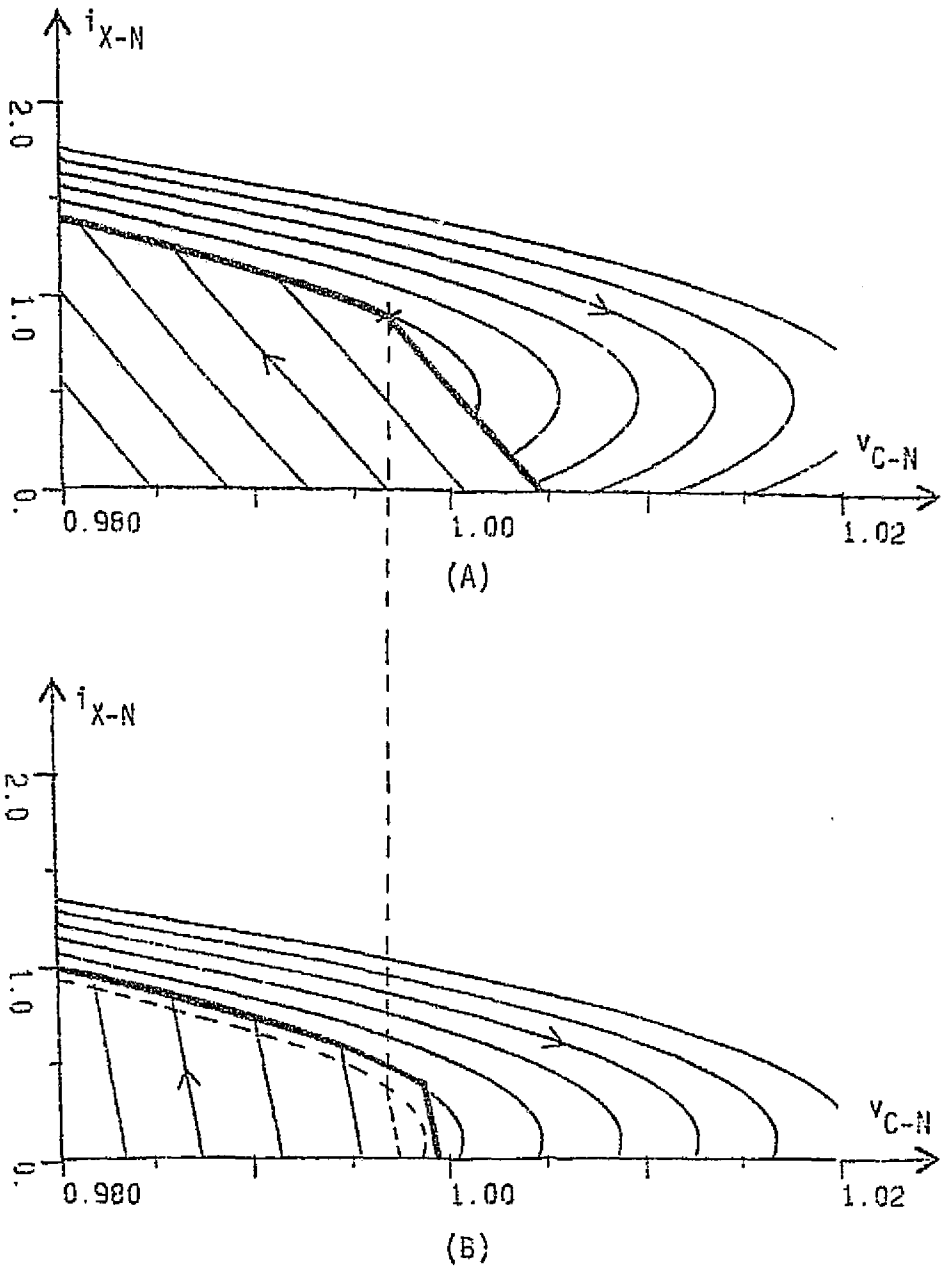

Fig. 5.10 State trajectories and switching boundaries (bold lines) for the voltage step-up converter of Fig. 2.1 modeled as shown in Fig. 2.5 with v_{I-N} = 0.75 and i_{O-N} = (A)0.5 and (B) 0.1. Dashed switching boundary in (B) results if the value of v_{B-N} computed for i_{O-N} = 0.5 is used to locate the steady-state switch-off point.

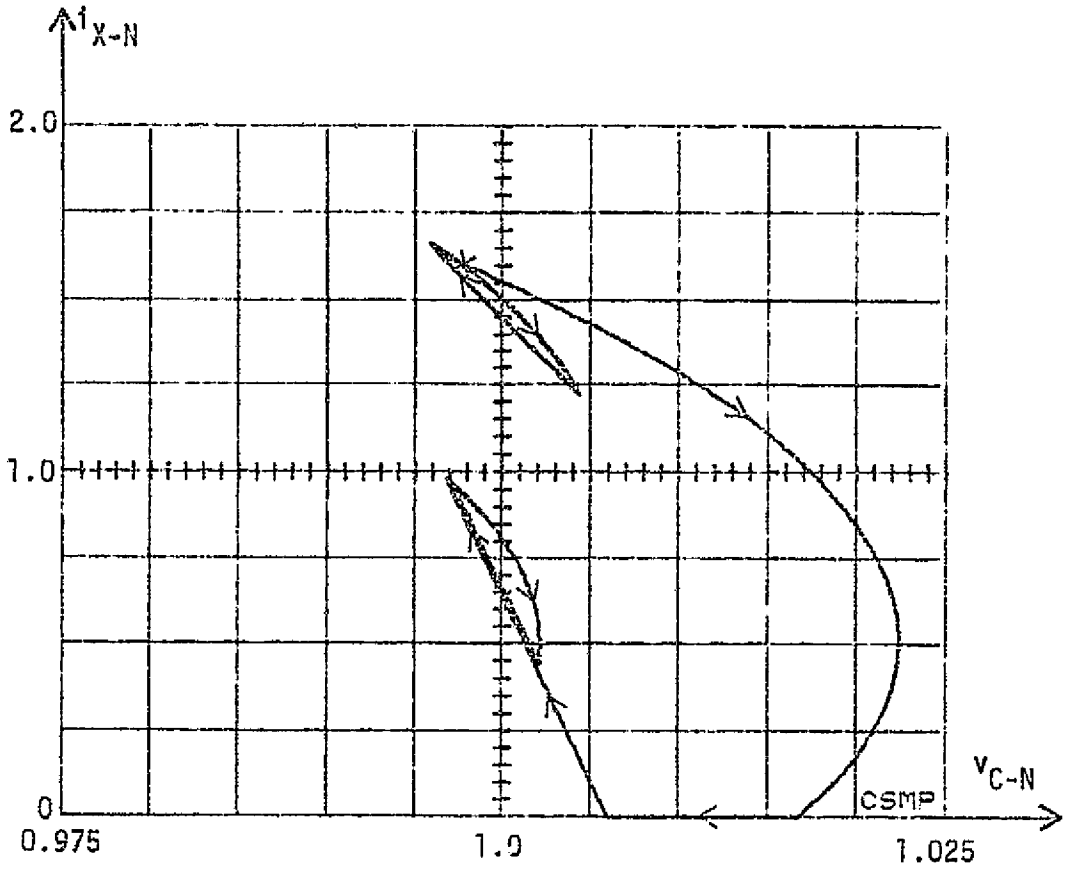

(A)

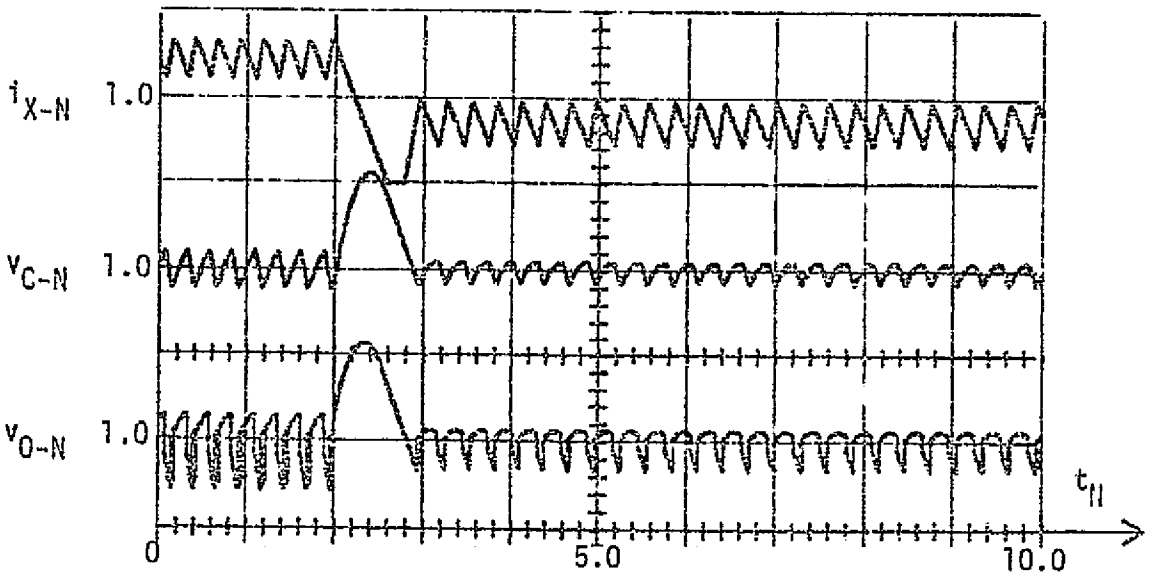

(B)

Fig. 5.11 CSMP generated response of the voltage step-up converter of Fig. 2.1 modeled as shown in Fig. 5.1 but controlled with the switching boundaries illustrated in Fig. 5.9. The operating conditions are $v_{I-N} = 0.75$ and i_{O-N} switches from 1.0 to 0.5 at $t_N = 2.0$. Scale factors for the time waveforms are, in normalized units per major division: i_{X-N}, 1.0/div; v_{C-N}, 0.02/div; and v_{O-N}, 0.02/div.

illustrated in Fig. 5.1, but the switching boundaries generated by the converter control function are the simplified implementations illustrated in Figs. 5.9 and 5.10, respectively, which are derived from the model of Fig. 2.5 but with the steady-state switch-off voltage fixed for all operating conditions rather than computed from equations (4.2) and (4.4). The response of the voltage step-up converter of Fig. 2.1 to a step change in output current from 100% to 50% of its rated value when operating in conjunction with this simplified state-trajectory control law is illustrated in Fig. 5.11. The test conditions illustrated in this figure are identical to those of Fig. 5.5 except that the steady-state switch-off voltage, v_{B-N}, is constant in Fig. 5.11 rather than computed as it is Fig. 5.5. As predicted from the graphical analysis of Fig. 5.9, the fixed value of v_{B-N} causes the steady-state trajectory to shift to the right for higher values of load current, which actually improves the converter performance in this case. The steady-state trajectory corresponding to $i_{O-N} = 0.5$ in Fig. 5.11 is also seen to yield a higher average output voltage than that in Fig. 5.5 because the constant value of v_{B-N} used in determining the switching boundary for the system of Fig. 5.11 was chosen to be slightly greater than the computed value from equation (4.2) in order to compensate for the losses in the converter power stage which are not incorporated in the converter switching boundary.

The response of this system to a step decrease in load current from 50% to 10% of its rated value is illustrated in Fig. 5.12. The final steady-state trajectory corresponding to $i_{O-N} = 0.1$ is seen to be in the discontinuous conduction mode and to yield an average output voltage slightly less than the desired value as predicted in Fig. 5.10. The effect of these approximations on the switching frequency of the system under the

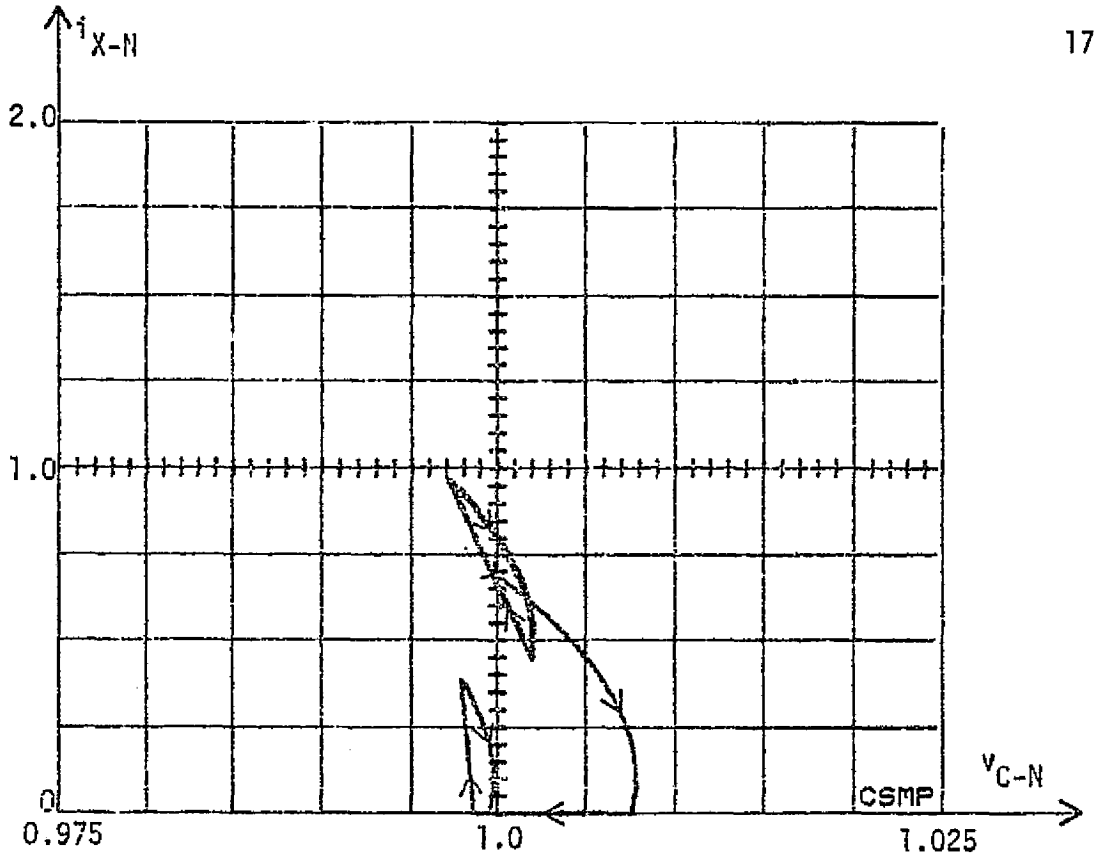

(A)

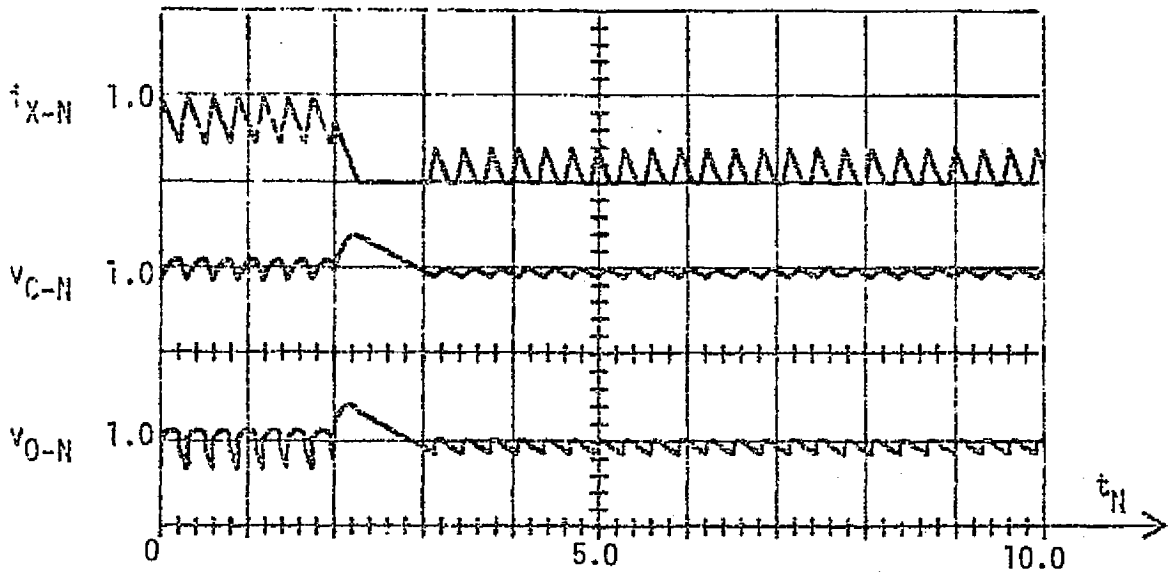

(B)

Fig. 5.12 CSMP generated response of the voltage step-up converter of Fig. 2.1 modeled as shown in Fig. 5.1 but controlled with the switching boundaries illustrated in Fig. 5.10. The operating conditions are $v_{I-N} = 0.75$ and i_{O-N} switches from 0.5 to 0.1 at $t_N = 2.0$. Scale factors for the time waveforms are, in normalized units per major division: i_{X-N}, 1.0/div; v_{C-N}, 0.02/div; and v_{O-N}, 0.02/div.

various load conditions can be seen in Figs. 5.10(B) and 5.11(B). For the examples presented in this chapter, the systems operating with the approximate switching boundaries tend to operate at higher frequencies than specified. This is due to the fact that the actual converter trajectories curl inside of the derived switching boundaries and thus switch sooner than they should. The resultant steady-state trajectories enclose smaller areas of the state plane which, as illustrated in Fig. 4.5, correspond to higher operating frequencies. In all of the examples presented in this chapter, however, the inherently stable, single cycle switching process is maintained through all transient disturbances, and only the converter steady-state performance characteristics are influenced by the switching boundary approximations.

5.5 Conclusions

The state-trajectory control law presented in this dissertation is based on a mathematical processing of information from the controlled system's power stage. The precise form of the equations which are used to implement this control function depends on the particular model chosen to represent the physical converter. Detailed converter models which include representations of the effects of lossy elements in the system power paths lead to more complex equations for the control law implementation. These more complex equations, in turn, enable converter performance that approaches the theoretically predicted response described in Chapter IV. Simplified converter models which ignore the effects of lossy elements on the system behavior lead to simpler expressions for the implementation of the state-trajectory switching boundary, but the performance of a converter operating under the influence of such a simplified control implementation does not

match the theoretical behavior predicted through analysis. The particular performance measures which degrade for given approximations can be predicted through the analytical framework used to derive the control law, and thus tradeoffs of system performance vs. controller complexity can be made.

After deriving a switching boundary from a given converter model which enables satisfactory performance with a control implementation of acceptable complexity, additional simplifications can be determined by examining the resultant mathematical expressions which represent the switching boundary. Neglecting terms in the expressions for i_{B-N} or v_{B-N} can result in simpler implementations with acceptable levels of performance. As illustrated in this chapter, it may even be possible to approximate one or more of the mathematical expressions by a constant value if it is found that the range of that value for the specified operating conditions is not too large.

Additional modifications to the state-trajectory switching boundary can be made to accomplish other desired circuit functions such as converter start-up or circuit protection features. The method for implementing such additional features can again be determined by examining the behavior of the converter in the system state plane and making the switching decisions based on the position of the system state relative to a derived boundary. A current limiting feature, for example, could be incorporated by imposing a third segment on the switching boundary which limits the on-time region of the plane to an area below a maximum reactor current level. The possibilities for adapting this control technique to particular applications are too numerous to describe in this dissertation, and the discussions and examples presented in this chapter are intended only to illustrate and give guidance for such investigations.

Chapter VI

EXPERIMENTAL VERIFICATION OF THE STATE-TRAJECTORY CONTROL LAW

6.1 Introduction

The control function derived in this dissertation can be represented mathematically by means of relatively simple algebraic equations. Thus, any physical device or combination of devices which can generate algebraic functions of measured signals can be used to physically realize this control concept. Currently available electronic components, both digital and analog, are capable of processing electronic signals in this manner and thus can be used to implement, in a straightforward manner, the state-trajectory control law derived in this dissertation. The purpose of this chapter is to demonstrate the physical realizability of this control technique and to discuss some possible approaches to such an implementation.

The particular implementation approach described in this chapter involves digitally computing the state-plane switching boundary and comparing the position of the monitored state of the system to this computed boundary. The implementation at this stage does not represent a practical development, but rather is designed to enable a maximum investigation of all aspects of the system behavior. After presenting a brief outline of this implementation procedure, oscillograms are presented which illustrate the behavior of an experimental voltage step-up dc-to-dc converter operating

under the control of this physical realization of the control technique. The performance of this experimental system is discussed with respect to the theoretically predicted performance and the computer simulated responses of such systems as presented in Chapters IV and V.

6.2 Implementation of the Control Law

For purposes of demonstration and experimentation, the control function derived in this dissertation has been programmed into a Digital Equipment Corporation PDP-11/45 digital computer. The signals from the converter power stage which are used in the control decision process are transmitted to the program through four separate analog to digital converter channels, and the resultant control signal is transmitted from the computer to the converter power switch via a single digital to analog converter channel. The program is written in an assembler language and all of the mathematical operations required by the program are performed by means of integer arithmetic. These required operations are performed sequentially in the central processing unit of the machine as instructed by the program and as described below.

A flow chart of this program is presented in Fig. 6.1. As indicated by the symbols in this figure, unnormalized system parameters and variables are used in this program and consequently throughout the discussions in this chapter. Also, two new symbols are introduced in this figure to help distinguish between physically measured system variables and the variables and parameters which are computed within the control program. Thus, throughout this chapter, measured values of variables from the converter power stage are indicated by a superscript asterisk, and computed values generated by the control program are indicated by a superscript circle.

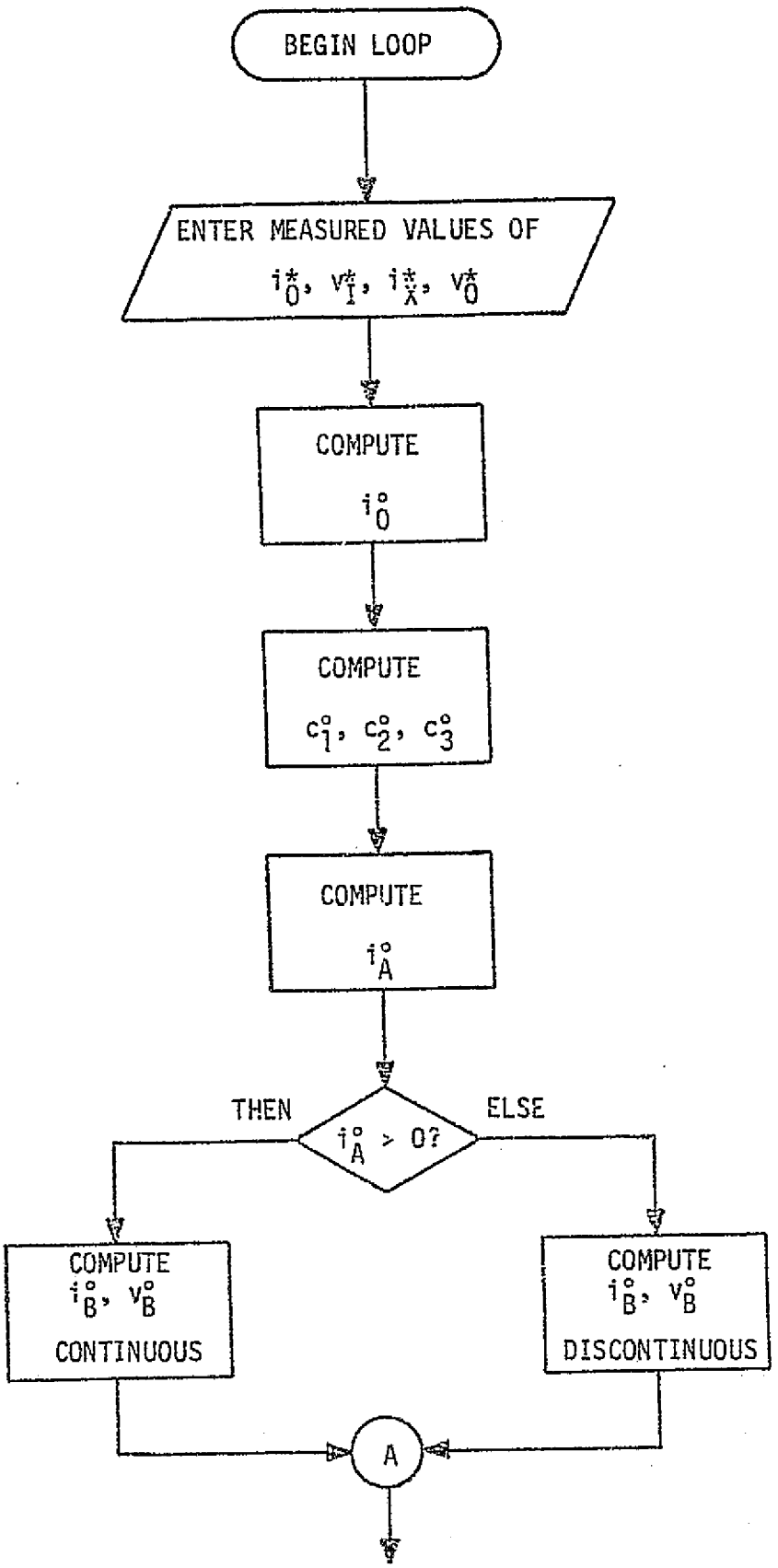
BEGIN LOOP
ENTER MEASURED VALUES OF
i_0^*, v_I^*, i_X^*, v_0^*
COMPUTE
i_0°
COMPUTE
c_1°, c_2°, c_3°
COMPUTE
i_A°
THEN
$i_A^\circ > 0$?
ELSE
COMPUTE
i_B°, v_B°
CONTINUOUS
COMPUTE
i_B°, v_B°
DISCONTINUOUS
A

Fig. 6.1 (1 of 3)

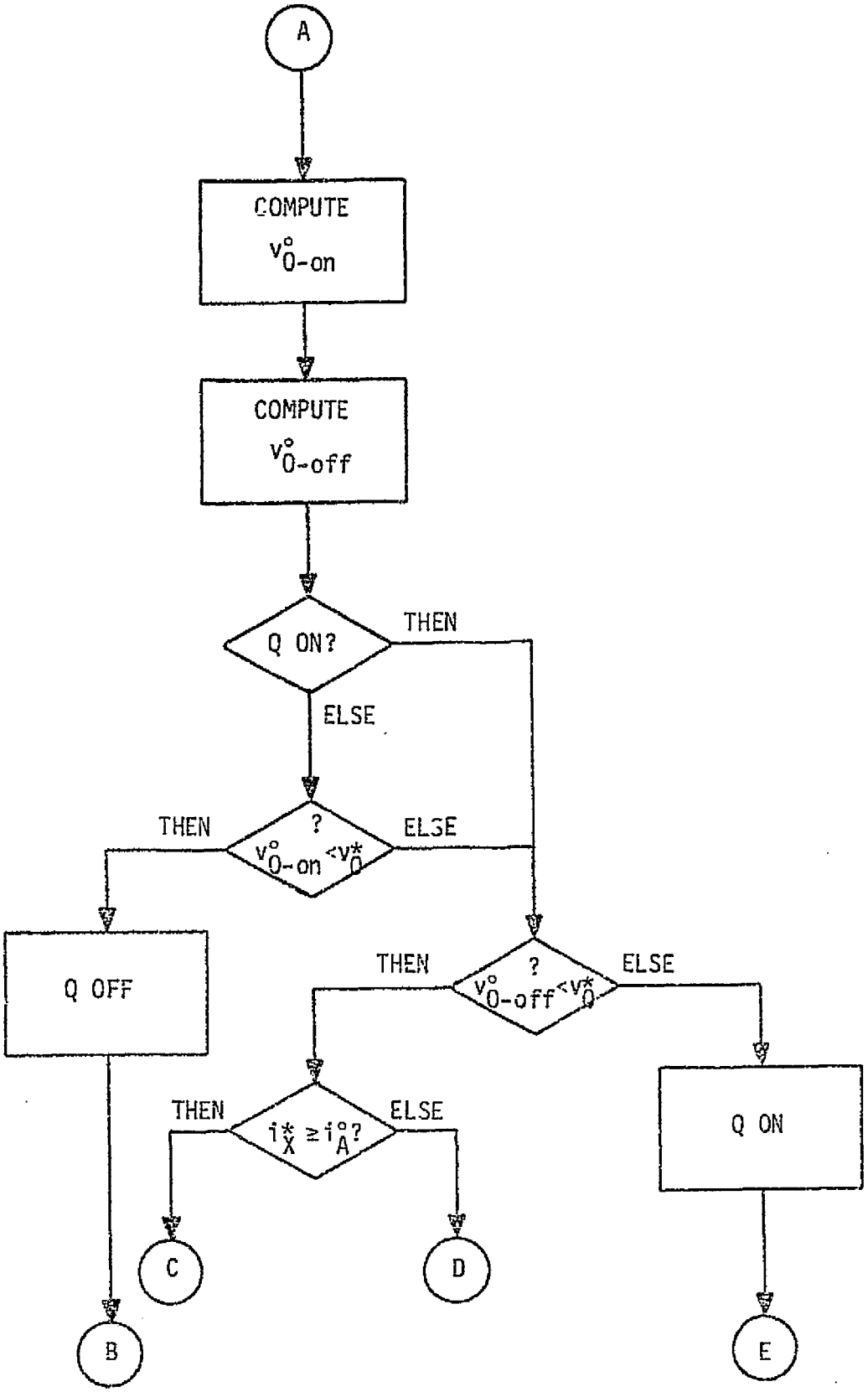
A
COMPUTE
$v^{\circ}_{0\text{-on}}$
COMPUTE
$v^{\circ}_{0\text{-off}}$
Q ON?
THEN
ELSE
THEN
?
$v^{\circ}_{0\text{-on}} < v^{*}_{0}$
ELSE
Q OFF
THEN
?
$v^{\circ}_{0\text{-off}} < v^{*}_{0}$
ELSE
THEN
$i^{*}_{X} \geq i^{\circ}_{A}$?
ELSE
Q ON
C
D
B
E

Fig. 6.1 (2 of 3)

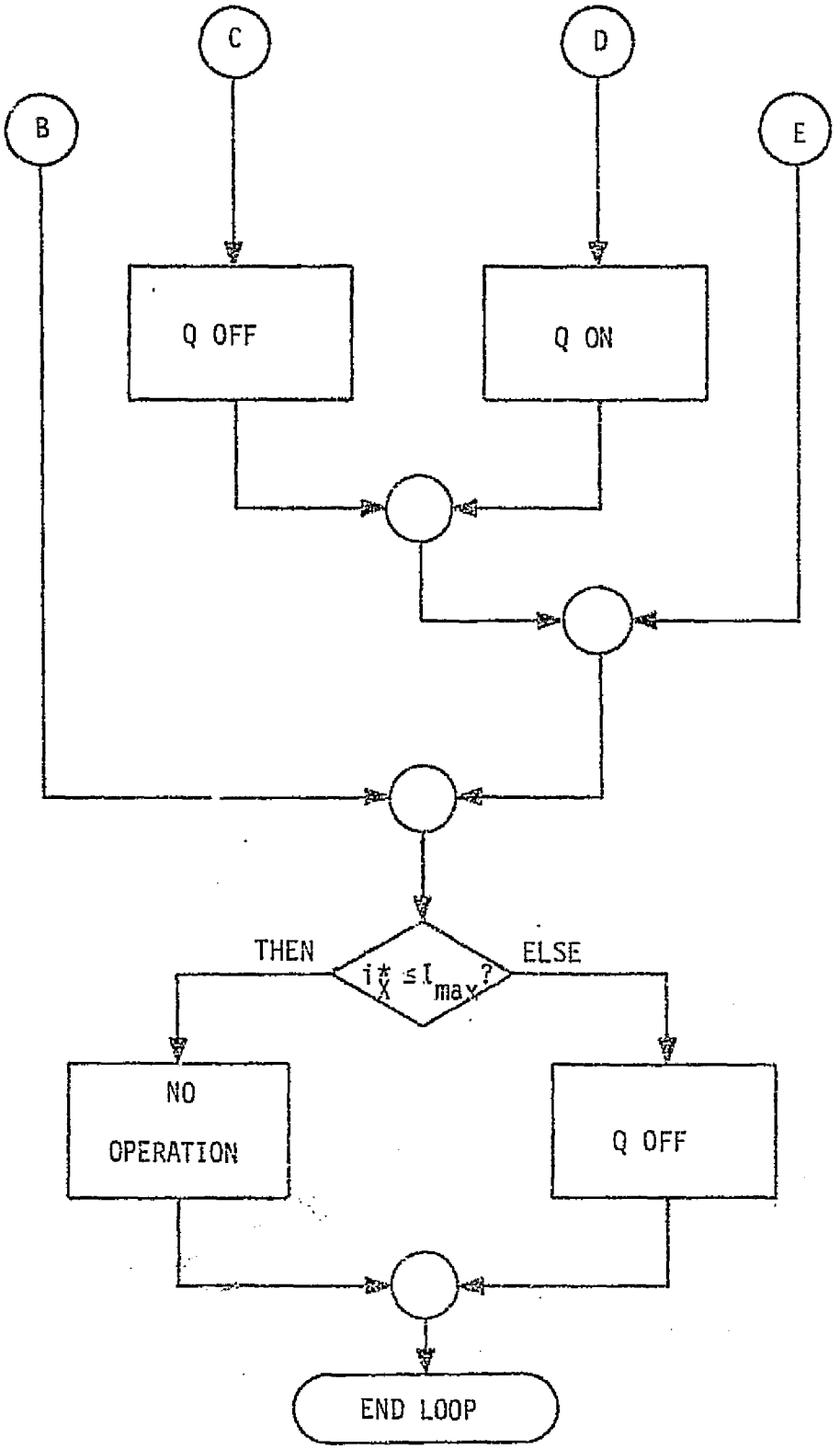

Fig. 6.1 Program flow chart for digital implementation of the state-trajectory control law.

The instructional loop depicted in this figure begins by taking measured values of the four signals from the converter power stage which are used in generating the control function. Two of these signals, i_0^* and v_I^*, represent the externally imposed operating conditions of the system, and the other two, i_X^* and v_0^*, represent the state of the system at the instant of sampling. The program then follows the sequence of operations depicted in the figure to determine whether the converter power switch should be turned on or off for those measured values of the power stage variables. By the time the program has reached the end of the loop, the control command has been updated to correspond to the most recently sampled values of these variables. After the loop is completed, the program immediately takes another set of sampled values and proceeds to process them to determine the next control command. A more detailed discussion of this control loop is presented in the following paragraphs.

The equations which generate the switching boundary used in this program are given in Appendix C as equations (C.3) and (C.4) and are rewritten below in a form which more clearly illustrates their use in the program. These equations are derived from the model of the voltage step-up converter given in Fig. 2.5.

$$v^\circ_{0\text{-off}} = c^\circ_1 \left(i^{*2}_X - i^{\circ 2}_B\right) + c^\circ_2 \left(i^*_X - i^\circ_B\right) + v^\circ_B - i^*_0 \, r_C \tag{6.1}$$

$$v^\circ_{0\text{-on}} = c^\circ_3 \left(i^*_X - i^\circ_B\right) + v^\circ_B + \left(i^*_X - i^*_0\right) r_C \tag{6.2}$$

where

$$c^\circ_1 = - \frac{L}{2C \left(V_0 - v^*_I\right)} \tag{6.3}$$

$$c^\circ_2 = \frac{i^\circ_0 \, L}{C\left(V_0 - v^*_I\right)} \tag{6.4}$$

$$c^\circ_3 = - \frac{i^\circ_0 \, L}{v^*_I \, C} \tag{6.5}$$

Equation (6.1) gives the value of voltage on the switch-off segment of the switching boundary as a function of the measured reactor current, i_X^*, and thus this computed value of voltage is given the symbol, $v_{0\text{-off}}^\circ$. This computed boundary is illustrated in Fig. 6.2 in the system state plane. The value of voltage on the switch-on segment of the switching boundary as a function of the measured reactor current is given by (6.2) and is represented by the symbol, $v_{0\text{-on}}^\circ$. This boundary is also depicted in Fig. 6.2. The coefficients used in these equations, c_1°, c_2° and c_3°, are functions of the values of the converter power stage components, L and C, the desired average output voltage, V_0, the measured value of input voltage, v_I^*, and the computed value of desired average output current, i_0°, which is discussed below.

The program loop illustrated in Fig. 6.1 consists of two principal segments--a computational segment in which $v_{0\text{-off}}^\circ$ and $v_{0\text{-on}}^\circ$ are determined, and a decision making segment in which the measured output voltage, v_0^*, is compared to these computed values and a control command is issued accordingly. After receiving a set of measured system signals, the program proceeds to process these signals, together with the programmed power stage component values and specified steady-state operating characteristics, to determine the system switching boundary. As indicated in Fig. 6.1, the first computation performed determines the value of average output current, i_0°, which is commensurate with the desired average output voltage, V_0, and the externally applied load. The computation is given by equation (6.6)

$$i_0^\circ = \frac{V_0}{R_0^\circ} \qquad \text{where} \quad R_0^\circ = \frac{v_0^*}{i_0^*} \tag{6.6}$$

which is based on the assumption that the converter load is purely resistive, and thus can be determined from Ohm's Law for the measured values of output current and output voltage. This computed value of current is the value which

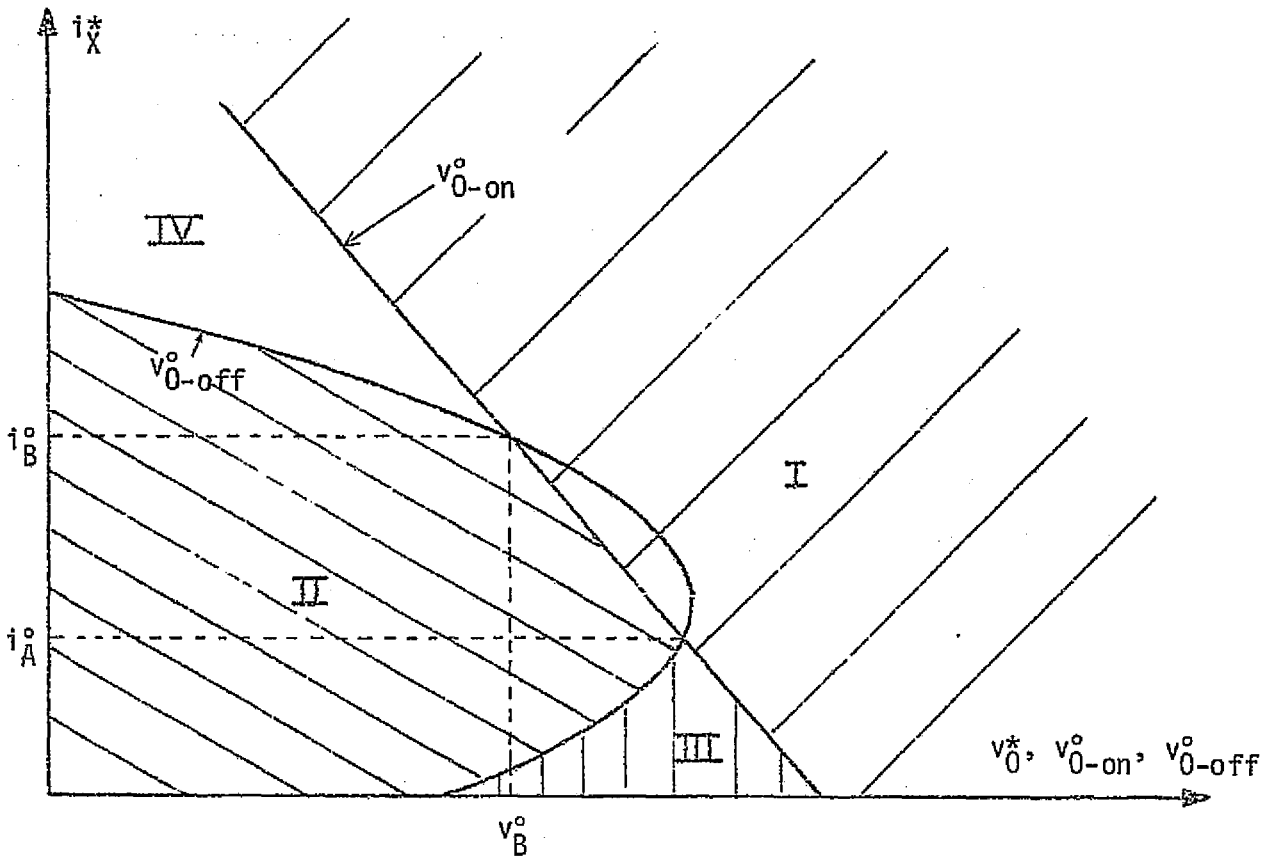

Fig. 6.2 Computed switching boundaries and resultant regions of the system state plane which are sequentially monitored by the control program. Regions I and IV are off-regions, II and III are on-regions.

is used in determining the coordinates of the steady-state switch-off point and the coefficients of the equations which describe the system switching boundary.

Using this value of i_0° and the measured value of input voltage, v_I^*, the coefficients c_1°, c_2°, and c_3° are computed from equations (6.3)-(6.5) respectively. These coefficients determine the shape of the system switching boundary, but the desired steady-state switch-off point must also be computed to locate the particular on-time and off-time trajectories which yield the desired steady-state operating characteristics. The experimental converter being used to exercise this control law implementation is designed to operate in a constant frequency mode, and thus the equations given in Table 4.1(A) can be used to compute i_B° and v_B°. As indicated in Table 4.1(A), however, the equations which determine the coordinates of this point are not the same for both continuous and discontinuous conduction operation. Thus, before this point is computed, the program determines in which mode of operation the converter should function under the measured operating conditions. This can be done by computing the value of the steady-state switch-on current, i_A°, which is given by equation (6.7) for the voltage step-up converter.

$$i_A^\circ = \frac{i_0^\circ V_0}{v_I^*} - \frac{T v_I^* (V_0 - v_I^*)}{2 L V_0} \tag{6.7}$$

This expression can be derived from equations (A.1), (A.2), and (A.5) of Appendix A. If this computed value of current is greater than zero, steady-state operation for this converter under the measured operating conditions is in the continuous conduction mode. If i_A° is less than or equal to zero, the converter should operate in the discontinuous conduction mode. Thus, depending on the computed value of i_A°, either equations (4.1) and (4.2) or (4.3) and (4.4) of Table 4.1(A) are used to compute values of i_B° and

v_B°, the coordinates of the steady-state switch-off point. Having determined the values of the coefficients c_1°, c_2°, and c_3°, and the values of i_B° and v_B°, values for $v_{0\text{-off}}^\circ$ and $v_{0\text{-on}}^\circ$ can be computed from equations (6.1) and (6.2) respectively. These computations are the final steps in the computation segment of the program, and with these computed values and the measured values taken at the beginning of the control loop, the program has all of the information it needs to determine whether the converter power switch should be on or off.

The first step in the decision segment of the program is to determine the current state of the converter power switch. If the power switch is off, the measured value of output voltage, v_0^*, is compared to the computed value of the switch-on line, $v_{0\text{-on}}^\circ$, at the measured value of reactor current, i_X^*. If the measured value of voltage is greater than the computed value, the state of the system at the sampling instant is to the right of the switch-on line, region I of Fig. 6.2, and thus the power switch should remain off. If the state of the system is to the left of the switch-on boundary, however, its position relative to the switch-off boundary must be determined. Likewise, if the converter power switch is found to be on at the beginning of the loop, the position of the system state relative to the switch-off boundary must be determined. If the computed value of voltage, $v_{0\text{-off}}^\circ$, is greater than the measured value, v_0^*, then the state of the system is in region II of Fig. 6.2, and the converter power switch should be on. If $v_{0\text{-off}}^\circ$ is less than or equal to v_0^*, however, the system state could be in either region III, an on-region, or region IV, an off-region. Thus, the measured value of reactor current, i_X^*, must be compared to the value of the steady-state switch-on current which was computed in the computational segment of the program to determine whether the system

state is in region III or IV, and thus whether the power switch should be on or off.

At this stage in the program a control decision has been made based on the most recently measured values of the state of the system and its externally imposed operating conditions. However, before the program returns to the beginning of the loop to take the next set of measured signal values, the value of the measured reactor current is compared to a specified maximum value, I_{max}. If i_X^* exceeds this maximum value, a power switch turn-off signal is issued, if it has not already been issued, to prevent the reactor current from rising to a level which might damage the converter power stage components. If i_X^* is less than I_{max}, no operation is performed. This step is a simple current limit protection feature as discussed in the preceding chapter.

6.3 Performance of Experimental Voltage Step-Up Converter

The time required for the PDP-11/45 to perform the operations called for in this control loop from start to finish is approximately 200 microseconds. Thus, in order to be able to compute a control signal sufficiently often per cycle of operation to enable accurate system performance, converters operating with this control implementation must switch at relatively low frequencies. An experimental voltage step-up dc-to-dc converter designed to operate at 100 Hz so that the control loop could be processed approximately 50 times during each switching cycle, has been built and exercised in conjunction with the digital implementation of the state-trajectory control law described above. The component values used in this converter power stage are listed in Table 6.1. The rated average output voltage for the converter is 28.0 volts, the rated output current is 4.0

Table 6.1

System Component and Parameter Values for the Experimental Voltage Step-Up Converter

Component or Parameter	Measured or Specified Value
L	9.7 mH
C	12,900 μF
r_C	0.017 Ω
V_O	28.0V
T	10.0 msec
i_O	0.4 - 4.0 A
v_I	16.0 - 24.0 V

amperes, and the specified range of input voltage is 16 to 24 volts. Small current sensing resistors are used to measure the instantaneous values of reactor current and output current.

The response of this voltage step-up converter system to a step change in load current from 100% to 50% of its rated value is presented in Fig. 6.3. As predicted by the theory presented in Chapter IV, and as demonstrated in digital computer simulations in Chapters IV and V, this converter operating under the influence of the state-trajectory control law is able to move from one steady-state condition to another in one cycle of control. In this case, the decrease in load current occurs during a power switch off-time interval, and the switch remains open until the state of the system crosses the new switch-on boundary. As can be seen from the current waveform, the converter momentarily operates in the discontinuous conduction mode during the transient cycle, but steady-state operation for both load conditions is in the continuous conduction mode.

The average output voltage at the lighter load condition is approximately .3 V, or 1%, lower than the value at the rated load. This shift in the average output voltage is due to inaccuracies in the computation of the steady-state switch-off voltage, v_B°. As can be observed in the simulation data presented in Chapters IV and V, the difference in the magnitude of v_B° over a range of output currents is quite small relative to the magnitude of the average output voltage, V_0. For example, the case illustrated in Fig. 4.17 shows a difference in v_B° of approximately 0.2% for a change in load current from 100% to 50% of the rated value. Consequently, given the limits in the accuracy of integer arithmetic, this difference is not transmitted through the control loop and the system effectively operates in a fixed v_B° mode as discussed in section 5.4. As described in that section,

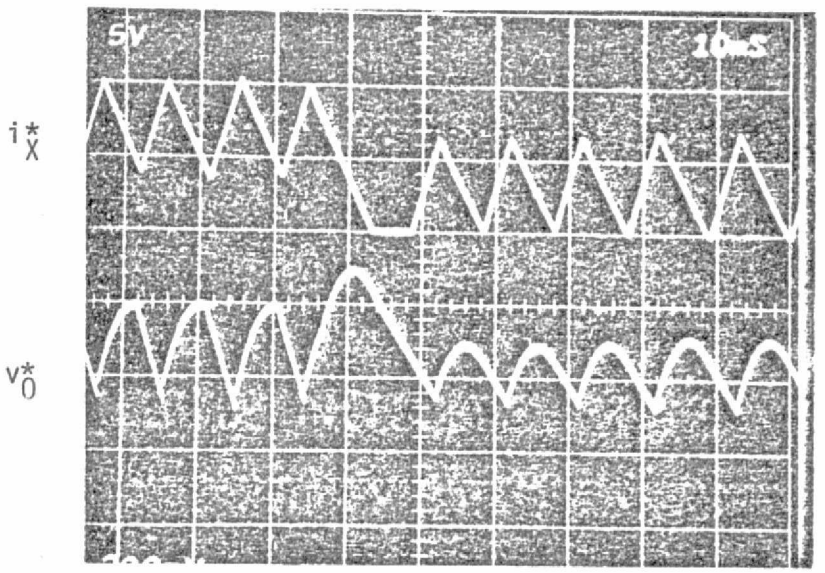

Fig. 6.3 Response of experimental voltage step-up converter system to a step decrease in load current from 100%, 4A, to 50%, 2A, of the rated value with v_I^* = 21 V. Scale factors are: i_X^*, 5 A/div; v_0^*, 0.8 V/div; time, 10 mS/div.

the fixed value of v_B° causes the steady-state trajectories at lighter loads to shift to the left yielding lower average output voltages, and causes the steady-state trajectories at higher loads to shift to the right yielding higher average output voltages. The same test condition as is illustrated in Fig. 6.3 is simulated in Fig. 5.11 although applied to a different voltage step-up converter. Although the details are not the same, the same basic response is seen to occur in the physical converter as occurs in the simulation.

A second example of the response of the experimental converter system is presented in Fig. 6.4. In this example, the system is subjected to a step change in output current from 100% to 25% of its rated value. The new steady-state condition is again achieved in one cycle of control, and the system is seen to be in the discontinuous conduction mode of operation at the lighter load condition. As discussed in the preceding paragraph, the average output voltage at i_0 = 1A is less than it is at i_0 = 4A. The frequency of operation at the lighter load condition is seen to be approximately 75 Hz rather than the specified 100Hz as it is at the higher load conditions. This change in frequency is again due to the fact that the change in the steady-state switch-off voltage, v_B°, cannot be detected by the control program and as illustrated in Fig. 4.5, the frequency of operation of converters operating in conjunction with this control law is very much dependent on the location of the system switching boundary in the state plane. The response depicted in the oscillogram of Fig. 6.4 is quite similar to the digital computer simulated response of Fig. 5.12. Two other test cases are presented in Figs. 6.5 and 6.6. These oscillograms again illustrate the single cycle transient response which can be achieved with the state trajectory control law.

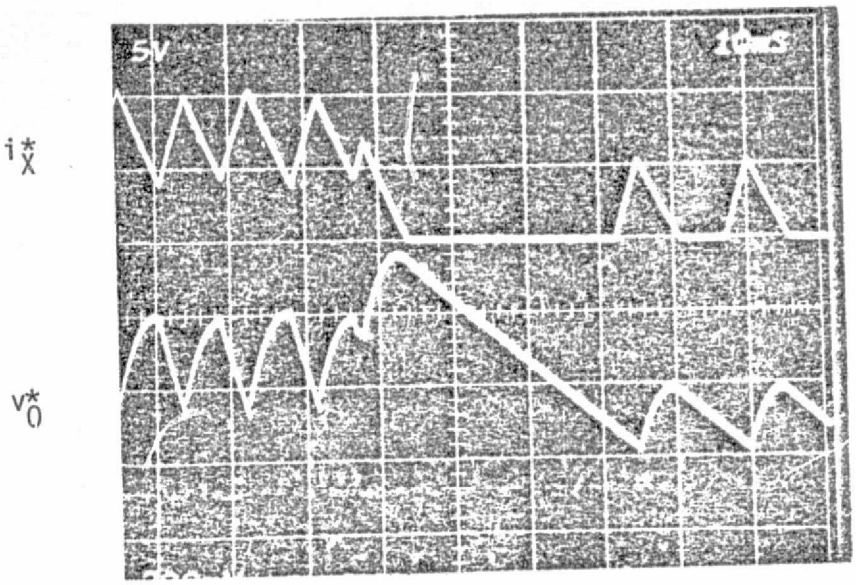

Fig. 6.4 Response of experimental voltage step-up converter system to a step decrease in load current from 100%, 4A, to 25%, 1A, of the rated value with $v_T^* = 21V$. Scale factors are: i_X^*, 5A/div; v_0^*, 0.8V/div; time, 10 mS/div.

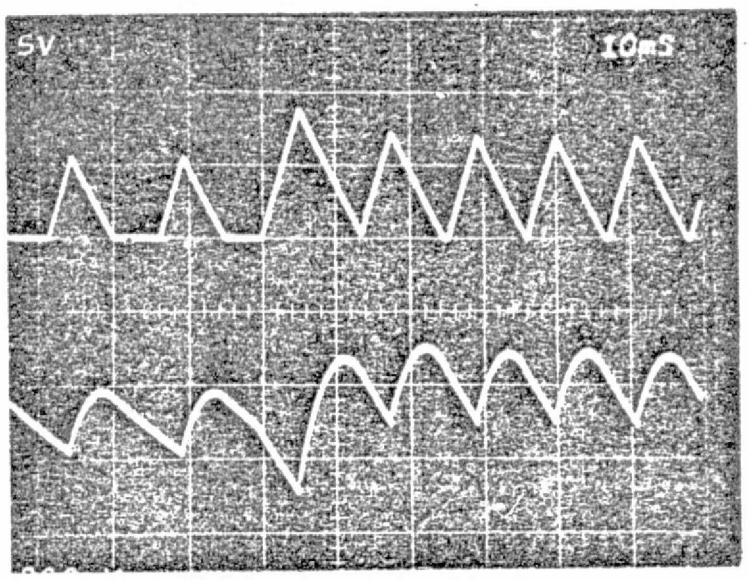

Fig. 6.5 Response of experimental voltage step-up converter system to a step increase in load current from 25%, 1A, to 50%, 2A, of the rated value with v_I^* = 21V. Scale factors are: i_X^*, 5A/div; v_0^*, 0.8V/div; time, 10 mS/div.

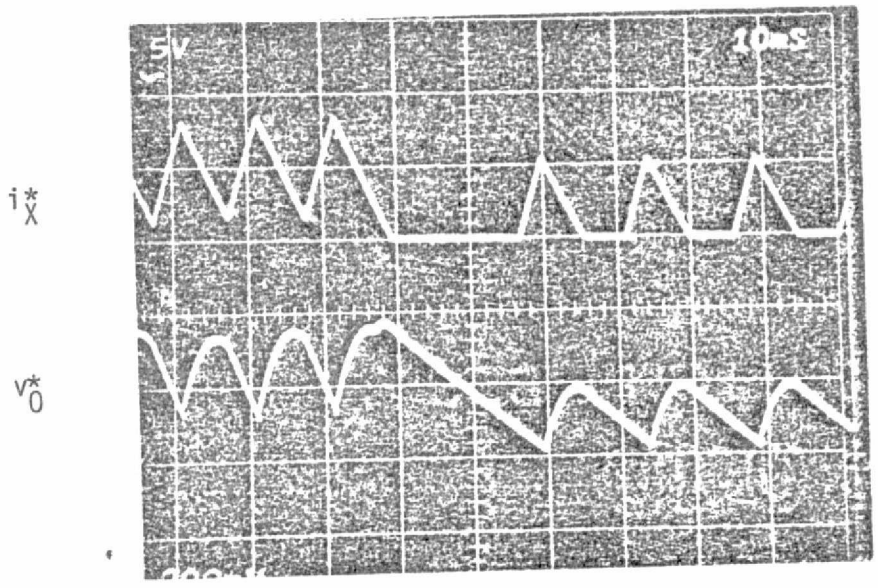

Fig. 6.6 Response of experimental voltage step-up converter system to a step devrease in load current from 75%, 3A, to 25%, 1A, of the rated value with v_I^* = 21 V. Scale factors are: i_X^*, 5A/div; v_0^*, 0.8V/div; time, 10 ms/div.

6.4 Conclusions

This chapter presents a brief description of the early stages of an experimental implementation of the state-trajectory control law derived in this dissertation. The implementation is, of course, not practical for normal use, but rather is intended to enable an experimental investigation of the theoretical discussions and predictions presented throughout this dissertation. It is believed that the oscillograms presented in this chapter conclusively demonstrate the feasibility of implementing the analytically derived converter control function.

Another approach to the implementation of this control law is currently being pursued whereby the algebraic expressions required to establish the state-plane switching boundary are generated by means of analog function modules. The same computations and control decisions as are illustrated in Fig. 6.1 are employed in this analog implementation, but the processes are all accomplished concurrently, and thus it is being applied to a converter which operates at 10KHz. Preliminary investigations of this approach have yielded encouraging results, and it is believed that with currently available electronic components, practical implementations of this control technique are feasible, whether they be digital in nature (e.g., microprocessors), analog, or hybrid combinations of these two approaches.

CHAPTER VII

CONCLUSIONS

A general, qualitative investigation of three representative members of a widely used class of energy-storage dc-to-dc power converters has been presented. The state-plane analysis approach employed in this investigation reveals families of trajectories which the state of a converter power stage must follow during the power switch on-time and off-time intervals as determined by the governing physical laws of the system. An understanding of these trajectories and knowing how they change with changes in system parameters and externally imposed operating conditions reveal certain fundamental limitations in the performance of the converter power stages which cannot be exceeded no matter what type of converter control technique is employed. This ability to observe the movement of the system state enables one to examine and compare various control techniques which can be used to determine a converter power stage switching sequence and to determine strengths and weaknesses in each of these techniques. Such a graphical visualization of the converter behavior is of course limited to second order systems, because higher order systems require more than two state variables to completely represent the behavior of the system. However, each of the power stages of the converters studied in this dissertation are second order and consequently their behavior can be portrayed in a plane even though the complete state of the system cannot.

In addition to revealing considerable qualitative insight into the behavior of dc-to-dc converters in general, this state-plane analysis approach has led to the postulation of a state-trajectory control law which enables converter performance that approaches the theoretical limits revealed in the analysis. This control law is conceptually quite simple and is easily visualized in the converter state plane. It can be represented mathematically by means of relatively simple algebraic equations which can be used to implement the graphical conception. Furthermore, because of its sound mathematical basis, the nature of the operation of this control technique is easily understood and additional developments and extensions of it can be readily accomplished to meet particular application requirements or system performance constraints as desired. These modifications can take the form of simplified implementations with less precise converter performance, or the incorporation of additonal control features such as current limiting protection or converter startup procedures.

The principal function of energy-storage dc-to-dc power converters is to extract electrical energy from a given source at some unregulated voltage level, but at a controlled rate, in order to deliver energy to an electrical load at a different specified voltage level and particular power level. The only means available for controlling this rate of energy extraction is the switching on and off of the converter power switches, which is of course the principal task of any converter controller. Wich such an *a priori* limitation in the ability to continuously control this flow of energy, further restrictions imposed on the control process such as fixing the power switch on-time or, even more restrictive, fixing

the converter switching frequency can only cause degradation from the theoretically achievable converter performance. Likewise by restricting converter reference levels to constant values which are established for a nominally specified operating point, the converter system is prohibited from accommodating all operating conditions equally well. Thus, only by utilizing all of the information which is available from the system, and by allowing the power switch to remain on and off for variable periods of time can the theoretical limits in converter performance which are revealed by analysis be approached.

The control technique proposed in this dissertation enables converters to operate in such a free-running mode and thus to avoid the degradation in system performance which often accompanies imposed switching restrictions. At the same time the control law is such that a particular system timing characteristic can be incorporated during steady-state operation if desired. Likewise the sensitivity of the converter controller to changes in the system operating conditions and the lack of dependence on fixed reference levels enables the converter to adapt to all changes in externally imposed operating conditions and to precisely achieve the desired system output characteristics over the entire range of specified operating conditions. However, while providing superior performance, this approach also requires considerably more complex circuitry to implement than the more conventional control techniques in widespread use today. Thus, as is often the case, more complex circuitry and the resultant decrease in system reliability must be weighed against the desired improved converter performance. However, with the current rapid advances in electronic component development, it is believed that control circuitry of this complexity is viable.

The brief discussion presented in Chapter VI concerning the implementation of the state-trajectory control law is intended only to demonstrate the feasibility of physically realizing such an analytically derived function. Given the quality of modern electronic components and design techniques, it is believed that a practical and cost effective implementation can be developed. Furthermore it is believed that this implementation could be general in nature so that a single control design could be applied to all of the converter configurations discussed in this dissertation. The nature of the control process is the same for each case, and the input signals which are required from the converter power stage are also the same. Thus, by incorporating external adjustment capabilities, the particular converter parameters and desired output characteristics as well as the type of converter power stage being controlled could be conveniently specified for a standard control module.

Because of the general nature of the state-plane analysis techniques employed in this work, these same approaches and theories should apply to other types of power processing systems in particular and to any other second order systems which employ on/off control in general. The approach is quite straightforward and can be applied to any system which can be adequately represented by piecewise linear models. By observing the shapes of the trajectories which the state of the system must follow during each of the possible combinations of switch states in the system power stage, and by analytically locating the desired equilibrium trajectory of the system, one should be able to construct switching boundaries which always turn the movement of the state of the system toward the desired equilibrium trajectory. Such an approach yields inherently stable systems which respond very quickly to transient disturbances and which achieve

excellent static performance as well.

The mathematical nature of the control law is such that additional explorations into modifying and extending the control switching boundary are possible. One such modification with immediate applicability would be to rederive the switching lines so that the converter could regulate the output current rather than the output voltage. One example of the use of such current regulated converters is to recharge batteries onboard orbiting spacecraft. Such a modification can be easily accomplished by interchanging the roles of the desired output voltage and the desired output current in the equations which determine the steady-state switch-off point for the given converter and operating conditions.

APPENDIXES

APPENDIX A

DERIVATION OF STEADY-STATE SWITCH-OFF POINT

The equations which specify the location of the steady-state switch-off point for the three dc-to-dc converter power stages treated in this dissertation are derived below. Equations for the reactor current, i_{B-N}, and the output capacitor voltage, v_{B-N}, for both continuous conduction and discontinuous conduction operation are derived for each of the converter configurations. The resultant equations are given in Table 4.1 as equations (4.1) through (4.12). These equations are derived from the models of the converter power stages presented in Chapter II, and consequently the equations and figures presented there are used as the baseline for these derivations.

Voltage Step-Up Converter: Continuous Conduction Operation

Reactor Current, i_{B-N}:

The average steady-state reactor current, I_{X-N}, can be determined geometrically from the waveform of i_{X-N} vs. t_N given in Fig. 2.9(A).

$$I_{X-N} = \frac{i_{B-N} + i_{A-N}}{2} \tag{A.1}$$

For the voltage step-up configuration, the average reactor current is equal to the average input current. Also, for the lossless models presented in Chapter II, the average input power equals the average output power which can be expressed mathematically as follows:

$$v_{I-N}\ I_{X-N} = V_{O-N}\ i_{O-N} \tag{A.2}$$

(since v_{I-N} and i_{O-N} are constant in steady-state operation).
From equation (2.1),

$$i_{B-N} = \frac{v_{I-N}}{L_N}\ T_{on-N} + i_{A-N} \tag{A.3}$$

Combining (A.1), (A.2) and (A.3) to eliminate I_{X-N} and i_{A-N} yields

$$i_{B-N} = \frac{i_{O-N}\ V_{O-N}}{v_{I-N}} + \frac{v_{I-N}}{2L_N}\ T_{on-N} \tag{A.4}$$

Substituting (4.13) into (A.4) to eliminate T_{on-N} yields

$$i_{B-N} = \frac{i_{O-N}\ V_{O-N}}{v_{I-N}} + \frac{T_N\ v_{I-N}\ (V_{O-N} - v_{I-N})}{2L_N\ V_{O-N}} \tag{A.5}$$

which is equation (4.1) of Table 4.1(A).

Capacitor Voltage, v_{B-N}:

During steady-state operation, the average output voltage equals the average voltage across the output capacitor, C_N. Thus, integrating the expressions for $v_{C-N}\ (t_N)$ given in (2.1) and (2.2) over one cycle, and dividing the resultant integral by the period, T_N, yields

$$V_{O-N} = \frac{1}{T_N} \left\{ \int_0^{T_{on-N}} \left(- \frac{i_{O-N}}{C_N}\ t_N + v_{A-N} \right) dt_N \right.$$

$$\left. + \int_0^{T_{off-N}} \left(- \frac{V_{O-N} - v_{I-N}}{2L_N\ C_N}\ t_N^2 + \frac{i_{B-N} - i_{O-N}}{C_N}\ t_N + v_{B-N} \right) dt_N \right\} \tag{A.6}$$

From equation (2.1),

$$v_{A-N} = v_{B-N} + \frac{i_{O-N}}{C_N} T_{on-N} \tag{A.7}$$

Substituting (A.7) into (A.6) and combining terms yields

$$V_{O-N} = \frac{1}{T_N} \left(\frac{i_{O-N}}{2C_N} T_{on-N}^2 - \frac{V_{O-N} - v_{I-N}}{6L_N C_N} T_{off-N}^3 + \frac{i_{B-N} - i_{O-N}}{2C_N} T_{off-N}^2 + (T_{on-N} + T_{off-N}) v_{B-N} \right) \tag{A.8}$$

Substituting (4.1), (4.13) and (4.14) into (A.8) to eliminate i_{B-N}, T_{on-N} and T_{off-N} and combining terms yields

$$v_{B-N} = V_{O-N} - \frac{(V_{O-N} - v_{I-N}) i_{O-N} T_N}{2C_N V_{O-N}} - \frac{(V_{O-N} - v_{I-N}) v_{I-N}^3 T_N^2}{12L_N C_N V_{O-N}^3} \tag{A.9}$$

which is equation (4.2) of Table 4.1(A).

Voltage Step-Up Converter: Discontinuous Conduction Operation

Reactor Current, i_{B-N}:

The average steady-state reactor current, I_{X-N}, can be determined geometrically from the waveform of i_{X-N} vs. t_N given in Fig. 2.9(B).

$$I_{X-N} = \frac{i_{B-N} (T_{on-N} + T'_{off-N})}{2 T_N} \tag{A.10}$$

From (A.2),

$$I_{X-N} = \frac{V_{O-N} i_{O-N}}{v_{I-N}} \tag{A.11}$$

From (B.1),

$$T'_{off-N} = \frac{v_{I-N}}{V_{O-N} - v_{I-N}} \; T_{on-N} \tag{A.12}$$

Substituting (A.11) and (A.12) into (A.10) yields

$$i_{B-N} = \frac{2\, T_N\, i_{O-N}\, (V_{O-N} - v_{I-N})}{v_{I-N}\, T_{on}} \tag{A.13}$$

From (2.1),

$$i_{B-N} = \frac{v_{I-N}}{L_N} \; T_{on-N} \tag{A.14}$$

(since $i_{X-N}\,(t_N^0) = 0$ for discontinuous conduction operation).
Substituting (A.14) into (A.13) to eliminate T_{on-N} yields

$$i_{B-N} = \sqrt{\frac{2T_N\, i_{O-N}\, (V_{O-N} - v_{I-N})}{L_N}} \tag{A.15}$$

which is equation (4.3) of Table 4.1(A).

Capacitor Voltage, v_{B-N}:

From equations (2.1), (2.2), and (2.3),

$$V_{O-N} = \frac{1}{T_N} \left\{ \int_0^{T_{on-N}} \left(- \frac{i_{O-N}}{C_N}\, t_N + v_{A-N} \right) dt_N \right.$$
$$+ \int_0^{T'_{off-N}} \left(- \frac{V_{O-N} - v_{I-N}}{2L_N\, C_N}\, t_N^2 + \frac{i_{B-N} - i_{O-N}}{C_N}\, t_N + v_{B-N} \right) dt_N$$
$$\left. + \int_0^{T''_{off-N}} \left(- \frac{i_{O-N}}{C_N}\, t_N + v_{C-N}\,(t_N^2) \right) dt_N \right\} \tag{A.16}$$

where $v_{C-N}\ (t_N^2)$ is the value of capacitor voltage at the instant the reactor current falls to zero. From (2.1) and (2.3),

$$v_{B-N} = - \frac{i_{O-N}}{C_N}\ T_{on-N} + v_{A-N} \tag{A.17}$$

and

$$v_{A-N} = - \frac{i_{O-N}}{C_N}\ T''_{off-N} + v_{C-N}\ (t_N^2) \tag{A.18}$$

Combining (A.17) and (A.18) yields

$$v_{C-N}\ (t_N^2) = v_{B-N} + \frac{i_{O-N}}{C_N}\ (T''_{off-N} + T_{on-N}) \tag{A.19}$$

Substituting (A.17) and (A.19) into (A.16) to eliminate v_{A-N} and $v_{C-N}\ (t_N^2)$ and integrating the resultant equation yields

$$V_{O-N} = \frac{1}{T_N} \left[- \frac{V_{O-N} - v_{I-N}}{6L_N\ C_N}\ T'^{\,3}_{off-N} + \frac{i_{B-N} - i_{O-N}}{2C_N}\ T'^{\,2}_{off-N} + \frac{i_{O-N}}{2C_N} \left(T_{on-N} + T''_{off-N} \right)^2 + \left(T_{on-N} + T'_{off-N} + T''_{off-N} \right) v_{B-N} \right] \tag{A.20}$$

From (A.12) and (B.7),

$$T'_{off-N} = \sqrt{\frac{2\ i_{O-N}\ L_N\ T_N}{V_{O-N} - v_{I-N}}} \tag{A.21}$$

Since $T_{on-N} + T''_{off-N} = T_N - T'_{off-N}$,

$$T_{on-N} + T''_{off-N} = T_N - \sqrt{\frac{2\ i_{O-N}\ L_N\ T_N}{V_{O-N} - v_{I-N}}} \tag{A.22}$$

Substituting (A.21) and (A.22) into (A.20) to eliminate T_{on-N}, T'_{off-N}, and T''_{off-N}, and substituting (A.15) into (A.20) to eliminate i_{B-N} yields

$$v_{B-N} = V_{O-N} - \frac{i_{O-N}\, T_N}{2C_N} + \frac{i_{O-N}}{3C_N}\sqrt{\frac{2\, i_{O-N}\, L_N\, T_N}{(V_{O-N} - v_{I-N})}} \qquad (A.23)$$

which is equation (4.4) of Table 4.1(A).

Current Step-Up Converter: Continuous Conduction Operation

Reactor Current, i_{B-N}:

Following the pattern established for deriving the equations for the voltage step-up converter, the average steady-state reactor current, I_{X-N}, is again given by

$$I_{X-N} = \frac{i_{B-N} + i_{A-N}}{2} \qquad (A.24)$$

For the current step-up con iguration, the average steady-state reactor current is also equal to the average output current so that

$$i_{O-N} = \frac{i_{B-N} + i_{A-N}}{2} \qquad (A.25)$$

From the equations presented in Fig. 2.6, the steady-state solutions for i_{X-N} and v_{C-N} as functions of time can be found to be

$$\begin{aligned} i_{X-N} &= \frac{v_{I-N} - V_{O-N}}{L_N}\, t_N + i_{A-N} \\ v_{C-N} &= \frac{v_{I-N} - V_{O-N}}{2L_N\, C_N}\, t_N^2 + \frac{i_{A-N} - i_{O-N}}{C_N}\, t_N + v_{A-N} \end{aligned} \qquad (A.26)$$

during the power switch on-time interval,

$$i_{X-N} = - \frac{V_{O-N}}{L_N} t_N + i_{B-N}$$

$$v_{C-N} = - \frac{V_{O-N}}{2L_N C_N} t_N^2 + \frac{i_{B-N} - i_{O-N}}{C_N} t_N + v_{B-N} \qquad (A.27)$$

during T'_{off-N}, the power switch off-time interval with $i_{X-N} > 0$, and

$$i_{X-N} = 0$$

$$v_{C-N} = - \frac{i_{O-N}}{C_N} t_N + v_{C-N}\,(t_N^2) \qquad (A.28)$$

during T''_{off-N}, the power switch off-time interval with $i_{X-N} = 0$, where again $v_{C-N}\,(t_N^2)$ is the value of the output capacitor voltage at the instant that the reactor current falls to zero.

From (A.26),

$$i_{A-N} = i_{B-N} - \frac{v_{I-N} - V_{O-N}}{L_N} T_{on-N} \qquad (A.29)$$

Substituting (4.17) into (A.29) to eliminate T_{on-N} and substituting the resultant expression for i_{A-N} into (A.25) yields

$$i_{B-N} = i_{O-N} + \frac{V_{O-N}\,(v_{I-N} - V_{O-N})\,T_N}{2L_N\,v_{I-N}} \qquad (A.30)$$

which is equation (4.5) of Table 4.1(B).

Capacitor Voltage, v_{B-N}:

Again following the pattern established for the voltage step-up configuration, the desired expression for v_{B-N} can be found from (A.26) and (A.27) as follows:

$$V_{O-N} = \frac{1}{T_N}\left[\int_0^{T_{on-N}}\left(\frac{v_{I-N} - V_{O-N}}{2L_N C_N}t_N^2 + \frac{i_{A-N} - i_{O-N}}{C_N}t_N + v_{A-N}\right)dt_N + \int_0^{T_{off-N}}\left(-\frac{V_{O-N}}{2L_N C_N}t_N^2 + \frac{i_{B-N} - i_{O-N}}{C_N}t_N + v_{B-N}\right)dt_N\right] \quad (A.31)$$

From (A.25), (A.30), and (A.27), i_{A-N}, i_{B-N}, and v_{A-N}, respectively, can be eliminated from (A.31). From (4.17) and (4.18), T_{on-N} and T_{off-N} can be eliminated, and after integrating and recombining terms, equation (4.6) of Table 4.1(B) results.

Current Step-Up Converter: Discontinuous Conduction Operation

Reactor Current, i_{B-N}:

From Fig. 2.9(B),

$$I_{X-N} = \frac{i_{B-N}\,(T_{on-N} + T'_{off-N})}{2\,T_N} \quad (A.32)$$

From (B.15),

$$T'_{off-N} = \frac{V_{I-N} - V_{O-N}}{V_{O-N}} \; T_{on-N} \tag{A.33}$$

Substituting (A.33) and $I_{X-N} = i_{O-N}$ into (A.32) yields

$$i_{B-N} = \frac{2T_N \; i_{O-N} \; V_{O-N}}{V_{I-N} \; T_{on-N}} \tag{A.34}$$

From (A.26),

$$i_{B-N} = \frac{V_{I-N} - V_{O-N}}{L_N} \; T_{on-N} \tag{A.35}$$

since $i_{A-N} = 0$ for discontinuous conduction operation. Substituting (A.35) into (A.34) to eliminate T_{on-N} yields

$$i_{B-N} = \sqrt{\frac{2 \; T_N \; i_{O-N} \; (V_{I-N} - V_{O-N}) \; V_{O-N}}{L_N \; V_{I-N}}} \tag{A.36}$$

which is equation (4.7) of Table 4.1(B).

Capacitor Voltage, v_{B-N}:

From (A.26), (A.27), and (A.28), one can obtain the following expression for the average output voltage, V_{O-N}, where again $i_{A-N} = 0$ for discontinuous conduction operation.

$$V_{O-N} = \frac{1}{T_N}\left[\int_0^{T_{on-N}}\left(\frac{v_{I-N} - V_{O-N}}{2L_N C_N}t_N^2 - \frac{i_{O-N}}{C_N}t_N + v_{A-N}\right)dt_N\right.$$

$$+\int_0^{T'_{off-N}}\left(-\frac{V_{O-N}}{2L_N C_N}t_N^2 + \frac{i_{B-N} - i_{O-N}}{C_N}t_N + v_{B-N}\right)dt_N$$

$$\left.+\int_0^{T''_{off-N}}\left(-\frac{i_{O-N}}{C_N}t_N + v_{C-N}\,(t_N^2)\right)dt_N\right] \qquad (A.37)$$

From (A.28),

$$v_{C-N}\,(t_N^2) = v_{A-N} + \frac{i_{O-N}}{C_N}T''_{off-N} \qquad (A.38)$$

Substituting (A.38) into (A.37) and integrating yields

$$V_{O-N} = \frac{1}{T_N}\left[\frac{v_{I-N} - V_{O-N}}{6L_N C_N}T_{on-N}^3 - \frac{i_{O-N}}{2C_N}T_{on-N}^2 + v_{A-N}\,T_{on-N}\right.$$

$$-\frac{V_{O-N}}{6L_N C_N}T'^3_{off-N} + \frac{i_{B-N} - i_{O-N}}{2C_N}T'^2_{off-N} + v_{B-N}\,T'_{off-N}$$

$$\left.+\frac{i_{O-N}}{2C_N}T''^2_{off-N} + v_{A-N}\,T''_{off-N}\right] \qquad (A.39)$$

From (A.26),

$$v_{A-N} = v_{B-N} - \frac{v_{I-N} - V_{O-N}}{2L_N C_N}T_{on-N}^2 - \frac{i_{O-N}}{C_N}T_{on-N} \qquad (A.40)$$

Also, since

$$T''_{off\text{-}N} = T_N - T_{on\text{-}N} - T'_{off\text{-}N}, \tag{A.41}$$

from (4.19) and (A.33),

$$T''_{off\text{-}N} = \frac{V_{I\text{-}N}\,(V_{I\text{-}N} - V_{O\text{-}N})}{2L_N\, i_{O\text{-}N}\, V_{O\text{-}N}}\, T^2_{on\text{-}N} - \frac{V_{I\text{-}N}}{V_{O\text{-}N}}\, T_{on\text{-}N} \tag{A.42}$$

Substituting (A.40), (A.35), (A.33), and (A.42) into (A.39) to eliminate $v_{A\text{-}N}$, $i_{B\text{-}N}$, $T'_{off\text{-}N}$, and $T''_{off\text{-}N}$ respectively, one obtains an expression for $v_{B\text{-}N}$ in terms of $T_{on\text{-}N}$. Substituting the value of $T_{on\text{-}N}$ from (4.19) into that expression yields equation (4.8) of Table 4.1(B).

Current-or-Voltage Step-Up Converter: Continuous Conduction Operation

Reactor Current, $i_{B\text{-}N}$:

From the equations presented in Fig. 2.7, the steady-state solution for $i_{X\text{-}N}$ and $v_{C\text{-}N}$ as functions of time can be found to be

$$\begin{aligned} i_{X\text{-}N} &= \frac{V_{I\text{-}N}}{L_N}\, t_N + i_{A\text{-}N} \\ v_{C\text{-}N} &= -\frac{i_{O\text{-}N}}{C_N}\, t_N + v_{A\text{-}N} \end{aligned} \tag{A.43}$$

during the power switch on-time interval,

$$\begin{aligned} i_{X\text{-}N} &= -\frac{V_{O\text{-}N}}{L_N}\, t_N + i_{B\text{-}N} \\ v_{C\text{-}N} &= -\frac{V_{O\text{-}N}}{2L_N C_N}\, t_N^2 + \frac{i_{B\text{-}N} - i_{O\text{-}N}}{C_N}\, t_N + v_{B\text{-}N} \end{aligned} \tag{A.44}$$

during T'_{off-N}, the power switch off-time interval with $i_{X-N}>0$, and

$$i_{X-N} = 0$$

$$v_{C-N} = - \frac{i_{O-N}}{C_N} t_N + v_{C-N} (t_N^2) \tag{A.45}$$

during T''_{off-N}, the power switch off-time interval with $i_{X-N} = 0$, where again $v_{C-N} (t_N^2)$ is the value of the output capacitor voltage at the instant that the reactor current falls to zero.

From Fig. 2.7, one can see that the average steady-state output current, i_{O-N}, is equal to the reactor current during the power switch off-time interval averaged over the whole period, T_N. Thus,

$$i_{O-N} = \frac{(i_{B-N} + i_{A-N}) T'_{off-N}}{2 T_N} \tag{A.46}$$

From (A.43),

$$i_{A-N} = i_{B-N} - \frac{v_{I-N}}{L_N} T_{on-N} \tag{A.47}$$

Substituting (A.47) into (A.46) and recombining terms yields

$$i_{B-N} = \frac{i_{O-N} T_N}{T'_{off-N}} + \frac{v_{I-N} T_{on-N}}{2L_N} \tag{A.48}$$

Substituting equations (4.21) and (4.22) into (A.48) to eliminate T_{on-N} and T'_{off-N} respectively yields

$$i_{B-N} = \frac{i_{O-N}\,(v_{I-N} + V_{O-N})}{v_{I-N}} + \frac{T_N\, V_{O-N}\, v_{I-N}}{2L_N\,(V_{O-N} + v_{I-N})} \qquad (A.49)$$

which is equation (4.9) of Table 4.1(C).

Capacitor Voltage, v_{B-N}:

The desired expression for v_{B-N} can be found from (A.43) and (A.44) as follows:

$$V_{O-N} = \frac{1}{T_N}\left[\int_0^{T_{on-N}} \left(-\frac{i_{O-N}}{C_N}\,t_N + v_{A-N}\right) dt_N + \int_0^{T_{off-N}} \left(-\frac{V_{O-N}}{2L_NC_N}\,t_N^2 + \frac{i_{B-N} - i_{O-N}}{C_N}\,t_N + v_{B-N}\right) dt_N\right] \qquad (A.50)$$

From (A.47), (A.49), and (A.44), i_{A-N}, i_{B-N}, and v_{A-N}, respectively, can be eliminated from (A.50). From (4.21) and (4.22), T_{on-N} and T_{off-N} can be eliminated, and after integrating and recombining terms, equation (4.10) of Table 4.1(C) results.

Current-or-Voltage Step-Up Converter: Discontinuous Conduction Operation

Reactor Current, i_{B-N}:

From (A.46), with $i_{A-N} = 0$,

$$i_{B-N} = \frac{2\, i_{O-N}\, T_N}{T_{off-N}} \qquad (A.51)$$

From (B.20),

$$T'_{off-N} = \frac{v_{I-N}}{V_{O-N}} \; T_{on-N} \tag{A.52}$$

Substituting (A.52) into (A.51) yields

$$i_{B-N} = \frac{2 \; i_{O-N} \; V_{O-N} \; T_N}{v_{I-N} \; T_{on-N}} \tag{A.53}$$

But from (A.47), with $i_{A-N} = 0$,

$$T_{on-N} = \frac{L_N}{v_{I-N}} \; i_{B-N} \tag{A.54}$$

Thus, substituting (A.54) into (A.53) yields

$$i_{B-N} = \sqrt{\frac{2 \; T_N \; i_{O-N} \; V_{O-N}}{L_N}} \tag{A.55}$$

which is equation (4.11) of Table 4.1(C).

Capacitor Voltage, v_{B-N}:

The desired expression for v_{B-N} can be found from (A.43), (A.44), and (A.45) as follows:

$$V_{O-N} = \frac{1}{T_N} \left[\int_0^{T_{on-N}} \left(- \frac{i_{O-N}}{C_N} t_N + v_{A-N} \right) dt_N + \right.$$

$$\int_0^{T'_{off-N}} \left(- \frac{v_{O-N}}{2L_N C_N} t_N^2 + \frac{i_{B-N} - i_{O-N}}{C_N} t_N + v_{B-N} \right) dt_N$$

$$+ \int_0^{T''_{off-N}} \left(- \frac{i_{O-N}}{C_N} t_N + v_{C-N} (t_N^2) \right) dt_N \Bigg] \qquad (A.56)$$

From (A.45),

$$v_{C-N} (t_N^2) = v_{A-N} + \frac{i_{O-N}}{C_N} T''_{off-N} \qquad (A.57)$$

Also, from (A.43),

$$v_{A-N} = v_{B-N} + \frac{i_{O-N}}{C_N} T_{on-N} \qquad (A.58)$$

Substituting (A.57) and (A.58) into (A.56) to eliminate $v_{C-N} (t_N^2)$ and v_{A-N}, and integrating yields

$$V_{O-N} = \frac{1}{T_N} \Bigg[- \frac{V_{O-N}}{6L_N C_N} T'^3_{off-N} + \frac{i_{B-N} - i_{O-N}}{2C_N} T'^2_{off-N} + v_{B-N} T'_{off-N}$$

$$+ \frac{i_{O-N}}{2C_N} (T_{on-N} + T''_{off-N})^2 + v_{B-N} (T_{on-N} + T''_{off-N}) \Bigg] \qquad (A.59)$$

From (A.51),

$$T'_{off-N} = \frac{2 i_{O-N} T_N}{i_{B-N}} \qquad (A.60)$$

Also, since $T_{on-N} + T''_{off-N} = T_N - T'_{off-N}$,

$$T_{on-N} + T''_{off-N} = T_N - \frac{2\, i_{O-N}\, T_N}{i_{B-N}} \tag{A.61}$$

Substituting (A.60) and (A.61) into (A.59) to eliminate T'_{off-N} and $(T_{on-N} + T''_{off-N})$, respectively, and substituting (A.55) into the resultant equation to eliminate i_{B-N}, yields

$$v_{B-N} = V_{O-N} - \frac{i_{O-N}\, T_N}{2\, C_N} + \frac{i_{O-N}}{3\, C_N} \sqrt{\frac{2\, i_{O-N}\, L_N\, T_N}{V_{O-N}}} \tag{A.62}$$

which is equation (4.12) of Table 4.1(C).

APPENDIX B

DERIVATION OF STEADY-STATE TIME RELATIONSHIPS

Equations which specify the relationships between the power switch off-time and on-time intervals and the total switching period for each of the three converter configurations in steady-state operation in the continuous and the discontinuous conduction modes are derived below. For discontinuous conduction operation, the off-time interval consists of two subintervals to distinguish the time that the reactor current is greater than zero, T'_{off-N}, from the time that the reactor current is equal to zero, T''_{off-N}. Thus, for discontinuous conduction operation,

$$T_N = T_{on-N} + T'_{off-N} + T''_{off-N}$$

In the continuous conduction mode of operation, however,

$$T_{off-N} = T'_{off-N}$$

and

$$T_N = T_{on-N} + T'_{off-N}$$

The equations derived in this appendix are presented in Table 4.2 as equations (4.13) through (4.24).

Voltage Step-Up Converter: Continuous Conduction Operation

During steady-state operation, the increase in reactor current during the power switch on-time interval is equal to the decrease in reactor current during the switch off-time interval. Thus, from (2.1) and (2.2),

$$\frac{V_{I-N}}{L_N} T_{on-N} = \frac{V_{O-N} - V_{I-N}}{L_N} T'_{off-N} \tag{B.1}$$

For continuous conduction operation,

$$T'_{off-N} = T_N - T_{on-N} \tag{B.2}$$

Substituting (B.2) into (B.1) and rearranging terms yields

$$T_N = \frac{V_{O-N}}{V_{O-N} - V_{I-N}} T_{on-N} \tag{B.3}$$

or

$$T_N = \frac{V_{O-N}}{V_{I-N}} T_{off-N} \tag{B.4}$$

which are (4.13) and (4.14) respectively of Table 4.2(A).

Voltage Step-Up Converter: Discontinuous Conduction Operation

From equation (A.15),

$$i_{B-N}^2 = \frac{2\ T_N\ i_{O-N}\ (V_{O-N} - v_{I-N})}{L_N} \tag{B.5}$$

From (A.14),

$$i_{B-N} = \frac{v_{I-N}}{L_N}\ T_{on-N} \tag{B.6}$$

Substituting (B.6) into (B.5) and recombining terms yields

$$T_N = \frac{v_{I-N}^2}{2\ L_N\ i_{O-N}\ (V_{O-N} - v_{I-N})}\ T_{on-N}^2 \tag{B.7}$$

which is equation (4.15) of Table 4.2(A).

Since

$$T_{on-N} = T_N - T_{off-N} \tag{B.8}$$

$$T_{on-N}^2 = T_N^2 - 2\ T_N\ T_{off-N} + T_{off-N}^2 \tag{B.9}$$

Substituting (B.9) into (B.7) and recombining terms yields

$$T_N^2 - 2\ (T_{off-N} + \frac{L_N\ i_{O-N}\ (V_{O-N} - v_{I-N})}{v_{I-N}^2}\ )\ T_N + T_{off-N}^2 = 0 \tag{B.10}$$

which is equation (4.16) of Table 4.2(A) with $T_N = T_R$. Solving for T_N yields

$$T_{N+},\ T_{N-} = \tau \pm \sqrt{\tau^2 - T_{off-N}^2} \tag{B.11}$$

where

$$\tau \triangleq T_{off-N} + \frac{L_N\, i_{O-N}\, (V_{O-N} - v_{I-N})}{v_{I-N}^2} \tag{B.12}$$

Since

$$(\tau - T_{off-N})^2 < \tau^2 - T_{off-N}^2 \tag{B.13}$$

it follows that

$$T_N^- = \tau - \sqrt{\tau^2 - T_{off-N}^2} \quad < T_{off-N} \tag{B.14}$$

which is a contradiction. Thus, T_N equals the larger root of the quadratic as stated in Table 4.2(A).

Current Step-Up Converter: Continuous Conduction Operation

From (A.26) and (A.27),

$$\frac{v_{I-N} - V_{O-N}}{L_N}\ T_{on-N} = \frac{V_{O-N}}{L_N}\ T'_{off-N} \tag{B.15}$$

Substituting (B.2) into (B.15) and recombining terms yields

$$T_N = \frac{v_{I-N}}{V_{O-N}}\ T_{on-N} \tag{B.16}$$

and

$$T_N = \frac{v_{I-N}}{v_{I-N} - V_{O-N}}\ T_{off-N} \tag{B.17}$$

which are (4.17) and (4.18) respectively of Table 4.2(B).

Current Step-Up Converter: Discontinuous Conduction Operation

Combining (A.34) and (A.35) to eliminate i_{B-N} yields

$$T_N = \frac{v_{I-N}\,(v_{I-N} - V_{O-N})}{2\,L_N\,i_{O-N}\,V_{O-N}}\;T_{on-N}^2 \tag{B.18}$$

which is equation (4.19) of Table 4.2(B).

Substituting (B.9) into (B.18) and recombining terms yields

$$T_N^2 - 2\left(T_{off-N} + \frac{i_{O-N}\,L_N\,V_{O-N}}{v_{I-N}\,(v_{I-N} - V_{O-N})}\right)T_N + T_{off-N}^2 = 0 \tag{B.19}$$

which is equation (4.20) of Table 4.2(B) with $T_N = T_R$. Following the argument given in equations (B.11) through (B.14), T_N equals the larger root of the quadratic as stated in Table 4.2(B).

Current-or-Voltage Step-Up Converter: Continuous Conduction Operation

From (A.43) and (A.44),

$$\frac{v_{I-N}}{L_N}\,T_{on-N} = \frac{V_{O-N}}{L_N}\,T'_{off-N} \tag{B.20}$$

Substituting (B.2) into (B.20) and recombining terms yields

$$T_N = \frac{V_{O-N} + v_{I-N}}{V_{O-N}}\;T_{on-N} \tag{B.21}$$

and

$$T_N = \frac{V_{O-N} + v_{I-N}}{v_{I-N}}\;T_{off-N} \tag{B.22}$$

which are (4.21) and (4.22) respectively of Table 4.2(C).

Current-or-Voltage Step-Up Converter: Discontinuous Conduction Operation

Combining (A.53) and (A.54) to eliminate i_{B-N} yields

$$T_N = \frac{V_{I-N}^2}{2 L_N i_{O-N} V_{O-N}} T_{on-N}^2 \tag{B.23}$$

which is equation (4.23) of Table 4.2(C).

Substituting (B.9) into (B.23) and recombining terms yields

$$T_N^2 - 2\left(T_{off-N} + \frac{i_{O-N} L_N V_{O-N}}{V_{I-N}}\right) T_N + T_{off-N}^2 = 0 \tag{B.24}$$

which is equation (4.24) of Table 4.2(C) with $T_N = T_R$. Following the argument given in equations (B.11) through (B.14), T_N equals the larger root of the quadratic as stated in Table 4.2(C).

APPENDIX C

SWITCHING BOUNDARIES f AND f'

This appendix presents the equations for the switching boundaries developed in Chapter IV. Boundary f is used if the ideal capacitor voltage, v_{C-N}, is monitored as one of the system state variables, whereas boundary f' is used if the output voltage, v_{O-N}, is monitored. Expressions for i_{B-N} and v_{B-N} are given in Table 4.1. The timing parameter can be changed by substituting the desired parameter from Table 4.2 into Table 4.1.

Voltage Step-Up Converter

$$f = - \frac{L_N}{2C_N (V_{O-N} - v_{I-N})} (i_{X-N}^2 - i_{B-N}^2) + \frac{i_{O-N} L_N}{C_N (V_{O-N} - v_{I-N})} (i_{X-N} - i_{B-N})$$

$$+ v_{B-N} - v_{C-N} \qquad \text{for } i_{X-N} \geq i_{B-N} \qquad \text{(C.1)}$$

$$f = - \frac{i_{O-N} L_N}{v_{I-N} C_N} (i_{X-N} - i_{B-N}) + v_{B-N} - v_{C-N} \qquad \text{(C.2)}$$

$$\text{for } i_{X-N} < i_{B-N}$$

$$f' = - \frac{L_N}{2\, C_n\, (V_{O-N} - v_{I-N})} \left(i^2_{X-N} - i^2_{B-N} \right) + \frac{i_{O-N}\, L_N}{C_N\, (V_{O-N} - v_{I-N})} (i_{X-N} - i_{B-N})$$

$$+ v_{B-N} - v_{O-N} - i_{O-N}\, r_{C-N} \qquad (C.3)$$

$$\text{for } i_{X-N} \geq i_{B-N}$$

$$f' = - \frac{i_{O-N}\, L_N}{v_{I-N}\, C_N} (i_{X-N} - i_{B-N}) + v_{B-N} - v_{O-N} + (i_{X-N} - i_{O-N})\, r_{C-N} \qquad (C.4)$$

$$\text{for } i_{X-N} < i_{B-N}$$

Current Step-Up Converter

$$f = - \frac{L_N}{2\, C_N\, V_{O-N}} (i^2_{X-N} - i^2_{B-N}) + \frac{i_{O-N}\, L_N}{C_N\, V_{O-N}} (i_{X-N} - i_{B-N}) + v_{B-N} - v_{C-N} \qquad (C.5)$$

$$\text{for } i_{X-N} \geq i_{B-N}$$

$$f = - \frac{L_N}{2\, C_N\, (V_{O-N} - v_{I-N})} (i^2_{X-N} - i^2_{B-N}) + \frac{i_{O-N}\, L_N}{C_N\, (V_{O-N} - v_{I-N})} (i_{X-N} - i_{B-N})$$

$$+ v_{B-N} - v_{C-N} \qquad (C.6)$$

$$\text{for } i_{X-N} < i_{B-N}$$

$$f' = - \frac{L_N}{2\, C_N\, V_{O-N}} \left(i^2_{X-N} - i^2_{B-N} \right) + \frac{i_{O-N}\, L_N}{C_N\, V_{O-N}} (i_{X-N} - i_{B-N})$$

$$+ v_{B-N} - v_{O-N} - i_{O-N}\, r_{C-N} \qquad (C.7)$$

$$\text{for } i_{X-N} \geq i_{B-N}$$

$$f' = - \frac{L_N}{2\, C_N\, (V_{O-N} - v_{I-N})} (i_{X-N}^2 - i_{B-N}^2) + \frac{i_{O-N}\, L_N}{C_N\, (V_{O-N} - v_{I-N})} (i_{X-N} - i_{B-N})$$

$$+ v_{B-N} - v_{O-N} + (i_{X-N} - i_{O-N})\, r_{C-N} \qquad \text{(C.8)}$$

$$\text{for } i_{X-N} < i_{B-N}$$

Current-or-Voltage Step-Up Converter

$$f = - \frac{L_N}{2\, C_N\, V_{O-N}} (i_{X-N}^2 - i_{B-N}^2) + \frac{L_N\, i_{O-N}}{C_N\, V_{O-N}} (i_{X-N} - i_{B-N}) + v_{B-N} - v_{C-N} \qquad \text{(C.9)}$$

$$\text{for } i_{X-N} \geq i_{B-N}$$

$$f = - \frac{i_{O-N}\, L_N}{v_{I-N}\, C_N}\, i_{X-N} - i_{B-N} + v_{B-N} - v_{C-N} \qquad \text{(C.10)}$$

$$\text{for } i_{X-N} < i_{B-N}$$

$$f' = - \frac{L_N}{2\, C_N\, V_{O-N}} (i_{X-N}^2 - i_{B-N}^2) + \frac{L_N\, i_{O-N}}{C_N\, V_{O-N}} (i_{X-N} - i_{B-N})$$

$$+ v_{B-N} - v_{O-N} - i_{O-N}\, r_{C-N} \qquad \text{(C.11)}$$

$$\text{for } i_{X-N} \geq i_{B-N}$$

$$f' = - \frac{i_{O-N}\, L_N}{v_{I-N}\, C_N} (i_{X-N} - i_{B-N}) + v_{B-N} - v_{O-N} + (i_{X-N} - i_{O-N})\, r_{C-N} \qquad \text{(C.12)}$$

$$\text{for } i_{X-N} < i_{B-N}$$

LIST OF REFERENCES

LIST OF REFERENCES

[1] E. T. Moore and T. G. Wilson, "Basic Considerations for DC to DC Conversion Networks," IEEE Transactions on Magnetics, Vol. MAG-2, No. 3, pp. 620-624, September 1966.

[2] F. N. Tompkins, "The Parallel Type Inverter," Transactions AIEE, Vol. 51, pp. 707-714, September 1932.

[3] "Voltage Regulation and Conversion in Unconventional Electrical Generator Systems," General Electric Company Report prepared under Bureau of Naval Weapons, Department of the Navy, Contract NOw 62-094-d, August 31, 1963.

[4] B. P. Schweitzer and A. B. Rosenstein, "Free Running - Switching Mode Power Regulator: Analysis and Design," IEEE Transactions on Aerospace and Electronic Systems, Vol. AS-2, pp. 1171-1180, October 1964.

[5] I. M. H. Babaa, T. G. Wilson, and Y. Yu, "Analytic Solutions of Limit Cycles in a Feedback - Regulated Converter System with Hysteresis," IEEE Transactions on Automatic Control, Vol. AC-13, No. 5, pp. 524-531, October 1968.

[6] O. A. Kossov, "Comparative Analysis of Chopper Regulators with LC Filter," IEEE Transactions on Magnetics, Vol. MAG-4, pp. 712-715, December 1968.

[7] F. F. Judd and C. T. Chen, "Analysis and Optimal Design of Self-Oscillating DC-to-DC Converters," IEEE Transactions on Circuit Theory, Vol. CT-18, No. 6, pp. 651-685, November 1971.

[8] G. W. Wester and R. D. Middlebrook, "Low-Frequency Characterization of Switched dc-dc Converters," IEEE Transactions on Aerospace and Electronic Systems, Vol. AES-9, No. 3, pp. 376-385, May 1973.

[9] D. Y. Chen, H. A. Owen, Jr., and T. G. Wilson, "Computer-Aided Design and Graphics Applied to the Study of Inductor-Energy-Storage dc-to-dc Electronic Power Converters," IEEE Transactions on Aerospace and Electronic Systems, Vol. AES-9, No. 4, pp. 585-597, July 1973.

[10] A. K. Ohri, H. A. Owen, Jr., T. G. Wilson, and G. E. Rodriguez, "Digital Computer Simulation of Inductor-Energy-Storage DC-to-DC Converters with Closed-Loop Regulators," S.P. 103, ESRO Spacecraft Power Conditioning Electronics Seminar, Frascati, Italy, May 1974.

[11] F. C. Schwarz, "Engineering Information on an Analog Signal to Discrete Time Interval Converter (ASDTIC)," NASA CR- 134544, June 1974.

[12] R. Prajoux, A. Giraud, and R. Valette, "A Modeling Technique Using A Recurrence for Some Control Systems Described by a Piecewise-Time-Invariant-Continuous State Equation," Conference Information Sciences and Systems, The John Hopkins University, Baltimore, Md., April 2-4, 1975.

[13] P. Burger, "Analysis of a Class of Pulse Modulated DC-to-DC Power Converters," IEEE Transactions on Industrial Electronics and Control Instrumentation, Vol. IECI-22, No. 2, pp. 104-116, May 1975.

[14] A. Capel, J. G. Ferrante, and R. Prajoux, "State Variable Stability Analysis of Multi-Loop PWM Controlled DC/DC Regulators in Light and Heavy Mode," IEEE Power Electronics Specialists Conference Record, IEEE Publication No. 75-CHO 965-4 AES, pp. 91-102, June 1975.

[15] R. P. Iwens, Y. Yu, and J. E. Triner, "Time Domain Modelling and Stability Analysis of an Integral Pulse Frequency Modulated DC to DC Power Converter," IEEE Power Electronics Specialists Conference Record, IEEE Publication No. 75-CHO 965-4 AES, pp. 80-90, June 1975.

[16] D. Y. Chen, H. A. Owen, Jr., T. G. Wilson, "Energy-Balance Constraints Affecting the Design of Energy-Storage DC-to-DC Converters," IEEE 1975 Applied Magnetics Workshop, IEEE Publication 75CH0964-7MAG, pp. 38-1 to 38-22, June 1975.

[17] J. Jalade, "Contribution à l'Étude des Systèms Nonlinéaires à Structure Linéaire par Morceaux: Application à l'Étude par un Modèle Discret des Convertisseurs Continu-Continu," Doctoral Thesis, University Paul Sabatier, Toulouse, France, 1976.

[18] J. C. Marpinard, "Contribution à l'Étude des Systèmes Nonlinéaires à Structure Linéaire par Morceaux: Application à l'Étude par un Modèle de Type Continu des Convertisseurs Continu-Continu," Doctoral Thesis, University Paul Sabatier, Toulouse, France, 1976.

[19] H. A. Owen, Jr., A. Capel, and J. G. Ferrante, "Simulation and Analysis Methods for Sampled Power Electronic Systems," IEEE Power Electronics Specialists Conference Record, IEEE Publication No. 76CH1084-3 AES, pp. 45-55, June 1976.

[20] R. D. Middlebrook and S. Cuk, "A General Unified Approach to Modeling Switching-Converter Power Stages," 1976 IEEE Power Electronics Specialists Conference Record, IEEE Publication No. 76CH1084-3 AES, pp. 18-34, June 1976.

[21] F. C. Lee, Y. Yu, and J. E. Triner, "Modeling of Switching Regulator Power Stages With and Without Zero-Inductor-Current Dwell Time," 1976 IEEE Power Electronics Specialists Conference Record, IEEE Publication No. 76CH1084-3 AES, pp. 62-72, June 1976.

[22] Y. Yu, J. J. Biess, A. D. Schoenfeld, and V. R. Lalli, "The application of Standardized Control and Interface Circuits to Three DC to DC Power Converters," 1973 IEEE Power Electronics Specialists Conference Record, IEEE Publication No. 73 CHO 787-2 AES, pp. 273-248, June 1973.

[23] A. D. Schoenfeld and Y. Yu, "ASDTIC Control and Standardized Interface Circuits Applied to Buck, Parallel, and Buck-Boost DC to DC Power Converters," NASA Report No. CR121106, February 1973.

BIOGRAPHY

BIOGRAPHY

WILLIAM WESLEY BURNS, III

Born: [redacted]

Education:
Harvard University, A.B., June 1968. Field of Concentration: Engineering and Applied Physics

Duke University, M.S., May 1974, Ph.D., May 1977. Major: Electrical Engineering

Professional Society Publications:

[1] ___(with T.G. Wilson, F.C.Y. Lee, and H.A. Owen, Jr.) "Relationships Among Classes of Self-Oscillating Transistor Parallel Inverters," IEEE Transactions on Aerospace and Electronic Systems, Vol. AES-11, No. 2, pp. 238-244, March 1975.

Also, IEEE 1974 Power Electronics Specialists Conference Record, IEEE Publication No. 74 CHO 863-1-AES, pp. 233-236, June 1974.

[2] ___(with H.A. Owen, Jr., T.G. Wilson, G.E. Rodriguez, and J. Paulkovich) "A Digital Computer Simulation and Study of A Direct-Energy-Transfer Power-Conditioning System," IEEE 1975 Power Electronics Specialists Conference Record, IEEE Publication No. 75-CHO 965-4 AES, pp. 138-149, June 1975.

[3] ___(with T.G. Wilson) "State Trajectories Used to Observe and Control DC-to-DC Converters," IEEE Transactions on Aerospace and Electronic Systems, Vol. AES-12, No. 6, pp. 706-717, November 1976.

Also, "State-Plane Trajectories Used to Observe and Control the Behavior of A Voltage Step-Up DC-to-DC Converter," IEEE 1976 Power Electronics Specialists Conference Record, IEEE Publication No. 76CH1084-3 AES, pp. 212-222, June 1976.

Professional Experience:

Project Engineer
United States Air Force, Kelly AFB, Texas, 1969 to 1972.

Teaching Assistant
Department of Electrical Engineering, Duke University, 1972 to 1974.

Research Assistant
Spacecraft Systems Research Laboratory, Duke University, 1972 to 1977.

Power Electronics Laboratory, Delft University of Technology, Delft, The Netherlands; in residence Fall 1975.

Laboratory of Automatic Control and Systems Analysis of the French National Center for Scientific Research, Toulouse, France; in residence Spring 1976.